Role of glycans in osteogenesis

Katherine Mary Wilson

PhD

University of York

Biology

July 2015

Abstract

Glycosylation is an abundant post translational modification of proteins, which occurs in the endoplasmic reticulum and Golgi. Nearly every secreted and plasma membrane localised protein is glycosylated. Mesenchymal stromal/stem cells (MSCs) are adult stem cells that can self-renew and differentiate into multiple cell types including: osteoblasts, adipocytes and chondrocytes. Due to their tri-lineage capacity and their immunoregulatory functions, MSCs are attractive tools for the treatment of multiple diseases and conditions. Key to their use in regenerative medicine is knowledge about what influences a MSC to differentiate into a particular cell type. Despite previous studies describing distinct glycan profiles of cells at different stages of development, whether glycans play a functional role in directing MSC differentiation is currently unknown.

Here, utilizing an immortalized primary human MSC line (hTERT-MSCs), the *N*-glycans from MSCs and osteoblasts were harvested using the Filter aided *N*-glycan Separation (FANGS) method. Following permethylation, *N*-glycans were analysed by mass spectrometry (MALDI-TOF/TOF). This method allowed the reliable, quantitative, relative abundance of different glycan structures to be compared between the two cell types for the first time. Complex *N*-glycans were significantly more abundant in osteoblasts compared to MSCs. The *N*-glycan profiles of different hTERT-MSC lines were not significantly different, despite variations in differentiation potential. The glycosylation pathway was genetically disrupted by targeting a subunit of the Conserved Oligomeric Complex (COG) with a shRNA. As predicted, since COG is responsible for the tethering of vesicles carrying Golgi resident enzymes, Cog4 knock-down hTERT-MSCs had disrupted *N*- and O-glycan synthesis. Interestingly, Cog4 knock-down hTERT-MSCs showed reduced osteogenic capacity with reduced levels of mineralised extracellular matrix (ECM). Surprisingly, the chemical inhibition of complex *N*-glycan synthesis increased ECM mineralisation, whilst inhibition of O-glycan synthesis or proteoglycan sulfation mimicked the Cog4 knock-down cells with reduced mineralisation. These results showed a novel role of both *N*-and O-glycans in osteogenesis.

Table of Contents

List of figures

List of tables

Acknowledgements

I would like to thank EPSRC for funding this project and both my supervisors, Dr. Paul Genever and Dr. Dani Ungar for their support and guidance throughout. I would also like to thank members of my thesis advisory panel, Dr. Betsy Pownall and Prof. Jenny Southgate for their input and guidance.

Many thanks also to Dr. Salina Abdul Rahman for teaching me FANGS and mass spectrometry methods. Thanks to all the staff at the Technology Facility at University of York, for technical assistance during imaging and flow cytometry work. In particular thanks to Graeme Park, whose friendly nature and generosity in time given to help with machine issues and dramas was much appreciated. Thanks to the Undergraduate project students: Alistair Jagger and Isabella Gomes Cantanhede for all their efforts in the lab and for showing such enthusiasm, you were a pleasure to supervise.

I would also like to thank all the members of the Cell Biology Laboratories at York, for their help and assistance in the laboratory. In particular I would like to thank: Charlotte, Becky, Julia, Sarah, Alice, Amanda and Dimi for their friendships, which have undoubtedly made my PhD experience more enjoyable. Thanks to Tom for supporting me through 1st year nerves and 2nd year blues and for being my rock for so long. Thanks to Andy and Team Dan, your friendships mean a lot to me and our sessions on the squash court and in the pub have helped me remain happy even whilst writing this thesis! Thanks lastly to my parents who have always encouraged me, I will eventually stop being a University student.

Author's declaration

The work presented in this thesis was performed by the author between October 2011 and July 2015 in the Department of Biology, University of York, in the laboratories of Dr. Dani Ungar and Dr. Paul Genever. All experiments were performed by the author, with the exception of a few experiments in Chapter 4 and 5, which were performed by Alistair Jagger and Isabella Gomes Cantanhede, both undergraduate students who worked in the lab under the authors supervision. Figure that contain data from their work are clearly marked. Neither this thesis nor any part of it has previously been submitted for acceptance of a higher degree.

Chapter 1: Introduction

1.1 The Golgi

In 1898 Camillo Golgi described an 'internal reticular apparatus' in the cytoplasm of nerve cells [1]. Following observations of the same structure in many different cell types, and the identification of the structure by electron microscopy 50 years later [2], the existence of the organelle was finally accepted and became widely known as the Golgi.

The Golgi is formed of stacks of individual membrane ribbons or cisternae that are spatially and functionally divided into different regions. The *cis* Golgi network is comprised of cisternae adjacent to the endoplasmic reticulum (ER) and receives vesicles containing newly translated proteins. As proteins move from the *cis* to the *trans* Golgi network they undergo post translational modifications such as glycosylation. Proteins are finally transported from the *trans* Golgi network, at the plasma membrane end of the stack, to their cellular destination such as the plasma membrane or lysosome (Figure 1.1).

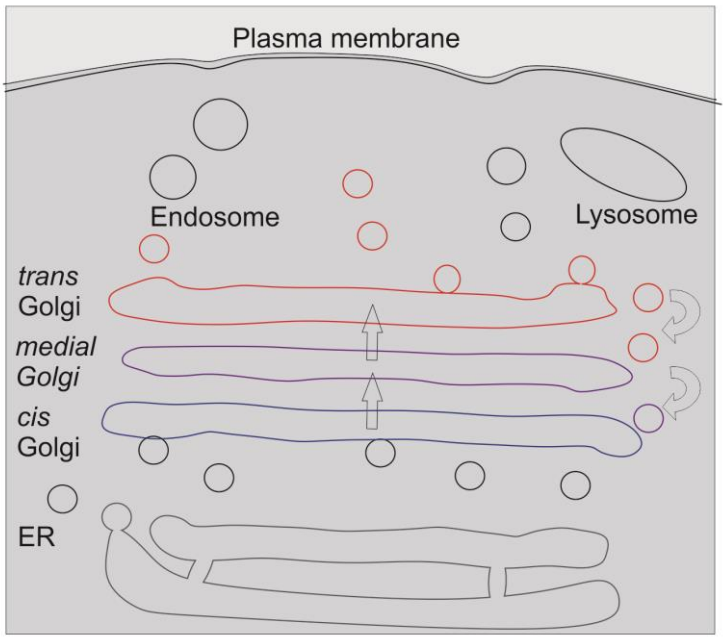

Figure 1.1 The Golgi

Diagram depicts location of the Golgi inside a cell, near the endoplasmic reticulum (ER). Cisternae of the Golgi are spatially and functionally separated, with the *cis* Golgi adjacent to the ER and the *trans* Golgi at the plasma membrane end of the stack. The content of cisternae changes or matures via retrograde transport vesicles that deliver Golgi enzymes back to newly formed cis cisterna. After post-translational modifications in the Golgi proteins are transported to their cellular location.

1.1.1 Models of protein traffic through the Golgi

In order for correct post translational modifications of proteins to occur, a distinct distribution of Golgi resident enzymes in the different cisternae must be maintained. Simultaneously, proteins are transported in an anterograde (forward) direction through the Golgi. Several models have been proposed for how this might be achieved. The vesicle transport model proposes that the cisternae are in fixed positions with anterograde vesicles transporting proteins from the *cis* to the *trans* Golgi network. Any mislocalized Golgi enzymes are retrieved to the correct cisternae by retrograde (backward) transport vesicles. Alternatively, the cisternal maturation model suggests that cisternae form by the fusion of vesicles containing proteins from the ER, which then moves itself in an anterograde direction (as depicted in Figure 1.1). The content of the cisternae changes or matures via retrograde transport vesicles that deliver Golgi enzymes back to newly formed *cis* cisterna. A third model described by Patterson *et al* (2008) [3], suggests that proteins are rapidly partitioned into either processing or export domains of individual cisternae. Although the exact process of protein traffic through the Golgi is still under debate, several studies have shown evidence for cisternal maturation using fluorescent microscopy techniques. For example, Rizzo *et al* (2013) modified a *cis*-Golgi resident enzyme so that it could be reversibly polymerized, and monitored its location within the Golgi using electron microscopy. When in monomer form, it was found in vesicles and localised between *cis* and *trans* Golgi markers. In agreement with the cisternal maturation model, after polymerization, which would prevent entry into vesicles, the enzyme then co-localised with *trans* Golgi markers [4]. Importantly, in all models the retrograde traffic of vesicles is required for the maintenance of correct enzyme distribution throughout the Golgi.

1.1.2 Retrograde vesicle traffic

The mechanism by which retrograde vesicles form, tether, bind, and then fuse to target cisternae involves a myriad of proteins. The exact mechanism of retrograde vesicle transport in the Golgi, especially how cargo is targeted to its specific destination, is still under investigation. The process is similar to other cellular vesicle trafficking events but uses Golgi specific coat proteins, Rabs, tethers and SNAREs. To begin with during vesicle budding, Arf1, a small GTPase, is recruited to the Golgi membrane. GTPases are a group

of GTP binding proteins found throughout the cell. They act as molecular switches, interchanging between inactive (GDP-bound) and active (GTP-bound) forms. At the Golgi, Arf1 recruits cargo from inside the Golgi and a vesicle coat protein from outside [5]. Coatomer protein complex-I (COPI) is a known coat protein involved in Golgi vesicle transport, as it is present on Golgi vesicles and at the rims of Golgi cisternae [6]. COPI polymerizes in order to bend the membrane and form a vesicle. As in other vesicle transport pathways in the cell, vesicle-SNARES and target-SNARES form trans-SNARE complexes that direct the fusion of vesicles with target membranes. Two different SNARE complexes have been identified at the Golgi, Syntaxin5-Ykt6-GOS28-GS15 at the *medial-trans*-Golgi, and Syntaxin5-membrin-Sec22-Bet1 at the *cis*-Golgi [7]. A gradiented distribution of the different v-SNARE and t-SNARE components of each complex influences the binding of vesicles to target membranes. Alongside SNARES several Ras-family small GTPases called Rabs, organise vesicle trafficking and transport via their interactions with downstream effectors. One group of effectors at the Golgi are golgins, which are tethering proteins responsible for engaging the vesicle. For example, Rab1 interacts with Golgin protein p115 to tether vesicles from the ER to the *cis* Golgi [8]. Different golgins interact with a different combination of Rab proteins that are expressed on vesicles carrying different cargo [9]. This selectivity also provides some specificity in intra-Golgi vesicle transport.

1.1.3 Conserved Oligomeric Golgi complex

The other major tethering factor in intra-Golgi retrograde transport is a multisubunit tethering complex called the Conserved Oligomeric Golgi (COG) Complex. The identification of COG began with the discovery of two mutant Chinese hamster ovary (CHO) cell lines that had poor low-density lipoprotein (LDL) uptake, named ldlB and ldlC [10]. The cause for poor LDL uptake was found to be low levels of LDL-receptor, due to rapid turnover at the plasma membrane. The rapid turnover of LDL-receptor was linked to poor Golgi associated glycosylation [11]. Simultaneous biochemical, yeast and CHO cell experiments, identified proteins which were later proved to be part of the same 8 subunit COG complex [12]. Further to this, electron microscopy of COG purified from bovine brain showed a bi-lobe structure. Together with studies on yeast homologue subunits, this identified the distribution of subunits, with lobe A containing subunits 1-4 and lobe B containing subunits 5-8 (Figure 1.2) [12, 13].

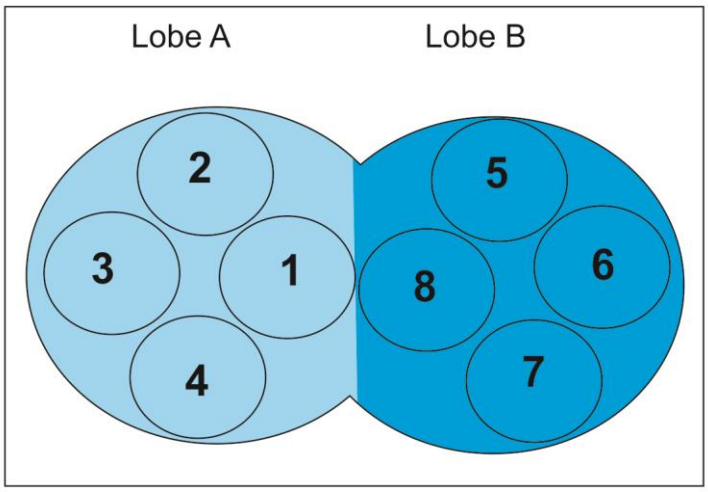

Figure 1.2 Structure of the Conserved Oligomeric Golgi Complex (COG)

Diagram depicting the distribution of subunits within COG. The bi-lobe structure was previously identified by electron microscopy. The distribution of subunits within the two lobes was previously determined in part through co-purification and in part, due to the similarity of the severity of mutations to subunits in the same lobe, in yeast.

The distribution of subunits shown in (Figure 1.2) was supported by the difference in severity of phenotypes in yeast when units from different lobes were mutated. Mutations to subunits in lobe A in yeast were lethal, whilst, mutations to subunits in lobe B lead to more mild phenotypes [13]. The vesicle transport role of COG was first indicated by the glycosylation defects observed in the COG CHO cell mutants, which had reduced *N*- and O-glycan sialylation, which is a predicted consequence of mislocalized Golgi resident enzymes [11]. Furthermore, the intra-Golgi transport in a cell free assay model was inhibited when antibodies against a COG subunit were used [14]. Measurements of vesicle transport at the Golgi using another cell free assay were also reduced when cytosol from patients with mutations in COG were used in the assay [15]. These *in vitro* experiments supported the notion that COG is an essential factor in vesicle traffic at the Golgi. Experiments in which Cog3 was knocked down using siRNA in HeLa cells, demonstrated that COG is a tethering factor of retrograde vesicles at the Golgi. Cog3 knock-down HeLa cells accumulated vesicles, which could be washed away from Golgi cisternae, showing that they were un-tethered. Furthermore, anterograde traffic of vesicular stomatitis virus G protein (VSVG) was not impaired; however, retrograde traffic

of Shiga toxin was impaired in the Cog3p knock-down cells [16]. Further evidence for COG's role in retrograde vesicle traffic is the interaction of different COG subunits with various Rabs, golgins, SNAREs, the SM protein Sly1 as well as with the COPI coat [17]. Through these interactions and functional studies, COG has been proposed to initiate docking of vesicles, support SNARE complex formation and vesicle fusion. Specificity of retrograde vesicle transport may be derived from the combinations of Rabs, golgins, COG subunits, and SNARE interactions that occur at different vesicle-cisternae sites.

1.1.3.1 Function of COG and COG subunits

The complete content of the retrograde vesicles, which COG tethers is still under investigation. Both models of protein transport through the Golgi, suggest that retrograde vesicles contain Golgi resident enzymes that need to be recovered to an earlier cisternae in order to maintain their distinct distribution between cisternae. The purpose of these enzymes is to modify glycan structures, which are attached to nearly every cell surface or secreted protein. There are several different types of glycan structure, which are described in the section below. In brief, glycans can be attached to lipids or proteins, and consist of short branched chains of oligosaccharides, or be large extended structures as in proteoglycans, which considerably add to the total molecular weight of the protein. COG through its vesicle tethering, may maintain the synthesis of numerous different types of glycan structures, which if abnormal can have consequences for protein function and following this have physiological effects.

Mutations to COG in cell lines such as CHOs mentioned earlier, had no effect on growth, but did perturb LDL uptake. In larger model organisms defects in COG have greater physiological effects, reflecting the difference in glycan sensitivity between simple cell lines and whole organisms. In *C.elegans* mutations to Cog1 resulted in reduced fucosylation of *N*-glycans, affecting the function of Mig17, a protein involved in gonadogenesis [18]. In *D. melanogaster,* deletion of the Cog5 homologue results in male fly sterility, with Cog5 indirectly affecting spermatogenesis, likely dependant on correct intracellular remodelling and key glycoproteins [19].

The yeast studies involved in identifying COG's bi-lobed structure, identified that mutations to subunits in lobe A were lethal, whilst mutations to lobe B subunits caused a milder phenotype with just reduce growth rates [13]. This lead to investigations in to whether the different individual subunits of COG, have different cellular functions.

Protein association studies of COG subunits with Golgi associated Rabs, SNAREs and golgins suggest different interaction hubs between different subunits, which could indicate separate functions of the lobes of COG. For example, Cog2 interacted with all golgins tested, but not with any Rabs or SNAREs indicating it could be a golgins hub, whilst through selective interactions with Rabs, Cog4 and Cog5 could be a Rab hub [17]. Cell lines and even patients with mutations in different COG subunits show different phenotypes and symptoms – although the variability among patients may be down to difference in the severity of the mutation. Cog5 loss in HeLa cells results in much more mild phenotype compared Cog1 or Cog2 mutations in CHO cells, with no effect on LDLR turnover in the Cog5 mutated HeLa cells [20]. Furthermore, studies monitoring the localization of specific *N*-glycan processing enzymes in cell lines with mutations to either lobe A or lobe B COG subunits, have shown that lobe A units are essential for correct Golgi architecture overall as well as *cis*/*medial* Golgi enzyme maintenance, whilst lobe B subunits contribute to the maintenance of *trans* Golgi enzyme trafficking [21, 22]. Importantly, mutation of any COG subunit has been shown to alter protein glycosylation to some degree and so is a valid target to perturb cellular glycosylation.

The main function of the Golgi is protein sorting and protein modification, such as glycosylation, prior to secretion. The next section will introduce types of glycosylation and explain how disruption of glycan synthesis, via COG mutations for example, can have physiological effects.

1.2 Glycosylation

Glycosylation involves the attachment of single sugars /monosaccharides or oligosaccharide chains to proteins or lipids and it is the most abundant post-translational modification. Nearly all cell surface proteins are glycosylated and it can double the predicted molecular weight of a protein. Therefore a cell's surface can be described as a forest of glycans, which can have many effects on a cell's behaviour and function. There are many different types of glycans that are processed in the ER and Golgi (Figure 1.3). The form of attachment can be broadly used to classify the different types of glycans, however, it is important to note that a single protein may have multiple types of glycan modifications and fluctuations in abundance of sugar donors or substrates may affect the synthesis of multiple glycan structures.

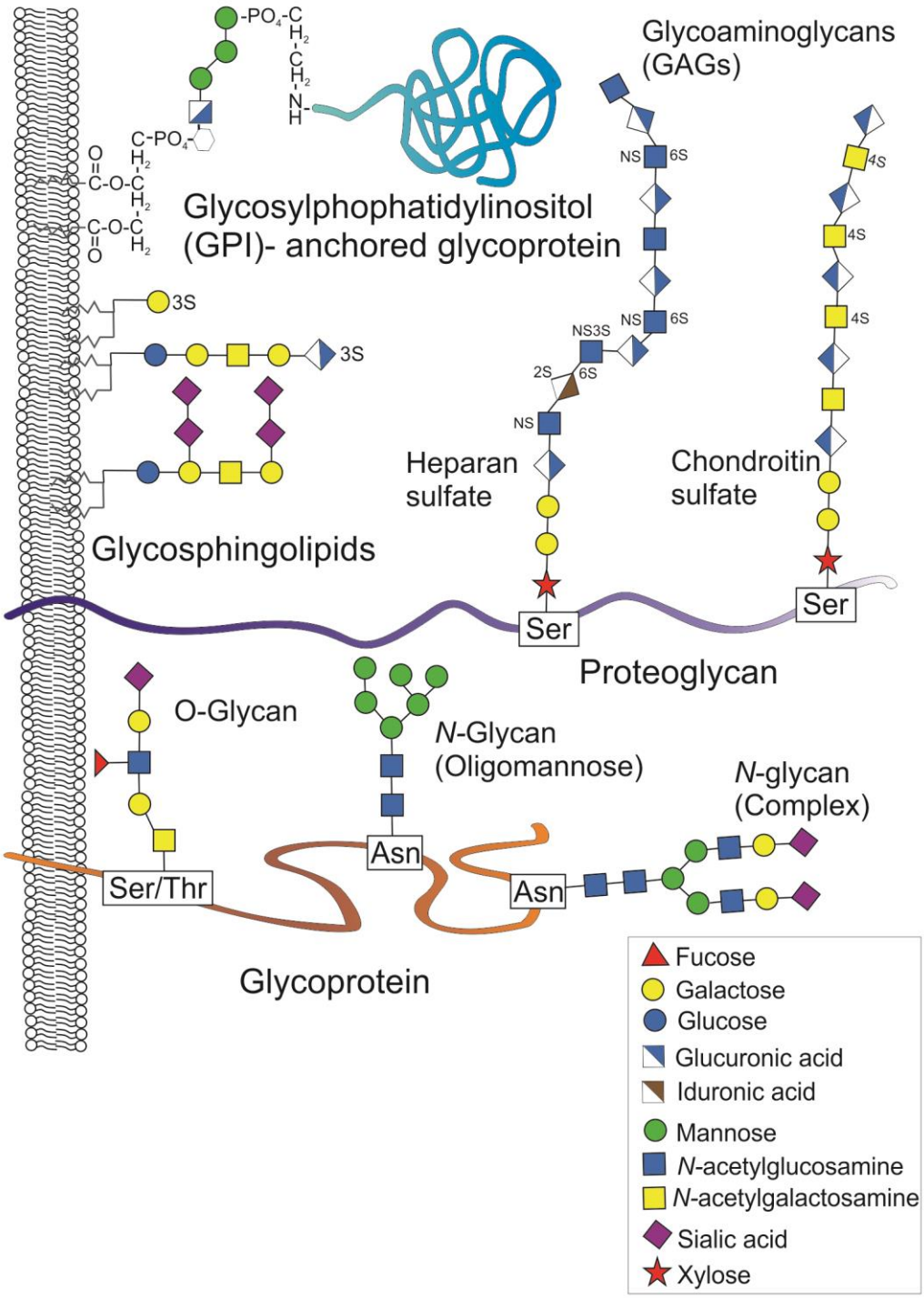

Figure 1.3 The diversity of glycans

Examples of the common types of glycans found on mammalian cells (not to scale). The structures shown are examples from a wide variety of structures that can be produced. Other less common glycan linkages to proteins also exist, such as O-fucose. A glycolipid often refers to a GPI anchored protein or a glycosphingolipid. A proteoglycan refers to a protein with glycoaminoglycan (GAGs) chains attached. Whilst a glycoprotein is a term used for proteins with *N*-or/and O-glycans attached. In reality a protein may have a mixture of different types of glycans attached to it. The types of glycosylation described above occur in the ER and Golgi, which is typical of membrane bound or extracellular proteins.

Adapted from: Varki A, Cummings RD, Esko JD, et al., editors. Essentials of Glycobiology. 2nd edition. Cold Spring Harbor (NY): Cold Spring Harbor Laboratory Press; 2009.

1.2.1 Glycolipids

Glycolipids are glycan structures attached to lipid moieties. The most common type is glycosphingolipids (GSL), which contain a glycan structure linked to a ceramide backbone by a β-glycosidic bond. The synthesis of GSL starts at the ER with the formation of the ceramide, following this, the synthesis pathway then branches; either the ceramide is galactosylated in the ER to form GalCer; or it is trafficked to the Golgi where it is glucosylated to form GlcCer. These two precursor GSLs are then extended in the Golgi by the step-wise addition of other monosaccharides. GSL can contain small linear glycan structures, or larger branched, sialylated structures. Some of the precursor structures are substrates for multiple glycotransferases, resulting in competition between the different enzymes. A running theme for all glycans, is that contributing to the final glycan structure, is the presence and abundance of different Golgi resident glycotransferases and donor sugars throughout the different Golgi cisternae. Since the ceramide can vary in chain length and saturation, and there is a wealth of potential glycan structures that can be attached, there is a large heterogeneity of possible GSL structures. GSL are transported from the Golgi to the plasma membrane where they cluster in "lipid rafts". Through this clustering GSL are thought to have a greater binding affinity for interacting proteins, which affects cell-cell interactions and the signalling of lipid-raft host proteins, such as the insulin receptor [23]. Inhibition of GSL synthesis at a cellular level *in vitro* has no effect on growth, however, the inhibition of GlcCer synthesis *in vivo* is embryonic lethal [24], showing a requirement of GSL in whole organism development. GalCer is the most abundant glycan in the brain and is produced by oligodendrocytes as a component of myelin sheaths. Through different knock-out mouse studies, phenotypes suggest that GSLs that are extended from GlcCer play roles in supporting neuronal development and function [25]. Although there aren't well known diseases of GSL synthesis, there are several well studied diseases of GSL degradation. Tay-Sachs and Gaucher's disease are both lysosomal storage disorders caused by errors in GSL catabolism, due to mutations in lysosomal enzymes that would normally degrade GSL into its subunits.

Alternative types of glycans, introduced below, share the GSL synthesis pathway and some of its glycotransferases. It is therefore possible that diseases that are associated with alterations in other types of glycans, described in each glycan section, also affect GSL synthesis and vice versa.

1.2.2 Glycosylphosphatidylinositol (GPI) - anchored glycoproteins

Another type of glycolipid are glycosylphosphatidylinositol(GPI)-anchored glycoproteins. Here a protein is attached to an ethanolamine phosphate that is linked to a glycan bridge. The glycan bridge contains 3 mannose (Man) and 1 glucosamine that is attached to a phosphatidylinositol(PI) group, which is anchored to the cell surface lipid bi-layer. This core structure (EtNP-6Manα1-2Manα1-6Manα1-4GlcNα1-6(PI)) is common to all GPI anchored proteins, however variation exists in terms of lipid substituents and the structure of additional glycan structures attached to the core structure [26]. The synthesis of the common core structure occurs at the ER, to start with on the cytoplasmic face and then onwards from the synthesis of the glycan bridge, in the lumen of the ER. The multi-subunit complex GPI transamidase transfers the preassembled GPI precursor onto the protein in the ER. The attachment occurs at a carboxy terminal GPI addition signal peptide, which contains 3 amino acids, followed by a polar domain of 5 residues, followed by a hydrophobic domain of 15-20 hydrophobic amino acids. Following the transfer of the protein onto the GPI anchor, lipid remodelling and addition of glycan side-chains to the glycan bridge occurs in the ER and Golgi.

One of the first GPI anchored glycoproteins identified was the variant surface glycoprotein (VSG) expressed by *T. brucei*, a parasite that causes sleeping sickness. Each trypanosome has $1x10^7$ GPI linked VSG molecules on its surface, in order to protect against complement mediated lysis. Although not essential for mammalian cell culture, GPI anchor synthesis has been shown to be essential for embryonic development in mice [27]. Relevant to this research, the enzyme alkaline phosphatase (ALP), which is highly expressed in bone tissue, has a GPI-anchor [28]. One disease caused by mutations in genes responsible for GPI-anchor synthesis is Hyperphosphatasia with Mental Retardation Syndrome (HMRS). Symptoms include, elevated serum ALP levels, hypotonia, neurological features such as seizures and intellectual disability [29]. Another disease caused by mutations to GPI-anchor synthesis genes is Paroxysmal nocturnal hemoglobinuria (PNH). The main symptom of PNH is haemolytic anaemia that is caused by a sequence of events starting with the somatic mutation of *PIGA*, which is a X linked gene that produces an enzyme involved in the first steps of GPI-anchor synthesis. Hematopoietic stem cells (HSCs) that gain mutations in *PIGA* produce erythrocytes that lack several GPI-anchored proteins, including CD55 and CD59. The absence of these protein leads to complement activation lysis of erythrocytes [30]. The continued survival of the mutated HSCs is

thought to be due to increased mobility, due to decreased binding of other GPI-anchor proteins to adhesion molecules at the HSC niche [31]. As genome sequencing technologies become more widely available, patients with mutations to other GPI-anchor synthesis genes are likely to be identified, and knowledge of the molecular roles of GPI-anchored glycoproteins will expand.

1.2.3 Proteoglycans

Proteoglycans are a diverse group of glycan modified proteins, which in general have chains of oligosaccharides attached to a glycan linker structure that is attached to a serine residue of a "core protein". The chains of oligosaccharides called glycoaminoglycans (GAGs) are made of repeating disaccharide units containing an amino sugar and an uronic acid or galactose. Several common GAGs are described in the chart below. The cellular location of proteoglycans varies, some are secreted into the extracellular matrix (ECM), some stored in intracellular granules, and others are inserted into the plasma membrane. Hyaluronan is an unusual GAG because it is secreted into the ECM without being covalently bound to a protein. As with other glycan types, proteoglycans are heterogeneous, for example the GAGs attached can vary in their epimerisation and sulfation pattern. Furthermore, the number of GAGs attached to a proteoglycan can vary from 1-100, with each chain potentially containing 80 oligosaccharides [32].

GAG	Disaccharide composition	Sulfation positions	Protein linkage
Chondroitin sulphate (CS)	N-acetylgalactosamine (GalNAc) – Glucuronic acid (GlcA)	4-O or 6-O sulfation of GalNAc	GluA-Gal-Gal-Xyl
Dermatan sulphate (DS)	N-acetylgalactosamine – Glucuronic/Iduronic acid (IdoA)	4-O or 6-O sulfation of GalNAc and 2-O sulfation of IdoA	GluA-Gal-Gal-Xyl
Heparan sulphate (HS)	N-acetylglucosamine (GlcNAc) – Glucuronic/Iduronic acid	6-O or N-position sulfation of GlcNAc and	GluA-Gal-Gal-Xyl

		2-O sulfation of IdoA	
Keratan sulphate (KS)	N-acetylglucosamine – Galactose	6-O sulfation of GlcNAc and 6-O sulfation of Galactose	*N*- or O-glycans
Hyaluronan (HA)	N-acetylglucosamine – Glucuronic acid	None	None

The glycan linker structure that attaches the GAG to the core protein is the same for all protein bound GAGs, apart from keratin sulphate. The common glycan linker structure is a tetrasaccharide formed by the sequential addition of xylose, two galactose units and a glucosamine. Xylosylation has been shown to occur in the ER and Golgi and does so without an apparent consensus site, preventing the prediction of GAG attachment sites to proteins [33, 34]. In the Golgi the addition of either β1-4 N-acetylgalactosamine or α1- N-acetylglucosamine initiates the formation of the repeating disaccharide chain that polymerizes into either chondroitin sulphate or dermatan sulphate, or, heparan sulphate GAGs respectively. As mentioned above keratin sulphate (KS) is a different type of GAG comprised of a sulphated poly-N-acetyllactosamine chain. Instead of a xylose linker structure, KS is found within *N*-or O-glycan structures (introduced later).

1.2.3.1 Function of Proteoglycans

Proteoglycans are found in nearly all tissues of the body and are the major component of ECM. The GAG sulphation makes the chains negatively charged that attracts Na^+ ions, which in turn increases the hydrophilic properties of the GAGs. In connective tissues such as cartilage, the GAGs in the extracellular matrix form a porous gel that provides supportive structure to the cells imbedded in it, and is capable of withstanding compressive forces. Other than acting as a hydrated-spacing agent in between cells, GAGs and proteoglycans can interact with proteins to influence cell signalling. For example, fibroblast growth factors bind to proteoglycans, which results in downstream signalling events leading to cell growth and proliferation [35]. The density of GAGs in the ECM can influence the mobility of signalling proteins and nutrients, thereby affecting the resident

cells' behaviour [36]. One of the earliest studied GAGs is heparin, which is a highly sulphated form of HS that is secreted in granules by mast cells. Due to its ability to bind to antithrombin, heparin is purified commercially and used as an anticoagulant. Proteoglycans are a major component of bone tissue and vary in their structure and function. Small leucine-rich repeat proteoglycans are abundant in bone matrix and influence mineralization through binding to collagen fibres, organising the ECM structure, and by interacting with growth factors regulating the activity and differentiation of osteoblasts [37]. Larger secreted proteoglycans such as aggrecan and membrane bound proteoglycans such as syndecan-3 are also present in bone tissue and affect bone development and structure. Due to the variety and abundance of proteoglycans in bone tissue, it is not surprising that mice in which different proteoglycans are knocked out show a variety of bone and cartilage symptoms, from dwarfism to osteoporosis [37].

In humans, Hereditary Multiple Exostoses (HME) is an autosomal dominant disease associated with cartilage/bony outgrowths called exostoses that form adjacent to the growth plate of long bones, ribs and pelvis. The exostoses protrude into neighbouring tissues causing pain and hinder the mobility of the limb affected. Patients undergo surgery to remove the exostoses, which don't reform after puberty, when the growth plate closes [38]. The genetic cause of HME in most cases is mutations in the genes EXT1 or EXT2, which encode for the glycosyltransferases responsible for HS chain elongation. *In vitro* studies have shown that knock-down of EXT1 or EXT2 results in shorter HS chains, and a combination of overexpression studies lead to the speculation that EXT1 and EXT2 form a complex, in which EXT1 is responsible for the enzymatic action, and EXT2 is a chaperone for EXT1 into the Golgi [39]. The mechanism by which shorter HS chain formation leads to exostoses formation is still under investigation, the basic reasoning is that shorter HS chains leads to impaired cell signalling, as growth factor gradients and signalling molecule interactions are no longer initiated by the shorter HS chains. Indian Hedgehog, Wnt and BMP signalling, which are all required for correct skeletogenesis, have been shown to be modulated by HS [40-42]. These interactions are likely reduced or absent in HME which leads to the altered growth plate development, showing that small changes to glycan formation can have developmental effects [40].

1.2.4 O-glycans

Proteins that have glycans attached to serine or threonine residues via an O-glycosidic bond are called O-glycans. There are less common types of O-glycans such as O-fucose and O-mannose, but here, O-glycans shall refer to the most common type - O-GalNAc – which starts with the addition of an N-acetylgalactosamine (GalNAc) to a hydroxyl group of a serine or threonine residue. In the Golgi, chains or branches are then elongated by the sequential addition of monosaccharides. There are 8 different O-glycan core structures (Figure 1.4), which can contain antigenic groups and be elongated by several branches of polysaccharides. Proteins that have clusters of O-glycans are known as mucins and are commonly found in mucous secretions in the body. The clustering of O-glycans occurs on mucins due to protein regions abundant in serine or threonine, called variable tandem repeat regions. In humans, the addition of the initial GalNAc is carried out by one of 24 different GalNAc-transferases, which are located throughout the Golgi [43]. Some GalNAc-transferases have carbohydrate-binding domains, and so the presence of nearby GalNAc units promotes the transfer of another, contributing towards the formation of densely O-glycosylated mucins. As with other types of glycans, O-glycosylation is heterogeneous with a large number of possible glycan structures and variety in potential site occupation. Mucin proteins may have 100 O-glycans attached, but there are proteins that are modified by just 1 O-glycan structure.

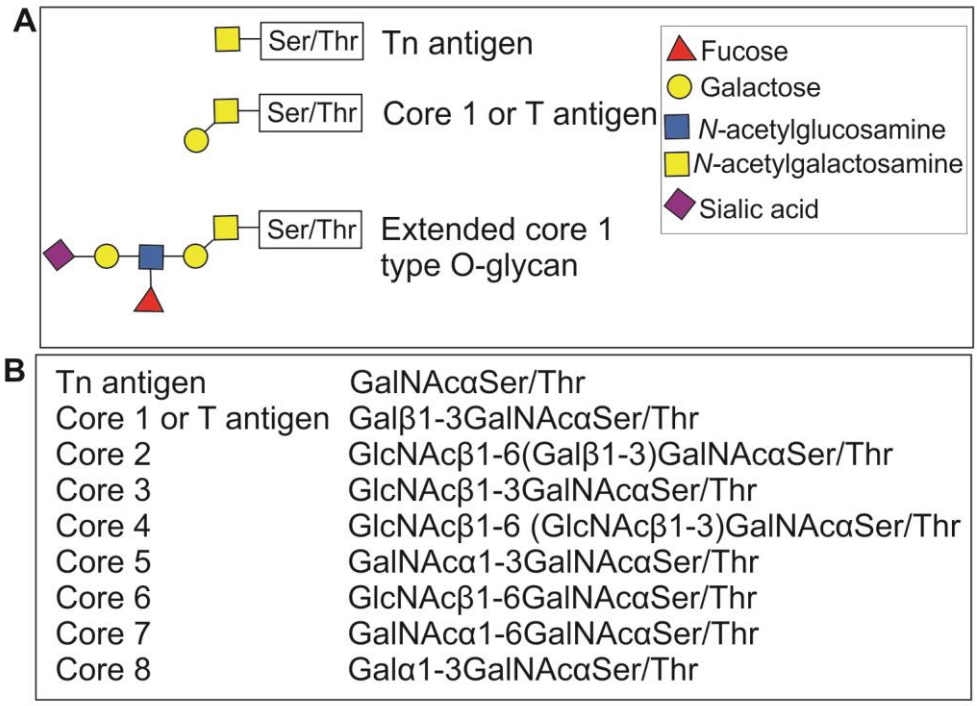

Figure 1.4 O-glycan structures

A) Diagram showing structure of Tn and T antigen, as well as an example of an extended core 1 type O-glycan. B) Structures of the 8 known O-glycan cores.

1.2.4.1 Function of O-glycans

As already mentioned O-glycosylated proteins are abundant in mucous secretions of the body. Similar to the GAG chains, the O-glycans are negatively charged and can attract water to form gels or mucous, which protects the tissues and traps pathogens. O-glycosylated proteins can span the membrane and act in signal transduction. The expression of O-glycan structures changes during cancer affecting the ability of cells to bind to lectins expressed on epithelial cells [44]. Small changes to the O-glycosylation of MUC1, a mucin transmembrane protein overexpressed in breast cancer, causes altered EGF, MAPK and Wnt signalling that favours tumour growth [45]. Human diseases associated with O-glycan synthesis have mostly been overlooked or understudied as many of the patients suffer from *N*-glycosylation defects as well, due to shared synthesis localization and some common synthesis components. One disease that occurs due to mutations in an O-glycan exclusive protein is familial tumoral calcinosis (FTC). Here, mutations to GalNAc-transferase3, one of the enzymes responsible for initiating O-glycan synthesis, affects FGF23 activity, mutations of which can also cause the disease as it regulates phosphate levels in the blood [46]. Patients have calcium deposits in skin and

subcutaneous tissues. Deposits can be asymptomatic, being identified after unrelated scans, or can grow quite large and restrict movement of joints and cause pain. Altered O-glycosylation has been identified in breast cancer samples. The symptoms of patients with defects in enzymes shared between O- and *N*-glycosylation pathways will be described after the introduction of *N*-glycosylation synthesis below.

1.2.5 *N*-glycans

Finally, *N*-glycans are also attached to protein residues but have different structures and are synthesized differently to O-glycans, as described in more detail below. A glycoprotein can refer to a protein with either *N*- or O-glycans, however, glycoproteins can have a mixture of the glycan modifications mentioned above. Importantly, most secreted and membrane proteins are *N*-glycosylated, explaining why it has been estimated that two thirds of all proteins (identified in the SWISS-PROT database) are *N*-glycosylated [47]. The abundance of this modification on secreted and plasma membrane proteins indicates how important *N*-glycosylation is to cellular processes.

1.2.5.1 *N*-glycan synthesis

N-glycosylation occurs in the ER and Golgi. During translation the protein is translocated into the lumen of the ER and the oligosaccharyl transferase (OST) complex recognises the *N*-glycosylation consensus site - Asn-X-Ser/Thr – (in which X cannot be Pro) and attaches a pre-formed 14 unit oligosaccharide, made up of a 2 N-acetylglucosamine (GlcNAc) unit base, a 9 mannose unit core, with 3 glucose units attached at the terminal end of one branch ($Glu_3Man_9GlcNAc_2$) [48]. The glucose residues are removed in the ER prior to the glycoprotein being transported to the Golgi, with the $Man_9GlcNAc_2$ precursor glycan attached. Here the precursor glycan is modified by sequential removal and addition of sugars by a variety of glycosidases and glycosyltransferases that are present at varying levels in the *cis*, *medial* and *trans* Golgi cisternae (Figure 1.5a). Again, which enzymes the glycoprotein encounters and when during its transport through the Golgi network, influences the form of the final glycan structure. The structure of the protein itself will also influence enzyme binding and the final glycan structure, which enables a cell to produce different glycoproteins with different glycan structures, using the same Golgi network. There is a vast variety of different glycan structures that can be produced. Glycans can have various numbers of branches, with different degrees of fucosylation and

a variety of terminal monosaccharides at the end of branches. Broadly, *N*-glycan structures can be grouped into 3 different types; 1) oligomannose that have terminal mannose sugars; 2) complex that have branches starting with an GlcNAc attached to the mannose core, which can be followed by galactose and then terminal sialic acid residues; or 3) hybrid that are a combination of the other two (Figure 1.5b). As with other types of glycan modifications, the presence of an *N*-glycan consensus site doesn't always result in the addition of a glycan. Some sites are always glycosylated whilst others are variably occupied. Added to this, the final glycan structure at the same site, on the same protein, can vary. For example a standard glycoprotein RnaseB has just one *N*-glycan site, yet 5 different *N*-glycan structures can be isolated from a sample of RnaseB (Figure 1.5c). The key points of *N*-glycan synthesis, which are common to all types of glycan synthesis, are that the process is a step-wise, enzymatic reaction. Also, glycan structure is dependent on the glycoprotein itself, the presence of sugar donors, and the presence/competition of specific glycosyltransferases during transport through the Golgi.

Despite most secreted and plasma membrane proteins being modified by *N*-glycans, the extent that *N*-glycans influence specific protein function remains unknown for most glycoproteins. The next sections will describe the known roles of *N* -glycans in regulating protein folding, cellular processes, and development.

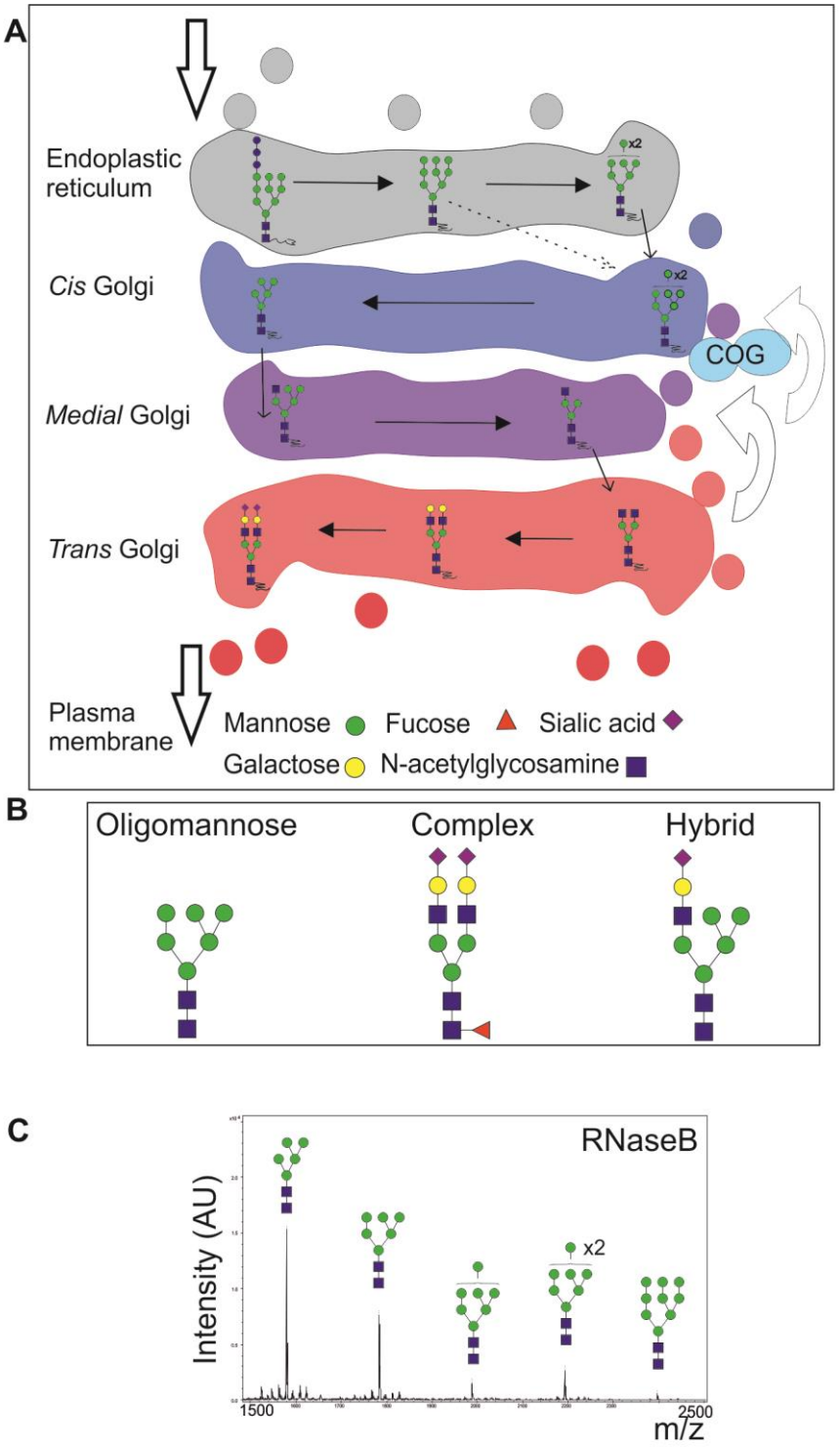

Figure 1.5 *N*-glycan synthesis and heterogeneity

A) Schematic of *N*-glycan synthesis in the ER and Golgi. For simplicity only one final *N*-glycan structure is shown in the trans Golgi. Black arrows indicate action of glycosidases and glycotransferases. B) Examples of the three classes of *N*-glycan structures. C) Mass spectrometry spectrum of *N*-glycans isolated from RNaseB. Peaks are annotated with predicted glycan structures based on the calculated mass of monosaccharide units and knowledge of the synthesis pathway. Spectrum shown covers 1500m/z to 2500m/z.

1.3 Biological functions of glycans

1.3.1 Protein folding

N-glycans are known to impact glycoprotein folding prior to exit from the ER. This is accomplished by two protein chaperones that are lectins called, calnexin and calreticulin. In the ER the chaperones selectively bind to a partially trimmed monoglucosylated *N*-glycan core structure on a glycoprotein. Following this, the two enzymes act in concert, one that trims the final glucose releasing the glycoprotein from the chaperones. The other enzyme binds only to unfolded glycoproteins and then attaches a terminal glucose, resulting in re-binding with the chaperones or eventual degradation of any unfolded protein [49]. This mechanism regulates the passage of proteins from the ER to the Golgi, ensuring only folded proteins traffic to the Golgi.

1.3.2 Protein and cellular function

As well as a role in regulating protein folding in the ER, *N*-glycans have been shown to influence protein function, thereby affecting multiple cellular processes. Since most cell surface proteins are *N*-glycosylated the first point of contact for a cell is its coat of glycans. It follows then, that *N*-glycans and lectins are involved in processes in the immune system and in immune system evasion. For example, the binding of influenza virus to host cells is glycan dependant [50]. Many studies have shown cancer cells to have altered *N*-glycosylation. Linking altered *N*-glycosylation and the increased migratory behaviour of cancer cells, a study showed integrin-fibronectin binding was dependant on correct *N*-glycosylation [51]. As well as lectin-glycan interactions, *N*-glycans have been shown to affect the function of the glycoprotein itself. For example, the presence of a core fucosylated *N*-glycan on epidermal growth factor receptor (EGFR) is required for epidermal growth factor simulated phosphorylation of EGFR [52]. Interestingly, Rabinovich *et al* (2007) described how formation of galectin lattices can reduce receptor turnover, thereby potentially influencing multiple cell signalling pathways [53]. Although there are many examples of functional *N*-glycans there are also glycoproteins whose function appears un-altered in the absence or modification of glycans. The effect of many *N*-glycans on their glycoprotein function is currently unknown. Clearly there are *N*-glycans that play a role in cellular function and in the next sections the known roles of *N*-glycans in development and human disease will be introduced.

1.3.3 *N*-glycans in development

Initial studies into the importance of *N*-glycans involved the mutation of different enzymes in the *N*-glycan synthesis pathway, using classic biological models such as mice and Arabidopsis. Metzler *et al* (1994), created mice which lacked UDP-N-acetylglucosamine: alpha-3-D-mannoside beta-1,2-N-acetylglucosaminyltransferase I (GlcNAc-TI). This enzyme initiates complex glycan branching in the *medial* Golgi, by the addition of GlcNAc to the core $Man_5GlcNAc_2$ structure. Demonstrating the importance of complex *N*-glycans, the knock-out mice died during embryonic development by day 10.5. Already at day 9, embryos had severe symptoms including reduced vascularization, impaired neural tube formation and altered left-right body asymmetry [54]. Using Arabidopsis, Boisson *et al* (2001) found that glucosidase I knock-out caused seeds to fail to develop, showing that *N*-glycans are important in plant as well as mammalian development [55].

The role of *N*-glycans in human development starts with fertilization. The sperm cell has a thick glycan coating called glycocalyx, which affects its ability to interact with epithelium during transport to the oocyte. The oocyte has its own specialized glycan-extracellular matrix coating called zona pellucida, which interacts with lectins on the sperm cell membrane, affects cell binding, and ultimately fertilization [56].

Alongside *in vivo* mouse studies, the role of *N*-glycans in human development can in part be elucidated by observing patients that have mutations in genes encoding proteins involved in the *N*-glycan synthesis pathway.

1.3.4 Congenital disorders of glycosylation

Congenital disorders of glycosylation (CDGs) are a fast expanding group of autosomal recessive diseases. Genes that code for proteins involved in any of the different glycan synthesis or processing pathways are estimated to make up 2% of the human genome [57]. Since 2000 an increasing number of patients have been diagnosed with CDG due to mutations in genes responsible for different steps of glycan synthesis and processing [58]. The increase in diagnosis is in part due to new diagnostic tools as well as increased awareness of CDGs, which can be difficult to identify due to multiple body-systems being affected and the variability of symptoms between patients. For example, patients can suffer a wide variety of impaired developmental symptoms including mild motor defects, dysmorphic face, hypotonia, frequent infections, epilepsy, neurological defects, or multi-

system failures resulting in death a few weeks after birth [59]. The standard diagnostic test for CDG is analysis of a serum glycoprotein called transferrin. Transferrin has two *N*-glycosylation sites that are normally both occupied by complex, biantennary *N*-glycans. Transferrin from a patient that is not glycosylated at all, points to a mutation in a gene involved in *N*-glycan precursor synthesis or transfer of the *N*-glycan to the protein. Alternatively, transferrin from a patient that has structurally altered *N*-glycans, points towards genes involved in *N*-glycan processing. The ease of this diagnostic test, which identifies *N*-glycosylation pathway related mutations, probably contributes towards why more patients have been diagnosed with defects in *N*-glycan synthesis, compared to others such as O-glycan and proteoglycan synthesis. In 2003, Wopereis *et al* developed a molecular test for aberrant O-glycan synthesis [60]. It involved the isoelectric focusing of a serum protein called Apolipoprotein C III (ApoCIII), which is normally modified by one O-glycan, and has 3 isoforms that correspond to varying O-glycan length and sialylation. Using this test Wopereis *et al* (2003) identified a CDG patient with a mutation in an unknown *N*-glycan processing gene that also had reduced O-glycan sialylation [60]. This test enables the identification of O-glycan mutations in other suspected CDG cases that show normal transferrin results, despite CDG symptoms.

The most common CDG with over 500 patients world-wide is PMM2-CDG (previously known as CDG1a) [59]. Here, phosphomannomutase is deficient, which is an enzyme that generates mannose 1-P, a sugar unit used to make GDP-mannose, used for building the precursor oligosaccharide. Symptoms include inverted nipples, abnormal subcutaneous fat pads, hypotonia and a mortality rate of 20% in the first year. Despite a high carrier frequency of 1/70 in Europe for one mutation in PMM2, there are currently no incidences of homozygotes for that particular mutation, indicating that it is lethal in the homozygous state. Trials using mannose supplements as a treatment proved unsuccessful for PMM2-CDG patients despite relieving symptoms in PMI-CDG patients, which have mutations in the gene upstream of PMM2 in the GDP-mannose biosynthesis pathway [59, 61]. Apart from mannose and fucose therapies for the PMI-CDG and GDP-fucose transporter deficiencies, all of the treatments for CDGs are aimed at managing the symptoms rather than treating the molecular cause of the disease.

1.3.4.1 COG related CDGs

Since 2004, a small number of CDG patients have been found to have mutations in subunits of COG. The first to be identified were two patients (siblings) who had mutations in Cog7 [62]. Since then patients with mutations in subunits 1, 2, 4, 5, 6, and 8 have also been identified [63-68]. Patients have reduced *N*-and O-glycan sialylation, shown using transferrin and ApoCIII isoelectric-focussing, lectin staining, mass spectrometry, or a combination of these techniques. Patient symptoms are similar to other CDG patients and vary dramatically, from the mildest (CDG-Cog5) involving mild neurological impairments to the much more severe (CDG-Cog7), involving growth retardation, microcephaly, epilepsy, feeding problems, body dysmorphia, hypothermia and death before 3 months of age (Table 1).

Since *N*-glycans are on nearly every cell surface it is unsurprising that CDG patients suffer a wide variety of symptoms, affecting nearly every system in the body. Although these diseases provide useful evidence that glycans are physiologically important, it is difficult to elucidate a molecular link between altered *N*-glycans and a specific developmental symptom. The differentiation of stem cells into mature cell types is a developmental process that can be easily studied *in vitro*. Research using this type of model enables a closer look at the role of *N*-glycans in a specific process of development, without the web of interconnected systems found in whole organisms. Before describing what is currently known about the role of *N*-glycans in this process, methods used to study glycans will be introduced.

Symptoms (+ indicates occurrence of symptom documented)	Lethality in first year	Growth retardation	Psychomotor retardation	Mental retardation	Microcephaly	Hypotonia	Developmental delay	Failure to thrive	Feeding problems	Dysmorphic features	Wrinkled skin	Adducted thumbs	Cerebellar atrophy	Hypothermia	Liver dysfunction/abnormalities	Skeletal abnormalities	Epilepsy/Seizures	Cardiac dysfunction	Anti-mongoloid eyelids	Hypocupremia (bone marrow deficiency)	Intracranial bleeding	Frequent infections	Vitamin K deficiency	Intolerance to wheat and dairy	Encephalopathy	PFAPA syndrome	Coagulation problems
Cog1 [63]		+	+		+	+		+	+				+			+		+	+								
Cog2 [64]			+		++		+						+		+		+			+							
Cog4 [65]			+	+	+	+				+			+			+	+					+					
Cog5 [69]				+		+							+														
Cog6 [66]	+																++				++		+				
Cog7 [62, 70]	++	+			++	+	+	+	+	+	+	+		+	+	+	++	+									
Cog8 [67, 68]			+	++	+	+				+			+											++	++	+	+

Table 1. Symptoms of COG related CDGs.

1.4 Methods used to study glycans

1.4.1 An introduction to lectins

Lectins are a widely used tool for studying glycans. Lectins are proteins that are capable of binding oligosaccharide structures. They were first discovered by Peter Hermann Stillmark in 1888, who isolated a compound capable of agglutinating erythrocytes, from the seeds of the castor tree (*Ricinus communis*) [71]. He named the hemagglutinin ricin, which rose to fame in 1978, after its toxic property was used in the "umbrella murder" of Georgi Markov. Following the work of Stillmark, Karl Landsteiner won the Nobel Prize for his discovery of the ABO blood groups, which had huge clinical impacts by improving the safety of blood transfusions. Blood sera from different individuals had different capabilities in agglutinating donor red blood cells, indicating specific antigens on red blood cells. Later experiments, using blood from different animals, showed varied ability of different bean extracts to agglutinate erythrocytes, suggesting specificity in binding (reviewed in [72]) . It wasn't until 1936, after the purification of concanavalin A (ConA) isolated from jack bean, which experiments showing that sucrose could inhibit ConA induced hemagglutination, indicated for the first time that agglutinins were binding to oligosaccharide structures on the surface of red blood cells [73]. Indeed following this discovery, the ABO antigens were shown to be specific sugar structures. In 1954, plant agglutinins were re-named lectins from the latin *legere,* to pick out/or choose, due to different plant agglutinins being able to distinguish between erythrocytes of different blood groups [74]. Since their discovery, hundreds of lectins have been purified, isolated from mostly plants but also from animals e.g. eel, snail and horseshoe crab.

1.4.2 Lectins as tools for glycobiology

The labelling of lectins with biotin, horseradish peroxidase (HRP) or fluorescein isothiocyanate (FITC) enables lectins to be used in the same way that antibodies are used to analyse protein expression and localization.

The relative ease of availability of lectins and their specificity to sugars independent on the underlying protein makes them variable over antibodies raised against oligosaccharide structures. However, different lectins have varied affinities for specific oligosaccharides. The binding of lectins to different oligosaccharide structures is dependent on the branching of the glycan structure, as well as the the total glycan structure in which the target sugar resides. For example, ConA binds to mannose within

N-glycan structures. It binds tightly to both the mannose within branched oligomannose glycans and to mannose branches of hybrid glycans. It binds more weakly to the core Man3 structure within all *N*-glycan structures however, binding does not occur to complex glycans that are tri- or tetraantennary. Due to this broad glycan specificity profile, the use of a panel of lectins is required to draw conclusions on the nature of glycan structure changes between samples. High-throughput lectin micro-arrays enable the comparison of binding to hundreds of lectins and can be used to elucidate specific differences between samples. A considerably cheaper, but also quantitative, alternative used in this study, is the use of multiple lectins and flow cytometry, to discern differences in glycan abundance on the cell surface of samples. Disadvantages to using lectins, includes the lack of information regarding the exact *N*-glycan structure to which the lectin is bound, i.e. ConA will bind the structures $Man_5HexNAc_2$ and $Man_9HexNAc_2$ equally. In the next section an alternative technique to lectin staining will be introduced, focussing on mass spectrometry which is relevant to this study.

1.4.3 Mass spectrometry for analysis of glycans

Similar to protein analysis, the use of analytical chemistry methods for analysis of glycans has several advantages over lectin/antibody based approaches. Importantly, detailed structural information of individual glycan species can be determined, as well as their relative abundance in a sample. If required tandem MS can be carried out to determine the exact linkage orientation in a single glycan species.

The basic process of analysing glycans by mass spectrometry involves purification of glycans from glycoproteins, glycan derivatization, followed by separation and analysis by mass spectrometry or chromatography methods. Depending on the type of glycan to be analysed, specific techniques are preferred for each step, for example O-glycans require chemical release from glycoproteins, via β-elimination method, whilst glycolipids, proteoglycans and *N*-glycans can be released enzymatically. Glycan samples are then derivatized and/or labelled in order to improve detection sensitivity by mass spectrometry or chromatography respectively.

Both matrix-assisted laser desorption/ionization mass spectrometry (MALDI-MS) and Electrospray ionization mass spectrometry (ESI-MS) are routinely used in glycan profiling. As with protein analysis by mass spectrometry, samples are ionized, and these ions are separated based on their mass-to-charge ratio, detected and represented as a spectrum.

In this study MALDI- time of flight (TOF) mass spectrometry was used, as it is regarded as one of the most sensitive methods for glycan profiling and produces spectrum in which glycan species are singly charged, so that the mass-to-charge ratio equals the predicted mass of the glycan structure, facilitating easier spectrum analysis (reviewed in [75]). Alternatively, ESI-MS is a 'soft' ionization technique and should therefore reduce the amount of in-source decay of samples. Unlike MALDI-MS as matrix is not used for ionization, spectra do not contain background matrix peaks. However, ESI-MS is considerably more labour intensive, as spectrum can contain a complex pattern of multiple charged states for each glycan species.

Earlier sections have described multiple types of glycans and some of their current known cellular functions and roles in diseases. As stated before, the study of stem cell differentiation *in vitro* is an ideal model to investigate the role of glycans in a specific process of development, without the web of interconnected systems found in whole organisms. Before describing what is currently known about the role of glycans in this process, mesenchymal stem cells and their differentiation *in vitro* and *in vivo* will be introduced.

1.5 Stem cells

Human embryonic stem cells (hESCs) are isolated from the inner cell mass of a pre-implantation embryo. These cells are capable of differentiating into every cell type in the body, apart from extra-embryonic supporting tissues such as the placenta, and are therefore called pluripotent. Later during development, and residing in tissues throughout life, there are cells capable of self-renewal and differentiation into several adult cell types. These adult stem cells are called multipotent. When tissues need to be renewed due to damage caused by injury or age, the adult stem cells divide asymmetrically in order to self-renew and provide cells that can differentiate into the required mature, functional cells for that tissue.

1.5.1 Mesenchymal stem cells

Mesenchymal stem cells or multipotent stromal cells (MSCs) are adult stem cells that act *in vivo* to differentiate into bone, fat and cartilage tissue when it is damaged or aged (Figure 1.6). In a paper by Pittenger *et al* (1999), MSCs were isolated from iliac crest bone

marrow and characterized *in vitro* [76]. MSCs were capable of multiple rounds of proliferation whilst retaining the ability to differentiate into different lineages when specific stimuli were added to the culture media. Experiments with single cell derived colonies suggested that MSC cultures are a heterogeneous population of cells. Within the population, some MSCs had the ability to differentiate into any cell type – osteoblast, adipocyte or chondrocyte – whilst others were less potent and more limited in their differentiation potential [76].

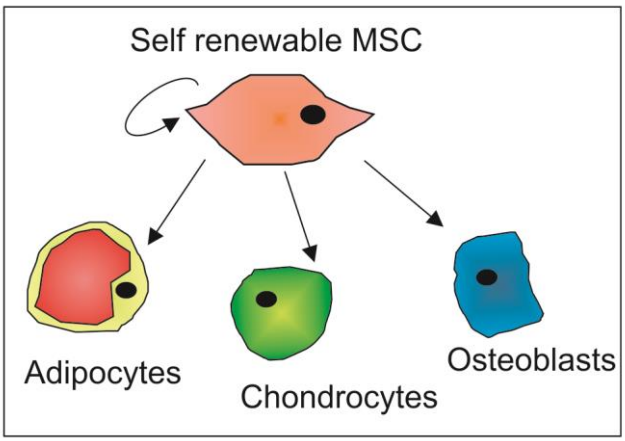

Figure 1.6 Differentiation capacity of MSCs

MSCs both *in vivo* and cultured with specific stimuli *in vitro* can differentiate into adipocytes, chondrocytes and osteoblasts.

1.5.1.1 Function of MSCs

MSCs are typically isolated from bone marrow but cells with MSC-like characteristics have been successfully isolated from nearly every tissue in the body including the brain [77]. Aside from differentiating into adipocytes, chondrocytes and osteoblasts, MSCs have been shown to have immuno-regulatory roles. Since MSCs reside in the bone marrow alongside HSCs, which differentiate into all types of blood cells, including immune cells, the ability of MSCs to regulate lymphocyte proliferation was tested. *In vitro* results showed that MSCs reduced lymphocyte proliferation, and tests using skin grafts suggested that MSCs had immune-regulatory properties *in vivo* [78].

The ability of MSCs to differentiate into different cell types means they could be used for regenerative medicine, for example by generating patient derived (autologous) new tissue to replace damage or diseased tissue. The application of MSCs in regenerative medicine began with the treatment of bone defects or diseases. Successful results in sheep, using scaffolds loaded with MSCs to repair critical-size tibia bone defects, were

recapitulated in clinical trials using patients with various bone defects [79, 80]. Following the discovery of the immune-regulatory capacity of MSCs, there has been some success in clinical trials for the treatment of graft versus host disease, using MSCs. The exact dose of MSCs and the risk of complications still requires further investigations [81]. The number of trials using MSCs to treat a variety of conditions and diseases, such as muscle repair after heart attacks, diabetes or stroke [82-84], is ever increasing. Their success is likely due to a combination of MSCs tri-lineage differentiation potential and their immuno-regulatory capabilities.

1.5.1.2 Defining an MSC

As the number of studies using MSCs was increasing, and research groups were isolating their MSCs from different tissues, using different selection conditions, a set of criteria for defining MSCs was published by the International Society for Cellular Therapy. This was to enable better comparison of studies and to ensure that the MSCs being used were the same population of cells between research groups. The criteria was for MSCs to be plastic adherent; capable of tri-lineage differentiation; and to express cell surface markers CD105, CD73, CD90; as well as be negative for HSC surface markers CD45, CD43, Cd14 or CD11b, CD79a or CD19 and HLA-DR [85].

1.5.1.3 Controlling differentiation of MSCs

Detailed understanding of the regulatory mechanisms that determine MSC fate would improve the success of MSCs in regenerative medicine, and could identify novel targets to treat or prevent disease. Currently, genomic and proteomic approaches have identified changes in gene expression and transcription factors, as well as the myriad of signalling pathways that influence MSC differentiation [86]. A combination of unique and shared mechanisms regulates the differentiation of MSCs into specific, mature, functioning cell types. Outlined below are the main transcription factors and signalling pathways involved in osteogenesis; the differentiated lineage that will be the focus of this research.

1.6 Osteogenesis

The major pro-osteogenic transcription factor is Runx2, which is expressed throughout osteogenesis. Studies that identified Runx2, found it bound to the promoter region of the osteoblast specific gene osteocalcin, as well as other osteogenic genes: α 1 collagen, bone sialoprotein (BSP) and osteopontin [87]. Expression of Runx2 was observed throughout

skeletal development and limited to osteoblast cells. Confirming its role in osteogenesis, the loss of Runx2 expression in mice was lethal and their skeletons showed a complete lack of bone ossification, indicating that Runx2 is required for osteogenesis [88]. Furthermore, overexpression of Runx2 in mouse-derived MSCs enhanced the expression of bone-related genes *in vitro*, and showed increased mineralization capacity *in vivo* [89]. Osterix is another pro-osteogenic transcription factor that acts downstream of Runx2, and is essential for bone formation [90]. Other pro-osteogenic transcription factors are Dlx3, Dlx5 and Dlx6, with overexpression of either transcription factor *in vitro* enhancing osteogenic differentiation [91, 92]. Transcription factors that inhibit osteogenic differentiation include Twist1 and to a lesser extent Msx2. Msx2 has been shown to promote osteoblast proliferation, which is required during early differentiation and inhibits matrix mineralisation, which is associated with later stages of osteogenesis [93]. Twist1 is another transcription factor that has roles in the timing of osteogenic differentiation. Overexpression studies *in vitro* showed that Twist1 can inhibit Bone morphogenetic protein 2 (BMP2) induced osteogenesis [94]. Patients with Saethre-Chotzen syndrome suffer from premature cranial ossification, which is caused by mutations in Twist1. Patient osteoblasts showed increased rates of growth and mineralization without increased osteocalcin expression [95]. These findings suggested that Twist1 is required for the correct temporal expression of pro-osteogenic factors.

The expression of transcription factors is modulated by several signalling pathways, which are activated by growth factors and signalling molecules from the cellular environment. Of the many signalling pathways that converge to regulate osteogenesis, BMP signalling is central. BMPs are members of the TGFβ superfamily that are morphogens, which are secreted as dimeric ligands. BMPs act at different stages of development and BMP2 is implicated in directing osteogenesis. Addition of BMP2 to culture media can induce osteogeneic differentiation of MSCs *in vitro*. The downstream signalling pathway of BMPs and TGF-β involves the binding to distinct receptors, which results in the phosphorylation of receptor SMAD proteins that form complexes with other SMAD proteins and translocate to the nucleus, where they affect transcription factor activity. BMP2 and TGF-β1 have been shown to activate Runx2 [96]. BMP2 also increases Osterix activity via Dlx5, independently of Runx2 [97]. Another major signalling pathway involved in osteogenesis is the canonical Wnt pathway. Through a signalling cascade active Wnt signalling prevents the phosphorylation and the following destruction of β catenin, this allows un-

phosphorylated β catenin to translocate to the nucleus and modulate gene transcription via the LEF/TCF family of transcription factors. Studies into the role of Wnt signalling in osteogenesis have been somewhat contradictory. Mice studies using a Wnt pathway inhibitor that protects β catenin from phosphorylation, showed an increase in osteogenesis *in vitro* and *in vivo* [98]. Further studies suggested Wnt signalling to promote osteogenesis, by identifying a TCF binding site in the promoter region of Runx2 [99]. However, studies using human MSCs showed that canonical Wnt pathway stimulation using Wnt3a inhibited osteogenesis, whilst, non-canonical Wnt pathway stimulation using Wnt5a promoted osteogenesis [100]. Quarto *et al* (2010) analysed MSCs at different stages of osteogenic differentiation and found stage-specific responses to Wnt3a, showing that Wnt signalling promoted osteogenesis of mature osteoblasts, but inhibited osteogenesis of MSCs [101]. Another signalling pathway active during bone development is the Hedgehog (Hh) signalling pathway. Similar to the Wnt pathway, binding of an Hh factor to a receptor prevents the suppression of a protein downstream, called Smoothened, which leads to the Gli family transcription factors being active. *In vitro* studies in which mouse MSCs were treated with the Hh signaling factor – Indian Hedgehog (IHh) – showed positive induction of osteogenesis after just 2 days of treatment [102]. In further support of this, IHh null mice showed reduced chondrogenesis and osteoblast formation, resulting in reduced endochondral bone formation [103]. Interestingly, the pro-osteogenic action of IHh has been shown to require active Wnt signalling *in vitro*, showing cross-talk between the signalling pathways regulating osteogenesis [102].

Osteogenesis is a complex process, with layers of proteomic and genomic control. Overlapping pathways interplay to insure the correct temporal and spatial stages of osteogenesis occur. Studies have also described how the MSC environment or niche is critical to its function [104]. However, although cells are covered in glycans that can interact with other cells and the ECM; and many of the components of osteogenic signalling pathways are glycoproteins (Table 2); there has been little research into the role of glycans in MSC differentiation. The next sections will describe the current knowledge of glycans and stem cells, as well as outline evidence that suggests glycans may have a role in MSC differentiation.

Signalling pathway	Lineage	Glycoprotein	Effect on function	Ref
Wnt	Osteoblast, Adipocyte and Chondrocytes	Wnt3a	Wnt3a has 2 N-glycan sites. Glycosylation required for secretion. Some hint at reduced binding to z8-CRD (post PNGase F).	[105, 106]
		Wnt1	Removal of 4 glycan sites shown not to affect ability of retroviral vector to transform a mouse epithelial line.	[107]
		Frizzled 1-10	Putative N-glycan sites identified only.	[108]
		LRP6	Mest reduced LRP6 secretion accompanied by a reduction in LRP6 glycosylation, which promoted adipogenesis.	[109]
Non canonical Wnt		Wnt5a	4 N-glycan sites identified. Removal didn't affect function, but secretion was lower.	[106]
Hedgehog pathway	Pro- osteogenic Anti-adipogenic	Patched	Patched receptor has 2 putative glycan sites. Treatment with tunnicamycin reduced ability of Smoothened (co-receptor) to bind to Patched.	[110]
TGF-β	Osteogenic, Chondrogenic and Anti-adipogenic	Type II TGF-β receptor	2 N-glycosylation sites, which affect localization to membrane thereby affecting TGF-β sensitivity.	[111, 112]
BMP	Osteogenic	BMP-6	Removal of glycosylation of BMP-6 blocks binding to receptor.	[113]
Insulin	Adipogenic	Insulin growth factor receptor	Alternative glycosylation induced by media glucose deprivation caused alternative proreceptor to be degraded which prevented tyrosine kinase activity.	[114]

Table 2 . Glycosylation of receptors and ligands in several pathways key to differentiation of MSCs.

Table includes some of the receptors and ligands identified as glycoproteins, which are involved in signalling pathways key to MSC differentiation. Many receptors and ligands have only putative glycosylation sites identified from sequence data, others have yet to be analysed for the presence of *N*-glycan consensus sites.

1.7 Glycosylation changes during cellular development

Studies have shown that the glycosylation profile of cells changes during development. In fact, several markers of hESCs, such as stage-specific embryonic antigens (SSEAs), are glycoproteins and glycolipids [115]. Lectin binding arrays have revealed differences in cell surface glycans between undifferentiated hESCs and 12-day-old differentiated embryoid bodies, such as the loss of α 1, 2 linked fucose after differentiation [116]. Furthermore, again using lectin binding arrays, differences in glycosylation between MSCs, neural progenitors cells (NPCs), and hESCs have been identified [117]. This shows that glycosylation is different not only between cells at different stages of differentiation, but also between cell types at the same level of differentiation – i.e. between MSCs and NPCs.

1.8 Glycan profile of MSCs and functional roles

Mass spectrometry has been used to analyse the glycome of MSCs and osteoblasts derived from them [118]. MSCs were shown to have more oligomannose type glycans than osteoblasts, which had more complex glycans as well as more glycans with terminal galactose, than MSCs [118]. Moreover, a study investigating the function of glycans compared the ability of MSCs, osteoblasts, or adipocytes to support myelopoiesis. Adipocytes were found to be less supportive than osteoblasts, and had decreased glycan branching compared to both MSCs and osteoblasts. When MSCs were treated with a mannosidase I inhibitor (deoxymannojirimycin), this resulted in both reduced glycan branching and reduced myelopoistic support, suggesting that glycosylation plays a functional role in the ability of cells to support myelopoiesis [119]. A study by Sackstein *et al* (2008), showed that MSC glycans have another cellular function. The glycosylation of CD44 on MSCs, was altered *ex vivo* in order to recognise the lectin found specifically in bone marrow vessels. This successfully improved bone infiltration rates of intravenously administered MSCs, without changing their ability to proliferate or differentiate, showing both the importance, and functional specificity of cellular glycans [120]. Together these studies have shown that glycans on MSCs can influence cellular function and that the glycan profile changes during differentiation. However, critically, none of the studies mentioned above have shown the role of glycans (if any) in the differentiation of MSCs.

Evidence that supports a role of glycans in determining MSC fate, includes the skeletal related symptoms, such as short stature; absent humerus and tibial; and clinodactyly

(bent little fingers), that many CDG patients suffer from [121]. Furthermore, many of the receptors and ligands in the signalling pathways already identified as key to MSC differentiation are known to be glycosylated (Table 2). The degree of glycosylation is known for some, and for a few glycoproteins the effect of glycosylation on function has been studied, by either altering the consensus site so a glycan is no longer attached at all, or by using glycosidase inhibitors to prevent complex glycan formation in the Golgi. A major change to cellular glycosylation would alter the glycosylation of many signalling molecules, and if an effect on cellular function was bought about, it would be challenging to dissect out a single culprit glycoprotein that has bought about the change. However, due to the redundancy in many signalling pathways, it is possible that an alteration to a single glycoprotein would not result in an observable cellular change.

1.9 Project rationale and aims

Glycosylation is an abundant post-translational modification, which can affect many cellular processes. Although most glycans are not required for *in vitro* cell culture, all types of glycan have been shown to be essential for embryonic development. Mouse studies and symptoms of CDG patients point towards a developmental role of glycans in many tissue types. The study of MSC differentiation provides an *in vitro* model of development, which can be easily manipulated and studied, without the web of interconnecting systems found in whole organisms. Research into what influences MSC differentiation is of importance to the regenerative medicine field, as it may improve differentiation techniques or identify novel targets that can be manipulated to influence stem cell behaviour *in situ.*

There are multiple lines of evidence that signify a speculative role for glycans in MSC differentiation. These include: the abundance of glycosylated proteins on MSCs cell surface; known examples of glycans impacting protein function; the change in glycan profile between MSCs and differentiated cells; the skeletal symptoms of CDG patients; and the involvement of many glycoproteins in signalling pathways. To investigate if glycans can influence MSC osteogenesis, I propose to use mass spectrometry to profile the *N*-glycans of MSCs and osteoblasts derived from them. The glycan profile of subpopulations of MSCs, with varied differentiation capacity, will be compared. Further to this, the glycan synthesis pathway will be disrupted genetically and chemically, and the ability of MSCs to differentiate with modified glycan profiles will be assessed. As a result of these experiments, any changes in differentiation capacity will be compared back to alterations in glycan profile, providing a novel assessment of the role of glycans in osteogenesis.

Chapter 2 Materials and methods

2.1 Chemicals

All chemicals were from Sigma unless otherwise stated.

2.2 Cell culture

2.2.1 Culture media

All tissue culture components were from Invitrogen and the plasticware from Sigma-aldrich unless otherwise stated. Cells were cultured in basal media composed of Dulbecco's Modified Eagle Media (DMEM, high glucose, pyruvate, no glutamine) supplemented with 10% fetal bovine serum (FBS), 1% Penicillin/streptomycin (P/S) and 1% Gluta-Max-I.

2.2.2 hTERT-MSCs

hTERT-MSCs were previously generated and characterized prior to this research [122]. These immortalized cell lines were created from primary human mesenchymal stromal cells that were isolated from a femoral head, and then transduced with lentivirus to drive the over expression of human telomerase. Single cell colonies derived from this transduction were isolated and expanded in culture. Lines used in this research were Y101, Y201 and Y202 hTERT-MSCs.

2.2.3 hTERT-MSC culture

Cells were grown in a humidified incubator at 37^{o}C and 5% $CO_{2.}$ Cells were grown in tissue culture flasks or 10cm petri dishes, before cells reached full confluence cells were split 1/6 or as required, by incubation with trypsin/EDTA for 5 minutes until detached.

2.2.4 Mycoplasma

Cells were tested for mycoplasma regularly throughout culture and whenever cells were bought up from liquid nitrogen storage. Briefly, cells were seeded into wells of a 24 well plate and serial diluted across several wells. After minimum of 2 days, culture media was removed and wells were washed with PBS twice followed by fixation with methanol for 5 minutes. After removal of methanol, cells were incubated in a solution of 2µg/ml DAPI in PBS, for 5 minutes at room temperature in the dark. Post removal of DAPI and several washes with PBS, cells were visualised using a UV lamp, and another lab member requested to confirm absence of none nuclear staining.

2.2.5 Osteogenic media

In order to induce osteogenesis cells were cultured in basal media described above that also contained 50µg/ml ascorbic acid, 5mM β-Glycerophosphate and 10nM dexamethasone. During differentiation (up to 28 days) media was changed every 3-4 days.

2.2.6 Adipogenic media

In order to induce adipogenesis cells were cultured in basal media described above that also contained 1µM dexamethasone, 500µM 3-isobutyl-1-methylxanthine (IBMX), 1 µg/ml insulin and 100µM indomethacin. During differentiation (up to 28 days) media was changed every 3-4 days.

2.3 Generation of Cog4KDs

To generate Cog4 knock-down MSC lines, Y101 hTERT-MSCs were seeded into tissue culture wells and allowed to settle for 6 hours. Following this, cells were incubated overnight in media containing, 6µg/ml polybrene and MISSION® lentiviral particles, containing one of five shRNAs targeted to Cog4, which were designed and produced by Sigma-Aldrich. The five shRNAs were assigned a letter A-E (Table 3). The plasmid-backbones used for the different shRNAs are shown in Figure 2.1. The difference between the two vectors is the presence of a Woodchuck Hepatitis Post-transcriptional regulatory element (WPRE), which has been shown to enhance transgene transcription.

shRNA I.D.	Plasmid backbone	Complement site	Exon	mRNA variant used	Sequence
A	TRC1.5	229-252	1	Variant 1	CGGCCATTGAAAGTA AGATGGTCACTCGAG TGACCATCTTACTTTC AATGGTTTTTTG
B	TRC1.5	1258-1282	10	Variant 1	CCGGGCAGGAGCTAA TTGGCTTATACTCGAG TATAAGCCAATTAGCT CCTGCTTTTTTG
C	TRC1.5	1895-1919	16	Variant 2	CCGGCCCTTGGGTAC AACAGTTCATCTCGA GATGAACTGTTGTAC CCAAGGGTTTTTTG
D	TRC2	817-841	6	Variant 2	CCGGCATCTTTGCAG ATACACTTACCTCGAG GTAAGTGTATCTGCAA AGATGTTTTTTG
E	TRC2	2181-2204	19	Variant 2	CCGGGTGACCGAGAT CCTCGATTACCTCGA GGTAATCGAGGATCT CGGTCACTTTTTTG

Table 3. Details of shRNAs against Cog4.

shRNAs were designed and produced by Sigma-Aldrich.

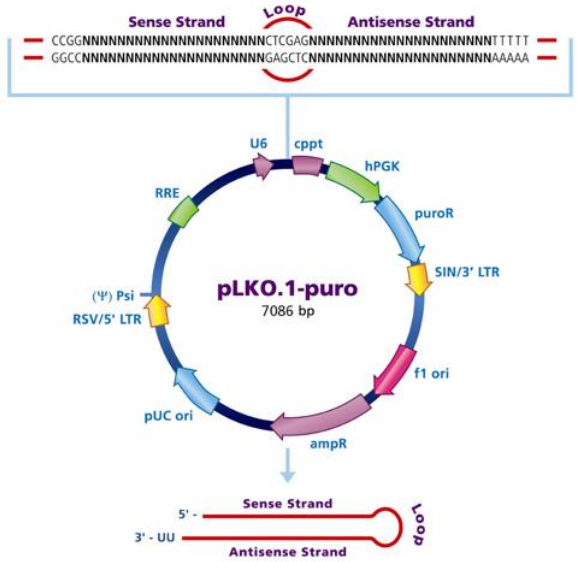

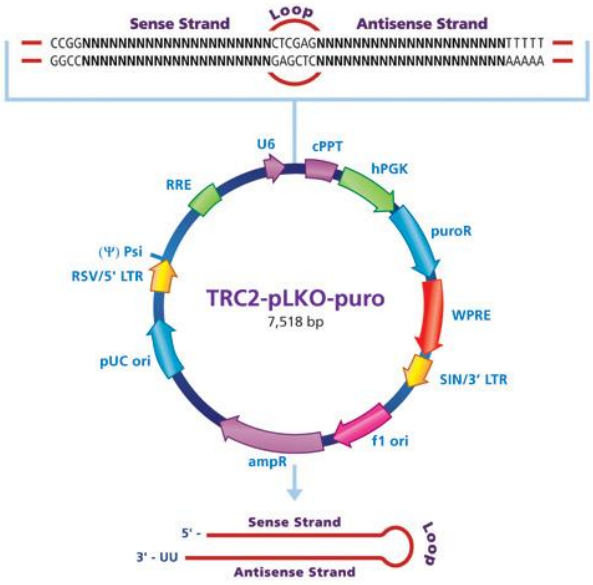

Name	Description
cppt	Central polypurine tract
hPGK	Human phosphoglycerate kinase eukaryotic promoter
puroR	Puromycin resistance gene for mammalian selection
WPRE	Woodchuck Hepatitis Post-Transcriptional Regulatory Element
SIN/LTR	3' self inactivating long terminal repeat
f1 ori	f1 origin of replication
ampR	Ampicillin resistance gene for bacterial selection
pUC ori	pUC origin of replication
5' LTR	5' long terminal repeat
Psi	RNA packaging signal
RRE	Rev response element

Figure 2.1 TRC1.5 and TRC2 Vector Maps (pLKO.1-puro).

Taken directly from http://www.sigmaaldrich.com/life-science/functional-genomics-and-rnai/shrna/library-information/vector-map.html (May 2015).

The multiplicity of infection (MOI) is the number of transducing lentiviral particles per cell. This was calculated as follows:

i) (Total number of cells per well) x (Desired MOI) = Total transducing units needed (TU)
ii) (Total TU needed) / (TU/ml reported on Certificate of Analysis) = Total ml of lentiviral particles to add to each well

A range of MOI were used as recommended by the manufacturer, in order to determine criteria for highest transduction efficiency. Following transduction, cells were cultured in normal media for 24 hours and then in media containing 2µg/ml puromycin, to select for positively transduced cells. Media was changed every 2 days and cells monitored until non-transduced control cells had died.

2.3.1 Single-cell derived line formation

To culture single-cell derived lines, transduced cells were trypsinized and 500 cells placed into a 10cm culture dish with 9ml clonal media. Clonal media was basal culture media supplemented with 10% Hyclone FBS; and was made with 50% conditioned media, which was collected from a T175 flask of non-transduced Y101 hTERT-MSCs and filtered before use; and contained 2µg/ml puromycin. Media was replaced every 3-4 days. Dishes were monitored regularly and single, adhered cells were circled using a lab pen. Once colonies contained at least 50 cells, plates were washed with 1xPBS and small metal clonal rings were adhered to the plate using sterile grease. Trypsin was added inside of the ring, and after 10 minutes incubation at 37^{o}C, colonies were pipetted into separate wells of a 24 well plate. Cog4KD hTERT-MSC colonies were named using the letter of the shRNA used during transduction, the MOI which was used, and finally a number given after initial transfer into a 24 well plate. For example, C1.6 was created using shRNA “C”, an MOI of 1 and was the 6th clone transferred into a 24 well plate.

2.4 Histochemistry

2.4.1 Crystal violet

Cells were washed twice in PBS before fixation in 95% ethanol at room temperature for 5 minutes. Cells were then washed with PBS before being incubated at room temperature in 0.5% w/v crystal violet made in 95% ethanol, for 30 minutes. After removal of stain, cells were washed several times in tap water to remove non bound stain. Plates were

then left to air dry, at room temperature overnight, prior to imaging by bright-field microscopy.

2.4.2 Alkaline Phosphatase (ALP) and phosphate (Von Kossa)

Cells were washed twice with PBS before addition of ALP stain solution which contained: 0.2mg/ml naphtol AS-MX in 1% N,N-dimethylformamide, 1mg/ml Fast Red TR diluted in 0.1M Tris pH 9.2. After 5 minutes incubation with the ALP stain solution, the cells were washed twice with PBS before being fixed in 4% paraformaldehyde (PFA) for 5 minutes at room temperature. Cells were then washed with PBS, followed by water, before addition of 1% v/w silver nitrate solution. Plates were then placed on a light box for 30 minutes. Cells were then washed three times with distilled water (dH_2O) and incubated for 5 minutes with 2.5% w/v sodium thiosulphate to remove non-specific staining. Finally, cells were then washed twice with dH_2O and stored in 20% glycerol in PBS before being imaged by bright-field microscopy.

2.4.3 Oil red O

Cells were washed 1x with PBS before being fixed with 4% PFA for 10 minutes. Following this, cells were washed 1x with dH_2O. Cells were then incubated in 60% isopropanol for 5 minutes, and then incubated for 10 minutes in 0.3% Oil red O solution. The 0.3% Oil red O solution was made by diluting a stock solution of 0.5% Oil red O (in isopropanol) with dH_2O (3:2), this was left overnight for precipitate to settle as well as being filtered before use. Cells were then washed 1x with 60% isopropanol and 3x with dH_2O. 100ul dH_2O was then added before imaging.

2.4.4 Alcian blue staining

Cells were washed once with PBS before fixation for 10 minutes at room temperature with 4% PFA. Cells were then washed twice with dH_2O, and then incubated overnight at room temperature in 0.5% w/v Alcian blue, 10% concentrated hydrochloric acid (HCL) v/v. Cells were then washed twice with dH_2O and 100µl of PBS added to each well. Images of stained cells were then taken using a bright-field microscope. To quantify degree of staining, the stain was eluted by addition of 100µl 6M guanidine-HCL to each well. After 48 hours, the guanidine solution was transferred into a new 96 well plate, and absorbance was read at 630nm.

2.5 Real time quantitative PCR methods

During the following procedures filter tips as well as plasticware and regents that were set aside for 'RNA work only', were used in order to limit contamination of samples with RNAases.

2.5.1 RNA extraction

Cells were grown in 6 well tissue culture plates to allow for sufficient cell numbers to extract RNA from. To harvest RNA, cells were washed with PBS twice and then incubated with 500µl per well TRIzol reagent (ambion, life technologies) for 2.5 minutes at room temperature. Plates were then gently rocked before a further incubation of 2.5 minutes at room temperature. Cell lysate in TRIzol was then transferred into an eppendorf tube and frozen at -80^{o}C. Samples were then defrosted at room temperature and 100µl of chloroform was added to each sample. Tubes were then shaken vigorously for 15 seconds and then incubated at room temperature for 15 minutes. Following this tubes were centrifuged at 12000g for 20 minutes at 4^{o}C. The clear, upper phase was transferred into a new tube and 250µl isopropanol was added. The tubes were then inverted several times before being incubated at room temperature for 30 minutes, to allow RNA to precipitate. Samples were then centrifuged at 12000g for 15 minutes at 4^{o}C, and the RNA pellet was then washed with 1ml 75% ethanol, before being centrifuged at 12000g for 5 minutes at 4^{o}C. Most of the supernatant was removed before allowing the pellet to air-dry for 10 minutes. Finally the RNA pellet was resuspended in 12µl nuclease-free water (Hypure, Molecular biology grade water, ThermoScientific) and stored at -80^{o}C.

2.5.2 DNase treatment of RNA samples

RNA samples were treated with RQ1 RNase-free DNase I (Promega) following the manufacture's guidelines. In brief, RNA samples were defrosted on ice, before 1µl of RQ1 RNase-Free DNase, 2µl of 10x reaction buffer and 5µl of nuclease-free water, were added to each sample. Samples were then incubated at 37^{o}C for 30 minutes. 2µl of 50mM EDTA was then added to each sample before being incubated at 65 ^{o}C for 10 minutes in order to inactivate the DNase.

2.5.3 cDNA synthesis

Firstly, the RNA concentration of each sample was measured using a nanodrop. Reverse transcription was carried out on 1µg of RNA from each sample and on a water control

sample. The RNA sample was pipetted into a PCR tube with 1µl of Oligo(dT)12-18 Primer (Invitrogen); 1µl 10mM dNTPs; and water to make the total volume 12µl. After mixing, by gentle pipetting, samples were incubated at 65 ^{o}C for 5 minutes. Samples were then chilled on ice for 2 minutes and then spun briefly. A mixture containing 4µl 1st Strand buffer; 2 µl 0.1M DTT; and 1 µl of water; was then added to each sample and gently mixed by pipetting. Samples were then incubated for 2 minutes at 42 ^{o}C, before 1 µl of SuperScript II reverse transcriptase (Invitrogen) was added. After further mixing, samples were then incubated at 42 ^{o}C for 1 hour and at 70 ^{o}C for 15 minutes. Samples were then either left neat or diluted as required with water, before being used in real-time PCR quantitative reactions.

2.5.4 Real time quantitative PCR reactions

Real time quantitative PCR reactions were carried out using Fast SYBR Green master mix (Applied Biosciences) and run using a StepOnePlus Real time PCR system (Applied Biosciences) and analysed using StepOne v.2.3 software.

To assay gene expression using real time quantitative PCR, a master mix containing 10µl of Fast SYBR Green reagent; 2µl of appropriate primer pair mix (each primer at 5mM); and 5µl of water was prepared, in triplicate, for each sample and pipetted into wells of a 96 well plate (MicroAmp® Fast optical 96 well reaction plate with barcode, Life Technologies). Following this 3µl of diluted cDNA was added in triplicate. Plates were briefly centrifuged to bring contents to the bottom of each well, before being loaded into the StepOnePlus PCR machine. Settings on the StepOnePlus system were chosen for SYBR Green use, to generate comparative CT data and, when doing primer validation, (described in more detail below) to include a dissociation curve. Program settings were 95^{o}C for 20 seconds, before 40 cycles of 95^{o}C for 3 seconds then 60^{o}C for 30 seconds. When a dissociation curve was required, following each cycle, temperatures changed to 95^{o}C for 15 seconds, 60^{o}C for 1 minute followed by 95^{o}C for 15 seconds.

2.5.5 Primers and validation

Primers were designed using NCBI GenBank and NCBI Primer blast online tools. Primers were tested on cDNA from Y101 hTERT-MSCs, after 21 days in osteogenic media. cDNA was serially diluted and added in triplicate to the PCR master mix (as above). Water only controls were also added in triplicate to check for primer dimerization. Plates were then run as above including a dissociation curve stage. To test the efficiency of primers, the CT

values were plotted against the Log concentration and the slope of the line compared to that of the housekeeping gene RSP27a. If primers are efficient the CT values should increase by 3.33 cycles after a 10 fold dilution of cDNA. The dissociation curves were used to confirm primer specificity. The primer sequences and the efficiency graphs are shown in Figure 2.2. For analysis of samples from a time-course experiment, the 20µl of cDNA from the cDNA synthesis was used after dilution of 1/3 for BMP2 and BSP primers, 1/2 for Runx2 and 1/10 for RPS27a.

A

Gene target	Forward primer sequence	Reverse primer sequnce
BMP2	5'-ACTCGAAATTCCCCGTGACC - 3'	5' - CCACTTCCACCACGAATCCA - 3'
BSP	5' - GAGGAGGAAGAGGAAGGAAATG - 3'	5' - TGGTACTGGTGCCGTTTATG - 3'
RPS27a	5' - TGGATGAGAATGGCAAAATTAGTC - 3'	5' - CACCCCAGCACCACATTCA - 3'
Runx2	5' - AGTGATTTAGGGCGCATTCCT - '3	5' - GGAGGGCCGTGGGTTCT -3'

B

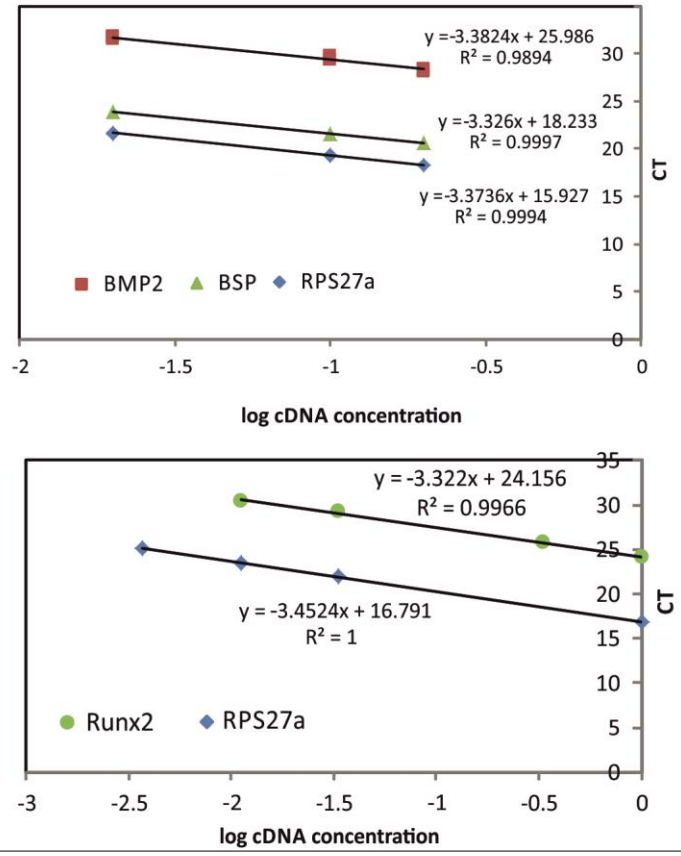

Figure 2.2 QPCR primer sequences and efficiencies

A) Primer sequences for primers used in real time quantitative PCR with SYBRE green reagents. B) Primer efficiencies were measured using a serial dilution of a test sample with each primer. CT values were plotted against log cDNA concentration and slope of the line calculated. For efficient primers the slope of the line should be -3.33 +/- 0.2.

2.5.6 Real time quantitative PCR data analysis

To analyse real time PCR data, the CT values from sample triplicates were averaged. This was done for gene of interest i.e. Runx2 and for the given housekeeping gene, which was RPS27a. Firstly the CT of RSP27a for that sample was taken away from the CT of the gene of interest to give "Delta CT". To compare samples back to a Day 0 time point sample, all Delta CT values were divided by the Delta CT of the Day 0 time point sample, which calculates "Delta Delta CT" values. In order to display these results as fold change from the Day 0 time point, the formula: $2^{-\text{Delta Delta CT}}$, was used, setting the Day 0 time point to 1. This was carried out for each gene of interest and when multiple cell types were used, the day 0 sample for untreated or wildtype was set to 1. Experiments were carried out twice, independently, to provide a biological replicate, resulting in n=6 for each sample.

2.6 Flow cytometry

Flow cytometry was used to assay the abundance of glycan structures on the cell surface. Samples were run using a flow cytometer (Beckman Coulter CyAn ADP analyser), and analysed using Summit 4.3 software.

2.6.1 Flow cytometry of glycans

Cells were first washed twice with PBS, and incubated with washing buffer (0.2% bovine serum albumin, 5mM EDTA in PBS) at 37^{o}C for 10 minutes until cells detached from the flask. Cells were collected into a falcon tube and centrifuged for 5 minutes at 450g. The cell pellet was then resuspended in PBS and a cell count performed. Cells were then centrifuged again for 5 minutes at 450g and resuspended in ice-cold PBS so that the suspension contained 10^6 cells/ml. 100µl of the cell suspension was placed into an eppendorf tube for each sample. Tubes were then incubated on ice for 15 minutes in order to limit lectin internalisation by endocytosis. Following this, lectins, diluted in 100 µl of ice-cold washing buffer, were added to each sample. Concentrations of lectins used are detailed in Table 4. Samples were then incubated on ice in the dark for 15 minutes, flicked, and then incubated for a further 15 minutes. If lectins were directly conjugated, 1ml of washing buffer was added and then the samples were centrifuged for 5 minutes at 450g. The cell pellet was resuspended in 100µl of washing buffer containing 1µg/ml DAPI and incubated on ice in the dark for 5 minutes. Following this 1ml of washing buffer was

added and samples were then centrifuged for 5 minutes at 450g. Finally the cell pellet was resuspended in 400µl PBS and stored on ice in the dark prior to analysis by flow cytometry. If the lectins were conjugated to biotin rather than directly to fluorescein, samples were incubated with 100µl of streptavidin-fluorescein and then incubated on ice in the dark for 15 minutes, before being flicked to mix, and incubated for another 15 minutes. 1ml of washing buffer was then added and samples centrifuged for 5 minutes at 450g. This was repeated 3 times to remove non-specifically bound streptavidin. Cell pellets were then resuspended in 100µl of washing buffer containing 1µg/ml DAPI and treated as described for directly conjugated lectins.

Name of lectin	Primary sugar specificity	Dilution	Conjugate
Concanavalin A (ConA)	Mannose	10µg/ml	Fluorescein
Wheat Germ agglutinin (WGA)	N-Acetylglucosamine	1µg/ml	Fluorescein
Peanut agglutinin (PNA)	galactosyl (β-1,3) *N*-acetylgalactosamine (T-antigen) unsialylated only	5µg/ml	Fluorescein
Vicia villosa (VVL)	N-Acetylgalactosamine (Tn-antigen) and galactosyl (β-1,3) *N*-acetylgalactosamine (T-antigen)	10µg/ml	Fluorescein
Jacalin (Jac)	N-Acetylgalactosamine (Tn-antigen) and galactosyl (β-1,3) *N*-acetylgalactosamine (T-antigen)	2µg/ml	Fluorescein
Sambucus Nigra (SNA)	Sialic acid (α-2,6 linkage)	10µg/ml	Biotin – use streptavidin secondary
Maackia Amurensis II (MAL II)	Sialic acid (α-2,3 linkage)	20µg/ml	Biotin – use streptavidin secondary
Secondary	Specificity	Dilution	Conjugate
Fluorescein- Streptavidin	Biotin	5µg/ml	Fluorescein

Table 4. Lectin binding and concentrations for use in flow cytometry.

2.6.2 Flow cytometry data analysis

Cells incubated with PBS only were run through the flow cytometry first, in order to adjust voltage of the lasers (405nm, 488nm and 633nm) so that the lower tail of the histogram was at 0, in all gates. Forward scattered light and side-scattered light were used to create a gate positively selecting cells, and negatively selecting cell debris, or cell clumps. Another gate selected negatively for violet fluorescence, thus selecting only live cells (unstained by DAPI). The count versus log green fluorescence of cells present in both gates was analysed and displayed as a histogram. The median fluorescence of the histogram was used in comparisons between samples. Also used was the coefficient of variation (half max) –CV(hm) –which is the width of a population at the point where the median value is half the maximum value of that population. The CV(hm) provided a numeric value of how wide or varied a population was.

2.7 Cell assays

2.7.1 p-Nitrophenyl Phosphate (pNPP) assay for ALP activity and picogreen assay for DNA content.

Cells were cultured in 96 well tissue culture plates. At required time points cells were washed once with carbonate buffer (0.133M Na_2CO_3, 0.066M $NaHCO_3$), then 150µl 0.1% Triton-X in carbonate buffer was added to each well. Plates were then frozen at -80^{o}C until all samples were gathered. Cells were then freeze/thawed (using a 37^{o}C incubator and -80^{o}C freezer) three times. Triton-X was pipetted up and down to insure full cell lysis. 50µl was transferred into a new clear 96 well tissue culture plate for pNPP assay and 50µl into a black opaque 96 well plate (Greiner 96 well microplate black, SLS) for the picogreen assay.

For pNPP assay, 50µl of substrate solution (0.33mg/ml pNPP in carbonate buffer with 3.3mM $MgCl_2$) was added to each well. pNP standards (0.5-0.0125 µmol/ml) were added in triplicate to the plate which was then incubated at 37^{0}C for 10-30 minutes. Absorbance was then read at 405nm and a standard curve used to calculate ALP activity per minute.

For the picogreen assay, salmon sperm DNA was diluted (8-0.25µg/ml) and pipetted in triplicate as standards. 50µl of the picogreen reagent (Quant-iT PicoGreen dsDNA Reagent, Invitrogen) diluted 1:50, in 100mM Tris, 1mM EDTA, pH7.5, was added to each well. Plates were covered with foil and left to rock for 5 minutes. Plates were read at

485nm excitation and 538nm emission, and a standard curve used to calculate amount of DNA per well, and used to make ALP activity relative to amount of DNA (µg PNP/min/µg DNA).

2.7.2 3-(4,5-dimethylthiazol-2-yl)-2,5-diphenyltetrazolium bromide (MTT) assay

For each cell line tested 1200 cells were seeded per well, into 6 wells of a 96 well culture plate. After 1, 2 and 4 days culture media was replaced with fresh media and 25µl MTT solution (5mg/ml in PBS). Plates were then incubated for 3 hours at 37^{o}C in 5% CO_2. MTT solution and media was removed from wells and 100µl of 0.04M HCL in isopropanol was added to each well. Plates were left to shake at room temperature for 10 minutes to allow for complete solubilisation. Absorbance was then read at 570nm, and average absorbance (with standard deviation) was used in comparisons.

2.8 Glycan profiling

2.8.1 Filter Aided *N*-glycan Separation (FANGS)

The FANGS method was carried out as described by Rahman *et al* (2014) [123]. For all experiments here, 1x10^{6} cells were seeded out into a 10cm tissue culture dish and allowed to settle for 24 hours (unless otherwise stated). Cells were then washed gently with 5ml of PBS (warmed to 37^{0}C), 6 times. 1ml of PBS was then added to the dish and a cell scrapper used to scrape cells into an eppendorf tube, which was placed on ice. The sample was then centrifuged at 16000g for 5 minutes, at 4^{o}C. The supernatant was removed and the pellet re-suspended in a volume of lysis buffer (4% SDS, 100mM Tris pH7.6, 100mM DTT), approximately 10x volume of the cell pellet. The sample was then heated at 95^{o}C for 5 minutes, followed by centrifugation at maximum speed (21000g) for 5 minutes. The supernatant was then placed into a new tube and stored at -80^{o}C if required. After defrosting, the supernatant was diluted 1:10 with 8M Urea and 100mM Tris pH 8.5. The sample was then concentrated through a concentrator filter system (millipore), by multiple centrifugation steps at 14000g for 5 minutes, by discarding the flow-through each time. The filter was then rinsed 2x with 8M Urea and 100mM Tris pH 8.5, solution. Afterwards, 300µl of 50mM iodacetamide in Urea and Tris solution was added to filter unit, and incubated in the dark for 15 minutes, before it was spun through

at 14000g. The filter was washed again with Urea and Tris solution and then washed 4x with 20mM ammonium bicarbonate solution made using HPLC grade dH_2O. 8-10 units of PNGaseF in total 100µl ammonium bicarbonate was added to each filter and mixed gently. Filter units were incubated for 16 hours at 37^{o}C. A new collection tube was added to filter, prior to centrifugation at 14000g for 10 minutes. Retaining flow through in the tube, 200µl HPLC grade dH_2O was added to the filter unit and mixed gently. Filter unit was then spun at 14000g for 10 minute and the last step repeated again. Flow through (500µl) was stored at -80^{o}C.

2.8.2 Permethylation

15ml glass tubes (SLS) were washed in 3%v/v Decon and flamed clean just before use. Glycan filtrate (final flow through from FANGS) was placed into a glass tube. Glycan filtrate was dried down under vacuum, and then 300µl of HPLC grade dH_2O was added to each tube. This was dried down under vacuum and repeated three times. Glycan samples were then stored at -20^{o}C for at least 1 week. Glass tubes were allowed to reach room temperature before 20 drops of DMSO was added using a glass Pasteur pipette. Following this, 2 microspatulas of freshly ground sodium hydroxide was added to each sample. 0.5 ml iodomethane was added to each sample and mixed once, by agitating the tube by hand. After 10 minutes this was repeated. After another 10 minutes, 1ml of iodomethane was added and mixed once by agitating the tube by hand. After 20 minutes 1ml of sodium thiosulphate (100mg/ml in H_2O), was added and tube vortexed briefly. 1ml of dichlormethane was added and sample vortexed again. Samples were then centrifuged for 10 seconds and the upper aqueous layer was removed. 1ml of dH_2O was added followed by a brief vortex and 10 second spin in centrifuge, and then removed as before. This was repeated 15x. The dichloromethane layer was then dried down under vacuum for 1 hour. Permethylated glycans were then stored at -20^{o}C.

2.8.3 Mass spectrometry

Permethylated glycans were dissolved in 20µl methanol unless otherwise stated. 2µl of sample; 1µl of sodium nitrate (0.5M in 70% methanol, 30% H_2O); and 2µl of 2,5-dihydroxybenzoic acid (DHB) 20mg/ml in 70% methanol, 30% H_2O; was mixed in a PCR tube. 2µl of this mix was placed onto a MALDI plate (Brucker) spot and allowed to air dry. Immediately after it dried 0.2 µl of ethanol was added to the spot in order for re-crystallisation. Samples were analysed using MALDI-TOF/TOF mass spectrometry

(UltraFlex, Bruker). The spectra were acquired using positive-ion mode, with 4000 shots in steps of 800, which were summed to give one spectrum per spot. The Smartbeam laser power was set to 50-65%. Mass spectra were recorded over the m/z range of 800-6000m/z.

2.8.3.1 Spectra analysis

Spectra were analysed using Flexi analysis 3.3 software (Bruker). Firstly, spectrum were all processed using Centroid peak detection algorithm, signal to noise limit of 3, and smoothed for 1 cycle at 0.1 mass/charge (m/z), using SavitzkyGolay alogrithm. Glycan peaks were identified from their mono-isotopic peak m/z value corresponding to a calculated m/z for known possible glycan structures. This was facilitated by the use of a simple algorithm that computes all possible combinations of the 4 main sugars (Mannose, GlcNAc, Fucose and Sialic acid), created by Dr. Peter Ashton (York). For a glycan to be included in analysis, at least 2 isotopic peaks had to be above noise, and the glycan had to have a comparable isotopic pattern to that which was predicted (Bruker Daltonics, Compass IsotopePattern software). The Peak intensity (height) of all isotope peaks for each glycan were summed (total peak intensity). In order to compare samples from different spectrum, the total peak intensity values were normalised using the formula: total peak intensity for a glycan X (100/total peak intensity identified in that spectrum). Normalised peak intensities could then be summed based on glycan structure characteristics and compared between samples.

2.9 Western blotting

2.9.1 Total cellular protein harvest

Cells were cultured in a well of a 24 well plate until confluent. Media was then removed and cells washed once with PBS. 150µl of sample buffer (5% glycerol, 50mM Tris 50mM DTT, 1% SDS, 0.74mM bromphenol blue) was added to each well. Plates were incubated at room temperature for 10 minutes. Sample buffer was then pipetted up and down before being placed into an eppendorf tube and heated at 95^{o}C for 5 minutes. Samples were then stored at -20^{o}C until required.

2.9.2 SDS-polyacrylamide gel electrophoresis (SDS-PAGE)

SDS-PAGE gels were prepared with a separating gel containing 10% acrylamide; 375mM Tris pH 8.8; 0.05% ammonium persulfate (APS); and 0.067% N,N,N',N'-Tetramethylethylenediamine (TEMED), and a stacking gel containing 4% acrylamide; 125mM Tris pH 6.8; 0.1% APS; and 0.1% TEMED. Samples were loaded into wells alongside 5µl of a pre-stained protein ladder (Page Ruler Plus, Thermo-scientific). Running buffer containing 25mM Tris, 250mM glycine and 0.1% SDS was added to the gel-tank prior to gels being run at 120V for 10 minutes and then at 180V until either the dye reached the bottom of the plate or the ladder had separated as much as required.

2.9.3 Semi-dry transfer

Prior to use polyvinylidene fluoride (PVDF) membrane (Immun-Blot, Bio-Rad) was placed briefly into methanol before being placed into semi-dry transfer buffer containing: 48mM Tris, 39mM glycine, 20% methanol and 0.0375% SDS, and stored at 4^{o}C until use. Two, 3mm thick, pieces whatman paper were also soaked at 4^{o}C, in transfer buffer. The SDS-PAGE gel was placed onto the PVDF membrane in-between the two whatman pieces and semi-dry apparatus connected to power supply at 20V for 60 minutes.

2.9.4 Immunoblotting and imaging

After transfer membranes were blocked with 5% w/v milk powder in PBS with 0.05% Tween (PBST) for 1 hour at room temperature on a plate rocker. If required, membranes were then cut at appropriate molecular weight using the pre-stained ladder as a guide. Primary antibodies were added in 5% milk PBST and incubated either overnight at 4^{o}C or for 1 hour at room temperature, on a shaker. Membranes were then washed 4 times with 5% milk PBST for 10 minutes at room temperature on a shaker. Secondary antibodies were then added in 5% milk PBST and membranes incubated on a shaker for 1 hour at room temperature. Details of specific antibodies used and concentrations are shown in Table 5. Membranes were then washed twice with 5% milk PBST, and at least 4 times with PBST for 10 minutes on a shaker at room temperature. Membranes were then imaged using Immobilon western chemiluminescent HRP substrate (Millipore) and photos processed using Abobe Photoshop.

Antibody	Concentration used
Rabbit anti human Cog4 (as used in [124])	1/500
Mouse anti-human β tubulin (gift from G.Waters, Princeton University)	1/2000
Mouse anti-human ALP (Santa-Cruz, #sc-137213)	1/6000
Mouse anti-human active β catenin (Millipore 050665)	1/2000
Goat anti-mouse HRP (BioRad)	1/3000
Goat anti-rabbit HRP (BioRad)	1/3000

Table 5. Details of antibodies used for immunoblotting.

2.10 Statistics

Data was analysed using SigmaPlot 12.3 software. Before statistical tests were applied a normality test (Shapiro-Wilk) and a test of equal variance was performed. If data passed and only two groups were being compared, a Student's T test was carried out. If more than one group was being compared, on a single factor, one-way ANOVA tests were carried out, followed by Holm Sidak post-hoc tests if required. If the data failed the normality or variance tests, equivalent non-parametric tests were applied instead. If two groups were being compared a Mann-Whitney test was carried out, and a Kruskal-Wallis One Way Analysis of Variance on Ranks, followed by Dunn's post hoc tests was carried out if more than one group was being compared on one factor. Throughout *=$P<0.05$, **=$P<0.01$ and ***=$P<0.001$.

Chapter 3: Comparison of the *N*-glycan profile of hTERT-MSCs and osteoblasts derived from them

3.1 Rationale for the comparison of the *N*-glycan profile of hTERT-MSCs and osteoblasts derived from them

Many studies have focused on discovering genomic and proteomic factors that influence MSC differentiation. Glycosylation is an abundant post-translational modification, which occurs to most cell surface proteins. Glycans have been shown to affect protein function and cellular behaviour. Previous studies have found differences in the glycan profile of MSCs compared to osteoblasts or adipocytes derived from them [118, 125]. The broad aim of this research was to investigate if glycans have a functional role in MSC differentiation. This was addressed utilizing immortalized human MSC cell lines (hTERT-MSCs). These lines were previously generated by inducing the overexpression of human telomerase in primary human MSCs [122]. The advantages of using an immortalised cell line include having an unlimited supply of cells, compared to the primary human MSCs that senesce after several passages in culture. Furthermore, it is known that there is variability in response to treatments, between primary human MSCs from different donors, which impedes comparisons between different experiments. As the hTERT-MSCs were expanded from single-cell colonies, they provide an unlimited supply of a single subtype of MSC. In agreement with the theory that primary human MSCs are a heterogeneous mixture of cells, three hTERT-MSC lines showed varying differentiation capacity ([122] and Figure 3.1). The Y101-hTERT-MSCs were capable of differentiating into osteoblasts, but showed limited adipogenic potential. The Y201 hTERT-MSCs were capable of differentiating into both osteoblasts and adipocytes, and the Y202 hTERT-MSCs did not differentiate into either cell type (Figure 3.1).

Although previous studies have compared the glycan profile of MSCs and osteoblasts, a heterogeneous mixture of primary MSCs were used [118]. Here, the Y101 hTERT-MSCs, which could be described as an osteoblast precursor or osteoblast progenitor line, were utilized. Differences that may have been missed due to the heterogeneity of the primary MSC population could be more pronounced in the Y101 hTERT-MSCs glycan profile. The Y101 hTERT-MSCs were differentiated into osteoblasts by culture in media supplemented with ascorbic acid, β-glycerophosphate and dexamethasome, which has been previously shown to induce osteogenesis [126]. Y101-hTERT-MSCs were cultured in osteogenic

media for 3 weeks prior to glycan analysis. There are many changes in gene expression and cellular physiology that occur during osteogenesis. During early stages and throughout osteogenesis ALP activity is known to increase. ALP is required for the initiation of mineralisation through increased localised phosphate production [127]. BMP2 is a bone morphogenetic protein that promotes osteogenesis by indirectly inducing Runx2 expression [128]. Runx2 is the major pro-osteogenic transcription factor that regulates the expression of several osteogenic genes [86]. BSP is one target of Runx2, and acts as a nucleator of hydroxyapatite crystal formation, required for matrix mineralisation [129], the process associated with later stages of osteogenesis. The functional readout of osteoblasts is mineralised ECM, which is visualised using Von kossa staining, which stains phosphates using the reduction of silver ions exposed to light [130]. In order to confirm osteogenic differentiation of the Y101 hTERT-MSCS, the expression of different markers of osteogenesis were monitored using histology, cell assays, and real time qPCR. As well as to confirm osteogenesis, these results provided an insight into the changes that occur at different cellular levels during osteogenesis, so that in later experiments the effect of altered glycosylation on differentiation can be monitored by comparing gene and protein expression, and functional activity back to control samples. This multi-parameter account of osteogenesis may provide mechanistic insight into the role of glycosylation in differentiation.

Despite lectin staining being a convenient way to assess the glycans present on the cell surface, it has several caveats. Lectins have varied specificity in glycan binding and staining doesn't provide detailed structural information of the glycans present, such as the degree of fucosylation. Mass spectrometry however can provide a more detailed profile with information on the relative abundance of specific glycan structures. Therefore, the *N*-glycans were profiled from the different cell types using mass spectrometry. Beforehand, the *N*-glycans were harvested using a medium through-put method called Filter Aided *N*-glycan Separation (FANGS) [123]. As this method required only $1x10^6$ cells per sample, it facilitated the profiling of biological repeats, which enabled a statistical comparison to be made between the cell types. Prior to analysis by mass spectrometry, *N*-glycan samples were permethylated. This was to stabilize the terminal sialic acids and facilitate more uniform ionization of glycans. This permethylation step reduces variation, allowing for relative quantitation of individual glycans within a mixture [131].

Following the comparison of glycan profiles of Y101 hTERT-MSCs and osteoblasts derived from them, the *N*-glycan profiles of Y201 and Y202 hTERT-MSCs were analysed. These immortalized subpopulations of MSCs had altered differentiation capacity compared to Y101 hTERT-MSCs. The glycan profiling of these lines was to assess if there was a link between MSC glycan profile or abundance of a particular glycan, and differentiation capacity. Could glycan profiles be used to predict the differentiation capacity of subsets of MSC populations? Furthermore, comparisons of the hTERT-MSC glycans profiles with the osteoblast profile were also made, to establish if an osteoblast precursor glycoform existed.

3.2 Chapter 3 Aims

Specifically, the aims were to differentiate an immortalized human MSC line into osteoblasts *in vitro*. Subsequently, to then confirm osteogenesis using histology, cell assays, and qPCR. Following this, the aim was to harvest *N*-glycans from undifferentiated MSCs and osteoblasts using the FANGs method, and then to permethylate the samples. Glycans from each cell type were to be analysed by mass spectrometry.

Furthermore, the aim was to obtain and compare the *N*-glycan profiles of 2 other immortalized MSC lines, each with varied differentiation capacities. Comparisons of the glycan profiles of different hTERT-MSCs lines and osteoblasts were then made, to determine if glycan profile could be used to predict differentiation capacity.

3.3 Chapter 3 Results

3.3.1 Single cell derived colonies of hTERT-MSCs have varied differentiation capacity

Prior to this research, primary human MSCs obtained from a single donor were immortalized by the over-expression of human telomerase [122]. Colonies derived from single cells were cultured into hTERT-MSC lines, named Y101, Y201, and Y202. Each line had a typical MSC phenotype, including plastic adherence and a fibroblast morphology, although the Y202 cells are more flattened (Figure 3.1 and [122]). To test their differentiation capacity each hTERT-MSC line was cultured for 21 days in osteogenic or adipogenic media. Cells cultured in osteogenic media were stained for phosphate (Von kossa). Cells cultured in adipogenic media were stained for fat using Oil-red O staining. The three hTERT-MSC lines showed varied differentiation capacity (Figure 3.1). The Y101 and Y201 hTERT-MSCs differentiated into osteoblasts, as seen by positive Von kossa staining. The Y101 hTERT-MSCs showed limited adipogenic differentiation compared to the Y201 hTERT-MSCs, which had visible fat droplets in most of the cells after 21 days in adipogenic media. The Y202 hTERT-MSCs did not appear to differentiate into either osteoblasts or adipocytes, as there was little phosphate or fat staining. These results support the notion of a heterogeneous population of MSCs, with individual MSCs having varied differentiation capacities. The Y101 hTERT-MSCs may represent osteoblast progenitor cells, which selectively differentiate into osteoblasts. Since previous work studying the glycan profile of MSCs and osteoblasts used a mixed primary population, the Y101 hTERT-MSC line provided the opportunity to profile an unmixed MSC /osteoblast progenitor population. Prior to this, a more thorough analysis of the osteogenic differentiation of Y101 hTERT-MSCs was carried out.

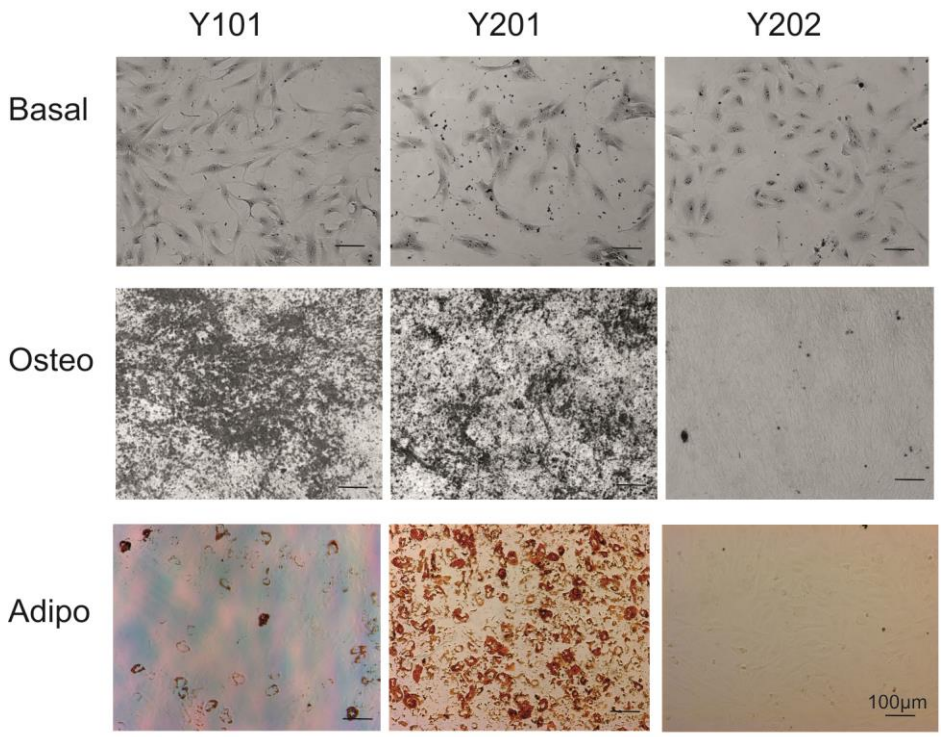

Figure 3.1 Differentiation capacity of 3 hTERT-MSC lines.

Brightfield microscopy images of 3 hTERT-MSCs lines named Y101, Y201 and Y202 hTERT-MSCs. Top row shows cells cultured in basal media and then stained with crystal violet. Second row shows cells after culture in osteogenic media for 21 days and stained for phosphate (Von kossa). Third row shows cells after culture in adipogenic media for 21 days and stained for fat (Oil red-O).

3.3.2 Y101 hTERT-MSCs are positive for several osteogenic markers

Increased ALP expression and activity is an early maker of osteogenesis. Y101 hTERT-MSCs were cultured in basal or osteogenic media for 21 days. The ALP activity of samples collected at weekly time points were compared (Figure 3.2A). The activity of ALP was significantly increased in cells cultured in osteogenic media for 21 days, compared to basal media (Student's T test, $P<0.05$, $n=3$).

A key property of functional osteoblasts is the mineralisation of extracellular matrix. Y101 hTERT-MSCs cultured in osteogenic media were stained for ALP and phosphate (Von kossa), at weekly timepoints (Figure 3.2). The amount of mineralisation steadily increased over 21 days in osteogenic media (Figure 3.2B). Y101 hTERT-MSCs were cultured in various sized tissue culture plates, for use in different assays. The degree of mineralisation was not affected by the size of the tissue culture plate or dish used, as seen by positive ALP and Von kossa staining after 21 days in osteogenic media (Figure 3.2B).

Alongside histological staining, changes in gene expression during osteogenic differentiation were used as indicators of osteoblast formation. Using real-time qPCR the expression of Runx2, BMP and BSP were made relative to the control gene RSP27a. Basal and osteogenic media samples were then expressed as fold change from day 0 samples. Runx2 is the dominant pro-osteogenesis transcription factor, which controls the expression of many osteogenic genes [86]. Expression levels of Runx2 increased over time, up 6 fold by day 7 and up 28 fold after 21 days in osteogenic media, compared to day 0 samples (Figure 3.2part Ci). These levels of increase are comparable to those seen by Frank *et al* (2002), who measured a 5 fold increase in Runx2 expression, between MSCs cultured for 3 or 20 days in osteogenic media [132]. Bone morphogenetic protein-2 (BMP2) is a pro-osteogenic cytokine. Through interactions with either, Dlx-5, Smad1 or Smad5, BMP2 increases the expression of Runx2 and Osterix, both pro-osteogenic transcription factors. The expression level of BMP2 increased over 21 days in osteogenic media, peaking at day 14 at 15 fold higher than day 0 samples (Figure 3.2Ci). Again this was similar to the 20 fold increase seen by Frank *et al*, between MSCs cultured for 3 or 20 days in osteogenic media [132]. Bone sialoprotein (BSP) is an abundant non-collagenous protein present in mineralised bone and facilitates hydroxyapatite crystal formation [129]. Levels of BSP expression increased over time in cells cultured in osteogenic media. After 21 days, Y101 hTERT-MSCs expressed over 2000 fold more BSP compared to day 0 samples (Figure 3.2C). Similar to results of Frank *et al* (2002), expression increased around 10 fold between day 7 and day 21. This showed that although BSP is associated with later stages of osteogenesis, its' expression increased 80 fold after 1 week in osteogenic media, when little phosphate staining was seen (Figure 3.2B). The Y101 hTERT-MSCs cultured in basal media for 21 days showed some increase in osteogenic gene expression, with levels above day 0 samples. However, expression levels were not as high as those for Y101-hTERT-MSCs cultured in osteogenic media (Figure 3.2Ci). Together, these results suggest that Y101 hTERT-MSCs express osteoblast markers after 3 weeks culture in osteogenic media. Following this the glycan profile of Y101 hTERT-MSCs and osteoblasts derived from them were compared.

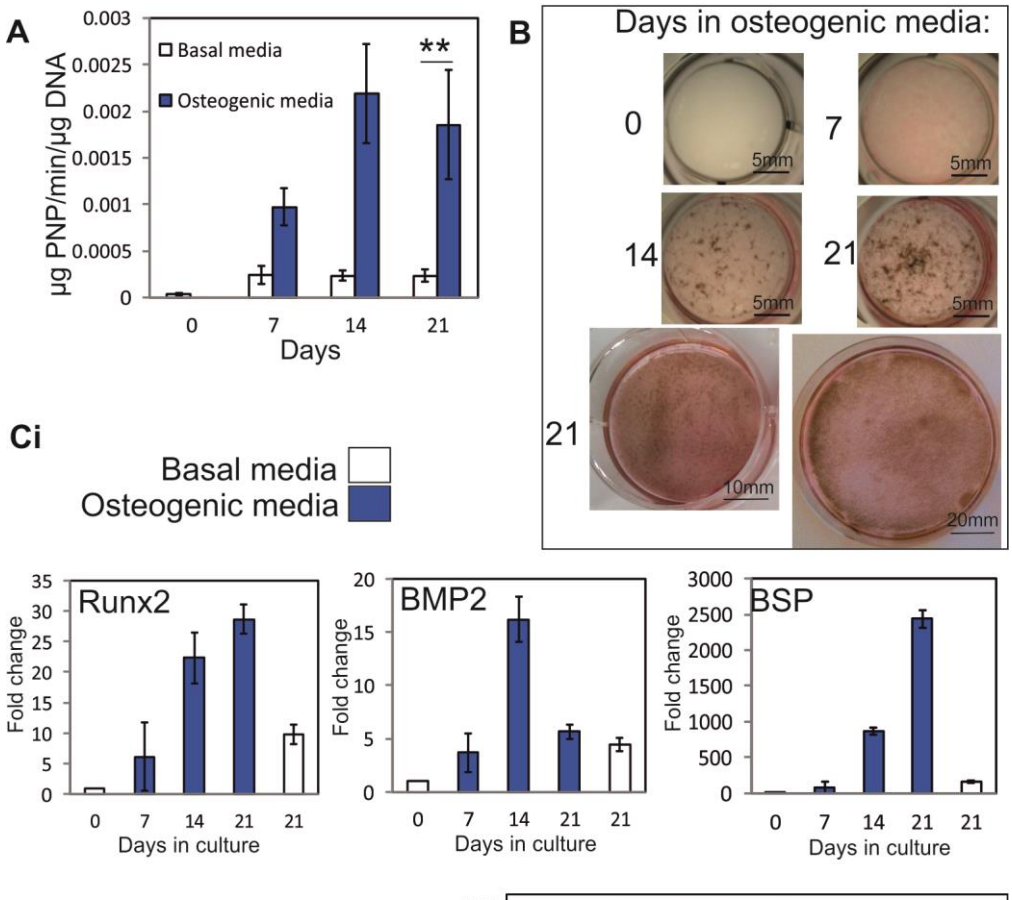

Cii

Average mean CT of repeats ± standard deviation			
	Runx 2	BMP2	BSP
0	30.3± 0.3	29.9± 0.9	32.6± 0.2
7	28.1± 0.6	27.6± 3.6	28.4± 2.7
14	26.6± 0.6	26.6± 0.2	23.4± 0.2
21	25.9± 0.2	27.8± 0.1	21.6± 0.2
21 (basal)	28.2± 0.2	28.9± 0.2	26.3± 0.1

Figure 3.2 Osteogenic differentiation of Y101 hTERT-MSCs.

Y101 hTERT-MSCs were cultured in basal or osteogenic media for 21 days and osteogenic differentiation assessed using several techniques and markers. A) Alkaline phosphatase activity was measured using pNP assay, after culture in basal or osteogenic media for 0, 7, 14, and 21 days. Activity was made relative to DNA content of each sample using a pico-green assay. Day 21 samples were compared using Student's T test, **=P<0.01, n=3. B) Bright-field images of alkaline phosphatase staining - seen as pink - and phosphate (von Kossa) staining - seen as brown - at weekly time points during culture in osteogenic media. Staining was positive at day 21, independent of the size of the culture plate or dish used - see scale bars. Ci) cDNA produced from cells grown in osteogenic media for either 0,7,14,or 21 days, were analysed using primers for Runx2, BMP2, BSP and RSP27a. cDNA produced from cells grown in basal media for 21 days was also analysed as a control. CT values were made relative to RSP27a values and then expressed as fold change relative to day 0 values. Triplicate technical replicates from 2 biological repeats are shown, error bars are standard deviation. Cii) Table shows mean CT values ± standard deviation of combined replicates.

3.3.3 Osteoblasts derived from Y101-hTERT-MSCs have an altered glycan profile

To generate *N*-glycan samples for analysis by mass spectrometry, Y101 hTERT-MSCs were cultured either in basal media overnight or, in osteogenic or basal media for 21 days. The latter sample was to control for any changes to glycan profile induced by time cultured at full confluency, rather than by differentiation into osteoblasts. The *N*-glycans were harvested from the different cell samples using the FANGS method (see methods for details). Afterwards, *N*-glycans were permethylated and analysed by mass spectrometry (MALDI-TOF/TOF). Glycans were identified from spectra using the calculated mass of monosaccharide units and knowledge of possible glycan structures produced by the *N*-glycan synthesis pathway. 65 different glycan structures were identified from the spectra of Y101 hTERT-MSCs (Figure 3.3). The spectra of osteoblasts derived from Y101 hTERT-MSCs contained the same peaks seen in Y101 hTERT-MSC spectra (Figure 3.4), when the spectrum were compared, there were significant differences in the relative abundance of individual glycan structures (Figure 3.5 and Figure 3.6). When the normalised peak intensity from each glycan structure, were grouped by structure type, significant differences between Y101 hTERT-MSCs and osteoblasts were identified. Oligomannose type glycans were significantly less abundant in osteoblasts (change from 44 to 19%), with complex glycans being significantly more abundant (change from 46 to 70%) (Student's T Test, **P<0.01, *P<0.05, n=3 and 5, (Figure 3.7)). There were also significantly more fucosylated glycans in osteoblast samples (63%) compared to Y101 hTERT-MSCs samples (42%) (Figure 3.7). The abundance of two specific oligomannose type glycan structures, Hex8HexNAc2 and Hex9HexNAc2, were significantly higher in Y101 hTERT-MSCs compared to osteoblasts (One way ANOVA, Holm Sidak post hoc test, ***P<0.001). The abundance of a singly sialylated, complex glycan structure: $NeuAc_1Fuc_1Hex_5HexNAc_4$, was significantly higher in osteoblast samples (One way ANOVA, Holm Sidak post hoc test, ***P<0.001)(Figure 3.7).

The *N*-glycan profile of Y101 hTERT-MSCs cultured in basal media for 21 days was overall more similar to Y101 hTERT-MSCs cultured overnight in basal media, than to osteoblast samples (Figure 3.5). When glycans were grouped by type there was no significant difference in abundance of oligomannose, hybrid or complex type glycans between Y101-hTERT-MSCs cultured in basal media for 24 hours or for 21 days (Figure 3.8). There was also no significant difference in abundance of fucosylated glycans (Figure 3.8). However,

there were some small differences between the 2 basal samples. The abundance of $Hex_9HexNAc_2$, the structure that enters the Golgi, had an average peak intensity of 10au in Y101 hTERT-MSCs cultured overnight in basal media. The intensity was 5au, and 2au in Y101 hTERT-MSCs cultured in basal media or osteogenic media for 21 days respectively. In order to allow for easier comparison of the *N*-glycan profiles of the different cell samples, the data was arranged into a heat-map format similar to that used in genomic studies (Figure 3.8a). The heat map conveys several aspects of the data set. For one, that despite oligomannose glycans being as prominent as complex glycans, there were fewer different oligomannose structures identified (rows on the heat map), compared to the number of different complex glycan structures. The similarity and differences in abundance of many glycans, between the cell samples is visible from the colour pattern. The partial similarity of the glycan profiles from cells cultured for 21 days might be due to some of the glycan structures being associated with time cultured at full confluency. However, another possibility is that the common structures could be associated with osteogenesis – as earlier qPCR data showed small increases in the expression of osteoblast associated genes, in samples cultured in basal media for 21 days.

Importantly, the *N*-glycan profile of Y101 hTERT-MSCs was significantly different from that of osteoblasts derived from them, which was not an artefact of time in culture. The question remaining was whether the other hTERT-MSCs, which had varied differentiation capacities, had similar *N*-glycan profiles to the Y101 hTERT-MSCs or not.

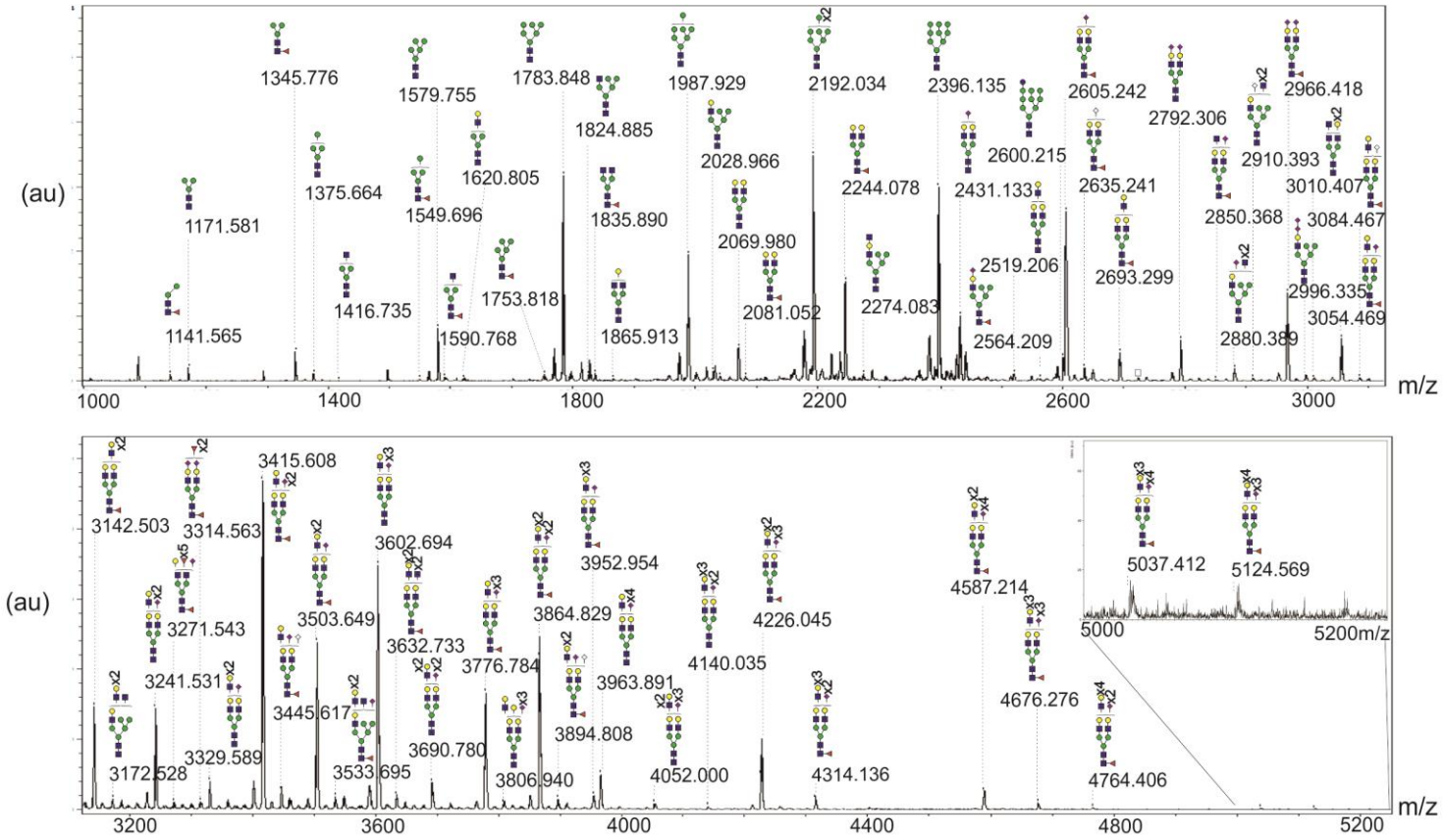

Figure 3.3 MALDI-TOF/TOF spectrum of N-glycans from Y101 hTERT-MSCs.

A representative spectrum (n=5) of *N*-glycans isolated from Y101 hTERT-MSCs. 1x10^6 cells were cultured in a 10cm dish, overnight before *N*-glycan harvest, and further processing. Glycan peaks were identified using calculated mass of monosaccharides and knowledge of the synthesis pathway. Glycans had to have two isotopic peaks, 3x above noise to be included. Mass of mono-isotopic peak is labelled, with predicted structure pictured above. Spectrum shown is from 1000m/z to 5250m/z split into two sections.

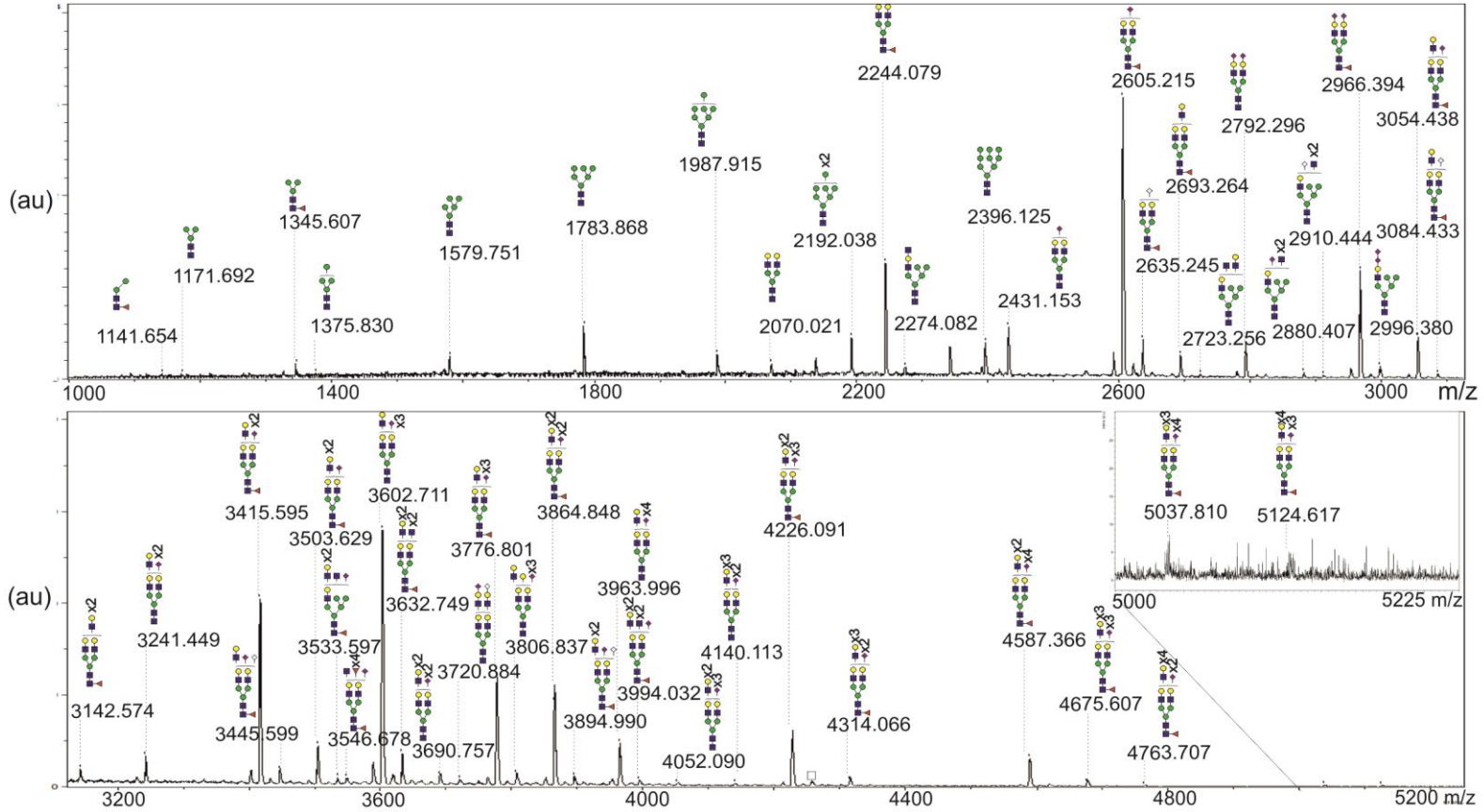

Figure 3.4 *N*-glycan spectrum of osteoblasts derived from hTERT-MSCs.

A representative spectrum (n=3) of *N*-glycans isolated from osteoblasts derived from WT hTERT-MSCs. 1x106 cells were cultured in a 10cm dish, for 21 days in osteogenic media, before *N*-glycan harvest, and further processing. Glycan peaks were identified using calculated mass of monosaccharide units and knowledge of the synthesis pathway. Glycans had to have two isotopic peaks, 3x above noise to be included. Mass of mono-isotopic peak is labelled, with predicted structure pictured above. Spectrum shown covers 1000m/z to 5250m/z.

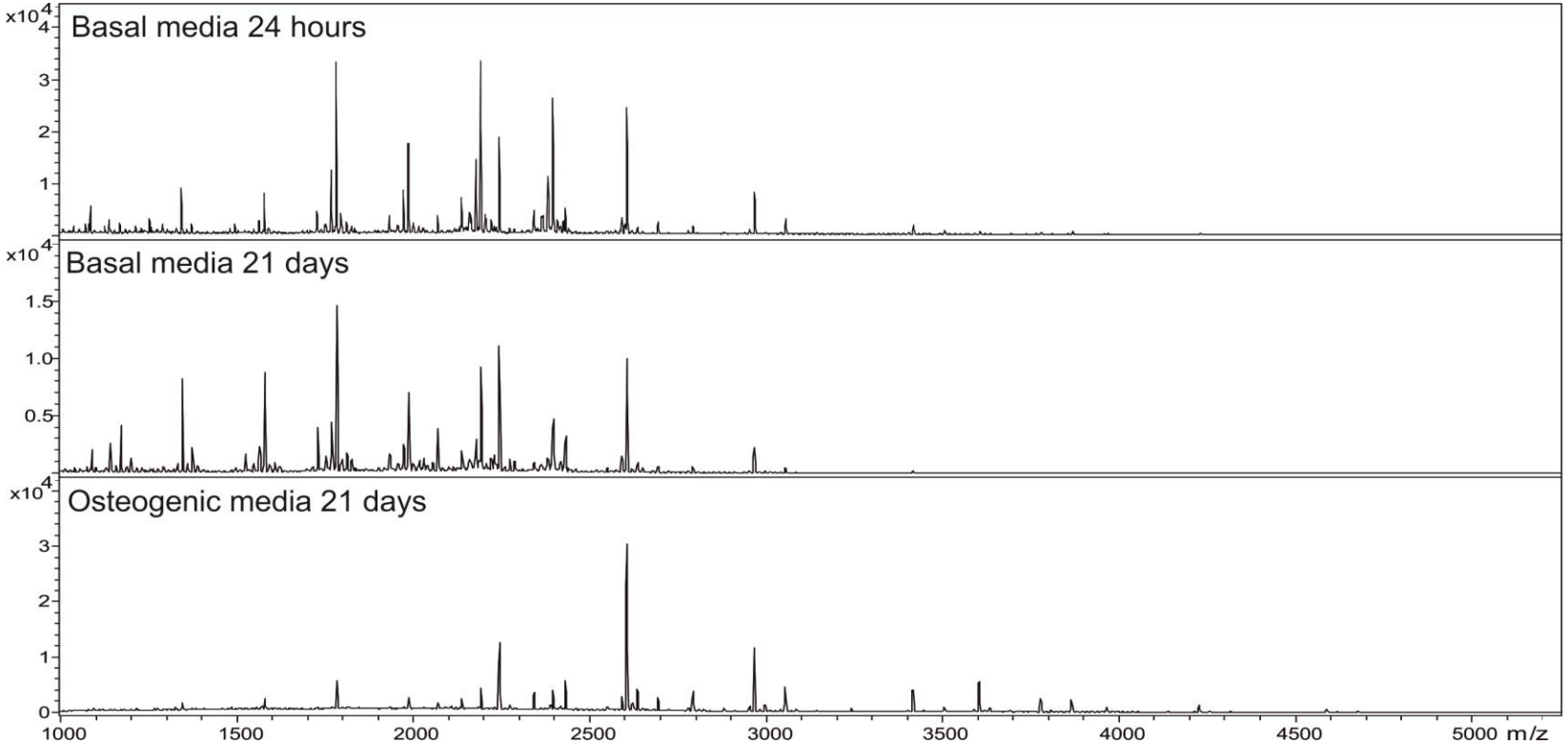

Figure 3.5 Comparison of spectrum from MSCs in basal media 24 hours, in basal media 21 days, or in osteogenic media 21 days.

A representative spectrum of *N*-glycans isolated from hTERT-MSCs cultured in basal media for 24 hours, n=5 (top), basal media 21 days, n=2 (middle) or MSCs in osteogenic media 21 days, n=3 (bottom). 1x106 cells were cultured in a 10cm dish for stated amount of time before *N*-glycan harvest, and further processing. Glycan peaks were identified using calculated mass of monosaccharide units and knowledge of the synthesis pathway. Glycans had to have two isotopic peaks, 3x above noise to be included. Major peaks between 1500m/z and 2400m/z are mostly oligomannose glycans, whilst those over 2500m/z are typically complex type glycans. Spectrum shown covers 1000m/z to 5250m/z.

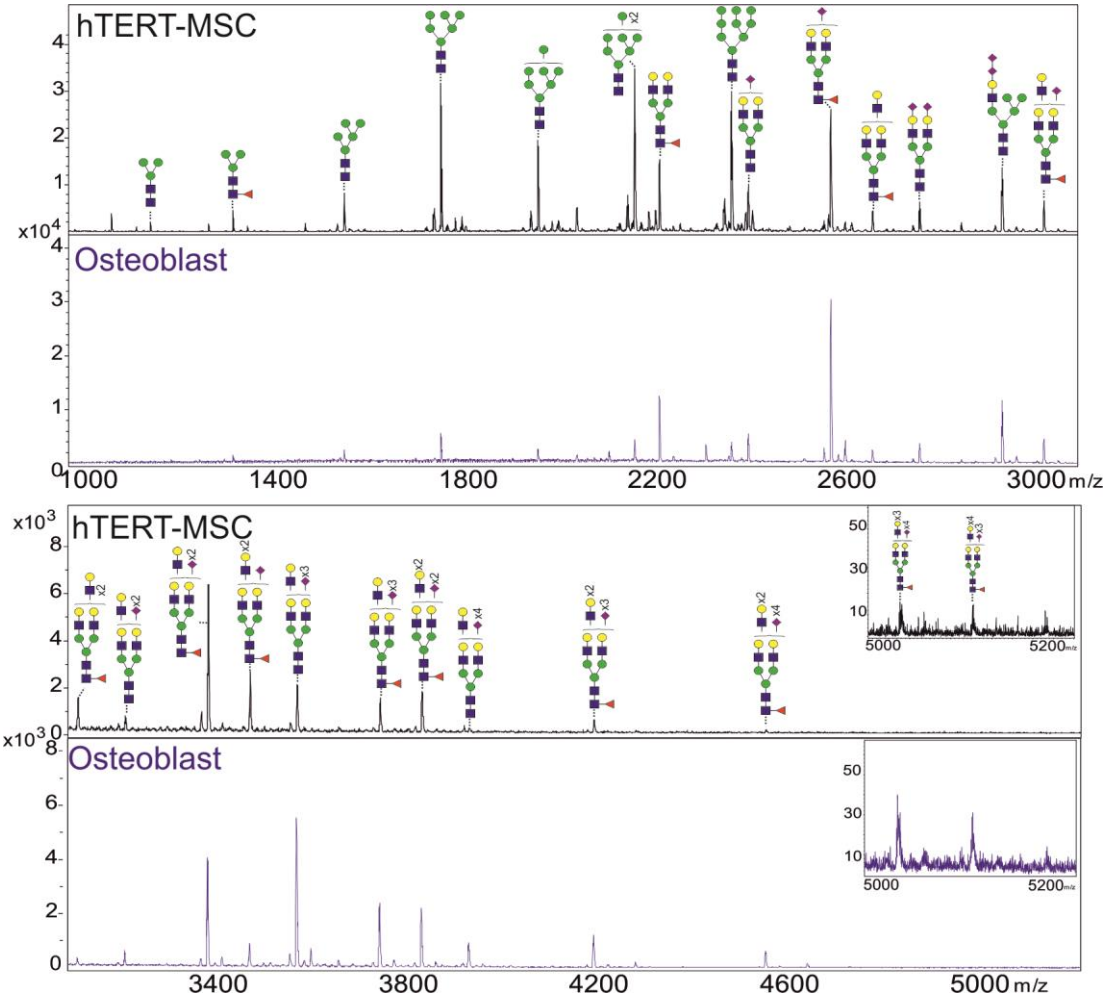

Figure 3.6 Comparison of mass spectrum of glycans isolated from MSCs or Osteoblasts.

hTERT-MSCs were cultured in either basal media for 24 hours (black spectrum) or osteogenic media for 21 days (blue spectrum), prior to glycan harvesting, further processing and analysis by mass spectrometry. Glycan peaks were identified using calculated mass of monosaccharide units and knowledge of the synthesis pathway. Glycans had to have two isotopic peaks, 3x above noise to be included. Spectrum shown are from 1000m/z to 5250m/z split into two sections.

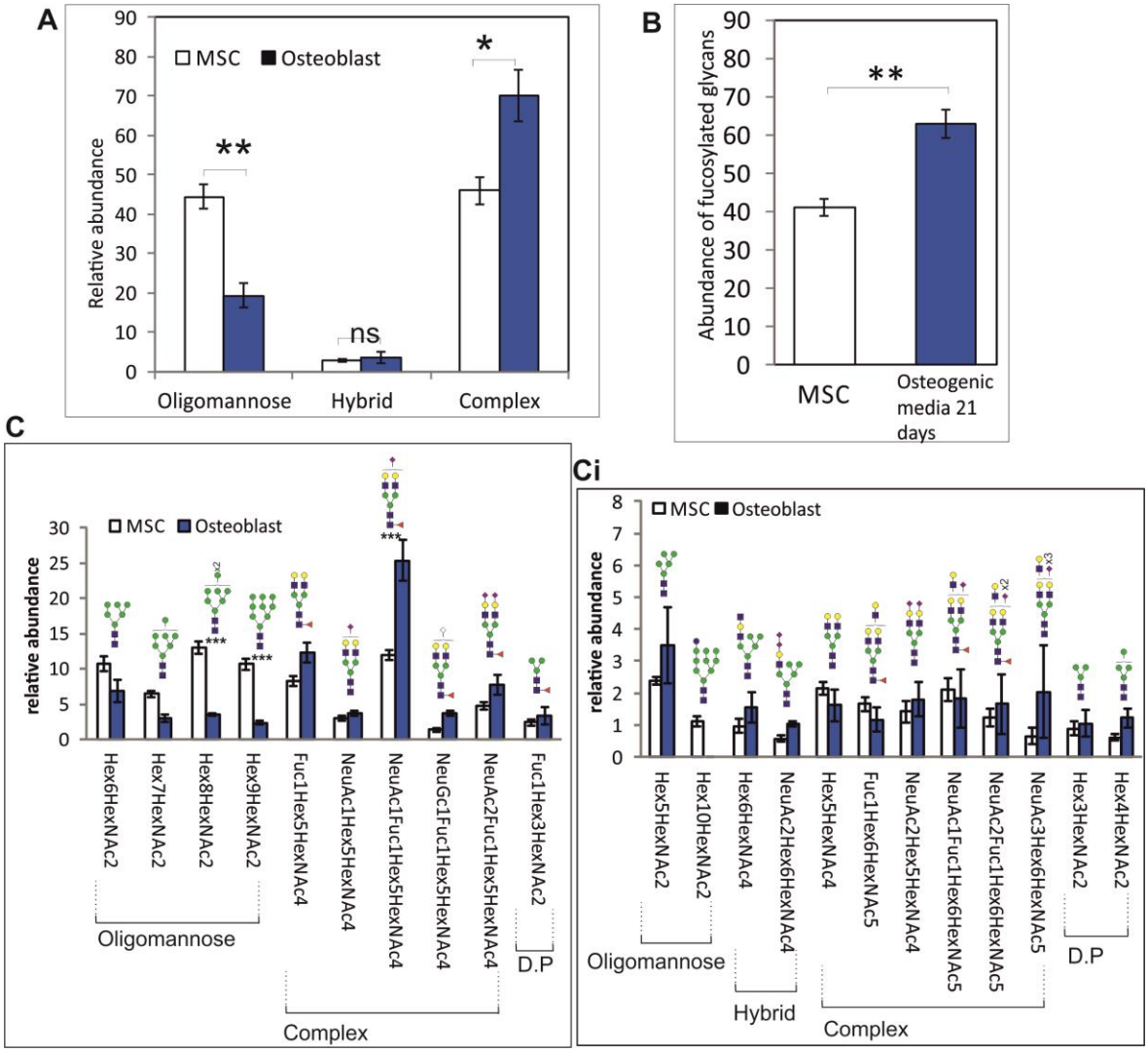

Figure 3.7 Glycan analysis of hTERT-MSCs and osteoblasts derived from them.

hTERT-MSCs were cultured in either basal media for 24 hours or osteogenic media for 21 days (osteoblast samples), prior to glycan harvesting, further processing and analysis by mass spectrometry. Glycans identified from spectrum were classed by type (A) and if they were fucosylated or not (B). Student's T Test, *=P<0.05, **=P<0.01, ns =not significant. The normalised, average peak intensity of individual glycan structures were also compared. Those present above 3 au (out of 100) in either MSC or osteoblasts are shown in (C) and those above 1 au in (Ci). One way ANOVA, with Holm Sidak post-hoc tests, ***=P<0.001, all other glycan pairs were not significantly different. Error bars show standard error of the mean.

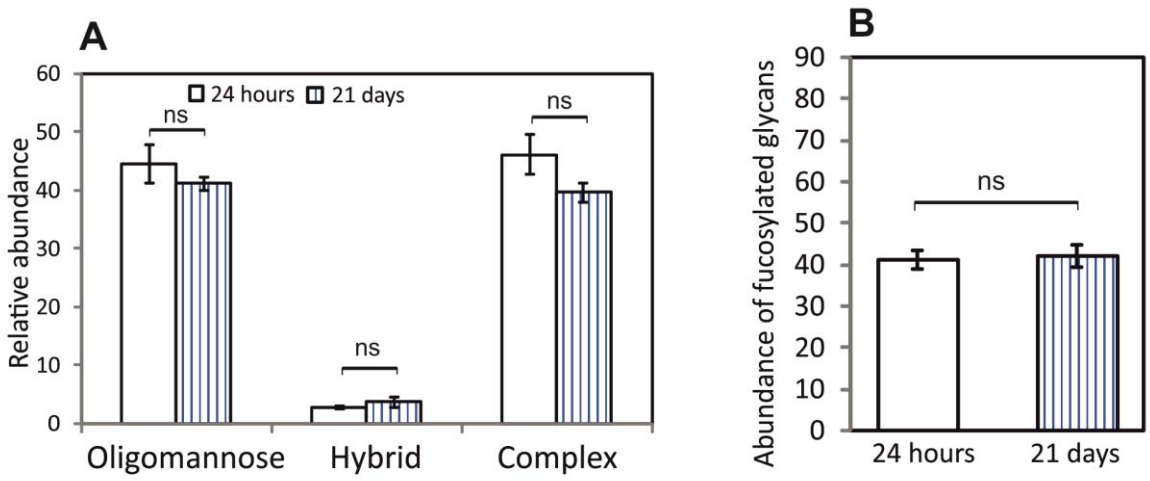

Figure 3.8 Glycan analysis of hTERT-MSCs in basal media for 24 hours or 21 days.

hTERT-MSCs were cultured in basal media for either 24 hours or 21 days prior to glycan harvesting, further processing and analysis by mass spectrometry. Glycans identified from spectrum were classed by type (A) and if they were fucosylated or not (B). Student's T Test, ns =not significant. Error bars show standard error of the mean.

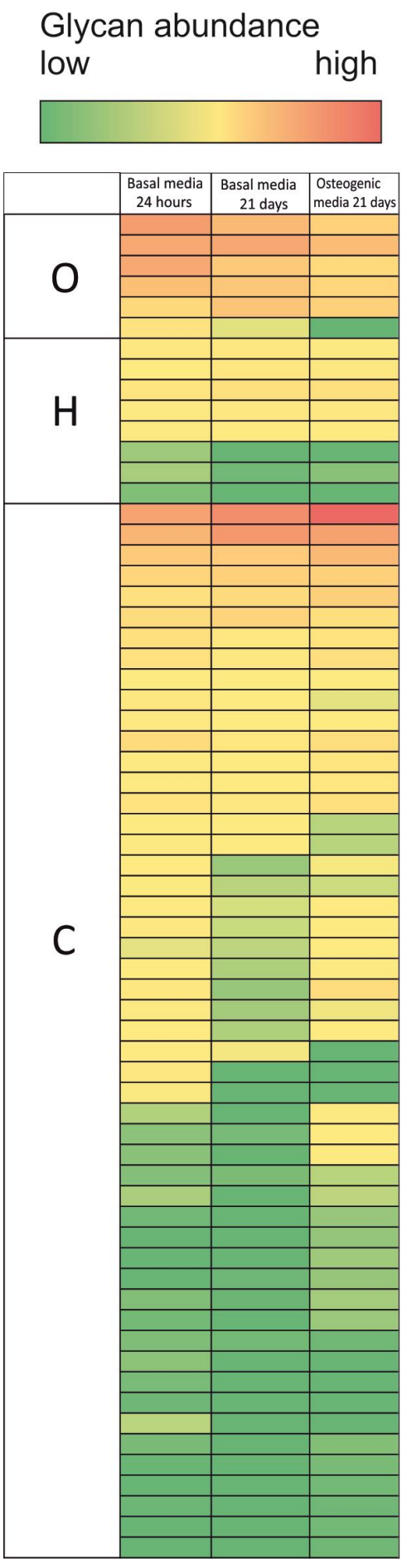

Figure 3.8a Heat map comparing glycan profile of hTERT-MSCs after culture for 24 hours in basal media, 21 days in basal media, or 21 days in osteogenic media.

Glycan peaks were identified from mass spectrometry spectra (basal media 24 hours n=5, cells in basal media for 21 days n=2, osteogenic media n=3). For each structure identified, the total peak intensities were summed, normalised and average (see materials and methods for details). Each row in the map shows average abundance of a single glycan structure in each of the cell types. Glycans have been grouped by type, O=Oligomannose, H= Hybrid and C=Complex type glycans. Colour denotes relative abundance, between all samples

3.3.4 The Y101, Y201 and Y202 hTERT-MSCs have similar glycan profiles

In order to compare the hTERT-MSC lines each cell type was cultured at a density of 10^6 cells/10cm dish, 24 hours in basal media, prior to harvest by FANGS. Spectrum from at least 4 biological repeats were averaged for each cell type (Y101 n=5, Y201 n=4, and Y202 n=5). The mass spectrometry spectra from the different hTERT-MSC lines appeared similar (Figure 3.9). When the abundance of individual glycans were grouped by structure type, there was no significant difference between the hTERT-lines (Figure 3.10 Comparison of glycans isolated from 3 hTERT-MSC lines.). However, there was a visible trend that the Y101 and Y202 hTERT-MSCs were more similar than the Y201 hTERT-MSCs, several oligomannose glycans, i.e. Hex6HexNAc2 and Hex9HexNAc2, were more abundant in Y201 cells compared to both Y101 and Y202 hTERT-MSCs (Figure 3.10). Analysis of individual glycan structures showed that $NeuAc_2Fuc_1Hex5HexNAc_2$, was significantly less abundant in Y201s compared to Y101 and Y202 hTERT-MSCs (One way ANOVA, Holm Sidak post hoc, $P<0.05$, n=4 or 5) (Figure 3.10 C). The heat-map display of the glycan profiles of the hTERT-MSC lines and osteoblasts shows visually, that the 3 hTERT-MSC lines are all similar (Figure 3.10a). Furthermore, the Y101 hTERT-MSCs, despite potentially representing osteogenic progenitors, were as distinguishable from the osteoblasts, as the other hTERT-MSC lines (Figure 3.10a).

Although these results showed that the *N*-glycan profile of the 3 hTERT-MSC lines was not as varied as their differentiation capacity, it did not rule out the contribution of glycans to differentiation. Differences in genome and proteome are likely responsible for the variation in the differentiation capacity of the hTERT-MSC lines. A genetic approach was used in the next chapter, to test the role of glycans in osteogenesis.

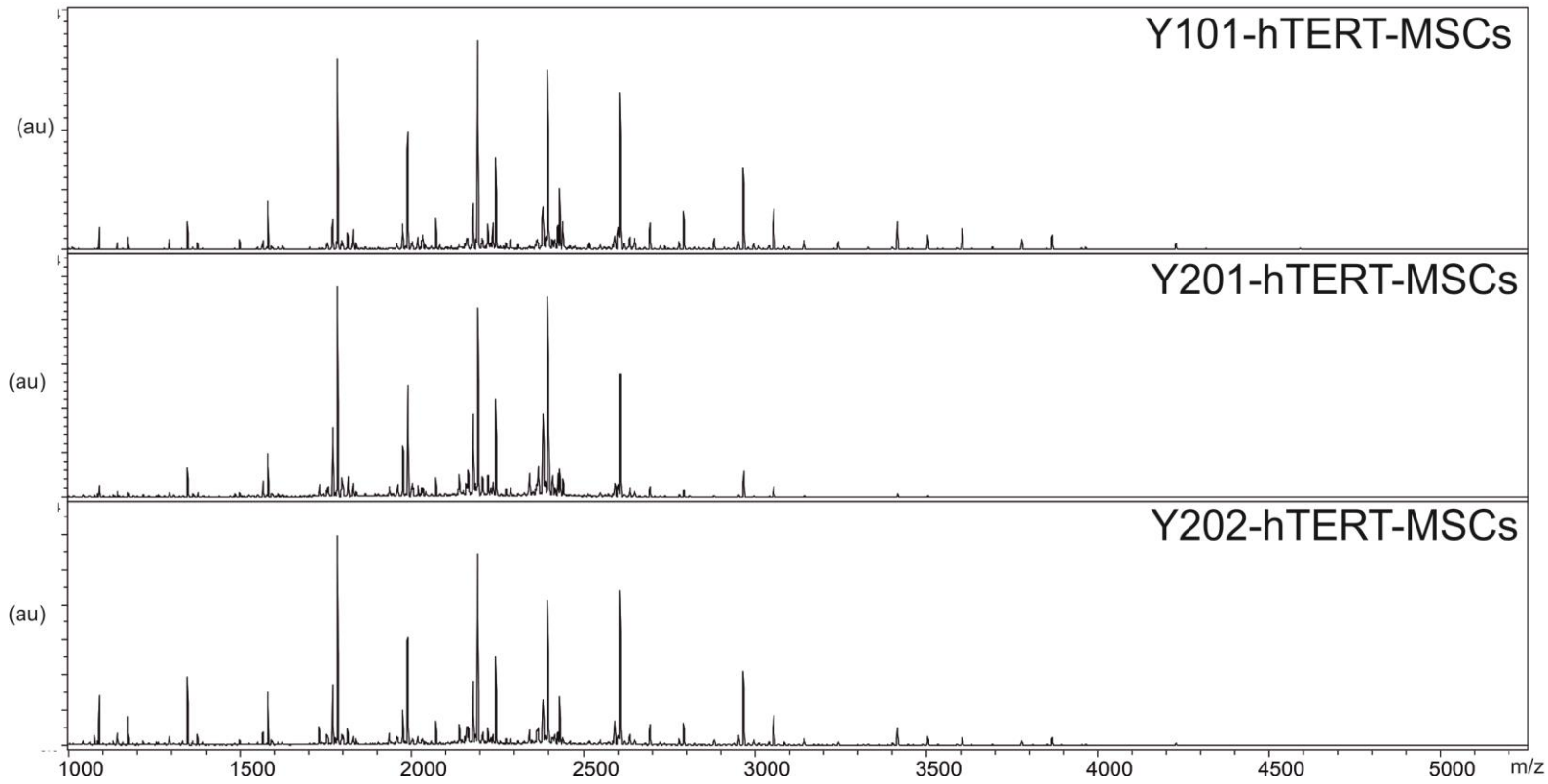

Figure 3.9 MALDI-TOF/TOF spectrum of *N*-glycans from 3 hTERT-MSC lines.

One representative spectrum of *N*-glycans isolated from Y101 hTERT-MSCs (n=5), Y201 hTERT-MSCs (n=4) and Y202 hTERT-MSCs (n=5). 1x106 cells were cultured in a 10cm dish, overnight prior to glycan harvest and further processing. Full spectrum from 1000m/z to 5250m/z shown above for each cell line.

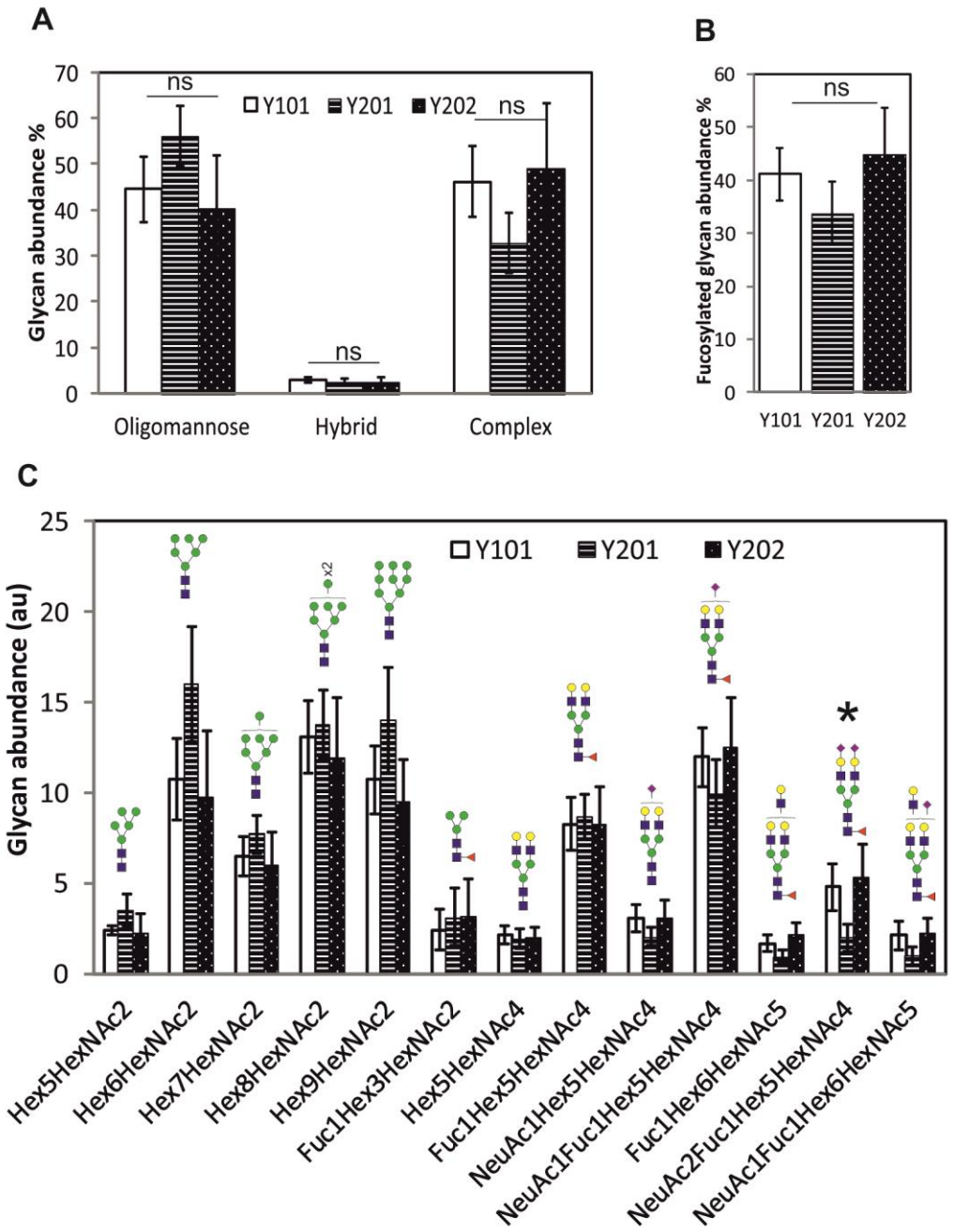

Figure 3.10 Comparison of glycans isolated from 3 hTERT-MSC lines.

Glycans identified from spectrum were classed by type (A) and if they were fucosylated or not (B). The normalised, average peak intensity of individual glycan structures identified were also compared. Those present above 2 (out of 100) in either hTERT spectrum are shown in (C), with predicted structure above. Error bars show standard deviation. One way ANOVA, ns = not significant, n=5, 4 and 5, for Y101, Y201 and Y202 respectively. In C, * highlights a differential expressed glycan, $NeuAc_2Fuc_1Hex_6HexNAc_5$, $P<0.05$ between Y101 and Y201, and Y201 and Y202. Abundance in Y101 and Y202 was not significantly different. One way ANOVA, Holm Sidak post-hoc test.

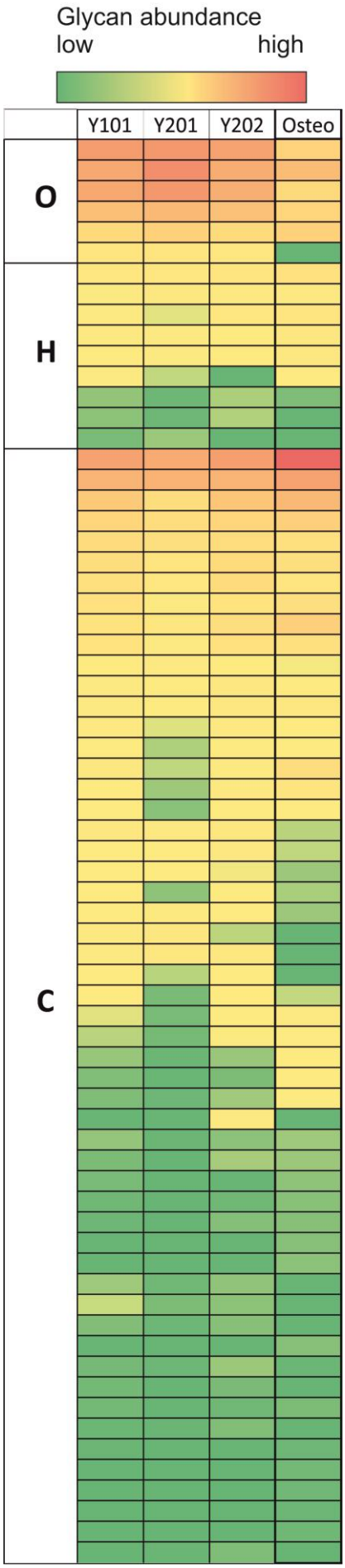

Figure 3.10a Heat map comparing glycan profile of Y101, Y201 and Y202 hTERT-MSCs, and osteoblasts derived from Y101 hTERT-MSCs.

Glycan peaks were identified from mass spectrometry spectra (Y101 n=5, Y201 n=4, Y202 n=5, osteoblasts (Osteo) n=3).For each structure identified, the total peak intensities were summed, normalised and average (see materials and methods for details). Each line in the map shows average abundance of a single glycan structure in each of the cell types. Glycans have been grouped by type, O=Oligomannose, H= Hybrid and C=Complex type glycans. Colour denotes relative abundance, between all samples.

3.4 Chapter 3 Conclusion

In order to investigate the role of glycans in MSC differentiation, the *N*-glycan profile of immortalised MSC lines and osteoblasts derived from them were compared. Three immortalised, primary human hTERT-MSC lines were shown to have varied differentiation capacity *in vitro*. These results supported the theory of a heterogeneous population of MSCs with mixed differentiation capacities. The ability of one line, Y101 hTERT-MSCs, to differentiate into osteoblasts was further characterised using several markers. During culture in osteogenic media the Y101 hTERT-MSCs had increased ALP activity and increased mineralised extracellular matrix compared to basal controls. Furthermore, Y101 hTERT-MSCs expressed increased levels of osteoblast associated genes Runx2, BMP and BSP, during culture in osteogenic media, compared to basal controls. Mass spectrometry was used to profile the *N*-glycans of Y101 hTERT-MSCs and osteoblasts derived from them. Osteoblasts had significantly more complex glycans and less oligomannose type glycans. The abundance of fucosylated glycans was significantly increased in the osteoblast samples.

To determine if a glycan profile could be used to predict differentiation capacity, the glycan profile of 2 other hTERT-MSC lines (Y201 and Y202) were compared to Y101 hTERT-MSCs and osteoblasts derived from them. Despite having varied differentiation abilities, the glycan profile of the 3 hTERT-MSC lines appeared very similar. There were no significant differences in the abundance of glycans when grouped by structure type. One individual glycan structure, which was a sialylated, biantennary, fucosylated, complex glycan, was significantly less abundant in Y201 hTERT-MSCs compared to the other two. There was a trend for Y101 and Y202 glycan profiles to group away from that of Y201s.

It is not possible to rule out the possibility that one of the hTERT-MSC lines has a single glycoprotein, which is alternatively glycosylated and functioning as consequence, differently, contributing to the lines differentiation capacity. Changes in glycosylation to single glycoproteins are likely beyond the detection limit of this total cellular, glycan profiling approach. Previous, studies have shown that small changes to single, glycoprotein can affect cell behaviour, such as changes to CD44's glycoform, affecting ability of MSCs to migrate to bone marrow [120]. Considering the dissimilarity in differentiation potential, and the overall resemblance of the glycan profiles, it was

concluded that the glycan profile of hTERT-MSC subpopulations, using this method, could not be used to predict their osteogenic differentiation capacity.

In the following chapter the glycan synthesis pathway was disrupted genetically, and the effect on osteogenic capacity assessed, using the same osteogenic assays introduced in this chapter.

Chapter 4 Genetic disruption of the glycosylation pathway

4.1 Rationale for genetic disruption of glycosylation pathway

The broad aim of this research was to investigate the role of glycans in MSC differentiation. In the previous chapter, mass spectrometry was used to profile the *N*-glycans of immortalised MSC lines and of osteoblasts derived from them. In agreement with previously published results, the *N*-glycan profile was significantly altered in the osteoblasts, which had a higher abundance of complex glycans [118]. However, MSC lines with varied osteogenic potential were found to have similar *N*-glycan profiles, disproving the idea that glycan profiles could be used to predict the osteogenic capacity of sub-populations of MSCs. Although *N*-glycans do not appear to be markers of differentiation potential, the question remains as to whether *N*-glycans have a functional role during the process of differentiation. In this chapter a genetic approach was used to determine the role of glycans in osteogenesis. Here, glycosylation synthesis was disrupted genetically and the ability of MSCs to then differentiate into osteoblasts was assessed.

A simple method to look at the function of glycans would be to target enzymes responsible for their synthesis and then observe the effect on phenotype. However, the strategy to knock-down or knock-out a single Golgi resident enzyme was not chosen for several reasons. For one, there are different isoforms of enzymes at each stage of glycan processing that provide redundancy and would each need to be targeted. For example there are at least 3 different α1,2-mannosidase enzymes [133], and 19 different mammalian galactosyltransferases [134]. Disruption of enzymes responsible for the production of precursor monosaccharides, or of enzymes in the ER at the beginning of the synthesis pathway, would inhibit *N*-glycan formation. However, this would impede the exit of glycoproteins from the ER, leading to ER and cellular stress [135], which would hinder the interpretation of any changes to cellular behaviour.

Instead, in the following chapter the Golgi organisation was perturbed by targeting COG with a shRNA. COG is responsible for the retrograde traffic of vesicles in the Golgi. This maintains the specific distribution of enzymes in different cisternae, which is required for glycan chain modulation. Although targeting COG should disrupt glycosylation, glycoproteins are likely to be trafficked to the cell surface. This allowed the role of the glycosylation to be tested, rather than the location of glycoproteins, or the effect of ER stress, unlike the strategies targeting specific enzymes in the E.R. This method, of

targeting COG is also advantageous, since several types of glycans are produced in the Golgi, disruption of COG may alter the processing or production of more than one type of glycan. Interestingly, COG related and other CDG patients display a wide variety of skeletal related symptoms such as: osteopenia, short limbs, and clinodactyly [121]. Added to this, Smits *et al* (2010) discovered that a form of lethal neonatal skeletal dysplasia is caused by mutations in Golgi microtubule-associated protein 210 (GMAP-210), which is responsible for maintaining Golgi architecture [136]. Altogether this indicates that the disruption of Golgi organisation, via COG-knock-down, should affect glycosylation and as a consequence may alter the differentiation of MSCs into osteoblasts.

COG is an 8 subunit protein with subunits divided into lobe A and lobe B. Out of the 8 subunits Cog4 was selected to be knocked-down by shRNA, in part because the crystal structure of a part of this subunit has been solved [124]. In the same study, HeLa cells with mutations to Cog4 had glycosylation defects [124]. Moreover, analysis of fibroblasts from a CDG patient, with a mutation in Cog4 showed reduced sialylation and galactosylation [65]. In addition, Cog4 is a subunit in lobe A and in yeast studies mutations to subunits in lobe A are lethal, whilst mutations in lobe B are less severe [12]. This may indicate that knocking-down Cog4 could have a greater effect than targeting a lobe B subunit. Together these studies suggest that Cog4 knock-down will cause glycosylation defects in MSCs.

Primary human MSCs senesce in culture after several passages. In light of this, the immortalised human MSC line - Y101 hTERT-MSC - characterised in the previous chapter was used. This allowed the production of Cog4 knock-down lines, derived from a single cell. Furthermore, the unlimited supply of cells enabled the same cell population to be tested in assays for phenotype, glyco-type and osteogenic potential. This avoided the variation of cell behaviour seen with primary MSCs isolated from different donors [137] to affect the interpretation of results. Some of the experimental work involving Cog4KD hTERT-MSCs was performed by an undergraduate student working under my supervision. Their contributions are acknowledged on the relevant figures.

4.2 Chapter 4 Aims

The aim of the work described in this chapter was to disrupt the glycosylation pathway genetically and to then assess the effect on osteogenesis.

More specifically, the aim was to generate single-cell-derived lines of Y101 hTERT-MSCs in which Cog4 is knocked down, using two different shRNAs. The use of two different shRNAs was to control for non-specific targets of a shRNA, which could mask the effect of reduced Cog4 levels. Following this, the aim was to verify the predicted effect of Cog4 knock-down on the glycosylation of MSCs, using lectins and flow cytometry, plus mass spectrometry. Finally, I assessed the effect of Cog4-knock down on MSC phenotype and osteogenic potential by comparing the change in gene and protein expression seen in wildtype Y101 hTERT-MSCs during osteogenesis to that of Cog4-knock down cells, as well as monitoring the functional capability of the cells, by testing for calcium phosphate deposition.

4.3 Chapter 4 Results

4.3.1 Generation of Cog4-knock-down (Cog4KD) hTERT-MSCs

In order to genetically disrupt the glycosylation pathway hTERT-MSCs were transduced using lentivirus containing shRNA targeting Cog4. Five different shRNAs were used and assigned a letter A-E (see methods for details). Initially, shRNAs A, C and D were tested. During transduction a multiplicity of infection (MOI) of 1 and 10 was used. After transduction, colonies derived from single cells were cultured and protein harvested for analysis by western blot (Figure 4.1part i and ii). The efficiency of knock-down varied amongst the different colonies. Transduction using an MOI of 10 did not appear to increase the level of Cog4 knock-down achieved. Also hTERT-MSCs that were transduced using shRNA 'C' using an MOI of 10, were viable, but failed to form any colonies. In light of this, a MOI of 1 and 3 was used during transduction with lentivirus containing the shRNAs B and E. Again there was varied efficiency in the degree of Cog4 knock-down between the shRNAs and among the colonies (Figure 4.1part iii and iv). Of the colonies isolated and tested, those produced with shRNAs B, C or E expressed less Cog4 protein compared to WT than those produced using shRNA A or D. Two colonies with the greatest reduction in Cog4 protein, which were produced using shRNA C and B, were further expanded. These were named Cog4KDshRNA1 and Cog4KDshRNA2 respectively (Figure 4.1 red boxes). In order to confirm that Cog4 knock-down had disrupted glycosylation, the glycan profile of the Cog4KD hTERT-MSCs was determined.

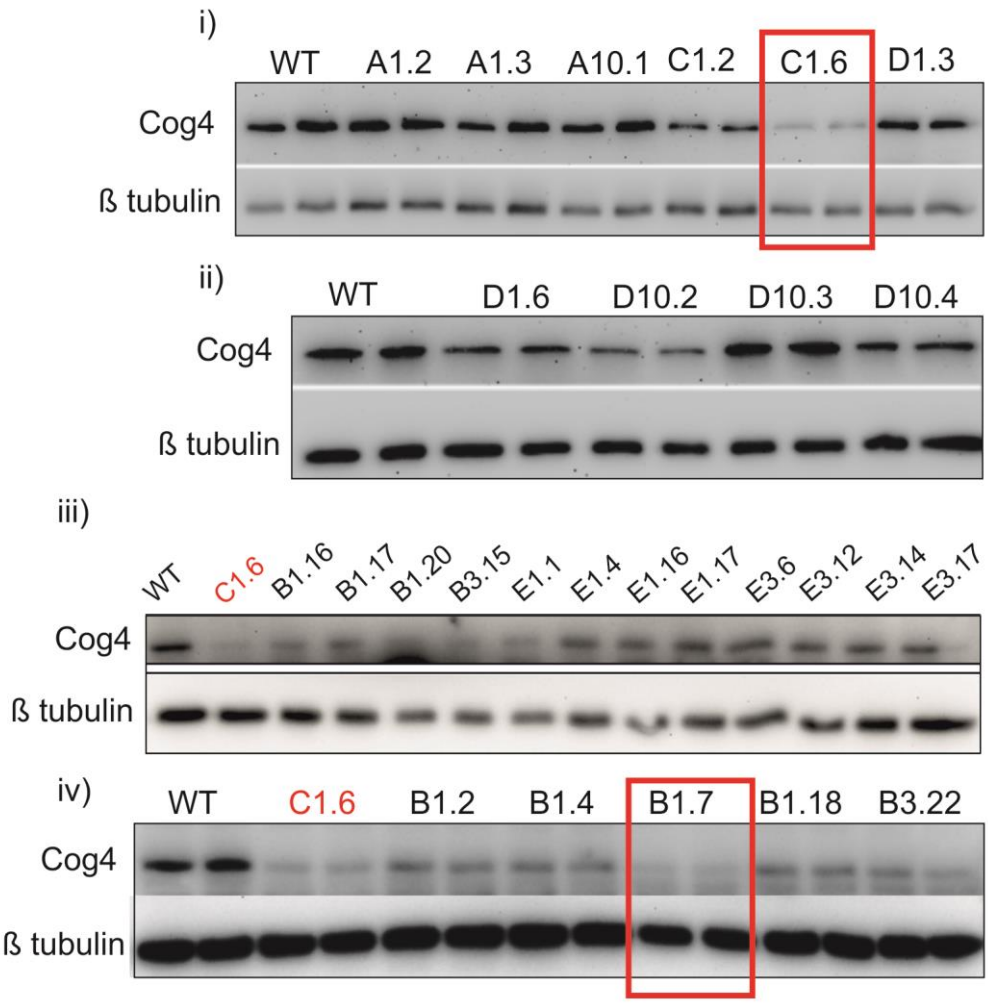

Figure 4.1 Western blots of single-cell derived colonies of Cog4KD hTERT-MSCs.

Whole cell lysates from wildtype (WT) hTERT-MSCs and colonies of Cog4KD hTERT-MSCs were run on SDS-gels prior to transfer onto PVDF membrane and immunoblotting using antibodies against Cog4 and ß tubulin. Cog4KD colonies were created using 5 different shRNAs named: A, B, C, D, and E. Different multiplicities of infection (MOI) were used, denoted by the first number in each colony name. The second number in each colony name was assigned during culture to distinguish between colonies with the same shRNA and same MOI. Samples were loaded in duplicate in blots i, ii, and iv. The red boxes highlight the colonies expanded in culture and used in further work. For simplicity C1.6 is referred to as Cog4KDshRNA1 and B1.7 is referred to Cog4KDshRNA2 in all further work.

4.3.2 Cog4KD hTERT-MSCs have an altered glycan profile

4.3.2.1 Flow cytometry identified similarities and differences in the glycosylation of WT and Cog4KD hTERT-MSCs

To find out if glycan synthesis was altered in Cog4KD hTERT-MSCs, cells were stained with several lectins and then analysed using flow cytometry. Prior to this experiment, WT hTERT-MSCs were used to test the affinity of each lectin. For all the lectins bar MAL II, the fluorescence histogram of the cells incubated with lectins alone shifted positively away from the histogram of cells incubated with lectins and an appropriate monosaccharide that competes with lectin binding. This demonstrated that the lectin staining was positive and specific (Figure 4.2). The lectin MAL II was conjugated to biotin and required incubation with streptavidin bound to fluorescein to analyse the cells by flow cytometry. The fluorescent histogram of cells stained with MAL II was not significantly different from that of cells incubated with streptavidin-fluorescein alone (Figure 4.2G)

To detect small differences in staining, 3 to 4 experimental repeats were carried out, and the data was normalised to WT in each repeat. This was to account for the variation in absolute fluorescence intensity between experimental runs. The staining of WT and Cog4KD hTERT-MSCs was positive with: ConA, WGA, PNA, SNA, Jacalin and VVL lectins (Figure 4.3, Figure 4.4, Figure 4.5). ConA binds to the core mannose structure present in all *N*-glycans, and is not known to bind to O-glycans. WGA binds to GlcNAc either terminally or within multiple glycan structures. There was no significant difference in staining with ConA or WGA lectins, between WT and Cog4KDhTERT-MSCs (Figure 4.3I and ii). The coefficient of variation (half-max) - CV(hm) – is a statistic used to measure the width of a population. The Cog4KDshRNA2 hTERT-MSCs stained with WGA (Figure 4.3B) had a significantly higher CV(hm) than WT (One-way ANOVA, Holm-Sidak post hoc, n=4, $P<0.001$). This suggested a more varied amount of staining among the cells, despite the similarity in median fluorescence (Figure 4.3). SNA and MAL II are lectins that bind to sialic acid residues of glycans. MAL II binds to sialic acid in a (α 2, 3) linkage, whilst SNA prefers structures with sialic acid in a (α 2, 6) linkage. Staining with MAL II was not above controls for all cell types (Figure 4.4A).SNA staining was significantly lower ($P<0.001$) in both Cog4KD hTERT-MSC lines compared to WT (Figure 4.4B). The CV(hm) of Cog4KDshRNA1 hTERT-MSCs stained with SNA was significantly higher ($P<0.05$), suggesting a greater variation in staining compared to WT hTERT-MSCs (Figure 4.4Biii).

This indicated that Cog4 knock-down in hTERT-MSCs resulted in significantly reduced glycan sialylation.

Some lectins, such as WGA described above, bind to glycan structures present in several types of glycans. PNA, Jacalin and VVL preferentially bind to structures present in O-glycans. Jacalin binds to the T-antigen structure (galactosyl (β-1,3) N-acetylgalactosamine), whether it is sialylated or not. Staining with Jacalin was positive for all cell types, with no significant difference between them (Figure 4.5A). Although PNA binds to the same structure as Jacalin, binding is inhibited if the structure is sialylated. Staining with PNA was increased in Cog4KD hTERT-MSCs (Figure 4.5B), indicating decreased O-glycan sialylation in Cog4KD hTERT-MSCs, which correlates with the reduced O-glycan sialylation seen in COG CDG patient ApoCII samples [63, 66, 70]. VVL binds to a single α-N-acetylgalactosamine linked to serine or threonine (Tn antigen). The Cog4KD hTERT-MSCs had a small, significant reduction in VVL staining compared to WT (Figure 4.5C). The Tn-antigen structure is the beginning of all O-glycan structures. A reduction in VVL staining could mean fewer O-glycan chain initiation sites, or fewer truncated O-glycans, with an increase in conversion of Tn-antigen into T-antigen structures instead. It is possible that disrupted Golgi-enzyme trafficking in Cog4KD hTERT-MSCs could lead to a combination of these changes occurring.

Altogether these results show the presence of similar glycan structures in WT and Cog4KD hTERT-MSCs. Yet importantly, the Cog4KD hTERT-MSCs had a significant reduction in sialylated O- and/or *N*-glycans, as well as reduced abundance of Tn antigen structures.

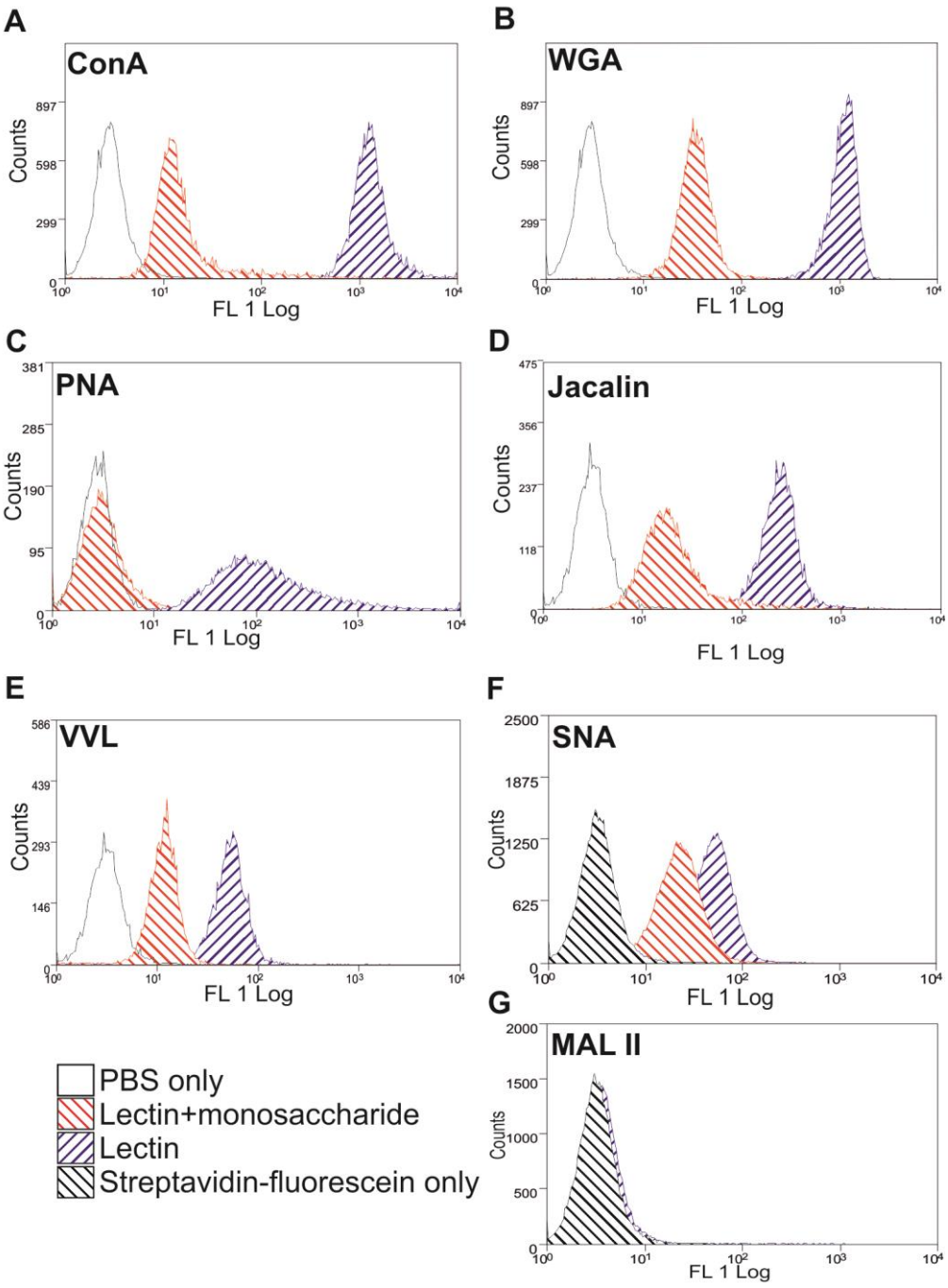

Figure 4.2 Flow cytometry analysis of lectin affinity.

To check the affinity of lectins for glycans, WT hTERT-MSCs were incubated with; PBS (black outline); lectin and appropriate monosaccharide at 0.5M (red stripe) ; or with lectin alone (blue stripe). All lectins apart from SNA and MAL II were directly conjugated to fluorescein. SNA and MAL II were biotin labelled and used streptavidin tagged with fluorescein. Staining with SNA and MAL II was compared to cells incubated with streptavidin-fluorescein alone (black stripe) instead of PBS. Histograms show log fluorescence of samples stained with A) ConA, B) WGA, C) PNA, D) Jacalin, E) VVL F) SNA and G) MAL II. MAL II was not tested with a monosaccharide, as staining was not above negative control levels.

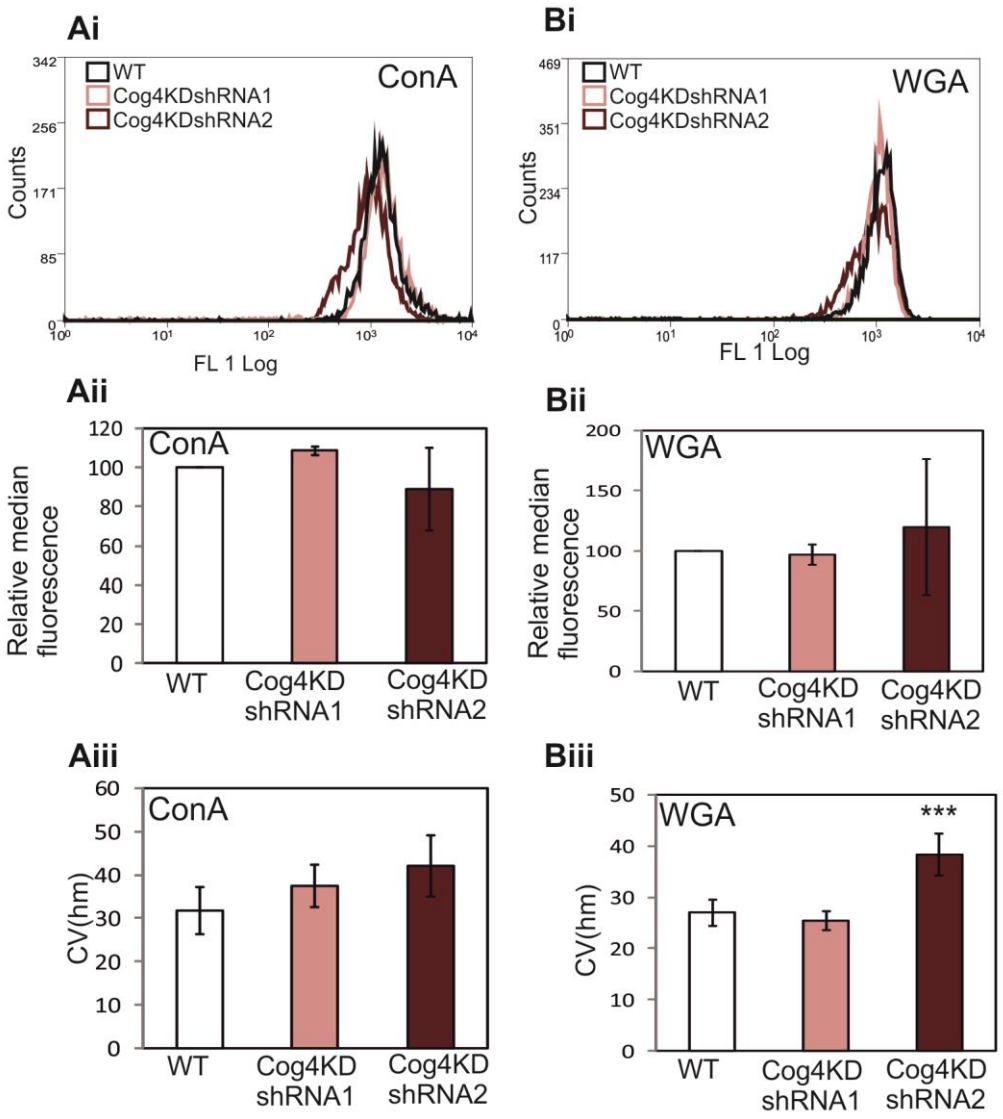

Figure 4.3 Flow cytometry analysis of WT, Cog4KDshRNA1 and Cog4KDshRNA2 hTERT-MSCs with ConA and WGA lectins.

WT, Cog4KDshRNA1 and Cog4KDshRNA2 hTERT-MSCs were probed with A) ConA and B) WGA lectins. Histograms i) show log fluorescence of WT (black), Cog4KDshRNA1 (pink) and Cog4KDshRNA2 (dark red) hTERT-MSCs after staining with lectin. The median fluorescence values were made relative to WT. The average relative fluorescence values of 4 independent experiments are shown in ii). The average Coefficient of variation (Half max) (CV (hm) are shown in iii). Error bars are standard deviation One way Anova, with Holm-Sidak post-hoc test, n=4, *** = P<0.001.

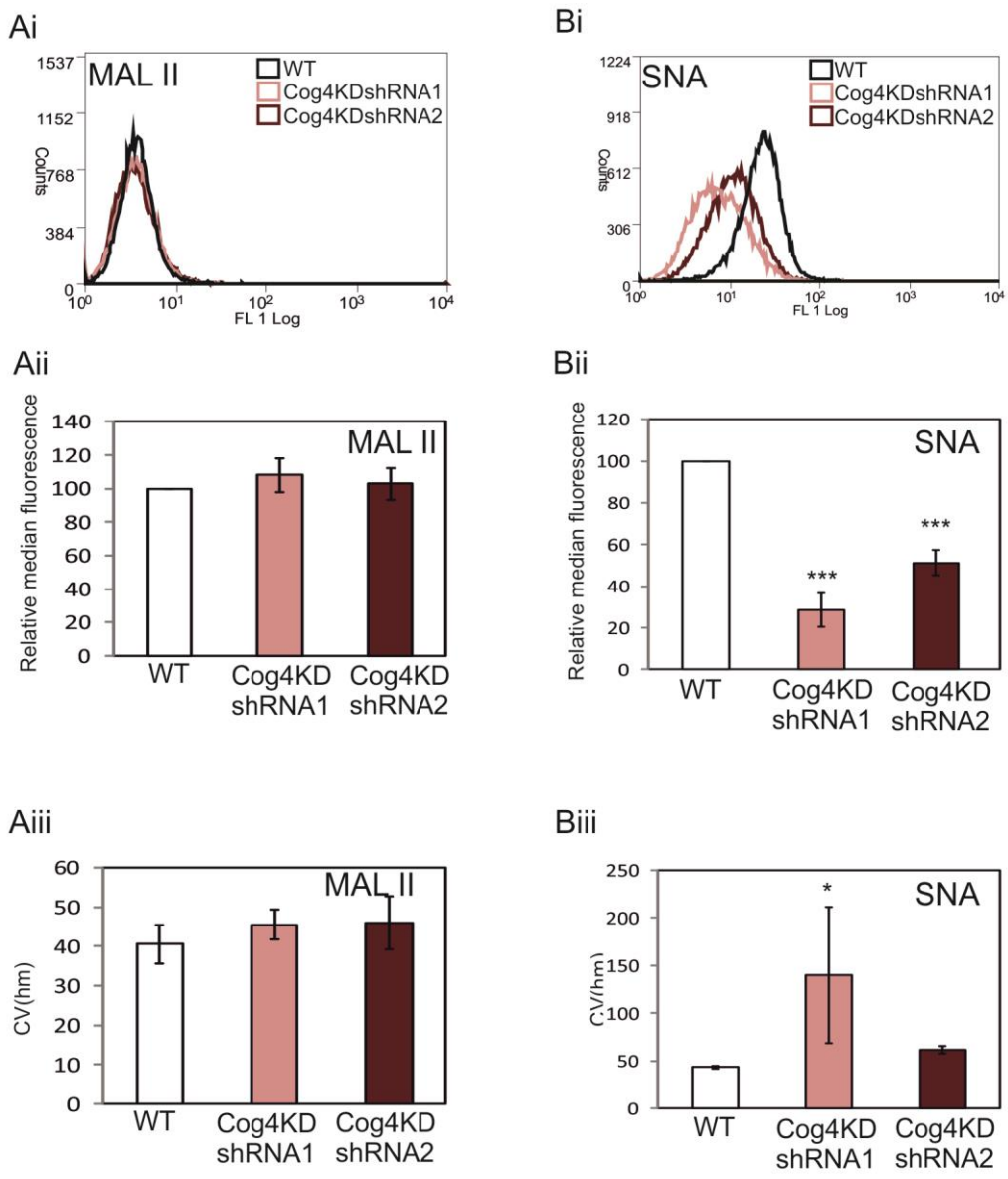

Figure 4.4 Flow cytometry analysis of WT, Cog4KDshRNA1 and Cog4KDshRNA2 hTERT-MSCs with MAL II and SNA lectins.

WT, Cog4KDshRNA1 and Cog4KDshRNA2 hTERT-MSCs were probed with A) MAL II and B) SNA lectins. Histograms i) show log fluorescence of WT (black), Cog4KDshRNA1 (pink) and Cog4KDshRNA2 (dark red) hTERT-MSCs after staining with lectin. The median fluorescence values were made relative to WT. The average relative fluorescence values of 3 independent experiments are shown in ii). The average Coefficient of variation (Half max) (CV (hm)) values, are shown in iii). Error bars show standard deviation. One way Anova with Holm-Sidak post-hoc test, n=3, * = P<0.05, ***= P<0.001.

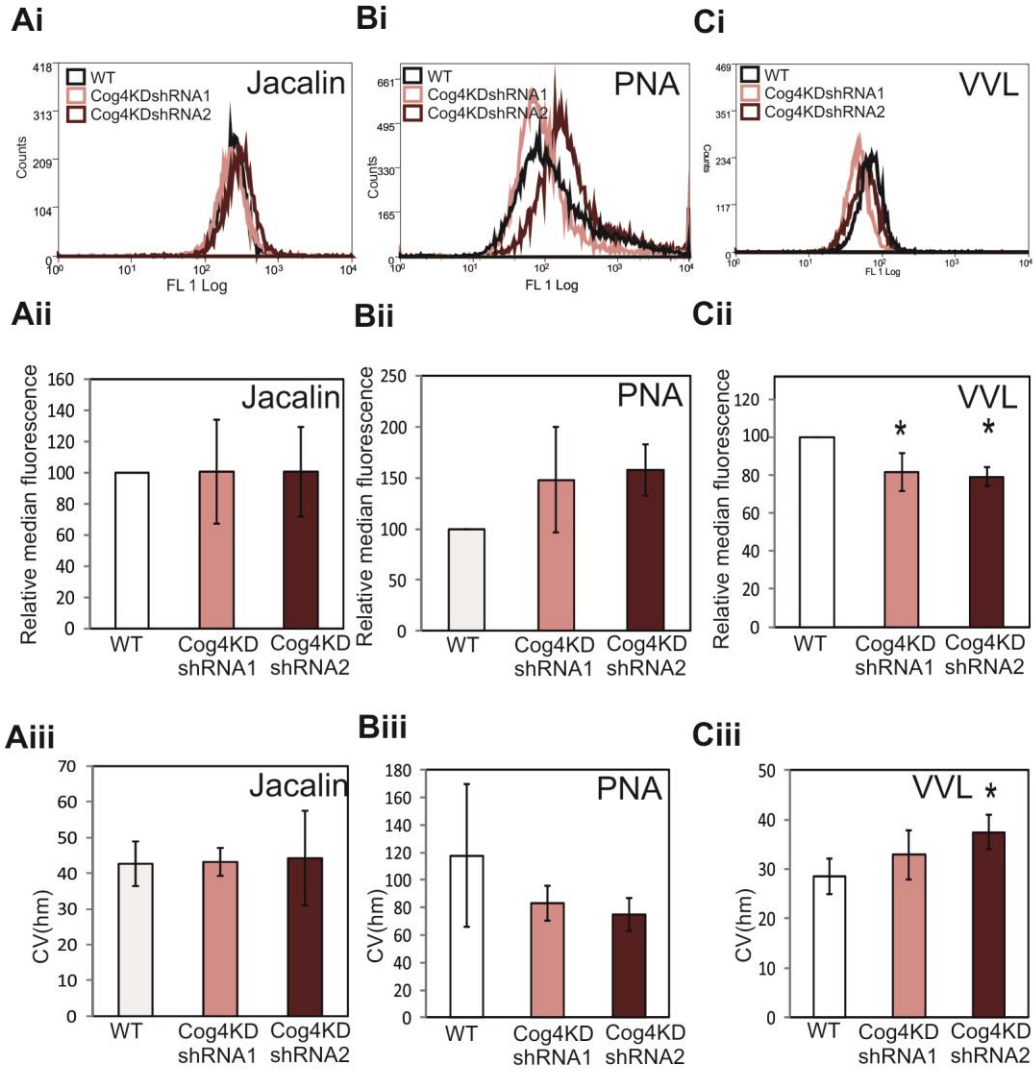

Figure 4.5 Flow cytometry analysis of WT, Cog4KDshRNA1 and Cog4KDshRNA2 hTERT-MSCs with Jacalin, PNA and VVL lectins.

WT, Cog4KDshRNA1 and Cog4KDshRNA2 hTERT-MSCs were probed with A) Jacalin, B) PNA and C) VVL lectins. Histograms i) show log fluorescence of WT (black), Cog4KDshRNA1 (pink) and Cog4KDshRNA2 (dark red) hTERT-MSCs after staining with lectin. The median fluorescence values were made relative to WT. The average relative fluorescence values of 4 independent experiments are shown in ii). The average Coefficient of variation (Half max) (CV (hm)) values, are shown in iii). Error bars show standard deviation. One way Anova on ranks, with Dunnett's post-hoc test using WT as control sample, n=4, * = $P<0.05$.

4.3.2.2 Cog4KD hTERT-MSCs are missing larger complex *N*-glycans

The largest difference in lectin staining between WT and Cog4KD hTERT-MSCs was in SNA staining. SNA can bind to sialic acid bound to terminal galactose, which is found in complex *N*-glycans, or, it can bind to sialic acid bound to GalNAc, found in O-glycans. In order to better determine the differences in *N*-glycan profile between WT and Cog4KD hTERT-MSCs, the more sensitive method of mass spectrometry was used. The *N*-glycans from Cog4KDshRNA1 were profiled, as this line showed the largest difference in SNA staining compared to WT.

The *N*-glycan profile of Cog4KD hTERT-MSCs contained 52 different *N*-glycan structures, all of which were present in the WT hTERT-MSC profile (Figure 4.6 and Figure 4.7). Complex type glycans were the most common (50%), followed by oligomannose (43%) and then hybrid type glycans (5%). The differences in abundance of each glycan type were not significantly different from WT hTERT-MSCs (Figure 4.8A). Of potential importance, 17 of the higher mass complex glycans, which were lowly abundant (<0.5 au) in WT hTERT-MSC spectrum, were absent from the Cog4KD hTERT-MSC spectrum in each biological replicate. Although not statistically significant, two smaller, complex glycan structures, $Fuc_1Hex_5HexNAc_4$ and $NeuAc_1Fuc_1Hex_5HexNAc_4$ were more abundant in Cog4KD than WT hTERT-MSCs (Figure 4.8C). When fucose containing glycan structures were grouped, there was no significant difference between cell types with 44% of the glycans from Cog4KD hTERT-MSCs containing at least one fucose sugar, compared to 41% of WT hTERT-MSCs glycans (Student's T Test, n=5 and 3) (Figure 4.8B). These results describe a similar *N*-glycan profile between WT and Cog4KD hTERT-MSCs. However, importantly the mass spectrometry data which showed Cog4KD hTERT-MSCs to have fewer high mass, complex *N*-glycans, indicates that reduced SNA staining was in part due to reduced *N*-glycan sialylation and not just reduced O-glycan sialylation.

In order to test if these higher mass complex *N*-glycans are required for osteogenesis, the osteogenic capacity of Cog4KDhTERT-MSCs was assessed. Prior to osteogenic analysis of Cog4KD hTERT-MSCs, the basic phenotypic attributes of shape and proliferation were assessed, as these can affect differentiation.

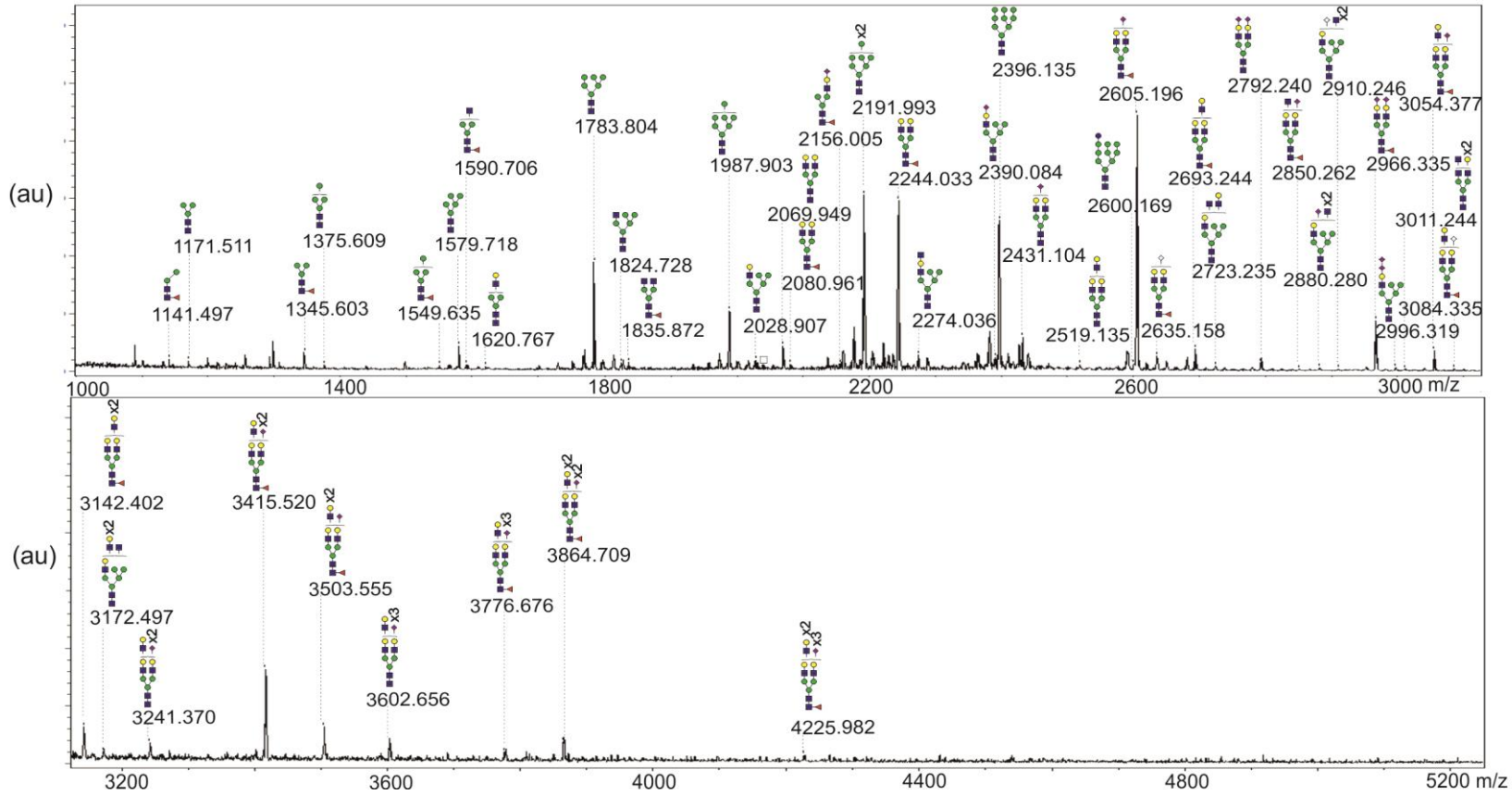

Figure 4.6 *N*-glycan spectrum of Cog4KD hTERT-MSCs.

A representative spectrum (n=3) of *N*-glycans isolated from Cog4KDshRNA1 hTERT-MSCs. 1x10^6 cells were cultured in a 10cm dish, overnight before *N*-glycan harvest, and further processing. Glycan peaks were identified using calculated mass of monosaccharides and knowledge of the synthesis pathway. Glycans had to have two isotopic peaks, 3x above noise to be included. Mass of mono-isotopic peak is labelled, with predicted structure pictured above. Spectrum shown is from 1000-5250m/z.

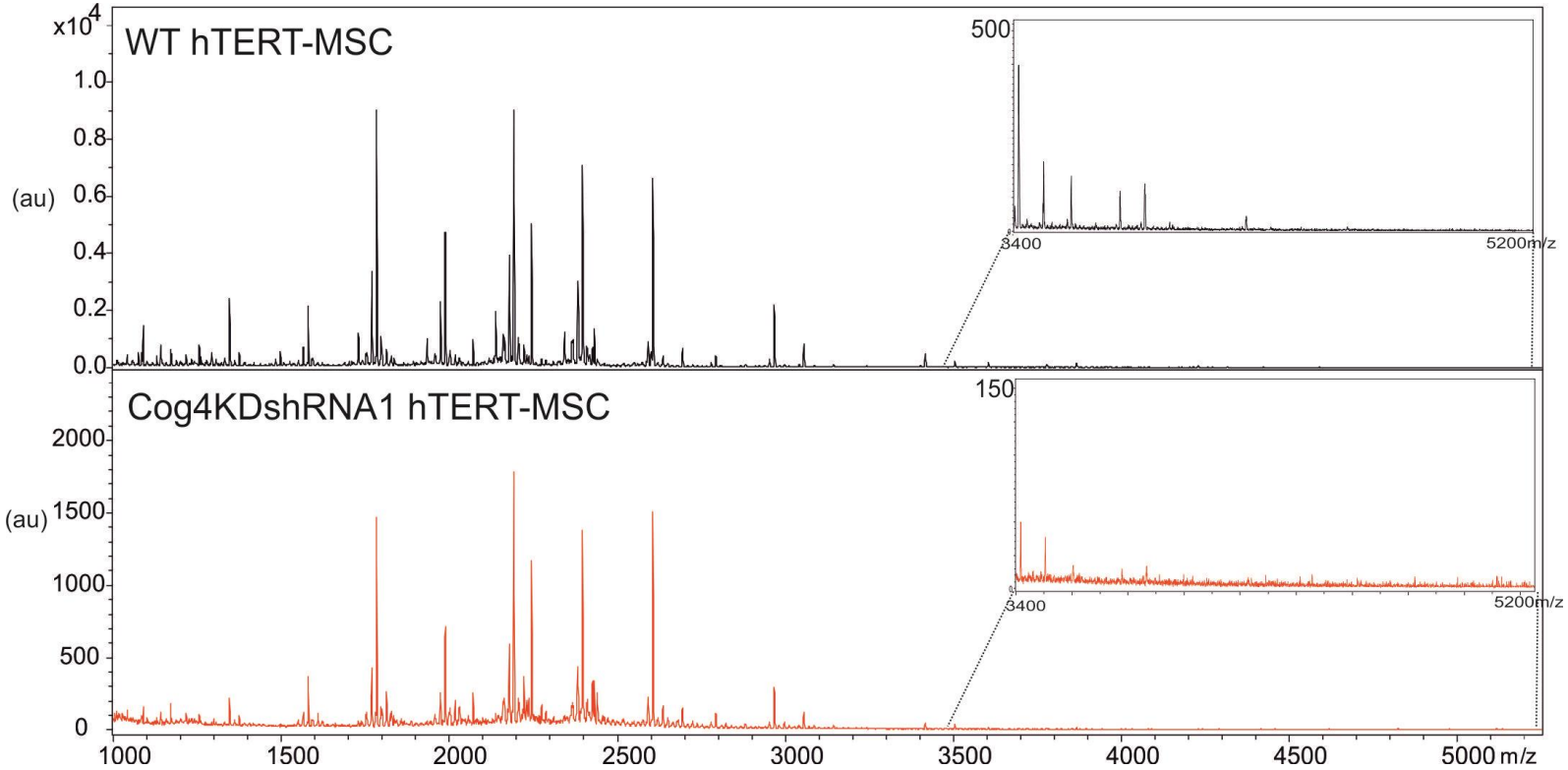

Figure 4.7 Comparison of *N*- glycan spectrum from WT and Cog4KDshRNA1 hTERT-MSCs.

Comparison of spectrum of *N*-glycans isolated from WT and Cog4KDshRNA1 hTERT-MSCs.1x10^6 cells were cultured in a 10cm dish, overnight before *N*-glycan harvest, and further processing. Spectrum shown is from 1000-5250m/z, with the inset focussed in from 3400m/z to 5250m/z showing decrease of high mass, complex glycans in Cog4KDshRNA1 hTERT-MSCs.

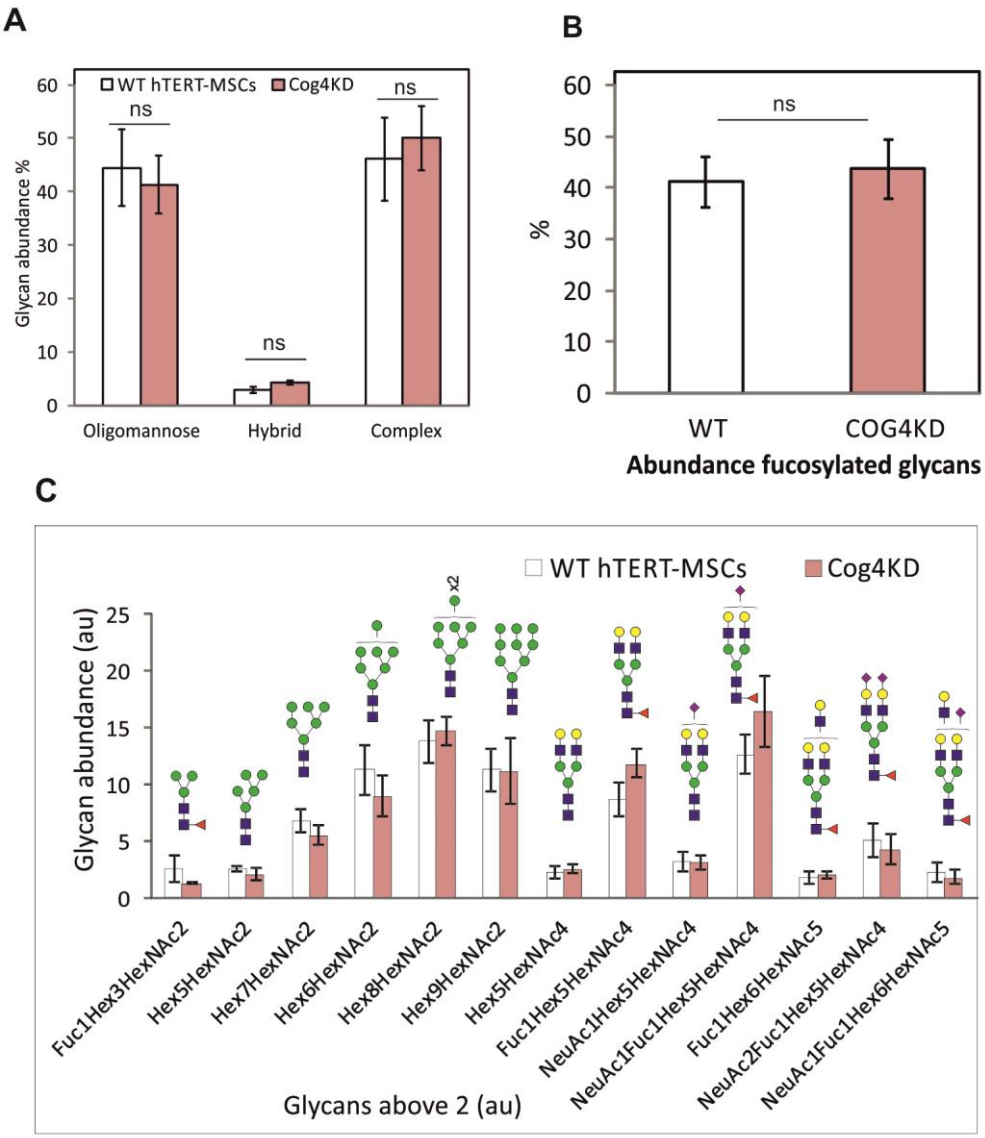

Figure 4.8 Comparison of glycans isolated from WT hTERT-MSCs and Cog4KDs.

Glycans identified from spectrum were classed by type (A) and if they were fucosylated or not (B). The normalised average peak intensity of individual glycan structures identified were also compared. Those present above 2 au in either WT or Cog4KD spectrum are shown in (C). Error bars show standard deviation. One way ANOVA (A) and Student's T test (B), ns = non significant, P>0.05, n=5 and 3.

4.3.3 Cog4KD hTERT-MSCs morphology and proliferation

The morphology of the Cog4KD hTERT-MSCs was unchanged from WT-hTERT-MSCs (Figure 4.9). Cog4KD hTERT-MSCs remained adherent to tissue culture plastic and had a fibroblastic appearance. The proliferation rate of Cog4KD-hTERT-MSCs was measured indirectly using an MTT assay. Cells were seeded into wells of a 96 well plate at sub-confluency and then assayed after 1, 2, 4, and 7 days. The metabolically active cells convert MTT into an insoluble purple product, which is dissolved in isopropanol and measured on a spectrophotometer at 570nm. Thus the measured absorbance in this case is directly proportional to the number of cells. The MTT assay results showed that the Cog4KDshRNA1 line had a higher proliferation rate than WT hTERT-MSCs. The Cog4KDshRNA2 line showed similar levels of proliferation to WT hTERT-MSCs (Figure 4.9). Although there was a difference in the proliferation rate between Cog4KDshRNA1 and WT hTERT-MSCs, the increase in proliferation should not negatively affect osteogenesis since all osteogenic assays begin at full confluency. With consideration of the proliferation data, several assays to test the osteogenic capacity of Cog4KD hTERT-MSCs were carried out.

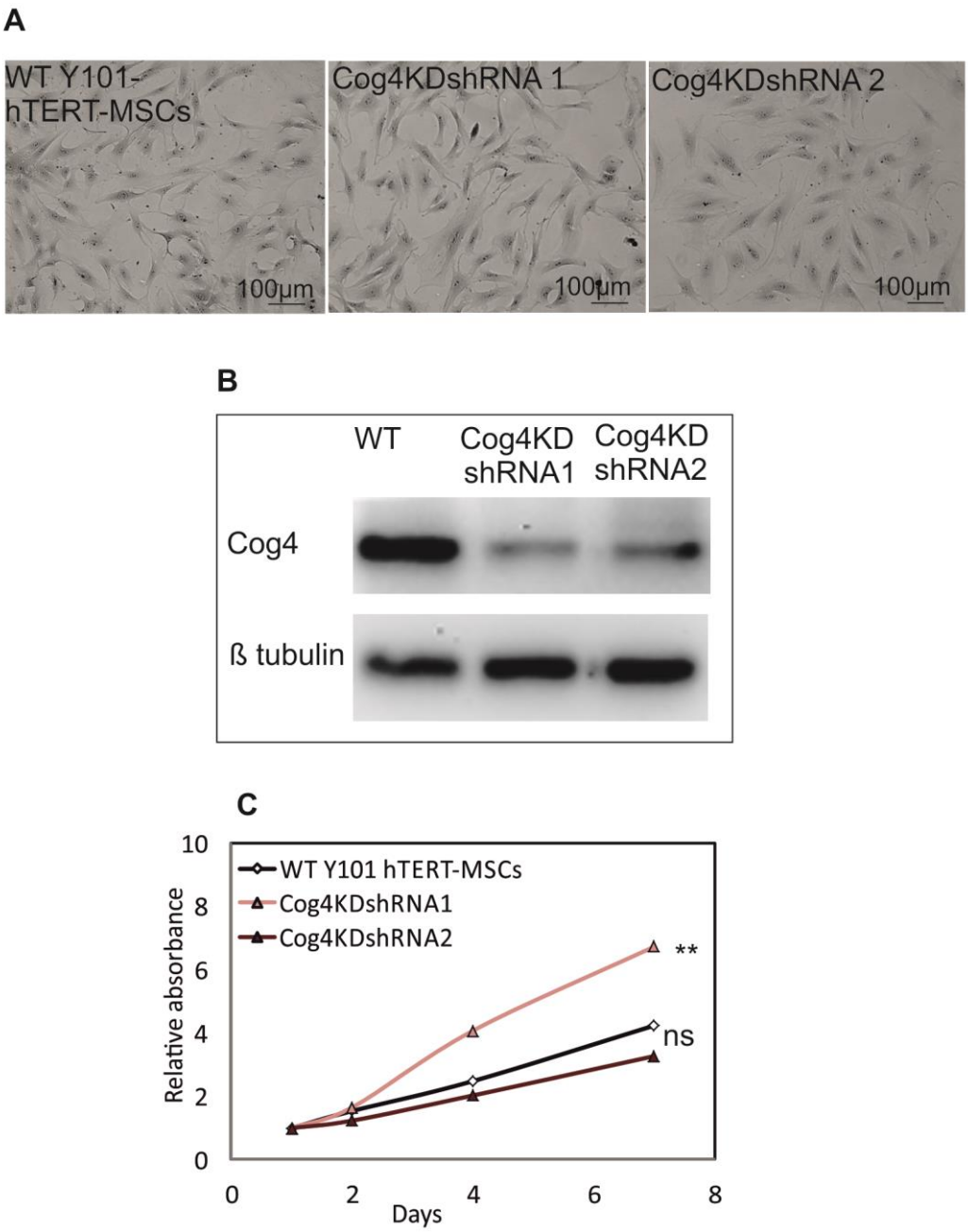

Figure 4.9 Phenotype of Cog4KD hTERT-MSCs.

A) Bright-field image of wildtype (WT) hTERT-MSCs, Cog4KDshRNA1 and Cog4KDshRNA2 cells after staining with crystal violet. B) Western blot of Cog4 protein levels in WT hTERT-MSCs and Cog4KDshRNA1 and Cog4KDshRNA 2 cells. ß-tubulin was used as a loading control. C) Proliferation of WT, Cog4KDshRNA1 and Cog4KDshRNA2 hTERT-MSCs was tested using a MTT assay, after 1,2,4 and 7 days in culture. Data was made relative to day 1 vaules. ** = P<0.01, ns = non significant, one way ANOVA, Holm-Sidak post hoc test, n=6.

4.3.4 Cog4KD hTERT-MSCs are less osteogenic

4.3.4.1 Cog4KD hTERT-MSCs have reduced phosphate staining after osteogenesis

WT and Cog4KD hTERT-MSCs were seeded at full confluency into wells of a 24 well plate and cultured in osteogenic media for 3 weeks. Every 7 days plates were stained for alkaline phosphatase (ALP - pink) and calcium phosphate mineral deposition (Von Kossa - brown). Increased ALP expression is associated with early osteogenesis whilst mineral deposition is carried out by functional active mature osteoblasts. Conveniently both of these stains can be carried out in parallel, on the same sample. WT and Cog4KD hTERT-MSCs stained positive for ALP, however, Cog4KD hTERT-MSCs had reduced levels of mineral deposition compared to WT (Figure 4.10).

4.3.4.2 Cog4KD hTERT-MSCs have lower ALP activity and reduced ALP protein levels compared to WT

In order to more closely examine ALP activity and ALP protein levels in WT and Cog4KD hTERT-MSCs, an assay measuring activity and western blots were carried out. The levels of ALP activity were measured every 7 days, during culture in osteogenic media. The ALP activity levels of WT hTERT-MSCs increased over time in osteogenic media. Although both Cog4KDshRNA1 and Cog4KDshRNA2 hTERT-MSCs showed an increase in ALP activity over time, the levels were significantly lower than WT hTERT-MSCs after 21 days in osteogenic media (Student's T test, $P<0.05$, $n=6$) (Figure 4.11). Western blot analysis of ALP protein showed that levels of ALP continued to increase in WT hTERT-MSCs cultured in osteogenic media, even after 4 weeks (Figure 4.12). The levels of ALP protein were reduced in both Cog4KD hTERT-MSC lines at all time-points compared to WT (Figure 4.12). The lower amounts of mineral deposition and ALP protein levels and activities in the Cog4KD hTERT-MSCs indicated reduced osteogenic capacity. To investigate this further, the expression levels of genes known to increase in osteoblasts derived from WT hTERT-MSCs were measured.

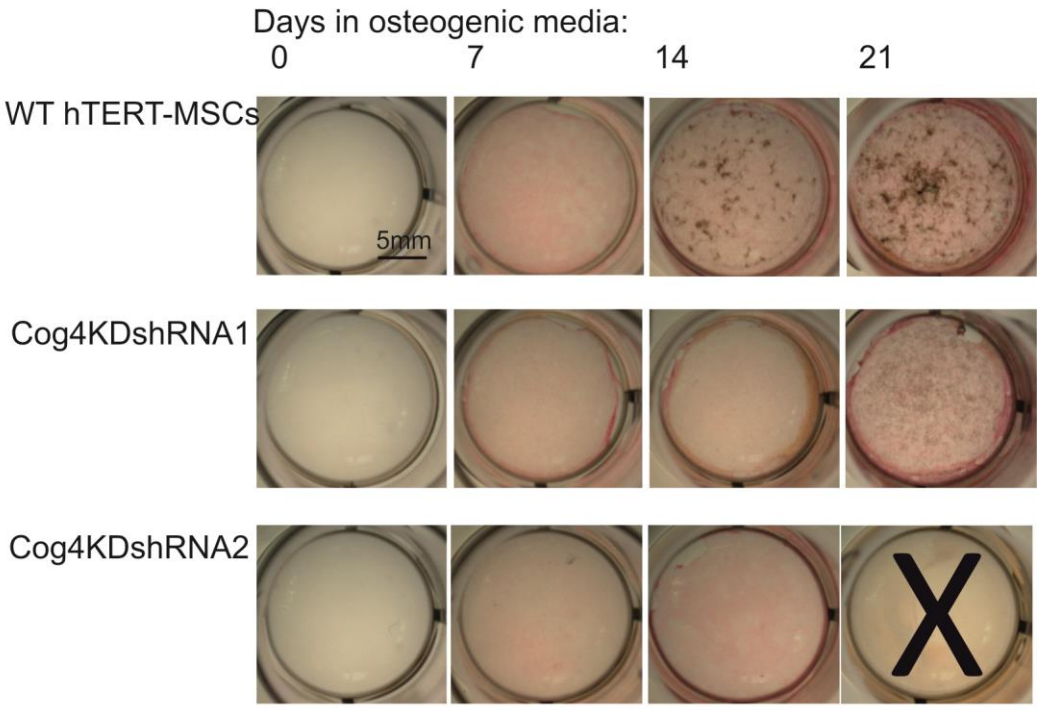

Figure 4.10 Osteogenic capacity of Cog4KDs.

Bright-field images of alkaline phosphatase staining - seen as pink - and phosphate (von Kossa) staining - seen as brown - of WT and Cog4KD hTERT-MSCs at weekly time points during culture in osteogenic media. X = cell layer peeled off.

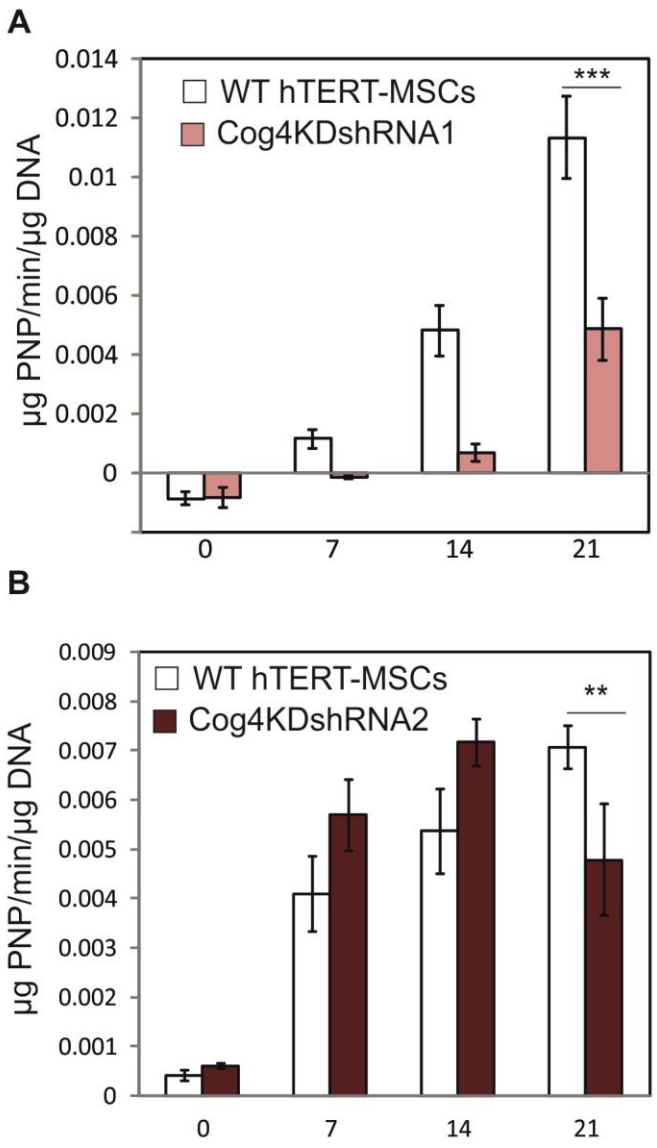

Figure 4.11 Alkaline phosphatase activity of WT and Cog4KD hTERT-MSCs.

Alkaline phosphatase activity was measured using pNP assay, after culture in osteogenic media for 0, 7, 14, and 21 days. Activity was made relative to DNA content of each sample using a pico-green assay. A) Comparison of WT and Cog4KDshRNA1 hTERT-MSCs. B) Comparison of WT and Cog4KDshRNA2 hTERT-MSCs. ALP activity of cells after 21 days in osteogenic media was compared using Student's T test, **=P<0.01, ***=P<0.001, n=6, error bars show standard deviation.

Data and image in A) printed with permission of A. Jagger who completed the experimental work for A).

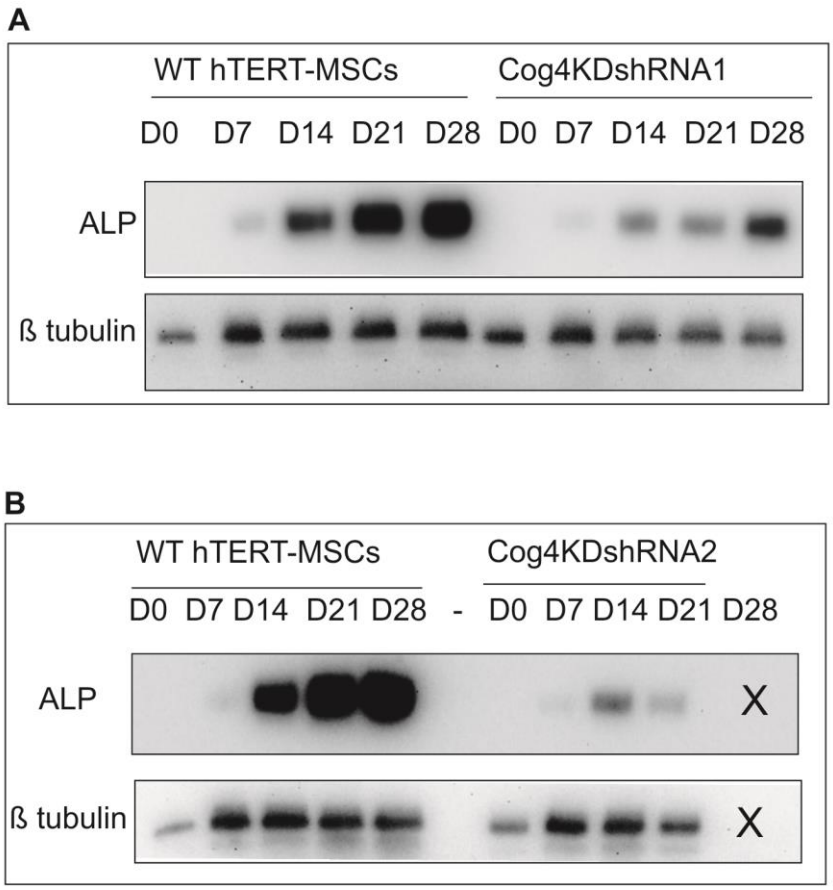

Figure 4.12 Western blot analysis of ALP levels in WT and Cog4KD hTERT-MSCs.

Protein samples were harvested after cells were cultured in osteogenic media for 0, 7, 14, 21 and 28 days. WT hTERT-MSC samples were run alongside (A) Cog4KDshRNA1 and (B) Cog4KDshRNA2. Western-blots were probed for ALP and ß tubulin as a loading control. 'X' indicates when the cell layer peeled off preventing sample harvest.

4.3.4.3 Expression of osteogenic markers is altered in Cog4KD-MSCs

In the previous chapter, the expression level of Runx2, which is a major pro-osteogenic transcription factor, was found to increase in WT hTERT-MSCs during incubation in osteogenic media. When testing the Cog4KD hTERT-MSC lines, however, I found differences in Runx2 expression patterns during osteogenic stimulation. The Cog4KDshRNA1 line showed the same expression pattern as WT hTERT-MSCs. In contrast, while the expression of Runx2 in the Cog4KDshRNA2 line did increase several fold in osteogenic media, at day 14 levels were notably lower than in WT or Cog4KDshRNA1 hTERT-MSCs (Figure 4.13A).

The expression level of BMP2, an osteogenic cytokine which can stimulate osteogenesis, was also different in the two Cog4KD hTERT-MSC lines. The Cog4KDshRNA1 hTERT-MSCs had expression levels as high as or higher than WT, which continued to increase overtime

(Figure 4.13B). The expression levels in Cog4KDshRNA2 hTERT-MSCs, were similar to WT at day 7, but failed to increase at day 14 unlike WT and Cog4KDshRNA1 hTERT-MSCs.

Although there was reduced phosphate staining in the Cog4KD hTERT-MSCs, the expression of BSP did increase to levels comparable with WT hTERT-MSCs after 7 and 14 days in osteogenic media (Figure 4.13C). BSP is a protein associated with the later, mineralisation stage of osteogenesis and in accordance with this, the expression in WT hTERT-MSCs was highest (2500 fold higher than day 0), after 21 days in osteogenic media. The level of BSP expressed by Cog4KDshRNA1 at day 21 was considerably lower than WT hTERT-MSCs, with levels unchanged from day 14. This supports the histology data (Figure 4.10), suggesting that Cog4KD hTERT-MSCs do differentiate but fail to mineralise. A sample from Cog4KDshRNA2 hTERT-MSCs after 21 days in osteogenic media was not obtained as the cell layer peeled off, in both biological repeats. This hinders the interpretation of the qPCR data for Cog4KDshRNA2, however the levels of BSP are lower than WT at day 14, which also suggests a reduced mineralization capacity.

The ability of the Cog4KD hTERT-MSCs to show any degree of positive osteogenesis, such as the small increase in ALP activity and the small increase in osteogenic gene expression during osteogenic stimulation, could be the result of Cog4 expression returning to WT levels whilst the cells are incubated in osteogenic media. Although Cog4KD hTERT-MSCs were maintained in culture media in the presence of the selective antibiotic, this was not included in media used for longer term assays. To test this theory, protein samples from WT and Cog4KD hTERT-MSCs cultured in osteogenic or basal media for 21 days were analysed for levels of Cog4 protein.

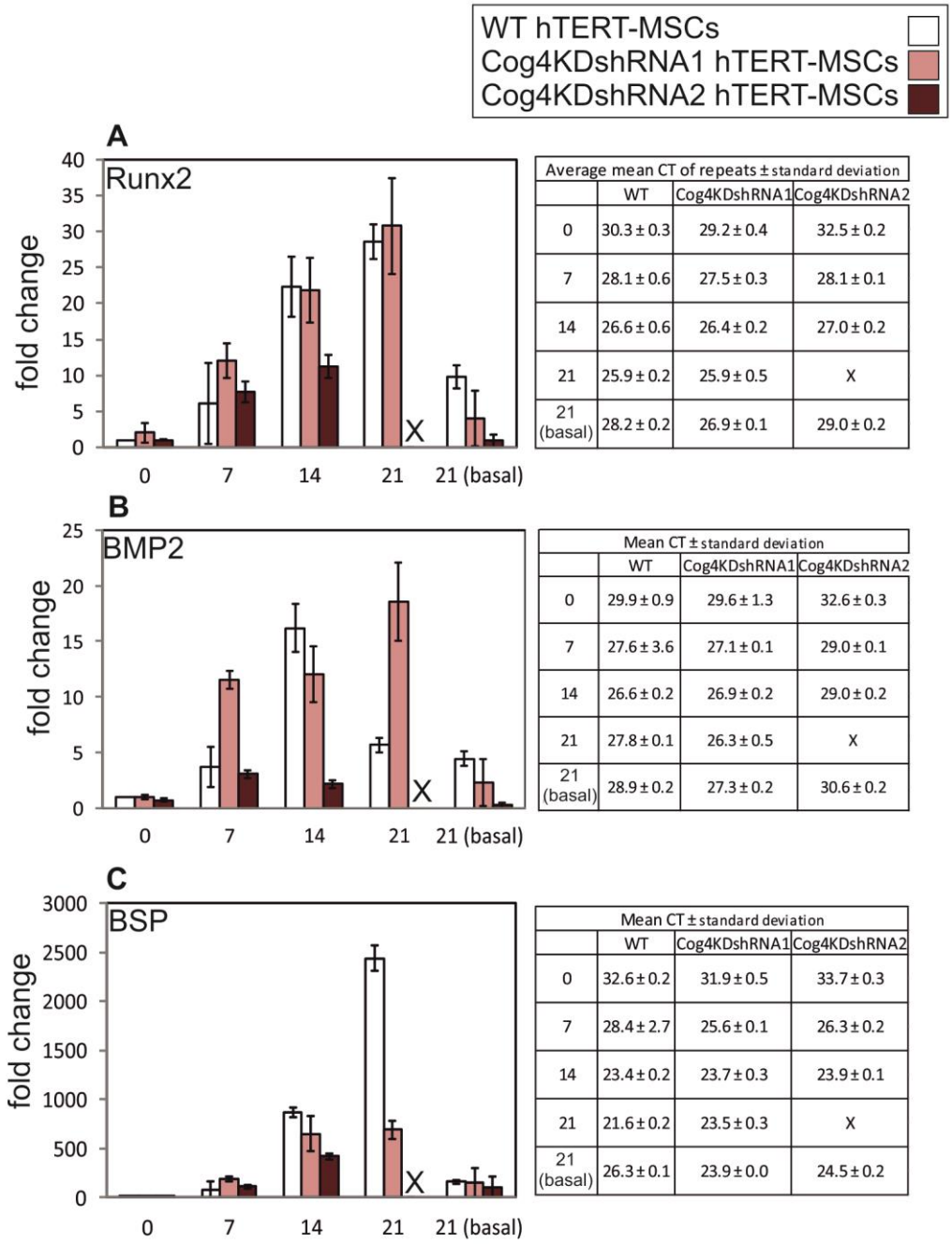

Average mean CT of repeats ± standard deviation			
	WT	Cog4KDshRNA1	Cog4KDshRNA2
0	30.3 ± 0.3	29.2 ± 0.4	32.5 ± 0.2
7	28.1 ± 0.6	27.5 ± 0.3	28.1 ± 0.1
14	26.6 ± 0.6	26.4 ± 0.2	27.0 ± 0.2
21	25.9 ± 0.2	25.9 ± 0.5	X
21 (basal)	28.2 ± 0.2	26.9 ± 0.1	29.0 ± 0.2

Mean CT ± standard deviation			
	WT	Cog4KDshRNA1	Cog4KDshRNA2
0	29.9 ± 0.9	29.6 ± 1.3	32.6 ± 0.3
7	27.6 ± 3.6	27.1 ± 0.1	29.0 ± 0.1
14	26.6 ± 0.2	26.9 ± 0.2	29.0 ± 0.2
21	27.8 ± 0.1	26.3 ± 0.5	X
21 (basal)	28.9 ± 0.2	27.3 ± 0.2	30.6 ± 0.2

Mean CT ± standard deviation			
	WT	Cog4KDshRNA1	Cog4KDshRNA2
0	32.6 ± 0.2	31.9 ± 0.5	33.7 ± 0.3
7	28.4 ± 2.7	25.6 ± 0.1	26.3 ± 0.2
14	23.4 ± 0.2	23.7 ± 0.3	23.9 ± 0.1
21	21.6 ± 0.2	23.5 ± 0.3	X
21 (basal)	26.3 ± 0.1	23.9 ± 0.0	24.5 ± 0.2

Figure 4.13 Real-time quantitative PCR analysis of Runx2, BMP2, and BSP expression in WT and Cog4KD hTERT-MSCs.

cDNA produced from WT, Cog4KDshRNA1 and Cog4KDshRNA2 hTERT-MSCs grown in osteogenic media for either 0,7,14,or 21 days, were analysed using primers for Runx2 (A), BMP2 (B), BSP (C) and RSP27a. cDNA produced from WT, Cog4KDshRNA1 and Cog4KDshRNA2 hTERT-MSCs grown in basal media for 21 days was also analysed as a control (21 basal). CT values were made relative to RSP27a values and then expressed as fold change relative to day 0, WT values. Triplicate technical replicates from 2 biological repeats are shown, error bars are standard deviation. Samples which peeled off and were not used are represented as X. Tables show mean CT values ± standard deviation of combined replicates.

4.3.5 Protein levels of Cog4 remain knocked down throughout differentiation

Puromycin was used as the selective antibiotic after hTERT-MSC transduction, in order to identify successfully transduced cells. Cog4KD hTERT-MSCs were cultured in media containing puromycin to ensure the cells maintained the shRNA for Cog4. As the effect of puromycin on differentiation was unknown, it was not included in the media used for osteogenic assays. To check that the levels of Cog4 remained knocked-down, protein samples were harvested from cells cultured for 21 days in either basal or osteogenic media (both without puromycin) (Figure 4.14). The western blot showed that Cog4 protein levels remained lower in both Cog4KD hTERT-MSC lines compared to WT after culture in either basal or osteogenic media. This confirms that the change to mineralization capacity - without affecting osteogenic differentiation altogether- is not due to Cog4 protein levels reverting to WT levels during osteogenic assays. The degree of Cog4 knock-down did not differ between the two Cog4KDshRNA lines. This suggests the difference in osteogenic gene expression between the Cog4KD lines, is not due to varying amounts of Cog4 protein. Interestingly, the protein level of Cog4 increased in WT cells after 21 days of culture in either media (Figure 4.14).

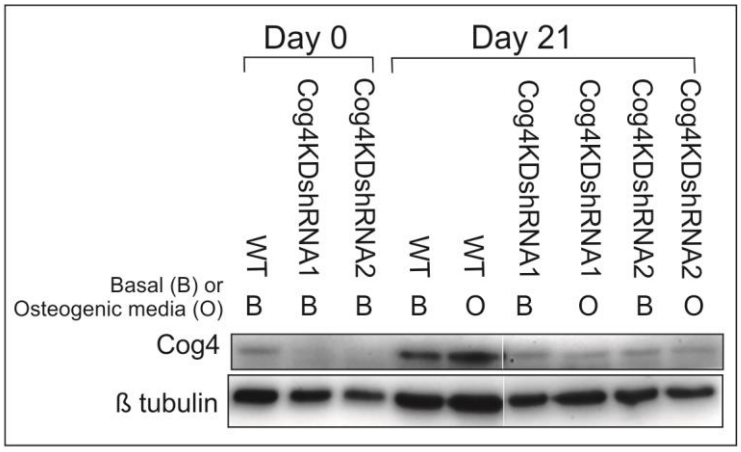

Figure 4.14 Western blot analysis of Cog4 levels after 21 days in media without puromycin.

WT and Cog4KD hTERT-MSCs were cultured in basal (B) or osteogenic (O) media for 21 days without puromycin. Protein harvested from day 0 and day 21 samples, were loaded to determine the effect of removing puromycin from Cog4KD hTERT-MSCs, on levels of Cog4 protein. ß tubulin was used as loading control. Samples were loaded on the same blot and exposed for the same amount of time, the images have been edited to exclude irrelevant samples.

4.4 Chapter 4 Conclusion

The glycosylation of hTERT-MSCs was successfully disrupted, using shRNA targeted to Cog4. Lectin staining with SNA and VVL was significantly lower in Cog4KD hTERT-MSCs, indicating decreased *N*- and/or O-glycan sialylation, which supports glycan analysis of COG CDG patient derived samples. Analysis of *N*-glycans using mass spectrometry confirmed that Cog4KD hTERT-MSCs had reduced levels of sialylated *N*-glycans, with large, complex glycans missing from the Cog4KDshRNA hTERT-MSC spectrum. Due to the Cog4KDshRNA2 hTERT-MSCs being produced late into the project, the *N*-glycan spectrum from this line was not obtained. Future experiments could investigate if this line also had reduced high mass, complex, glycans. Histology, western blots and qPCR data indicated that Cog4KD hTERT-MSCs were capable of osteogenic differentiation, however were unable to mineralise extracellular matrix. This change in differentiation capacity was rendered in the continued presence of reduced Cog4 protein levels, during osteogenic induction.

In the next chapter, to investigate if disrupted *N*-glycan sialylation caused the reduced ability of Cog4KD hTERT-MSCs to mineralise, the synthesis of different types of glycans were disrupted using chemical inhibitors.

Chapter 5 Chemical inhibition of glycosylation

5.1 Rationale

In chapter 3 the glycan profiles of hTERT-MSCs and osteoblasts derived from them, were identified by mass spectrometry. Osteoblasts had more complex type glycans than hTERT-MSCs. After genetic disruption of the glycan pathway, via Cog4 knock-down, the mineralisation capacity was reduced. Lectin staining and mass spectrometry were used to identify changes in the glycan profile. Cog4KD-hTERT-MSCs had reduced SNA staining and lacked several high mass, complex *N*-glycan structures, which was in agreement with the reported reduction in sialylation of O-and *N*-glycans from COG CDG patient samples. Due to the binding specificity of SNA, the reduction in staining with this lectin could have been caused by a reduced O or *N*-glycan sialylation. The disruption of the glycan synthesis pathway via COG knockdown, could have affected *N*-glycan, O-glycan, glycolipid or proteoglycan syntheses, as they all share some of the synthesis pathways in the Golgi. In order to elucidate which glycan structure disruptions in the Cog4KD hTERT-MSCs were functionally relevant, leading to reduced mineralization capacity, the effects of chemical inhibitors disrupting the different glycan synthesis pathways on osteogenesis were assessed.

Starting with the *N*-glycan synthesis pathway, the effects of two *N*-glycan synthesis inhibitors were tested. Swainsonine is an indolizidine alkaloid, originally derived from an Australian plant *Swainsona canescens*, which is toxic to cattle and horses [138]. It was initially identified as a lysosomal mannosidase inhibitor, as the cattle that ate it had symptoms similar to patients with lysosomal mannosidase deficiency. Later studies showed that swainsonine is a more potent inhibitor of Golgi mannosidase II [139, 140]. Mannosidase II resides in the *cis* Golgi and removes two mannose residues from the precursor oligosaccharide structure containing a single GlcNAc (Figure 5.1). This allows the addition of a further N-acetlyglucosamine, which is the beginning of a complex glycan branch. Inhibition of mannosidase II prevents complex glycan formation, allowing only oligomannose or hybrid type glycans to be formed (Figure 5.1). Several *in vitro* studies have confirmed that swainsonine decreases complex glycan formation and importantly, showed that swainsonine was non-toxic and had no effect on cell proliferation [141, 142]. However in cancer studies, swainsonine has been shown to have functional effects on cells in several ways. The proliferation of several cancer lines was reduced by swainsonine

treatment *in vitro* [143, 144]. Swainsonine treatment *in vivo* reduced tumour growth and metastasis [143-145]. Further studies showed that swainsonine modulated immune cell efficiency and promoted HSC proliferation *in vivo* [146-148]. Following these initial studies, swainsonine was tested in a clinical trial. Disappointingly, no clinical improvement was seen in the 17 kidney cancer patients treated with swainsonine [149]. Overall these studies suggest that swainsonine treatment of MSCs would be non-toxic and could have a functional effect.

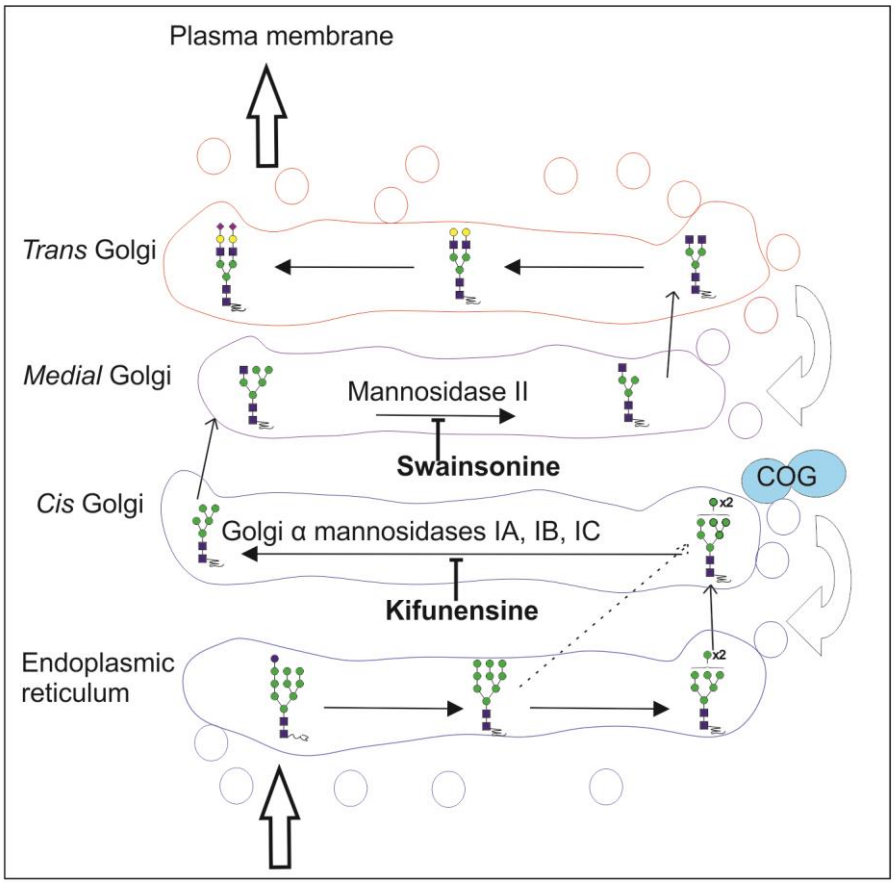

Figure 5.1 Chemical inhibition of N-glycan synthesis.

Schematic of *N*-glycan synthesis in the endoplasmic reticulum and Golgi. Kifunensine inhibits Golgi α mannosidase I in the cis Golgi. Swainsonine inhibits mannosidase II in medial Golgi. For simplicity only one possible complex *N*-glycan structure shown in the trans Golgi.

Although treatment with swainsonine inhibits complex glycan formation, hybrid glycans can also contain sialylated branches. Several types of lectins bind to sialic acid and are involved in a variety of cellular processes, including immunity and cell adhesion [150]. A study using MSCs showed that homing to bone marrow was improved by manipulating the glyco-form of CD44 in order to bind to E-selectin, a sialic acid and fucose binding

lectin [120]. Since sialic acid has cellular functions and the Cog4KDs showed reduced SNA lectin staining, an enzyme earlier in the glycosylation pathway was also targeted. Inhibition of Golgi mannosidase I prevents the removal of mannose from the precursor oligosaccharide which in turn prevents the formation of $Hex_5HexNAc_2$ (Figure 5.1). Subsequently only oligomannose type glycans can be produced. Kifunensine is small molecule that predominantly inhibits Golgi mannosidase I [151]. Unlike swainsonine, there have been few studies looking at the functional effect of kifunensine treatment. One study with epithelial cells used kifunensine to examine the role of glycans in the polarized secretion of Wnt3a and Wnt11 [152]. As this study found kifunensine to be effective at inhibiting Golgi mannosidase I *in vitro*, with no toxicity, kifunensine was used to test the effect of complete loss of sialylated *N*-glycans on MSC differentiation.

Another glycan synthesis pathway potentially disrupted in Cog4KD hTERT-MSCs is O-glycan synthesis. Evidence for this was the altered staining of Cog4KD-hTERT-MSCs, using VVL and PNA which are O-glycan binding lectins. SNA can bind to NeuAc-Gal, which is found in *N*- and O-glycans, or NeuAc-GalNAc which is found in O-glycans [153]. As such, the reduced SNA staining seen in Cog4KD-hTERT-MSCs may have been due to lower levels of sialylated O-glycans. To test if disrupted O-glycan synthesis was responsible for the loss of mineralisation in Cog4KD hTERT-MSCs, hTERT-MSCs were treated with an O-glycan inhibitor. **B**enzyl 2-**a**cetamido-2-**d**eoxy-α-D-**Gal**actopyranoside (BadGal) is a competitive substrate of the glycosyltransferase which normally adds galactose (Gal) to N-acetylgalactosamine (GalNAc), forming a core 1 or T-antigen O-glycan structure (Figure 5.2). BadGal treatment of colon carcinoma cells was shown to increase the amount of truncated O-glycan structures, comprising of just GalNAc attached to serine or threonine (Tn-antigen structure) [154]. The treated cells accumulated free intracellular BadGal-Gal disaccharides, which acted as a competitive substrate of sialyltransferases. This resulted in increased T-antigen abundance, along with decreased sialylated O-glycans compared to untreated controls [154]. To test if disrupted O-glycan synthesis affected osteogenesis, hTERT-MSCs were treated with BadGal.

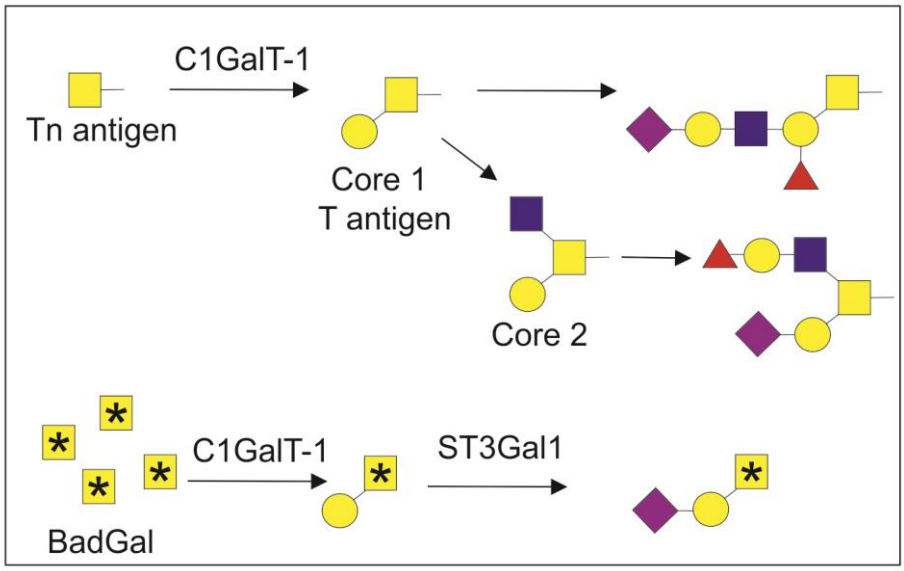

Figure 5.2 Competitive inhibition of O-glycan formation by BadGal.

Schematic showing competitive inhibition of T antigen formation and sialylated O-glycans by BadGal. C1GalT-1 = Core 1 β1-3 galactosyltransferase. ST3Gal1 = Core 1 α2-3 sialyltransferase.

Inhibitors of glycolipid and proteoglycan synthesis were also used to see if their disrupted syntheses were responsible for the altered mineralisation in Cog4KD hTERT-MSCs. Gaucher's disease is a lysosomal storage disease, caused by disrupted glycolipid degradation. Due to disrupted degradation, the cellular supply of glycolipid precursors may be altered resulting in disrupted glycolipid synthesis. Patients with Gaucher's disease can suffer from a variety of skeletal symptoms such as osteopenia, osteoporosis, osteolytic lesions, and osteonecrosis. Using Gaucher's disease mice models, *in vitro* analysis of osteoblasts found that osteoblasts had reduced proliferation and reduced osteogenic differentiation capacity compared to osteoblasts isolated from healthy control mice [155]. In view of this, disrupted glycolipid synthesis in the Cog4KD hTERT-MSCs could have contributed towards the reduction in mineralization capacity. In order to test this, hTERT-MSCs were treated with a glycolipid inhibitor called *N*-butyldeoxynojirimycin (NB-DNJ) [156] and the effect on osteogenesis was measured using ALP and Von kossa staining. As mentioned in the introduction (section 1.2.3), proteoglycans are a major component of bone tissue, forming the ECM that is then mineralized. *Ex vivo* and *in vitro* studies have shown that GAG synthesis and sulfation are required for osteogenesis [157, 158]. It is possible then, that the reduced mineralization capacity of Cog4KD hTERT-MSCs could also be due to improper GAG synthesis or sulfation, as both processes requires Golgi resident enzymes. Therefore, the influence of sodium chlorate, a GAG sulfation

inhibitor, on the osteogenesis of hTERT-MSCs was analysed using ALP and Von kossa staining. Some of the experimental work involving glycosylation inhibitors was performed by undergraduate students working under my supervision. Their contributions are acknowledged on the relevant figures.

5.2 Results for Chemical inhibition of glycosylation

5.2.1 Swainsonine treatment significantly alters the glycan profile of hTERT-MSCs

After 48 hours treatment with 10µg/ml swainsonine glycans were harvested from hTERT-MSCs and then analysed by mass spectrometry (MALDI-TOF-TOF). The change in *N*-glycan profile was consistent with mannosidase II inhibition. Spectra from swainsonine treated cells had several hybrid structures, which were not present in the untreated hTERT-MSC profile (Figure 5.3 and Figure 5.4). The abundance of oligomannose and complex glycans was significantly lower in swainsonine treated hTERT-MSCs (One way ANOVA, Holm-Sidak post hoc, $P<0.001$, n=3) Figure 5.5A). Hybrid type glycans were the most common, with the structure $NeuAc_1Fuc_1Hex_6HexNAc_3$ being the most abundant (Figure 5.4 and Figure 5.5C). The high intensity of this fucosylated structure contributed to the significant increase in fucosylation seen in swainsonine treated cells (Student's T test, $P<0.01$, n=3) (Figure 5.5B). As treatment with swainsonine successfully altered the *N*-glycan profile of hTERT-MSCs, tests were then carried out to see if this caused a change in phenotype.

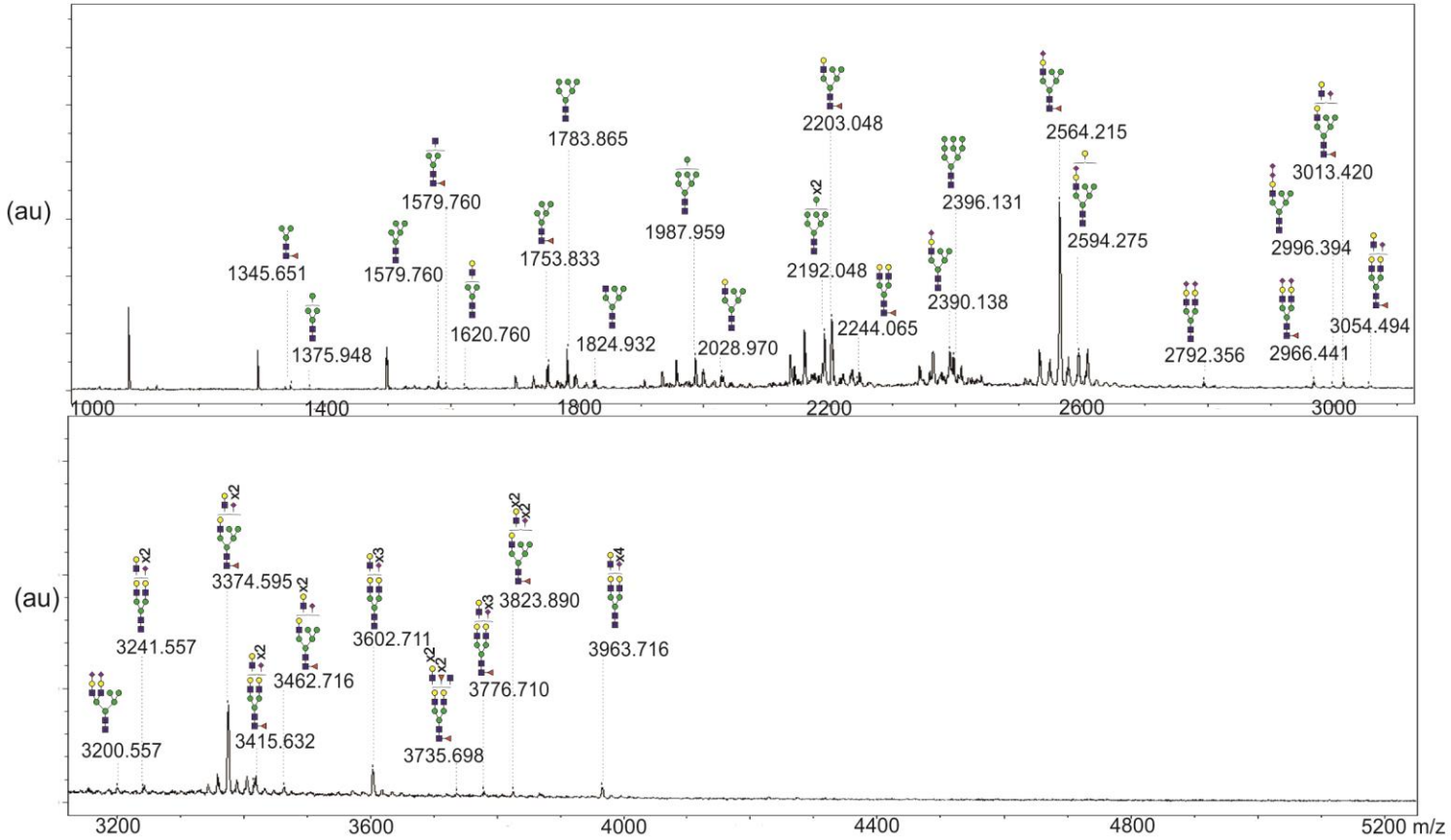

Figure 5.3 MALDI-TOF/TOF spectrum of *N*-glycans from hTERT-MSCs treated with swainsonine.

A representative spectrum (n=3) of *N*-glycans isolated from hTERT-MSCs treated with swainsonine.1x106 cells were cultured in a 10cm dish, in media with swainsonine (10µg/ml) for 48 hours, before *N*-glycan harvest, and further processing. Glycan peaks were identified using calculated mass of monosaccharide units and knowledge of the synthesis pathway. Glycans had to have two isotopic peaks, 3x above noise to be included. Mass of mono-isotopic peak is labelled, with predicted structure pictured above. Spectrum shown is from 1000-5250m/z.

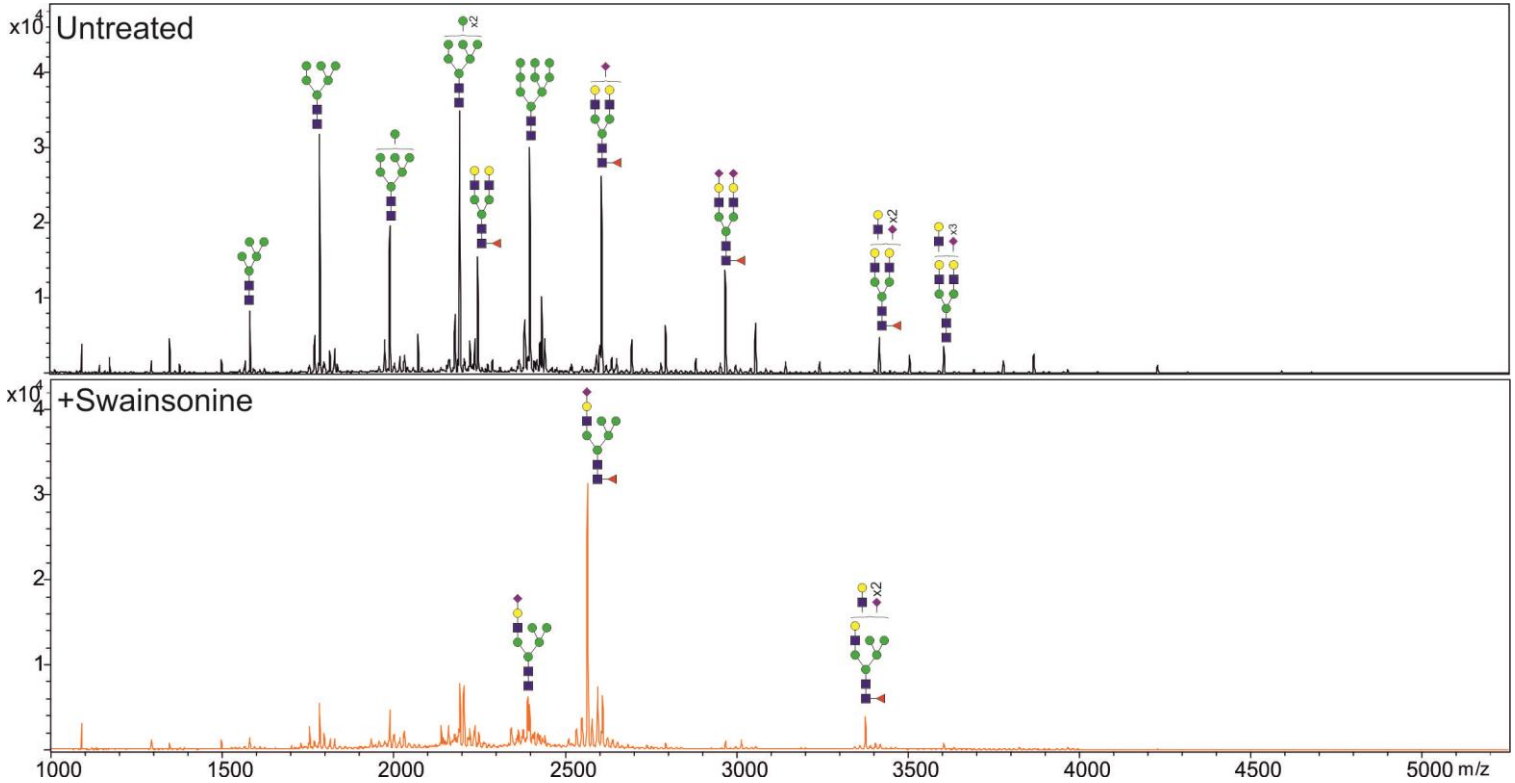

Figure 5.4 Comparison of spectrum from untreated and swainsonine treated hTERT-MSCs.

A representative spectrum (n=5 untreated, and n=3 treated with swainsonine) of *N*-glycans isolated from hTERT-MSCs.1x106 cells were cultured in a 10cm dish, in media with swainsonine (10µg/ml) for 48 hours, before *N*-glycan harvest, and further processing. Glycan peaks were identified using calculated mass of monosaccharide units and knowledge of the synthesis pathway. Glycans had to have two isotopic peaks, 3x above noise to be included. Mass of mono-isotopic peak is labelled, with predicted structure pictured above. Spectrum shown is from 1000-5250m/z.

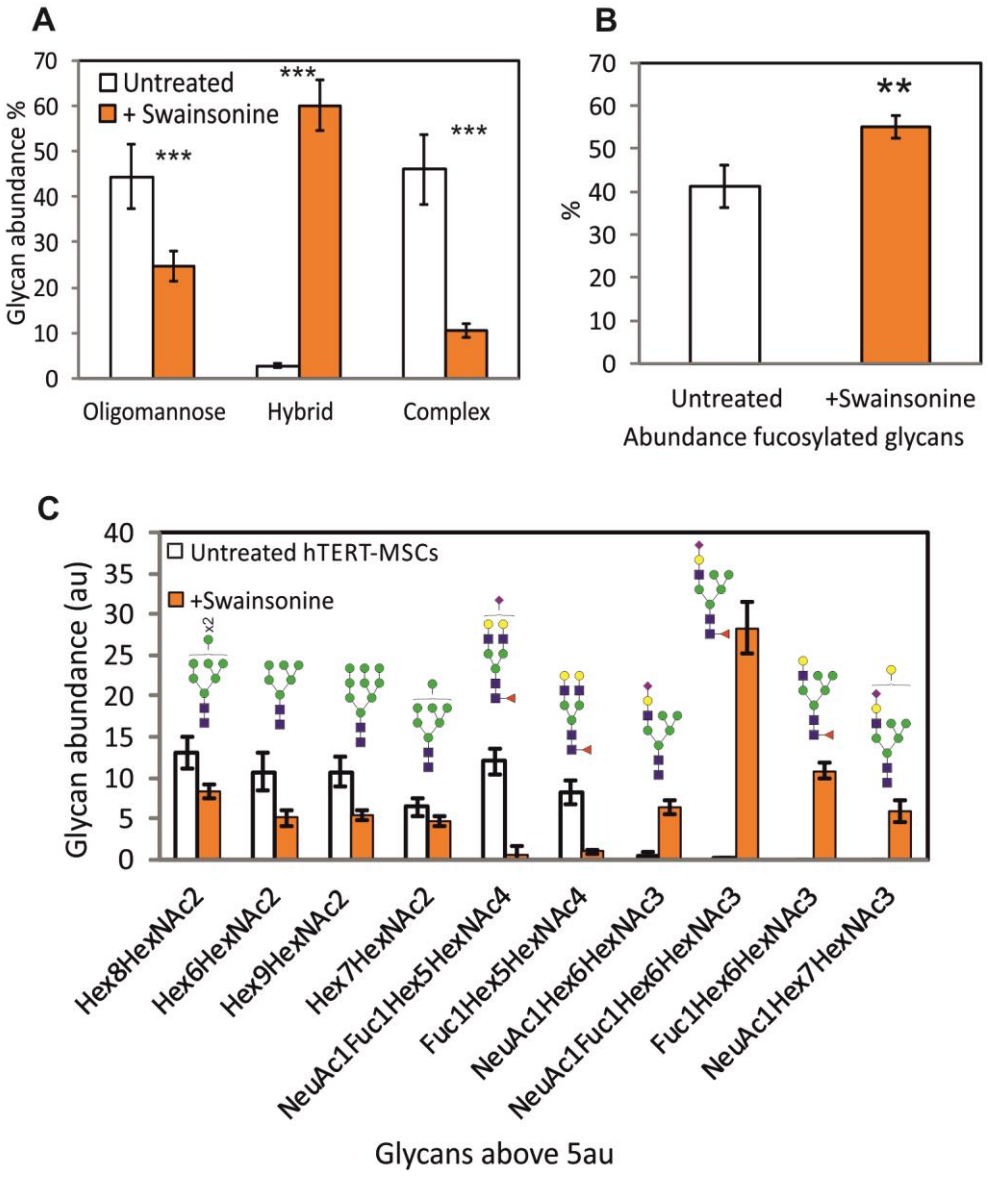

Figure 5.5 Comparison of glycans isolated from untreated hTERT-MSCs and swainsonine treated hTERT-MSCs.

Glycans identified from spectrum were classed by type (A) and if they were fucosylated or not (B). One way ANOVA, Holm Sidak post hoc test (A) Student's T test (B)**=P<0.01, ***=P<0.001, n=5 and 3. The normalised average peak intensity of individual glycan structures were also compared. Those present above 5au, in either spectrum are shown in (C). Error bars show standard deviation.

5.2.2 Swainsonine treatment does not affect morphology or proliferation of hTERT-MSCs

In order to check if swainsonine treatment affected cell morphology, hTERT-MSCs that had been treated with swainsonine for 48 hours were stained with crystal violet and imaged. No difference between untreated and swainsonine treated hTERT-MSCs was observed (Figure 5.6B). Results from a MTT assay indicated no significant difference in proliferation between untreated and swainsonine treated hTERT-MSCs (Figure 5.6B).

5.2.3 Swainsonine does not prevent osteogenesis

To determine if osteogenesis would still occur in the presence of swainsonine hTERT-MSCs were cultured in osteogenic media supplemented with 10µg/ml swainsonine for 21 days. Every 7 days cells were either stained for ALP and phosphate (Von kossa), or harvested for use in an ALP activity assay. Swainsonine treatment did not inhibit osteogenesis, as seen by positive ALP and phosphate staining (Figure 5.7). There was also no significant change in ALP activity of swainsonine treated cells (Figure 5.8).

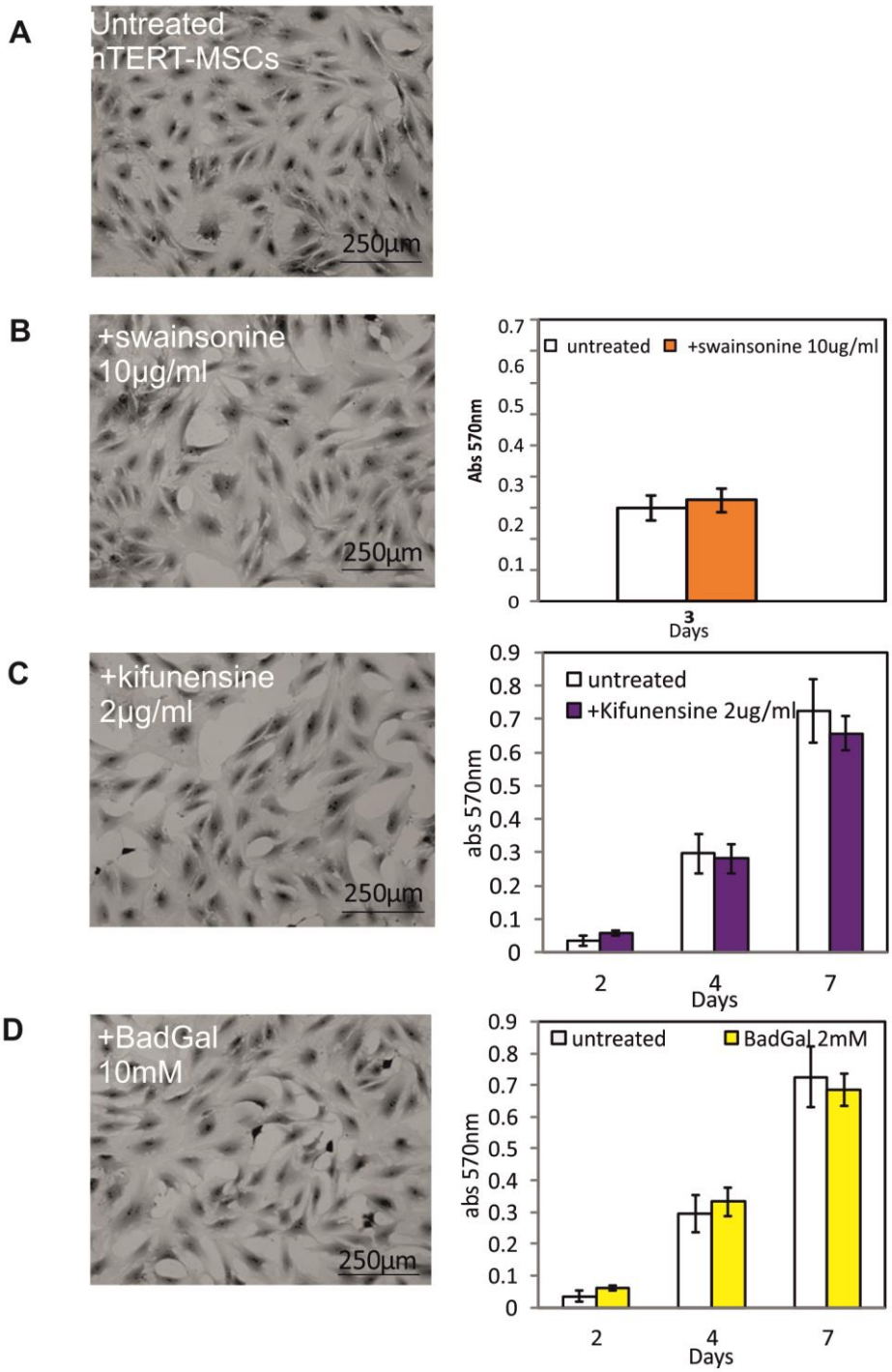

Figure 5.6 Effect of swainsonine, kifunensine or BadGal on phenotype.

A-D left-handside) Bright-field images of untreated hTERT-MSCs, cells treated with 10µg/ml swainsonine, 2µg/ml kifunensine or 10mM BadGal after staining with crystal violet. Right-handside B-D) Effect of treatments on proliferation was tested using MTT assays.

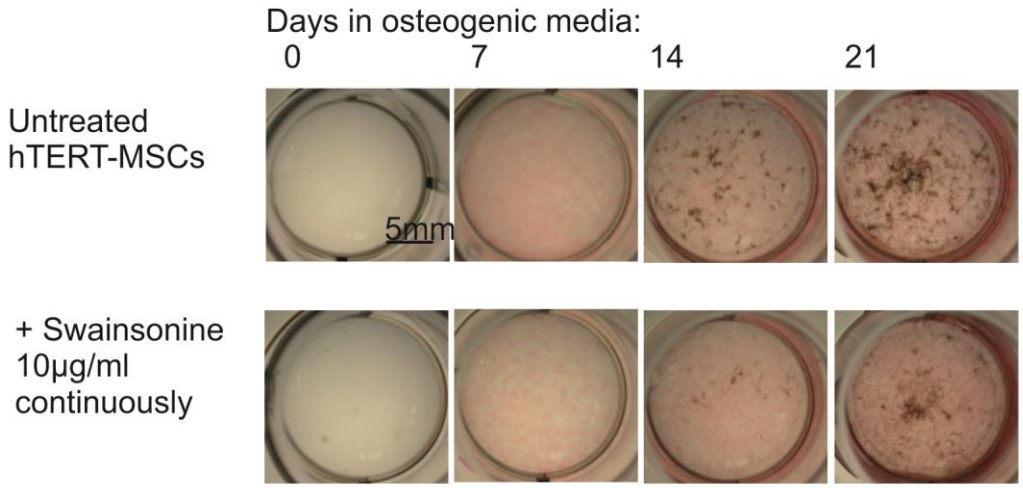

Figure 5.7 Effect of swainsonine on osteogenesis.

Bright-field images of alkaline phosphatase staining - seen as pink - and phosphate (von Kossa) staining - seen as brown - of hTERT-MSCs at weekly time points during culture in either normal osteogenic media or osteogenic media supplemented with 10µg/ml swainsonine.

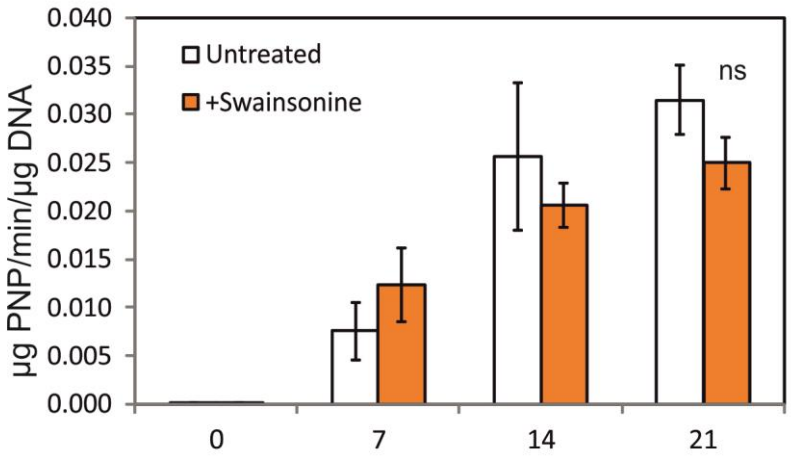

Figure 5.8 Effect of swainsonine on ALP activity.

ALP activity was measured using pNP assay, after culture in osteogenic media for 0, 7, 14, and 21 days. Activity was made relative to DNA content of each sample using a pico-green assay. White bars represent untreated hTERT-MSC, orange bars represent hTERT-MSCs treated continuously with 10µg/ml swainsonine. One way ANOVA on ranks, Dunn's post hoc test, ns=non-significant, n=6, error bars show standard deviation.

5.2.4 Kifunensine further decreased the abundance of complex glycans

As swainsonine treatment had no effect on osteogenesis, an enzyme earlier in the *N*-glycan synthesis pathway was targeted. Inhibition of mannosidase I should inhibit the production of any hybrid or complex glycans, resulting in only oligomannose type glycans. Indeed, hTERT-MSCs treated with kifunensine, a mannosidase I inhibitor, had an *N*-glycan profile dominated by oligomannose type glycans (Figure 5.9 and Figure 5.10). Of the 17 glycan structures identified in kifunensine treated profiles, $Hex_9HexNAc_2$ was the most abundant structure (Figure 5.10 and Figure 5.11C). Compared to the swainsonine treated cells there were 3x fewer complex glycans, indicating that kifunensine treatment was more potent than swainsonine. Phenotypic tests were then carried out to test the effect of this more extreme glycan profile alteration, on cell morphology and proliferation.

5.2.5 Kifunensine does not affect morphology or proliferation of hTERT-MSCs

As with swainsonine treatment, kifunensine did not affect the morphology of hTERT-MSCs. Crystal violet staining of kifunensine treated cells revealed similar cell morphology between treated and untreated cells (Figure 5.6C). Again using an MTT assay as an indicator of proliferation, there was no significant difference between untreated and kifunensine treated cells (Figure 5.6C). Following this, the effect of kifunensine on osteogenesis was tested by including kifunensine in the osteogenic media.

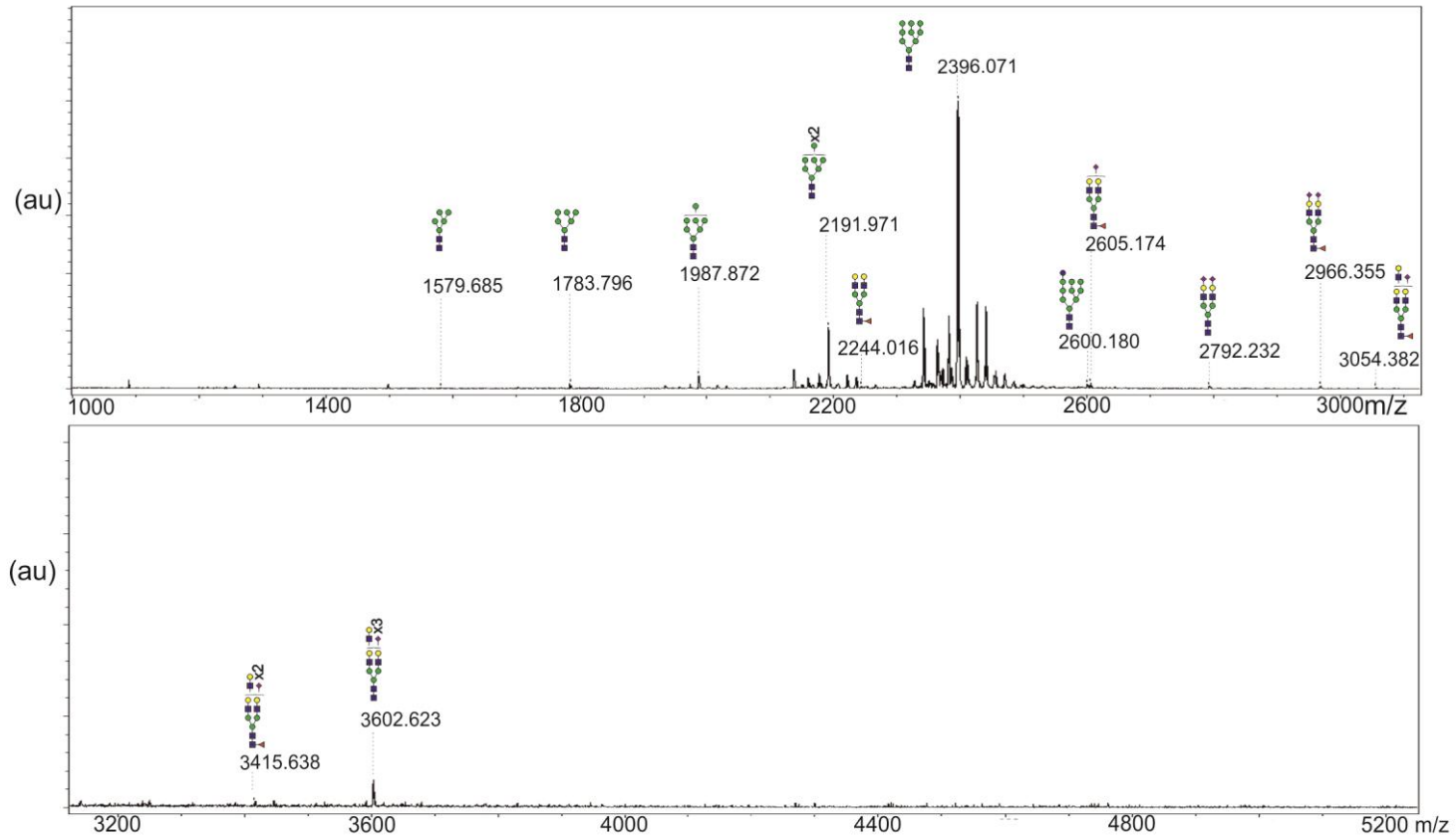

Figure 5.9 MALDI-TOF/TOF spectrum of *N*-glycans from hTERT-MSCs treated with kifunensine.

A representative spectrum (n=3) of *N*-glycans isolated from hTERT-MSCs treated with kifunensine.1x106 cells were cultured in a 10cm dish, in media with kifunensine (2µg/ml) for 48 hours, before *N*-glycan harvest, and further processing. Glycan peaks were identified using calculated mass of monosaccharide units and knowledge of the synthesis pathway. Glycans had to have two isotopic peaks, 3x above noise to be included. Mass of mono-isotopic peak is labelled, with predicted structure pictured above. Spectrum shown is from 1000-5250m/z.

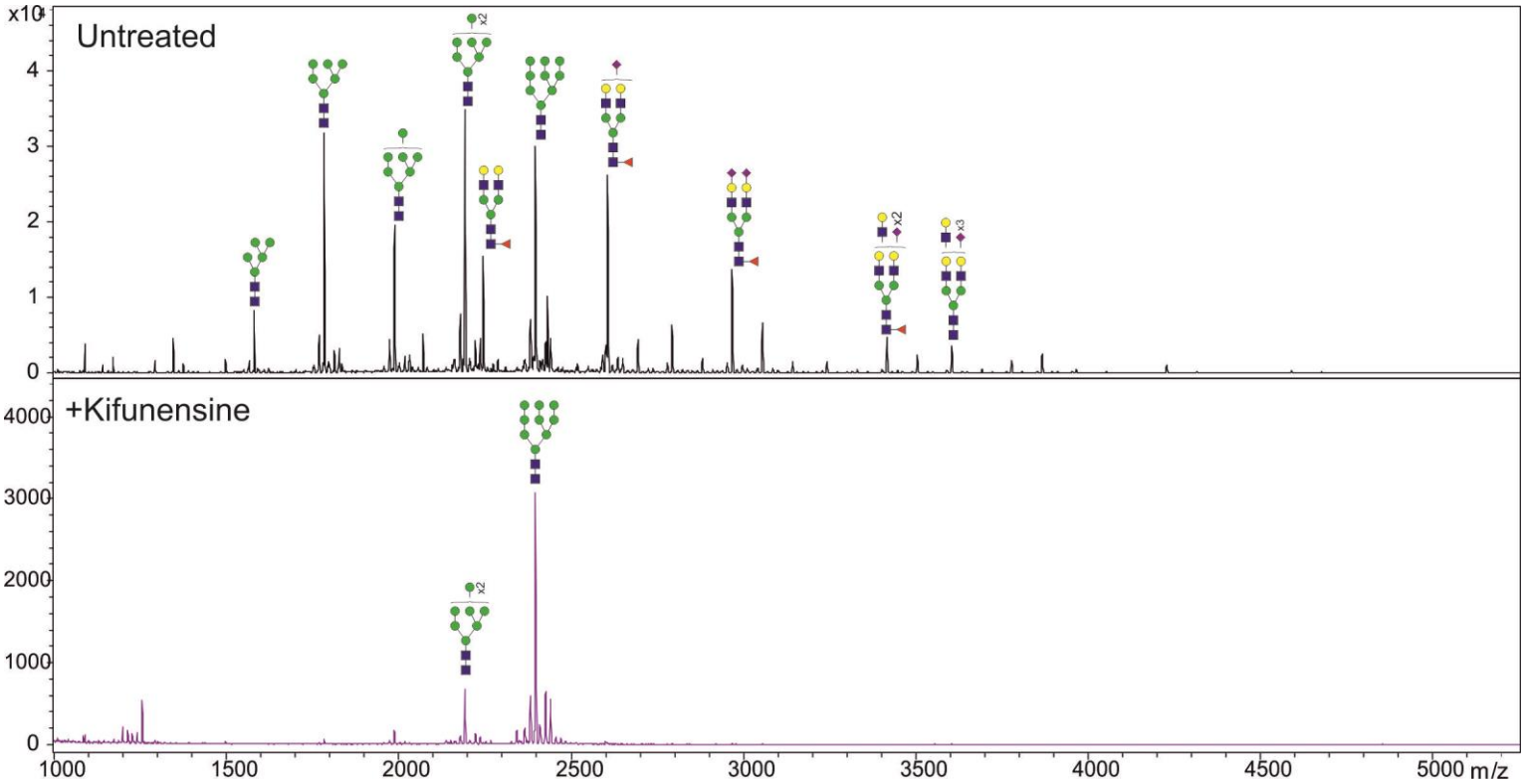

Figure 5.10 Comparison of spectrum from untreated and kifunensine treated hTERT-MSCs.

A representative spectrum of *N*-glycans isolated from hTERT-MSCs untreated or treated with kifunensine.1x106 cells were cultured in a 10cm dish, in basal media or media with kifunensine (2µg/ml) for 48 hours, before *N*-glycan harvest, and further processing. Glycan peaks were identified using calculated mass of monosaccharide units and knowledge of the synthesis pathway. Glycans had to have two isotopic peaks, 3x above noise to be included. Mass of mono-isotopic peak is labelled, with predicted structure pictured above. Spectrum shown is from 1000-5250m/z.

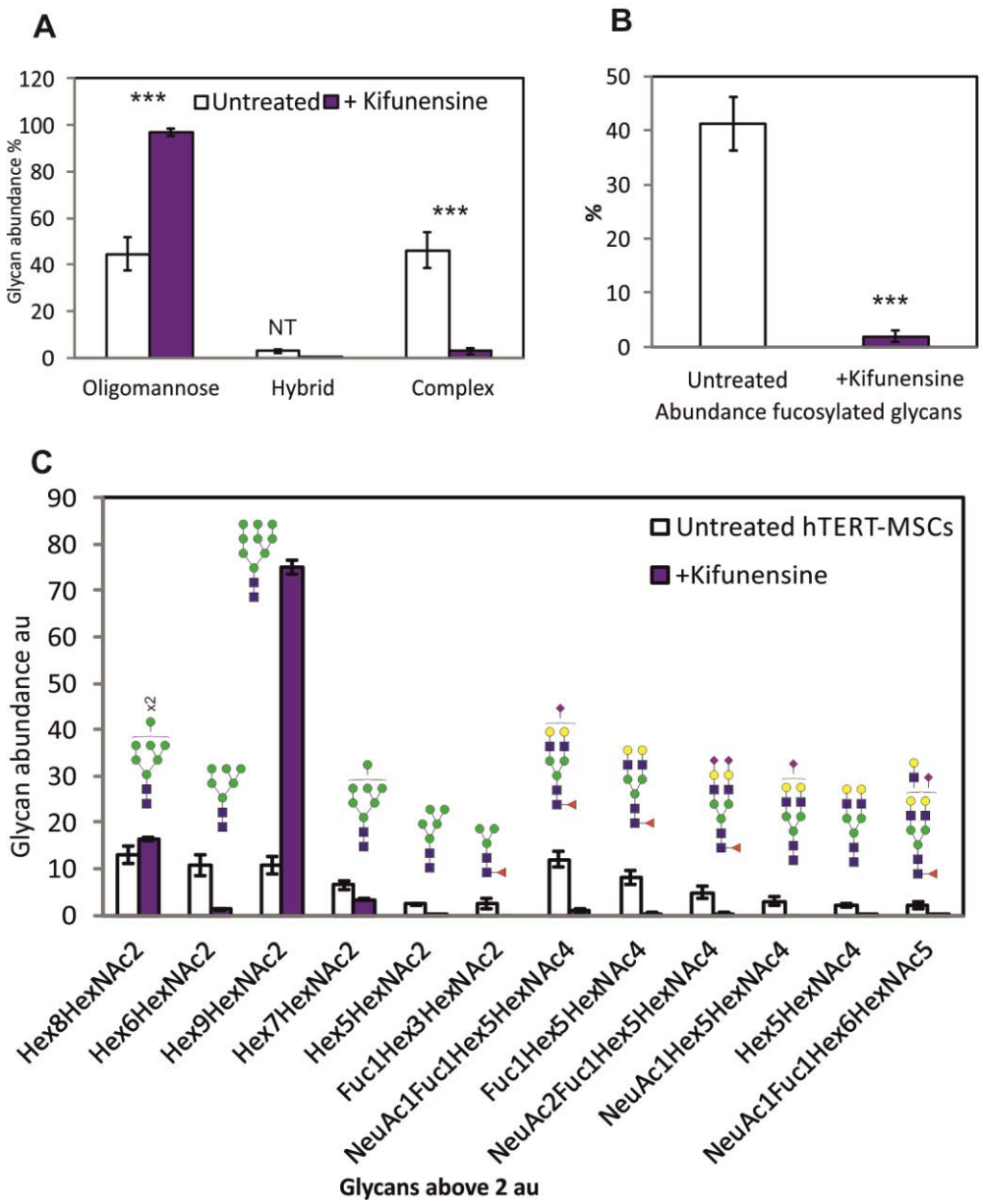

Figure 5.11 Comparison of glycans isolated from untreated hTERT-MSCs and hTERT-MSCs treated with kifunensine.

Glycans identified from spectrum were classed by type (A) and if they were fucosylated or not (B). One way ANOVA, Holm Sidak post hoc test (A) Student's T test (B)**=P<0.01, ***=P<0.001, NT =not tested, n=5 and 3. The normalised average peak intensity of individual glycan structures were also compared. Those present above 2au, in either spectrum are shown in (C). Error bars show standard deviation.

5.2.6 Altered osteogenesis with kifunensine treatment

5.2.6.1 Phosphate staining is increased after kifunensine treatment

To test the effect of kifunensine on osteogenesis cells were cultured in osteogenic media containing kifunensine (2µg/ml). Phosphate staining was notably increased in treated cells (Figure 5.12). The difference between untreated and kifunensine treated cells was visible in samples stained at day 14 and day 21. To help determine if kifunensine affected the differentiation of MSCs into osteoblasts, or, the mineralisation activity of osteoblasts, a pre-treatment with kifunensine, followed by culture in normal osteogenic media was tested. This pre-treatment also increased phosphate staining (Figure 5.12), suggesting that the differentiation of hTERT-MSCs had altered. Other osteogenic assays were then performed using pre-treatment and continuous kifunensine treatment, to further characterise and determine the mechanism by which kifunensine alters osteogenesis.

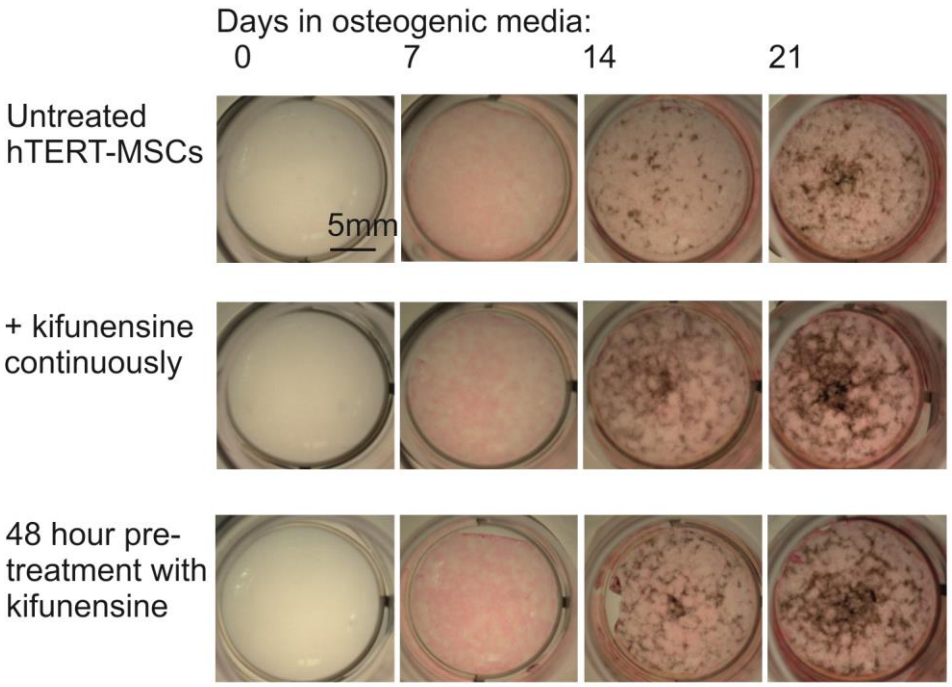

Figure 5.12 Effect of kifunensine on osteogenesis.

Bright-field images of alkaline phosphatase staining - seen as pink - and phosphate (von Kossa) staining - seen as brown - of hTERT-MSCs at weekly time points. Cells were cultured in either normal osteogenic media or osteogenic media supplemented with 2µg/ml kifunensine. The third row shows hTERT-MSCs treated for 48 hours with 2µg/ml kifunensine in basal media, prior to 21 days culture in osteogenic media.

5.2.6.2 ALP activity is unaffected by kifunensine

Following the results from the kifunensine pre-treatment tests, ALP activity and protein levels were measured, as ALP is used as an early marker of osteogenesis. There was no significant difference in ALP activity between untreated and hTERT-MSCs continuously treated with kifunensine (Figure 5.13A). Interestingly, western blots showed reduced levels of ALP protein after 14-28 days in osteogenic media with either kifunensine treatment (Figure 5.13B,C). As ALP is described as an early marker of osteogenesis, another time-course was carried out harvesting cells after 0, 2, 4, 6, 8 and 10 days. Samples were grouped by time so that the membranes could be cut and exposed for different lengths of time, to try and detect ALP at earlier time-points (Figure 5.14). Kifunensine pre-treatment reduced the amount of ALP in all of the samples, despite reaching close to untreated levels by day 28 (Figure 5.13 and Figure 5.14). Continuous treatment with kifunensine did not have the same effect with levels matching untreated samples until day 8, when ALP levels were lower in kifunensine treated cells. The ALP protein from continuously treated cells ran at a lower molecular weight, showing that ALP is *N*-glycosylated. The shift in molecular weight occurred in samples from day 4 onwards, the ALP from the kifunensine pre-treated samples ran at the same molecular weight as untreated, likely due to ALP turnover after the pre-treatment. To investigate what effect lower ALP protein levels and kifunensine treatment had on the expression of osteogenic associated genes, real time qPCR experiments were carried out.

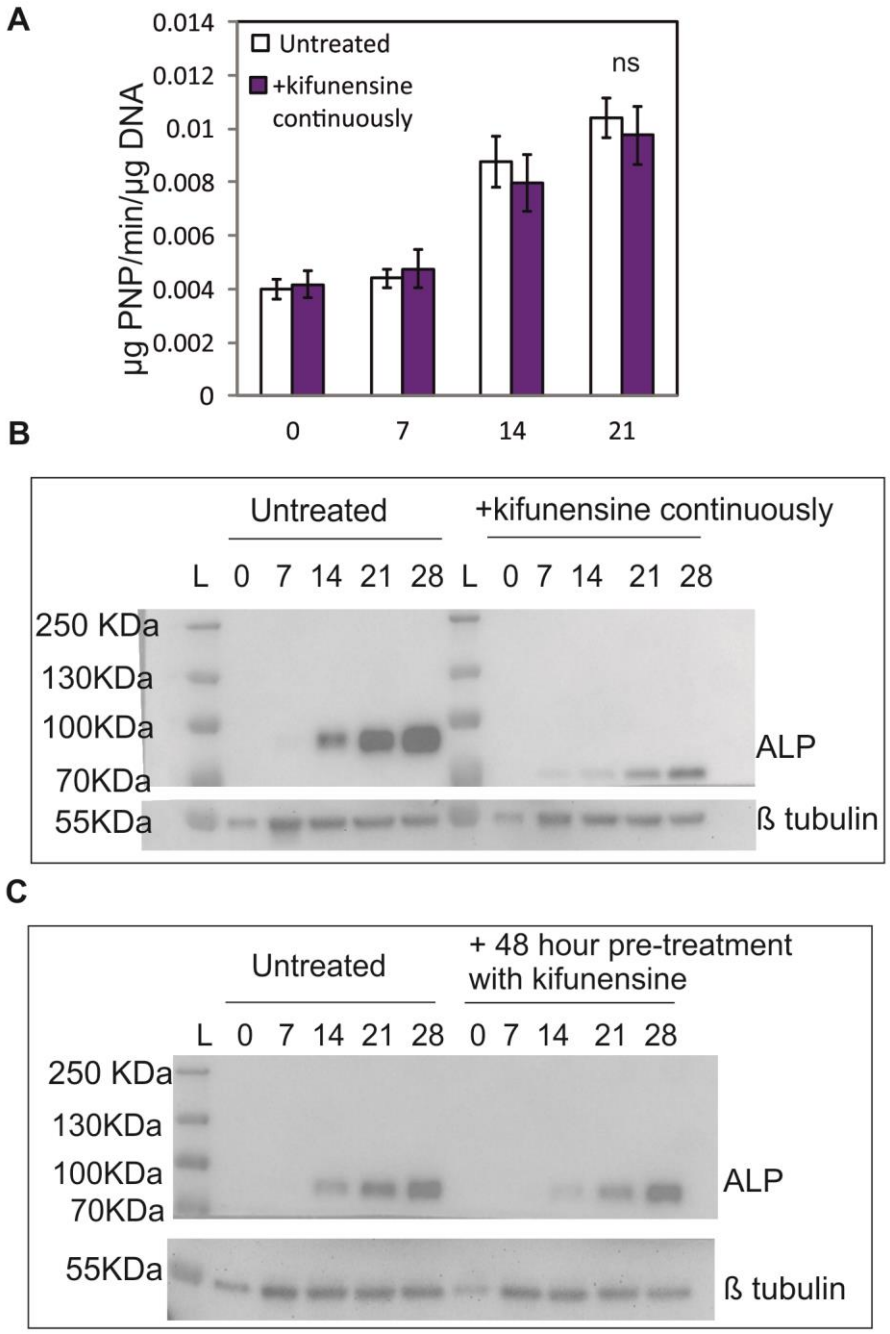

Figure 5.13 Effect of kifunensine on ALP activity and protein levels.

A) ALP activity was measured using pNP assay, after culture in osteogenic media for 0, 7, 14, and 21 days. Activity was made relative to DNA content of each sample using a pico-green assay. One way ANOVA, n=6, ns= non significant, error bars show standard deviation. Data and graph in A) is printed with permission of A.Jagger who carried out the experimental work for A). Protein samples were harvested after cells were cultured in osteogenic media for 0, 7, 14, 21 and 28 days. Untreated hTERT-MSC samples were run alongside hTERT-MSCs treated with kifunensine continuously (B) or for 48 hours prior to addition of osteogenic media (C). Western-blots were probed for ALP and ß tubulin as a loading control. L = protein ladder.

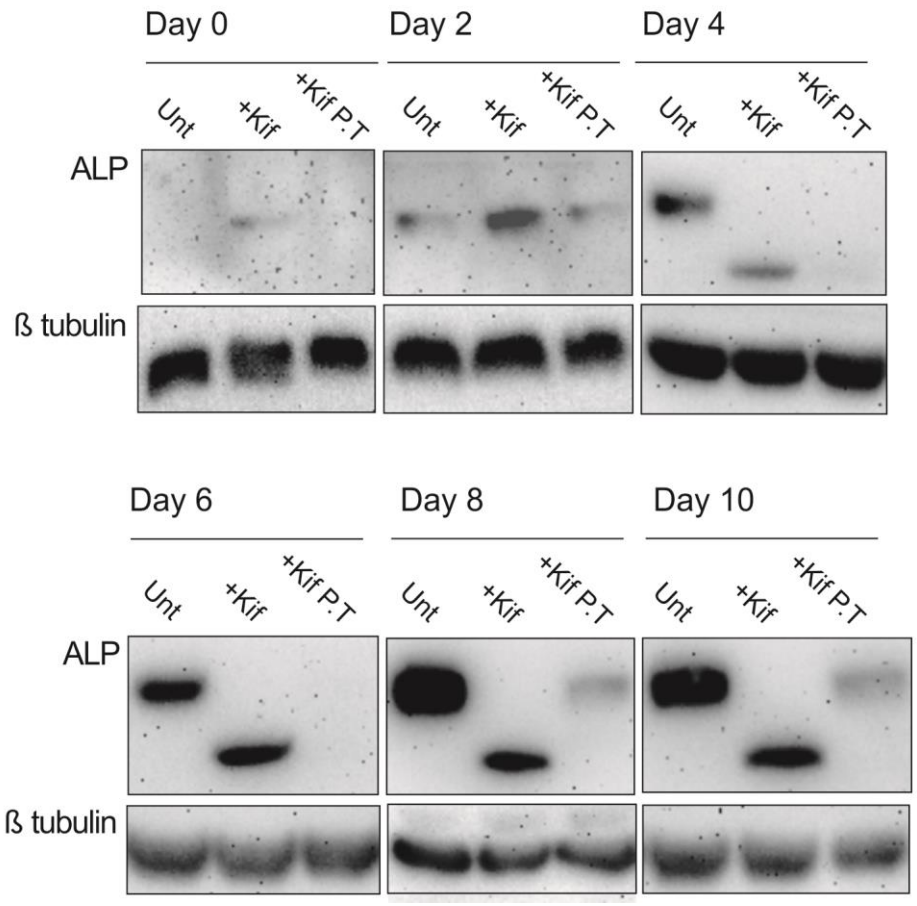

Figure 5.14 Effect of kifunensine treatments on ALP levels during early osteogenesis.

Protein samples were harvested after hTERT-MSCs were cultured in osteogenic media for 0, 2,4,6,8, and10 days. Cells received either normal osteogenic media (Unt), osteogenic media with kifunensine added continuously (+Kif), or a 48 hour pre-treatment with kifunensine in basal media then normal osteogenic media (+Kif P.T). Samples were run in time-point order and the membranes were cut into sections to enable varying exposure times, and avoid burning the membrane. Western blots were probed for ALP and ß tubulin as a loading control.

5.2.6.3 Kifunensine treatment reduces expression of BMP, BSP, and Runx2

In order to further characterise the effect of kifunensine treatment on osteogenesis, real time qPCR was used to analyse the expression level of 3 osteogenic markers used in previous chapters. BMP is a cytokine that stimulates osteogenesis via Smad-5 and Runx2. BMP expression levels in untreated hTERT-MSCs, peaked after 14 days in osteogenic media (Figure 5.15i). The BMP levels in the kifunensine treated samples did not peak at day 14, instead levels gradually increased matching untreated expression levels at day 7 and day 21. The expression of Runx2, which is activated downstream of BMP, increased over time in both kifunensine treated samples. However, levels were lower than untreated hTERT-MSCs at day 14 and day 21 (Figure 5.15ii). BSP is a major non-collagenous protein found in bone. As it plays a role in bone mineralisation, the expression levels were expected to be higher in kifunensine treated cells. In fact, the expression levels were notably lower in both kifunensine treated samples (Figure 5.15iii). Overall the qPCR results did not provide a mechanism of action of kifunensine treatment on osteogenesis. The reduced expression of Runx2 and BSP, together with reduced ALP protein levels, would be expected to result in reduced osteogenic differentiation in kifunensine treated cells. This contradicts the increased phosphate staining seen, which is indicative of functional osteoblasts. Further experiments are required to determine if the mineralisation observed via kifunensine treatment is the result of increased osteogenesis, or aberrant mineralisation by MSCs.

The purpose of testing glycosylation inhibitors was to identify the cause of reduced mineralisation by Cog4KD hTERT-MSCs. As kifunensine increased mineralisation a rescue experiment of Cog4KD hTERT-MSCs was then carried out.

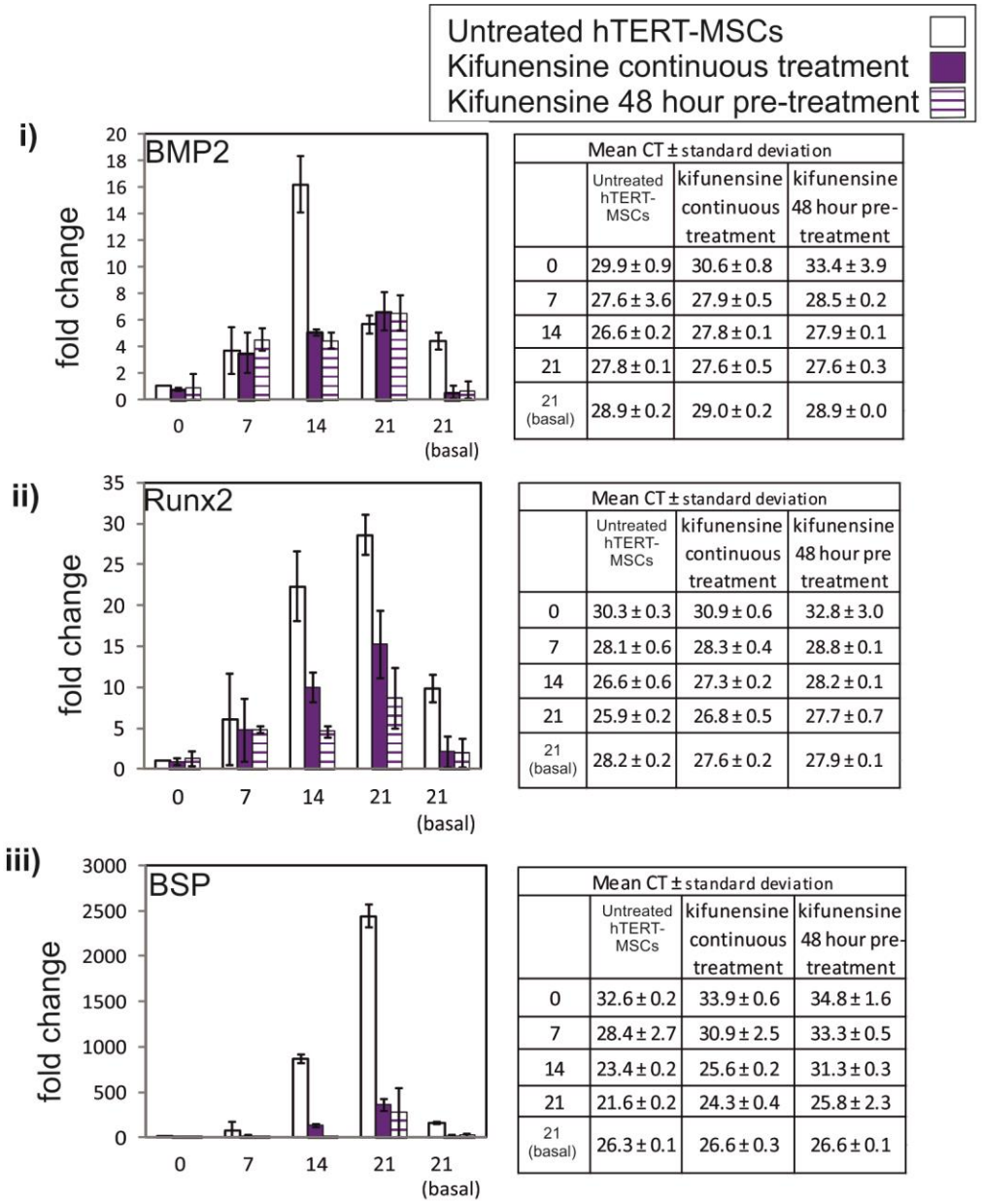

Mean CT ± standard deviation			
	Untreated hTERT-MSCs	kifunensine continuous treatment	kifunensine 48 hour pre-treatment
0	29.9 ± 0.9	30.6 ± 0.8	33.4 ± 3.9
7	27.6 ± 3.6	27.9 ± 0.5	28.5 ± 0.2
14	26.6 ± 0.2	27.8 ± 0.1	27.9 ± 0.1
21	27.8 ± 0.1	27.6 ± 0.5	27.6 ± 0.3
21 (basal)	28.9 ± 0.2	29.0 ± 0.2	28.9 ± 0.0

Mean CT ± standard deviation			
	Untreated hTERT-MSCs	kifunensine continuous treatment	kifunensine 48 hour pre treatment
0	30.3 ± 0.3	30.9 ± 0.6	32.8 ± 3.0
7	28.1 ± 0.6	28.3 ± 0.4	28.8 ± 0.1
14	26.6 ± 0.6	27.3 ± 0.2	28.2 ± 0.1
21	25.9 ± 0.2	26.8 ± 0.5	27.7 ± 0.7
21 (basal)	28.2 ± 0.2	27.6 ± 0.2	27.9 ± 0.1

Mean CT ± standard deviation			
	Untreated hTERT-MSCs	kifunensine continuous treatment	kifunensine 48 hour pre-treatment
0	32.6 ± 0.2	33.9 ± 0.6	34.8 ± 1.6
7	28.4 ± 2.7	30.9 ± 2.5	33.3 ± 0.5
14	23.4 ± 0.2	25.6 ± 0.2	31.3 ± 0.3
21	21.6 ± 0.2	24.3 ± 0.4	25.8 ± 2.3
21 (basal)	26.3 ± 0.1	26.6 ± 0.3	26.6 ± 0.1

Figure 5.15 Real-time quantitative PCR analysis of BMP2, Runx2 and BSP expression in hTERT-MSCs after kifunensine treatments.

cDNA was produced from hTERT-MSCs which were cultured for 48 hours in basal media containing 2µg/ml kifunensine prior to culture in osteogenic-inductive media, as well as from hTERT-MSCs cultured continuously in osteogenic media containing 2µg/ml kifunensine or standard osteogenic media. Samples were harvested at 0,7,14,or 21 days. Primers for BMP2 (i) Runx2 (ii), BSP (iii) and RSP27a were used in real-time qPCR experiments. cDNA produced from hTERT-MSCs grown in basal media for 21 days were also analysed as a control (21 basal). CT values were made relative to RSP27a values and then expressed as fold change relative to day 0 untreated values. Triplicate technical replicates from 2 biological repeats are shown, error bars are standard deviation. Tables show mean CT values ± standard deviation of combined replicates.

5.2.7 Kifunensine does not rescue Cog4KD hTERT-MSCs' mineralisation

Cog4KDshRNA1 hTERT-MSCs were treated continuously with kifunensine and osteogenic media. Phosphate staining remained reduced in the kifunensine treated Cog4KDshRNA1 hTERT-MSCs (Figure 5.16). This result as well as the increased phosphate staining seen in kifunensine treated cells, which have significantly reduced complex glycan abundance, indicates that disrupted *N*-glycosylation is not the cause of reduced mineralisation in the Cog4KD hTERT-MSCs.

Disrupted O-glycan synthesis is another potential cause of the Cog4KD hTERT-MSC phenotype. So the effect of an O-glycan inhibitor was tested next.

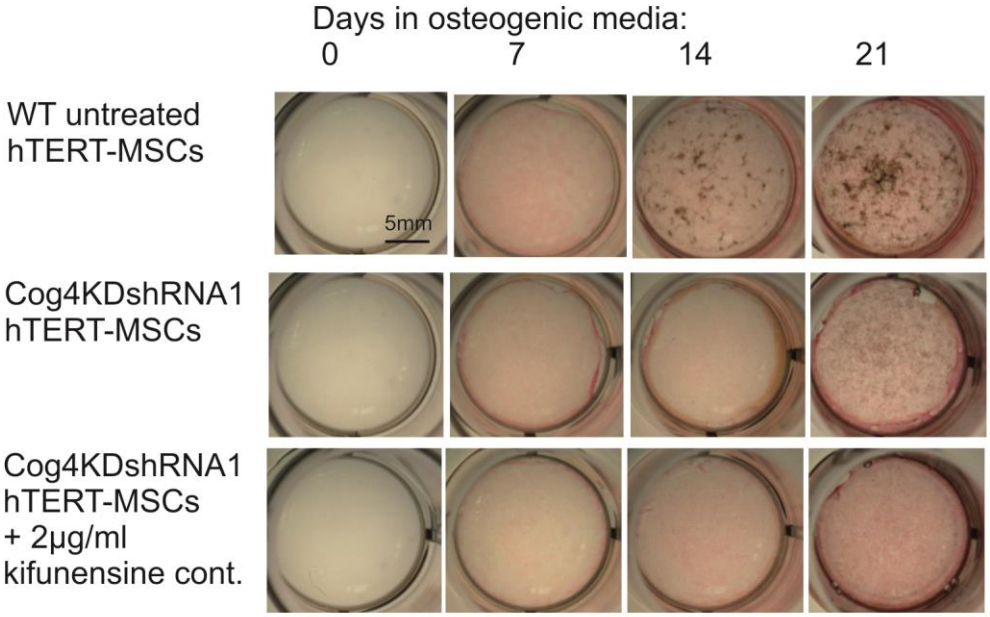

Figure 5.16 Effect of kifunensine on Cog4KD hTERT-MSCs.

Bright-field images of alkaline phosphatase staining - seen as pink - and phosphate (von Kossa) staining - seen as brown - of hTERT-MSCs at weekly time points. WT hTERT-MSCs were cultured in normal osteogenic media. Cog4KD hTERT-MSCs were cultured in normal osteogenic media or osteogenic media supplemented continuously with 2µg/ml kifunensine (bottom row). Kifunensine treatment started 48 hours prior to addition of osteogenic media.

5.2.8 BadGal treatment alters O-glycan synthesis

In order to test if disrupted O-glycan synthesis was the cause of reduced mineralisation in Cog4KD hTERT-MSCs, benzyl 2-acetamido-2-deoxy-α-D-galactopyranoside (BadGal) was used. BadGal is a competitive inhibitor of the glycosyltransferase that normally adds galactose to *N*-acetylgalactosamine, forming a core 1 or T-antigen O-glycan structure. Flow cytometry with lectins was carried out on BadGal treated hTERT-MSCs. Jacalin and VVL lectins can both bind to N-acetylgalactosamine or the Tn antigen structure. In line with glycosyltransferase inhibition BadGal treated hTERT-MSCs had significantly higher Jacalin and VVL staining ($P<0.05$ and $P<0.001$ respectively) (Figure 5.17A and Figure 5.17B). Staining with PNA, which binds to the T-antigen structure if unsialylated, was significantly increased in BadGal treated hTERT-MSCs ($P<0.001$) (Figure 5.17C). This could have been caused by binding of PNA to BadGal-galactose disaccharides, which have been shown to form in other cell types, however the staining should be preferential for surface glycans rather than intracellular structures. Alternatively, as PNA binding is inhibited by sialic acid, the BadGal-galactose disaccharide may have acted as a competitive inhibitor of sialyltransferases, resulting in fewer sialylated O-glycans. The binding of SNA increased significantly ($P<0.05$) (Figure 5.18A), but as binding can occur to sialylated *N*-glycans as well as sialylated O-glycans, it could be another consequence of altered sialyltransferase substrate competition. The binding of MAL II was not significantly different in BadGal treated hTERT-MSCs compared to untreated cells (Figure 5.18B). Overall the lectin staining indicated that BadGal treatment reduced O-glycan elongation. Phenotypic tests were then carried out to test the effect of reduced O-glycan synthesis.

5.2.9 BadGal treatment does not alter morphology or proliferation

BadGal treatment did not affect the morphology of hTERT-MSCs. Crystal violet staining of BadGal treated cells revealed similar cell morphology, between treated and untreated cells (Figure 5.6D). The proliferation of hTERT-MSCs were also unaffected by BadGal treatment, shown using an MTT assay (Figure 5.6D). Following this, the effect of altered O-glycan synthesis on osteogenesis was tested by adding BadGal (2mM) to osteogenic media.

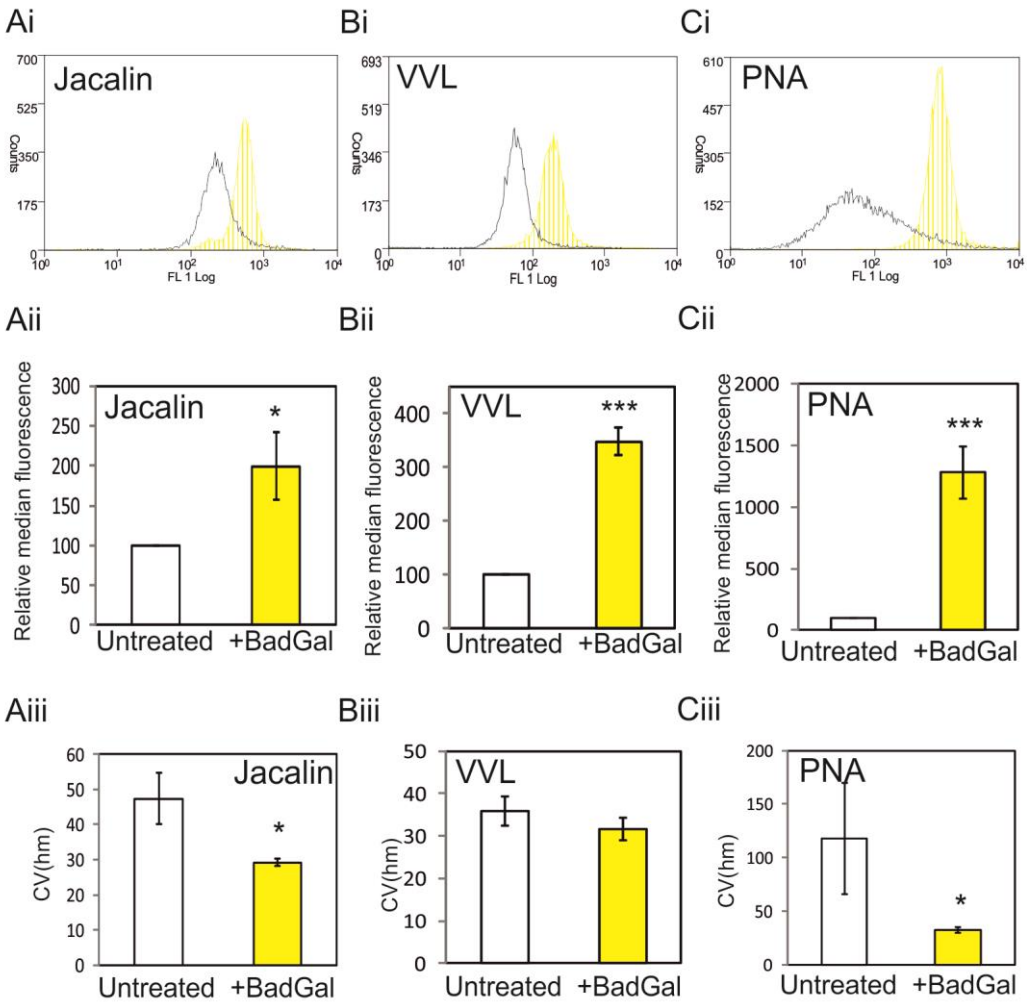

Figure 5.17 Flow cytometry analysis of BadGal treated hTERT-MSCs with lectins.

Untreated hTERT-MSCs and hTERT-MSCs treated with 2mM BadGal were probed with A) Jacalin B) VVL and C) PNA lectins. Histograms i) show log fluorescence of untreated hTERT-MSCs (black) and hTERT-MSCs treated with 2mM BadGal (yellow) after staining with lectin. Median fluorescence values were made relative to WT set at 100. Average relative values of 3 independent experiments are shown in ii). Coefficient of variation (Half max) (CV (hm)) values, average of 3 independent experiments are shown in iii). Student's T test, n=3, * = P<0.05, ***= P<0.001. Error bars are standard deviation.

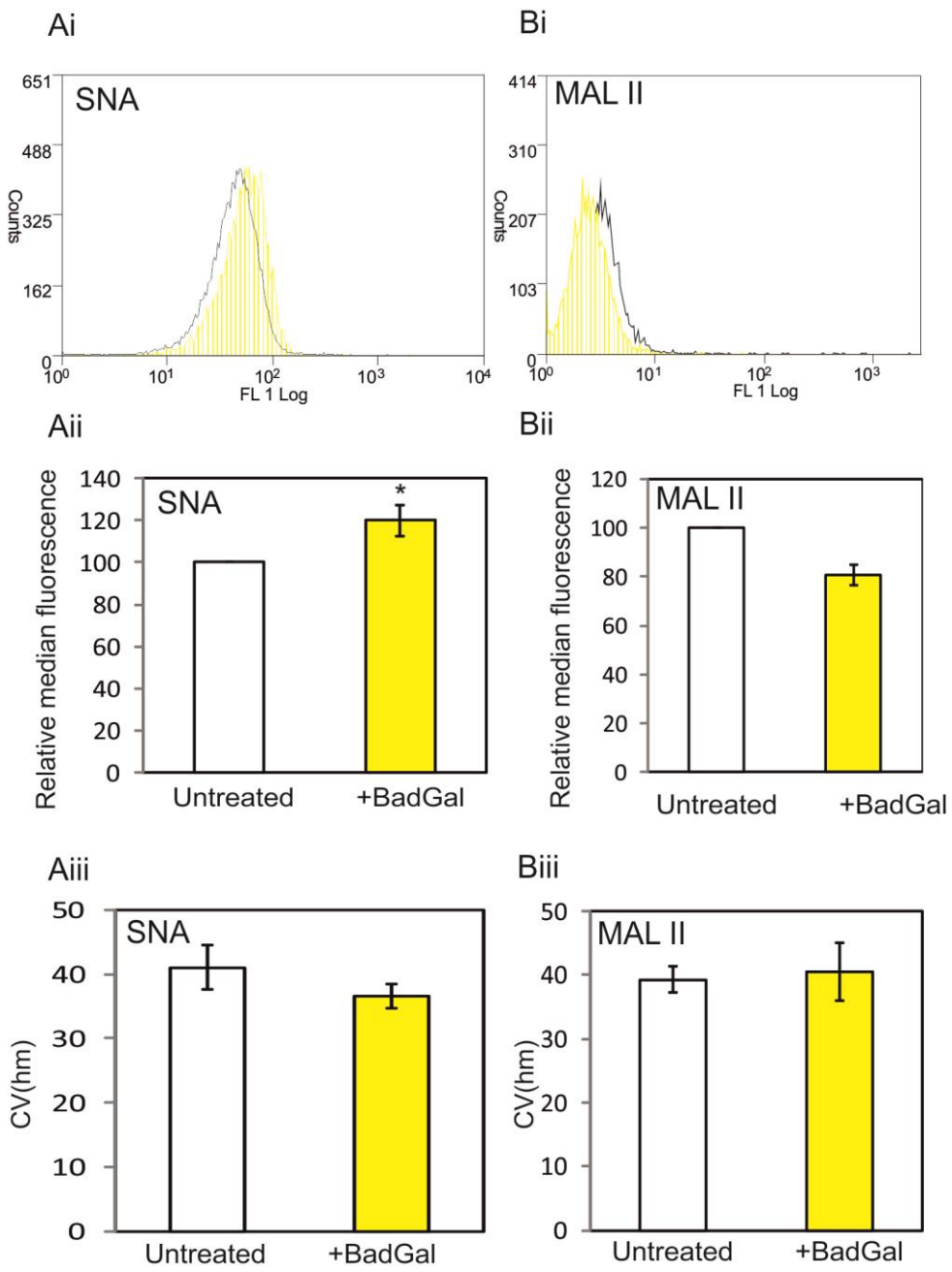

Figure 5.18 Flow cytometry analysis of BadGal treated hTERT-MSCs with lectins (continued).

Untreated hTERT-MSCs and hTERT-MSCs treated with 2mM BadGal were probed with A) SNA, and B) MAL II lectins. Histograms i) show log fluorescence of untreated hTERT-MSCs (black) and hTERT-MSCs treated with 2mM BadGal (yellow) after staining with lectin. Median fluorescence values were made relative to WT set at 100. Average relative values of 3 independent experiments are shown in ii). Coefficient of variation (Half max) (CV (hm)) values, average of 3 independent experiments are shown in iii). Student's T test, n=3, * = P<0.05. Error bars are standard deviation.

5.2.10 BadGal treatment mimics Cog4 knock down effect on osteogenesis

5.2.10.1 Phosphate staining is reduced in BadGal treated hTERT-MSCs

hTERT-MSCs were cultured in basal media containing BadGal (2mM) for 48 hours prior to the addition of osteogenic media, containing BadGal (2mM). Weekly ALP and phosphate (Von kossa) staining indicated reduced mineralisation in BadGal treated hTERT-MSCs (Figure 5.19). ALP staining (seen as pink) was unchanged between samples. As with the kifunensine treatments, to test if the change in mineralization capacity with BadGal treatment was due to impaired differentiation or impaired mineralisation, the effect of a pre-treatment of BadGal, prior to normal osteogenic media was assessed. This experiment showed that a reduction in mineralization occurred after a 72 hour pre-treatment with BadGal, seen by reduced phosphate staining, compared to untreated samples (Figure 5.20).

This reduction in phosphate staining was similar to the Cog4KD hTERT-MSCs. Following this, the effect of BadGal was tested using other osteogenic markers.

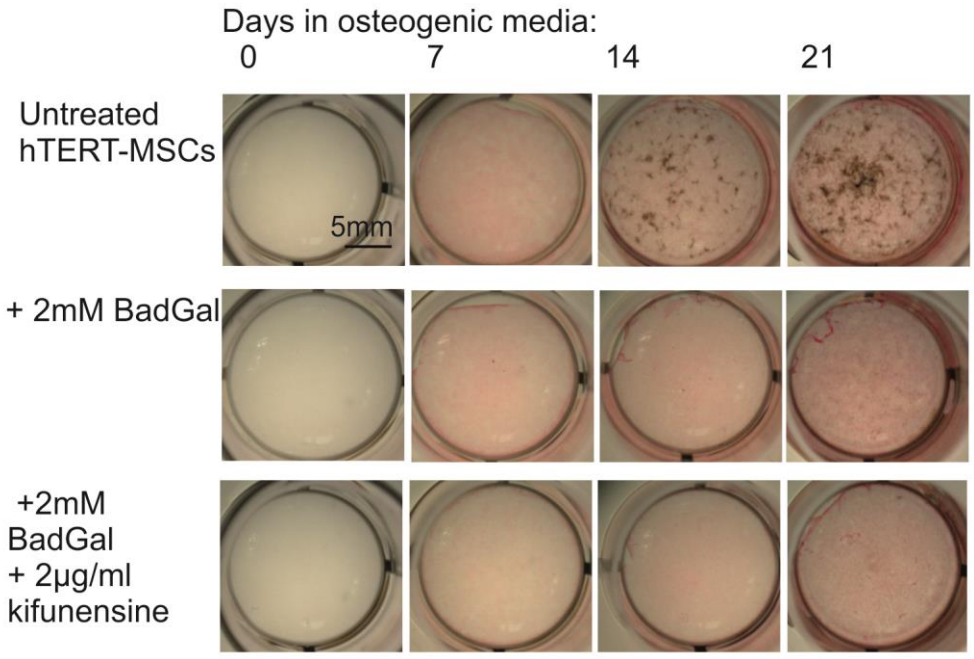

Figure 5.19 Effect of BadGal on osteogenesis.

Bright-field images of alkaline phosphatase staining - seen as pink - and phosphate (von Kossa) staining - seen as brown - of hTERT-MSCs at weekly time points during culture in either normal osteogenic media, osteogenic media supplemented with 2mM BadGal, or osteogenic media supplemented with 2mM BadGal and 2µg/ml kifunensine. Treatments started 48 hours prior to addition of osteogenic media.

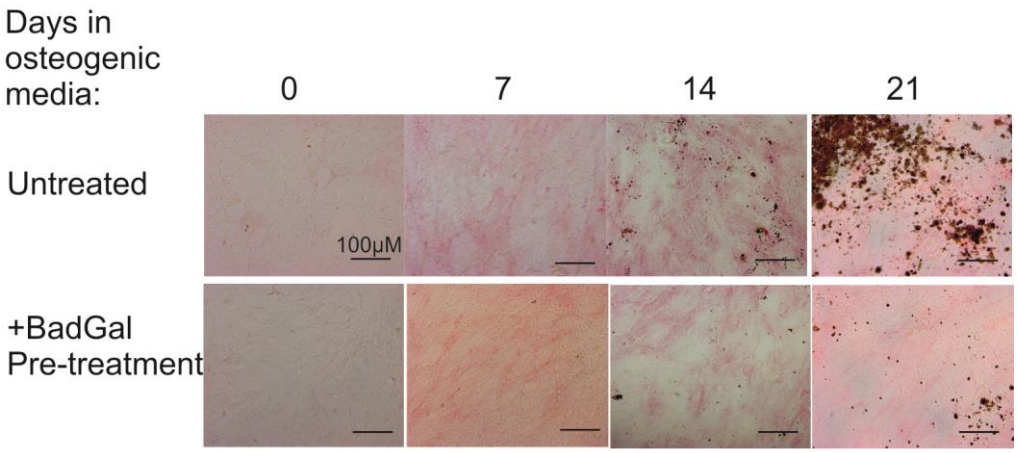

Figure 5.20 Effect of BadGal pre-treatment on osteogenesis.

Bright-field images of alkaline phosphatase staining - seen as pink - and phosphate (von Kossa) staining - seen as brown - of hTERT-MSCs at weekly time points during culture in osteogenic media. Untreated cells were grown in basal media for 72 hours prior to osteogenic media, whilst treated cells recieved 2mM BadGal for 72 hours prior to addition of normal osteogenic media. The images here are printed with the permission of I.G.Cantanhede who carried out the experimental work for this figure.

5.2.10.2 BadGal treatment does not affect ALP levels or, BMP, BSP, and Runx2 expression

To further test the effect of BadGal on osteogenesis, the activity and protein levels of ALP were measured in BadGal treated hTERT-MSCs. The activity of ALP was significantly lower in the BadGal treated hTERT-MSCs at day 21 (Figure 5.21A). Despite this, Western blots of ALP protein showed similar amounts of ALP between samples, although it ran at a lower molecular weight (Figure 5.21B). This suggests ALP is also O-glycosylated. This western differs from that of the Cog4KD hTERT-MSCs, which had reduced levels of ALP protein. During culture with osteogenic media containing BadGal the expression levels of osteogenic genes BMP2, BSP, and Runx2 were similar to untreated samples (Figure 5.22). Despite the lack of visible mineralisation seen by Von kossa staining of BadGal treated hTERT-MSCs, the levels of BSP were as high as untreated cells.

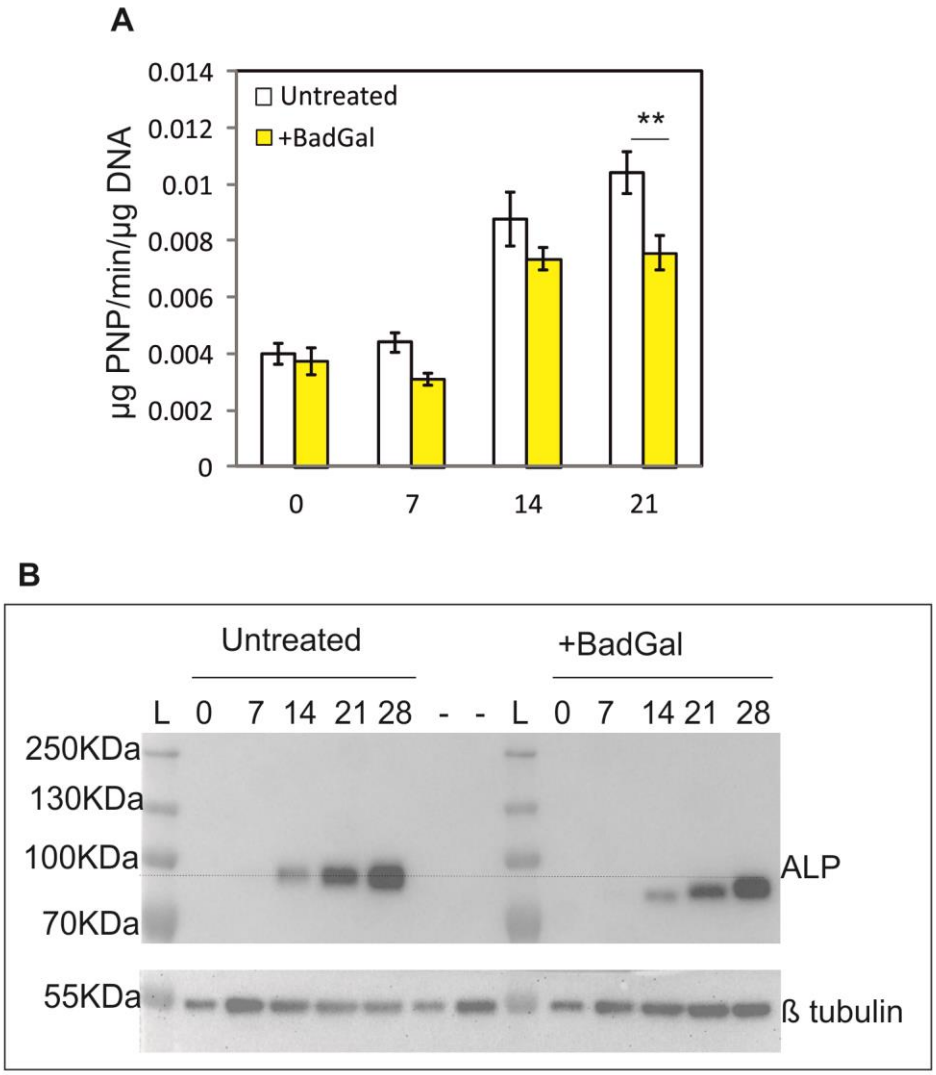

Figure 5.21 Effect of BadGal on ALP activity and protein levels.

A) ALP activity was measured using pNP assay, after culture in osteogenic media for 0, 7, 14, and 21 days. Activity was made relative to DNA content of each sample using a pico-green assay. White bars represent untreated hTERT-MSC, yellow bars represent hTERT-MSCs treated continuously with 2mM BadGal. Mann Whitney U test on day 21 data only, ** = $P<0.01$, n=6, error bars show standard deviation. B) Protein samples were harvested after cells were cultured in osteogenic media for 0, 7, 14, 21 and 28 days. Untreated hTERT-MSC samples were run alongside hTERT-MSCs treated with 2mM BadGal continuously. Western-blots were probed for ALP and ß tubulin as a loading control. L = protein ladder.

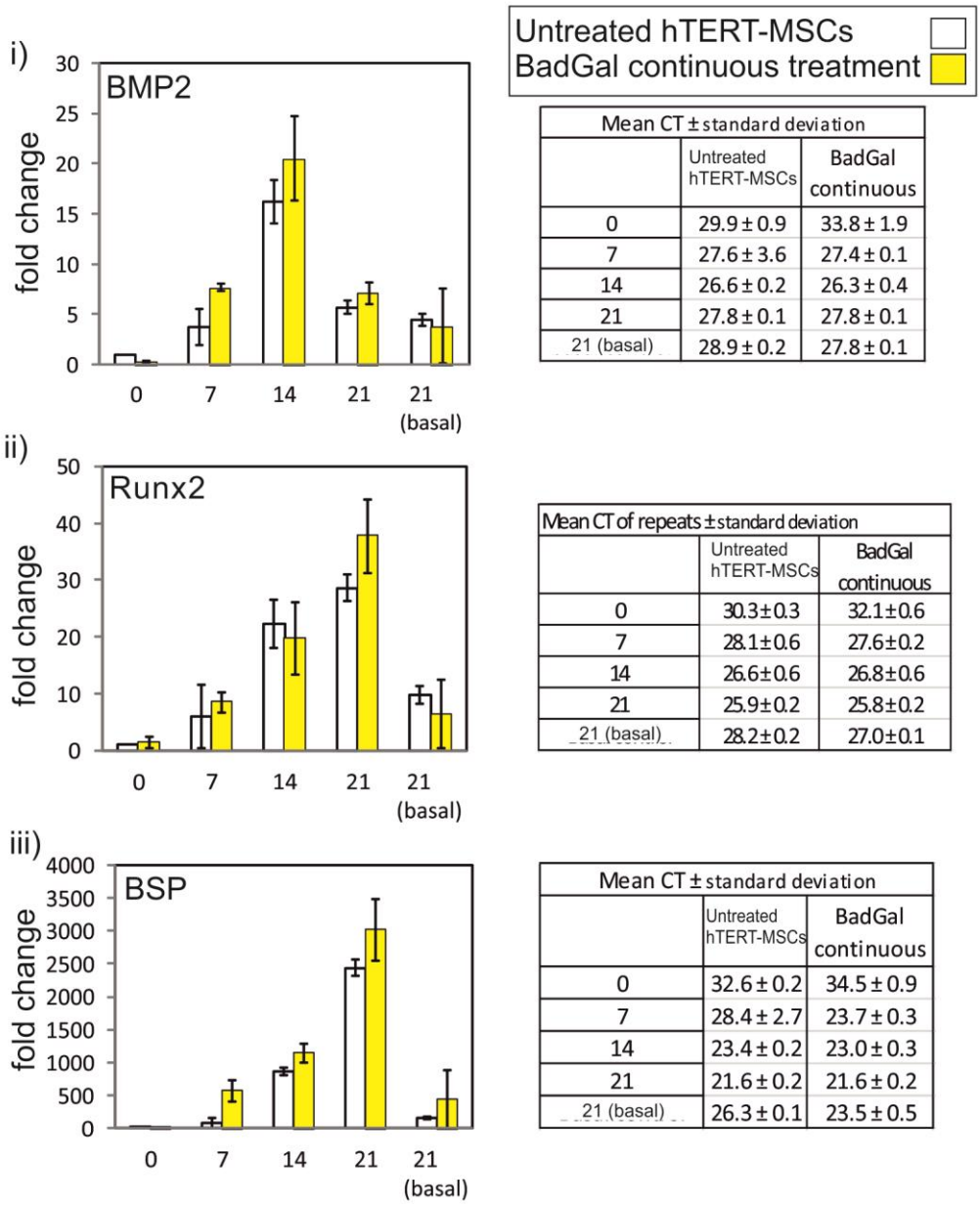

Mean CT ± standard deviation		
	Untreated hTERT-MSCs	BadGal continuous
0	29.9 ± 0.9	33.8 ± 1.9
7	27.6 ± 3.6	27.4 ± 0.1
14	26.6 ± 0.2	26.3 ± 0.4
21	27.8 ± 0.1	27.8 ± 0.1
21 (basal)	28.9 ± 0.2	27.8 ± 0.1

Mean CT of repeats ± standard deviation		
	Untreated hTERT-MSCs	BadGal continuous
0	30.3±0.3	32.1±0.6
7	28.1±0.6	27.6±0.2
14	26.6±0.6	26.8±0.6
21	25.9±0.2	25.8±0.2
21 (basal)	28.2±0.2	27.0±0.1

Mean CT ± standard deviation		
	Untreated hTERT-MSCs	BadGal continuous
0	32.6 ± 0.2	34.5 ± 0.9
7	28.4 ± 2.7	23.7 ± 0.3
14	23.4 ± 0.2	23.0 ± 0.3
21	21.6 ± 0.2	21.6 ± 0.2
21 (basal)	26.3 ± 0.1	23.5 ± 0.5

Figure 5.22 Real-time quantitative PCR analysis of BMP2, Runx2 and BSP expression after BadGal treatment.

cDNA was produced from hTERT-MSCs which were cultured in osteogenic media containing 2mM BadGal or normal osteogenic media. Samples were harvested at 0,7,14,or 21 days. Primers for BMP2 (i) Runx2 (ii), BSP (iii) and RSP27a were used in real-time qPCR experiments. cDNA produced from hTERT-MSCs grown in basal media for 21 days were also analysed as a control (21 basal). CT values were made relative to RSP27a values and then expressed as fold change relative to day 0 untreated values. Triplicate technical replicates from 2 biological repeats are shown, error bars are standard deviation. Tables show mean CT values ± standard deviation of combined replicates.

5.2.10.3 Kifunensine but not BadGal treatment significantly affects β catenin levels

Both kifunensine and BadGal treatments were able to affect mineralization capacity of hTERT-MSCs after a short treatment, prior to the addition of osteogenic media, which indicates a change in MSCs that affects the differentiation of the cells, rather than their mineralization machinery. Multiple signalling pathways initiate osteogenic differentiation, by inducing the expression of osteogenic transcription factors and genes. Active Wnt signalling involves unphosphorylated β-catenin translocating to the nucleus and affecting gene transcription. Since studies have shown active Wnt signalling to promote osteogenesis [98, 99], the levels of unphosphorylated β-catenin were assessed after kifunensine or BadGal treatments by western blot. The amount of unphosphorylated β-catenin was significantly increased after 48 hour kifunensine treatment (Figure 5.23). The level of unphosphorylated β-catenin after BadGal treatment, did also increase, but was not significantly different to levels in untreated hTERT-MSCs. This suggests that the mechanism of action of kifunensine could be via β-catenin, which is downstream of Wnt signalling. Further experiments are required to identify which signalling pathway BadGal acts on to affect osteogenesis. To further test the role of O-glycans in osteogenesis, a combined treatment of BadGal and kifunensine was carried out.

5.2.11 Reduced mineralisation with BadGal treatment is not rescued by kifunensine

WT hTERT-MSCs were treated with BadGal and kifunensine continuously during osteogenesis. The level of phosphate staining was the same as that of cells treated with BadGal alone (Figure 5.19). This supports the notion that O-glycosylation is disrupted in the Cog4KD hTERT-MSCs, as their mineralisation was also not restored by kifunensine treatment (Figure 5.16).

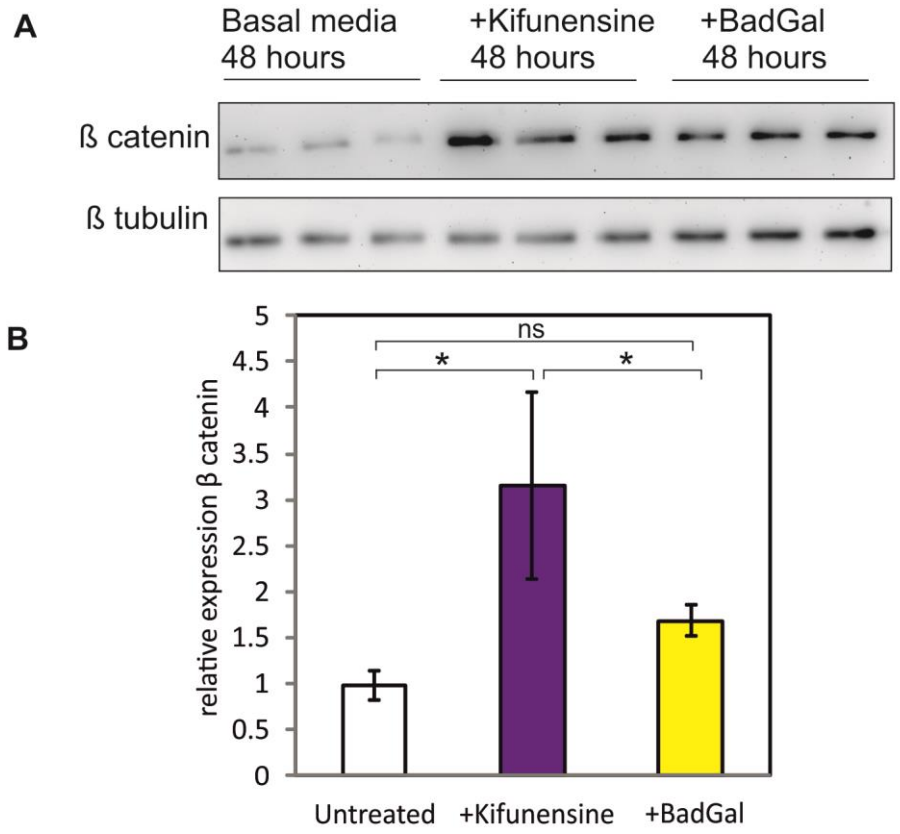

Figure 5.23 Effect of kifunensine or BadGal on ß catenin expression.

A) Protein samples were harvested from cells cultured in either basal media alone for 48 hours (untreated), or basal media supplemented with 2µg/ml kifunensine for 48 hours, or basal media supplemented with 2mM BadGal for 48 hours. Samples were run in triplicate on a SDS-page gel. After western blot, the membrane was cut, and blotted with antibodies against ß catenin or ß tubulin as loading control. Densitrometry was carried out on images of the blots in A) using ImageJ software. ß catenin density was made relative to ß tubulin density. The density of the first untreated lane was set to 1. Average relative ß catenin density is plotted in B). Error bars show standard deviation, ns = non-significant, * = $P<0.05$, One way ANOVA, with Holm Sidak post hoc test, n=3.

5.2.12 ALP is both O-and *N*-glycosylated and glycosylation levels correlate with protein levels

The protein harvested from cells treated with kifunensine, BadGal, or both was run alongside protein from untreated cells, and blotted for ALP (Figure 5.24). The ALP from untreated cells migrated at 95KDa whilst the ALP from BadGal treated cells migrated at 80KDa. This suggests ALP is O-glycosylated. The ALP from kifunensine treated cells migrated at 70KDa, showing ALP to be *N*-glycosylated as well. The amount of ALP protein varied depending on the glycan inhibitor treatment. The amount of ALP protein was reduced in cells treated with kifunensine. It was further reduced in cells receiving double treatment. One explanation for this is that *N*-and O-glycosylation contributes to the turnover rate of ALP. On the other hand, as glycan inhibitors were shown to affect osteogenesis, the altered levels could be a consequence of altered cell differentiation triggered by the change in cellular glycome.

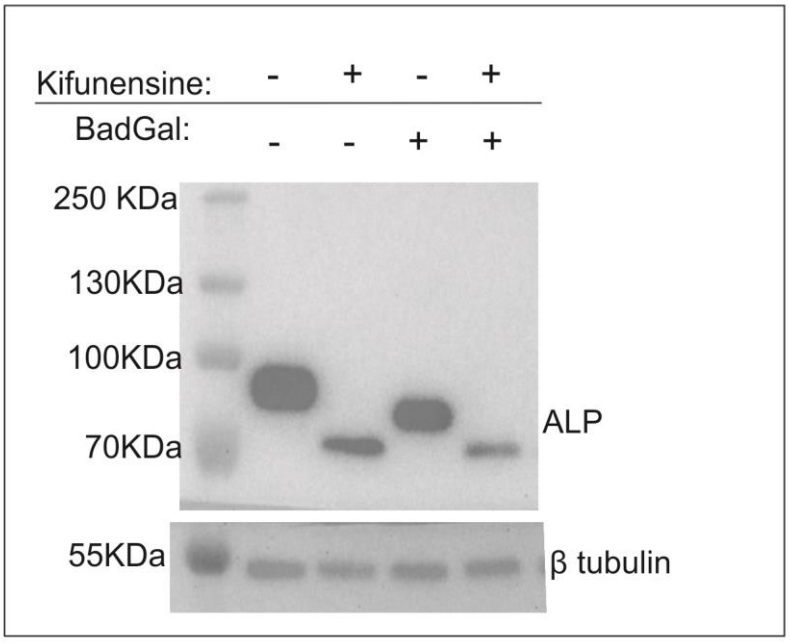

Figure 5.24 Effect of kifunensine and BadGal on ALP protein levels.

Protein samples of hTERT-MSCs cultured for 21 days in osteogenic media containing either no supplement, kifunensine, BadGal, or both kifunensine and BadGal supplements, were loaded (indicated by -/+). Western-blots were probed for ALP and ß tubulin as a loading control.

Despite the evidence implying that disrupted O-glycan sialylation in the Cog4KD hTERT-MSCs, could be causing the reduced mineralization capacity, other types of glycans that are also synthesised in the Golgi could be also affected by the Cog4 knock-down and contribute to their altered osteogenesis. In order to test this I.G.Cantanhede carried out experiments with a glycolipid inhibitor – deoxynojirimycin (NB DNJ) – and with sodium chlorate, an inhibitor of GAG sulfation.

5.2.13 Glycolipid inhibition by NB DNJ does not phenocopy Cog4KD hTERT-MSCs

NB DNJ is an imino sugar that has been shown to inhibit the synthesis of glycolipids that contain a glucose attached to ceramide at the start of the glycolipid chain [156]. Previous studies showed that treatment with 50μM NB DNJ could reduce cholera toxin (a protein that binds glycolipids) binding by 90% [156]. To ensure full inhibition hTERT-MSCs were treated with 150μM NB DNJ. This treatment did not affect proliferation of the cells, as shown by no change in absorbance in a MTT assay (Figure 5.25A). NB DNJ has been proposed to inhibit α-glucosidase I and II, which are responsible for cleaving the glucose units from the precursor oligosaccharide structure in the *N*-glycan synthesis pathway [156]. To test if NB DNJ was affecting *N*-glycan synthesis treated cells were stained with the lectin ConA and staining was compared to untreated hTERT-MSCs using flow cytometry. The ConA staining was unaffected by NB DNJ treatment, as seen by the overlapping fluorescence histograms from the flow cytometry (Figure 5.25B). This indicated that NB DNJ, at these concentrations, did not inhibit *N*-glycan synthesis, and could be used to test the role of glycolipid synthesis in MSC differentiation. The effect of glycolipid inhibition on osteogenesis was assessed by inclusion of NB DNJ in osteogenic media continuously, and by pre-treating cells with NB DNJ prior to normal osteogenic media. Staining of ALP and phosphate (von kossa) at weekly time-points indicated that pre-treatment or continuous treatment with NB DNJ had no effect on osteogenesis (Figure 5.25C). This indicated that disrupted synthesis of the most abundant type of glycolipid – glucosyl-ceramide based – was not responsible for the loss of mineralization capacity seen in the Cog4KD hTERT-MSCs.

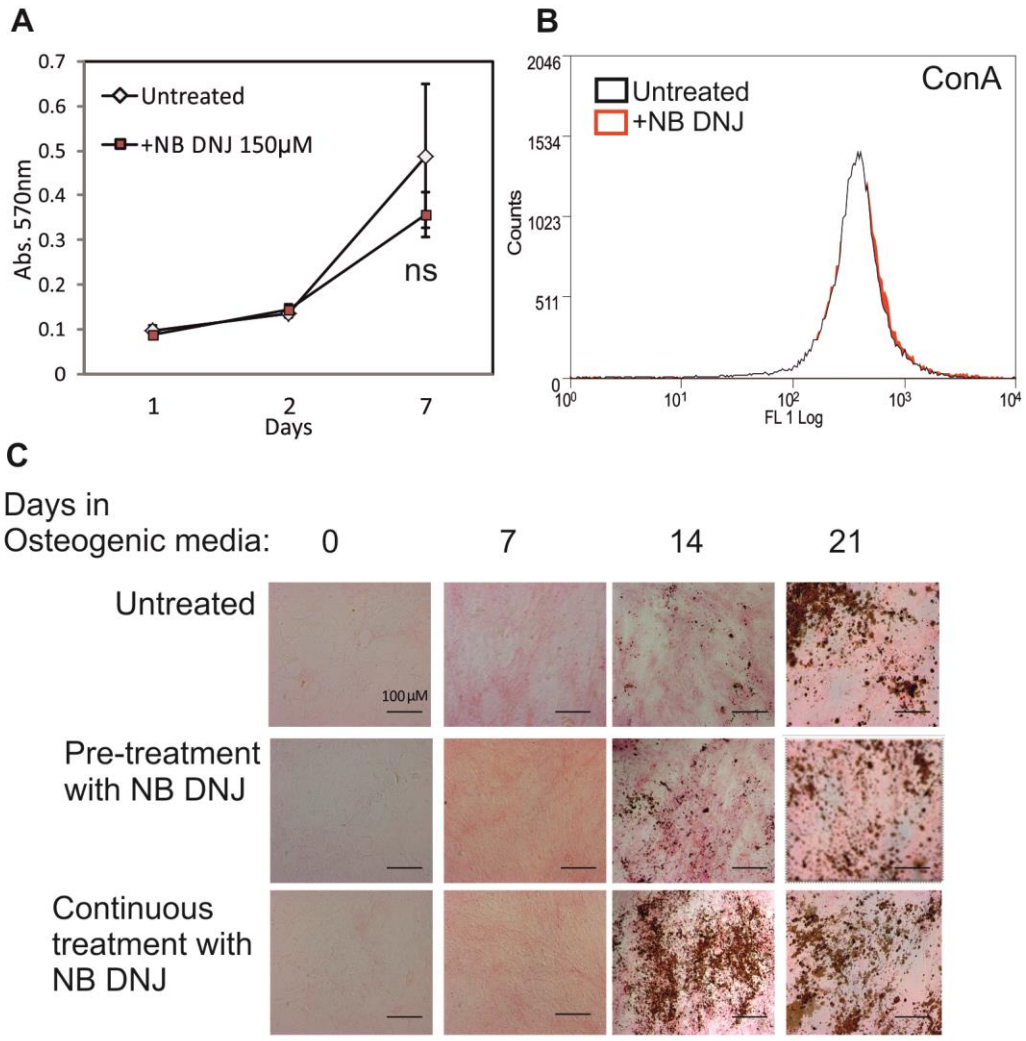

Figure 5.25 Effect of NB DNJ treatment on hTERT-MSCs.

A) Effect of continuous treatment with 150µM NB DNJ on the proliferation of hTERT-MSCs was estimated using an MTT assay, at days 1,2, and 7. ns= non-significant, One way ANOVA on Ranks, Dunn's post hoc test, n=6, error bars show standard deviation. B) Black histogram shows log fluorescence of untreated hTERT-MSCs after staining with ConA lectin. Red histogram shows log fluorescence of hTERT-MSCs treated with 150µM NB DNJ for 48 hours, after staining with ConA. C) Brightfield images of hTERT-MSCs after culture in osteogenic media with either no supplement, pre-treatment with NB DNJ, or continuous treatment with NB DNJ. Cells were stained for ALP and phosphate (Von kossa) at weekly timepoints.

These images and data are printed with the permission of I.G.Cantanhede who carried out the experimental work for this figure.

5.2.14 Continuous inhibition of GAG sulfation reduces mineralization capacity

As proteoglycans and GAG chains are synthesised in the Golgi alongside O-glycans, it is possible that proteoglycan synthesis was disrupted in the Cog4KD hTERT-MSCs. To test this, hTERT-MSCs were treated with sodium chlorate, which is a competitive inhibitor of ATP-sulfurylase an enzyme required for the synthesis of the sulfation substrate 3'-phosphoadenosine 5'-phosphosulfate (PAPS) [159]. Treatment of hTERT-MSCs with a range of sodium chlorate concentrations showed that 125mM sodium chlorate had a negative effect on proliferation, whilst 25mM or lower did not (Figure 5.26A). Following this, Alcian blue staining was carried out to test if 1, 5, and 25mM sodium chlorate treatment for 3 days, visibly reduced hTERT-MSC GAG sulfation. Only treatment with 25mM sodium chlorate significantly reduced GAG sulfation of hTERT-MSCs, shown by reduced absorbance at 630nm of the eluted Alcian blue stain (Figure 5.26B). Subsequently, hTERT-MSCs were either pre-treated with 25mM sodium chlorate for 48 hours, prior to culture in osteogenic media, or cultured continuously in osteogenic media supplemented with 25mM sodium chlorate. As osteoblasts produce a proteoglycan rich ECM, which is later mineralized, the ability of sodium chlorate to continue to inhibit GAG sulfation was assessed by Alcian blue staining at weekly time-points during incubation in osteogenic media. The Alcian blue staining (Figure 5.26C) and corresponding eluate (Figure 5.26D) showed that as expected levels of sulphated GAGs increased during osteogenesis. The levels of sulphated GAGs recovered to untreated levels, in cells which were pre-treated with sodium chlorate. Cells which were continuously treated with osteogenic media supplemented with sodium chlorate, did show some increase in Alcian blue staining over the time-course. However, levels of sulphated GAGs were significantly lower after 21 days compared to untreated controls (Figure 5.26C, D) (One way ANOVA on ranks, Dunn's post hoc test, $P=<0.05$, $n=6$). The effect of disrupted GAG sulfation on osteogenesis was assessed by ALP and phosphate staining at weekly time-points during osteogenic treatments. The pre-treatment with sodium chlorate had no effect on ALP or phosphate staining after 21 days osteogenic differentiation (Figure 5.26C). However, the continuous inclusion of sodium chlorate in osteogenic media, did not affect ALP staining, but did clearly reduce the level of phosphate staining (Figure 5.26C). This suggested that GAG sulfation is required for ECM mineralization by osteoblasts. To determine if Cog4KD hTERT-MSCs have altered proteoglycans further experiments are required, such as the staining of cells with Alcian blue, or a more sensitive dye such as 1,9-dimethylmethylene

blue or alternatively, immunohistochemistry staining with antibodies directed against sulphated heparan sulphate.

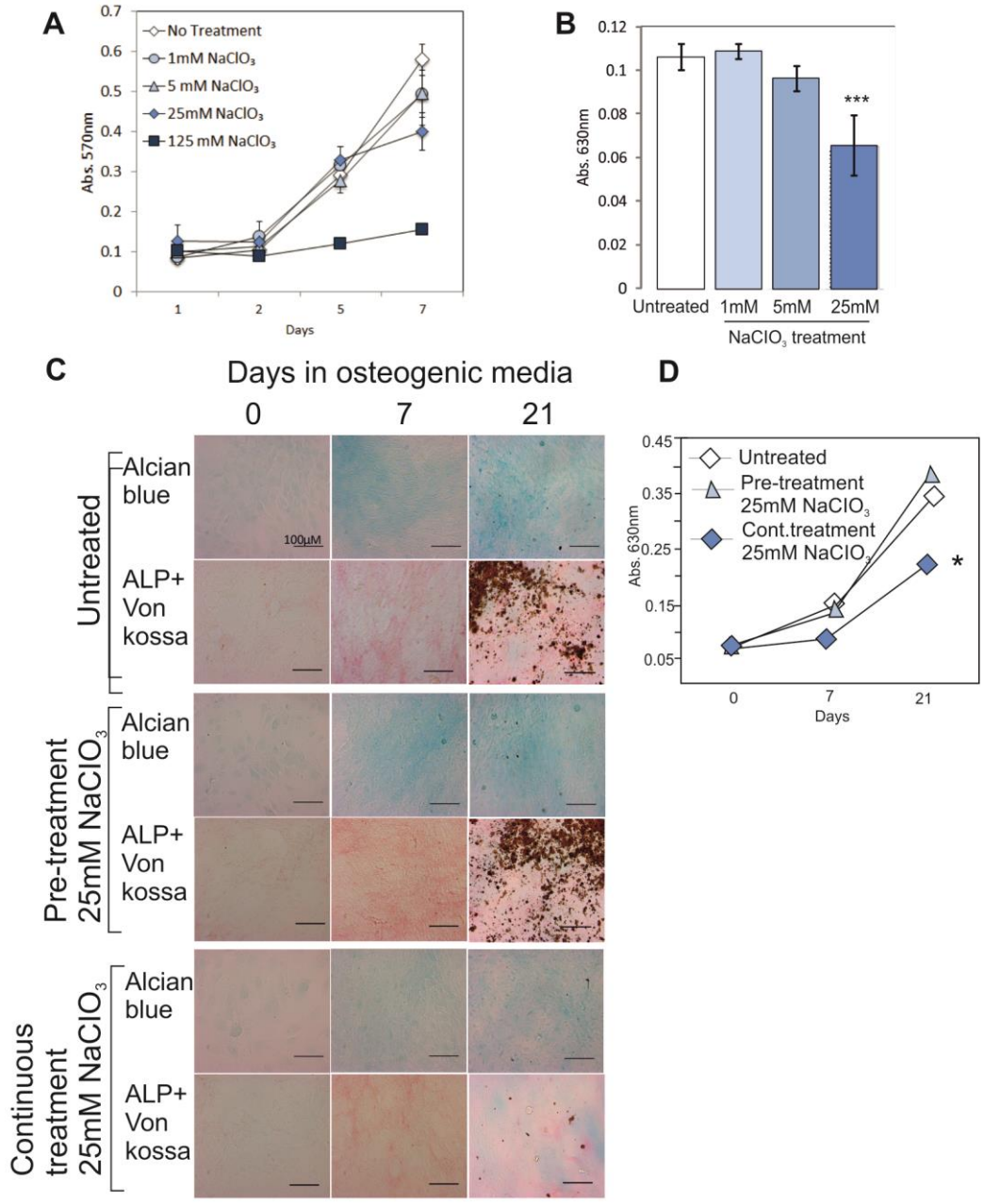

Figure 5.26 Effect of sodium chlorate (NaClO3) on osteogenesis.

A) The effect of different concentrations of NaClO3 on proliferation of hTERT-MSCs, was estimated using an MTT assay, after 1, 2, 5, and 7 days of treatment. B) hTERT-MSCs were stained with Alcian blue after treatments with NaClO3 for 3 days. The stain was then eluted and absorbance at 630nm measured. One way ANOVA, Holm Sidak post hoc test,***=P<0.001, n=6. C) The long term effect of NaClO3 pre-treatment (48 hours) or continuous treatment was assessed. Bright field images of Alcian blue or ALP von kossa staining of hTERT-MSCs in osteogenic media for 0, 7 and 21 days. The Alcian blue stain was quantified in D) after elution and absorbance read at 630nm. One way ANOVA on Ranks, (day 21 data), Dunn's post hoc test, *=P<0.05, n=6.

The data and images here are printed with the permission of I.G.Cantanhede who carried out the experimental work for this figure.

5.3 Chapter 5 Conclusion

Disruption of the glycosylation synthesis pathway genetically, via Cog4 knock-down, altered the ability of hTERT-MSCs to differentiate, with cells showing some positive osteogenic markers, but unable to mineralize ECM. Many types of glycan are synthesised in the Golgi and could be affected in the Cog4KD hTERT-MSCs. To determine which altered glycan structures were functionally responsible for the change in phenotype, inhibitors of different glycan syntheses were used, and the effect on osteogenesis monitored.

Due to the altered lectin staining and *N*-glycan profile of Cog4KD hTERT-MSCs, *N*-glycan synthesis was disrupted first. Swainsonine treatment changed the *N*-glycan profile of hTERT-MSCs to one dominated by hybrid type glycans. This shift was consistent with mannosidase II inhibition. The large change in *N*-glycan profile did not affect cell viability, morphology or proliferation. Swainsonine treated hTERT-MSCs underwent normal osteogenesis, as seen by positive ALP staining and ALP activity assays. There was a small reduction in phosphate staining, after 21 days in osteogenic media compared to untreated hTERT-MSCs, but this did not compare to the absence of phosphate staining seen with Cog4KD hTERT-MSCs.

Rather than dismiss *N*-glycans as potential mediators of the reduced mineralization capacity, an enzyme earlier in the *N*-glycan synthesis pathway was targeted. This was to reduce the presence sialic acid at the cell surface even further, as hybrid *N*-glycans can contain some sialic acid. Evidence to suggest that the sialic acid may be involved in altering the osteogenic potential in the Cog4KD hTERT-MSCs includes the mass spectrometry profiles that identified the absence of several complex glycans in the Cog4KD hTERT-MSCs. Furthermore, osteoblast *N*-glycan profiles contained significantly more sialic acid containing complex glycan structures, than MSCs. Siglecs are a group of sialic acid binding lectins that are known to have diverse, functional roles in the immune system, modifying cell-cell interactions and cell signalling [160].Besides regulating immune cell behaviour, siglecs (Siglec-15) has been shown to affect osteoclast differentiation [161]. Their role in osteoblast function is currently not known, it is possible that siglecs mediate cell-signalling required for mineralization.

In order to further reduce the presence of sialic acid containing *N*-glycans on hTERT-MSCs, cells were treated with a mannosidase I inhibitor called kifunensine. The *N*-glycan profile of hTERT-MSCs treated with kifunensine contained mostly oligomannose type glycans. The amount of complex glycans in kifunensine treated cells was 3x lower than in swainsonine treated cells. The phenotype of hTERT-MSCs was unaffected by kifunensine treatment, with no change in morphology or proliferation observed. Unexpectedly, kifunensine treatment altered the osteogenic capacity, with notably increased phosphate staining. This suggested that loss of complex *N*-glycans was not responsible for loss of mineralisation in Cog4KD hTERT-MSCs. An increase in mineralization was also seen with a pre-treatment of kifunensine prior to addition of normal osteogenic media. This result suggested a change in differentiation capacity rather than mineralisation ability. The mechanism by which kifunensine affected osteogenesis did not involve BMP2 or Runx2 signalling pathways, as their expression was not up-regulated in kifunensine treated cells. Despite the increase in phosphate staining, kifunensine treated cells showed decreased expression of BSP and decreased levels of ALP protein suggesting a defective differentiation capacity with aberrant ECM mineralisation. This phenotype may be caused by altered Wnt signalling indicated by an increase in β catenin levels in kifunensine treated cells.

Since the phosphate staining in the Cog4KD hTERT-MSCs was lower than WT, a rescue experiment with kifunensine was carried out. Cog4KDshRNA1 hTERT-MSCs that were cultured with osteogenic media supplemented with kifunensine, remained negative for phosphate after 21 days. This showed that the defect in Cog4KD hTERT-MSCs is dominant over the alteration caused by kifunensine. To identify which glycan structures were responsible for the Cog4KD hTERT-MSCs altered differentiation, the synthesis of another type of glycan structure was disrupted.

The effect of Cog4 knock-down on O-glycan synthesis was assessed in the previous chapter using lectin staining and flow cytometry. Cog4KD hTERT-MSCs had reduced VVL staining that binds to Tn and T antigen O-glycan structures. The reduced SNA staining of Cog4KD hTERT-MSCs could also indicated reduced O-glycan elongation, as SNA can stain sialic acid present in both *N*- and O-glycan structures. To test if these changes in O-glycan synthesis were responsible for the Cog4KDhTERT-MSCs mineralisation defect, cells were treated with an O-glycan synthesis inhibitor. Lectin staining and flow cytometry confirmed

that BadGal treatment altered O-glycan synthesis with reduced O-glycan elongation. Treatment with BadGal did not alter morphology or proliferation of hTERT-MSCs. Similar to the Cog4KD hTERT-MSCs, pre-treatment or continuous treatment with BadGal resulted in reduced phosphate staining after 21 days in osteogenic media. This suggested altered O-glycan synthesis may be responsible for the reduced mineralisation capacity of the Cog4KD hTERT-MSCs. The ability to influence differentiation capacity with a pre-treatment of BadGal suggested the effect was via a cell signalling pathway. Unlike kifunensine treatment, β catenin levels were not altered by BadGal treatment, indicating a different signalling pathway was responsible. Western blots showed that levels of ALP protein were unchanged after BadGal treatment, and that ALP is normally O-glycosylated. The expression of BMP, BSP and Runx2 were also unchanged by BadGal treatment. Further experiments are required to identify the osteogenic signalling pathway sensitive to changes in O-glycan synthesis. In further support of O-glycans mediating the change in differentiation capacity of Cog4KD hTERT-MSCs, hTERT-MSCs co-treated with BadGal and kifunensine did not stain for phosphate after 21 days in osteogenic media, just as kifunensine treatment of Cog4KD hTERT-MSCs did not restore phosphate staining. This suggests a hierarchy of functional importance of glycans in osteoblast mineralisation, with O-glycans being above *N*-glycans.

Finally, since glycolipids and proteoglycans are also synthesised in the Golgi, the effect of inhibitors of these synthesis pathways on osteogenesis, were also tested. Inhibition of the synthesis of glycolipids (starting with glucose attached to ceramide) did not affect osteogenesis. The continued inhibition of proteoglycan sulfation with sodium chlorate during osteogenesis did reduce mineralisation, whilst pre-treatment alone did not. This result is not surprising as bone ECM is rich in proteoglycans, and is required as a scaffold for mineralisation. The selectivity of BadGal on O-glycan inhibition requires further testing, as it is possible that BadGal can act as an alternative substrate to GalNAc, and inhibit the elongation of GAG chains, CS and DS both of which contain GalNAc. This would mimic EXT1/2 mutations, which results in reduced HS chain elongation and causes Hereditary multiple exostoses, in which skeletogenesis defects are the prominent symptom [39].

Further experiments identifying if proteoglycans are affected by the Cog4 knock-down are required to ascertain if a combination of O-glycan and proteoglycan changes mediate the loss of mineralisation in Cog4KD hTERT-MSCs.

This chapter has shown using chemical inhibitors that disruption of either O or *N*-glycan synthesis or proteoglycan sulfation can affect osteogenesis. Treatment with kifunensine shifted the glycan profile towards only oligomannose type *N*-glycans and increased ECM mineralisation. Treated cells had increased β catenin levels, implicating the Wnt signalling pathway in this *N*-glycan mediated effect. On the other hand, O-glycan inhibition or proteoglycan disruption ablated mineralization seen by reduced phosphate staining. This showed a novel functional role of O-glycans in MSC osteogenesis. Furthermore, co-treatment experiments with kifunensine and BadGal, suggested a hierarchy of importance of glycans in mineralisation, with O-glycans above *N*-glycans. Since chemical inhibition of either O-glycan or proteoglycan synthesis mimicked the loss of mineralisation seen in Cog4KD hTERT-MSCs, changes to both glycan structures may be responsible for the loss of mineralization. Further experiments identifying if proteoglycans are also affected by the Cog4 knock-down are required. The positive effect of kifunensine on osteoblast mineralisation is an interesting finding, and experiments in additional models are required to confirm the effect and further characterise the mechanism of action.

Chapter 6: Discussion

The use of MSCs in regenerative medicine is an exciting area of science. Their multi-lineage potential and relatively easy extraction from patients make them potential tools for the treatment of multiple diseases. Being able to understand and manipulate stem cell fate decisions would improve the efficiency of MSC differentiation *in vitro* and could identify targets for manipulation *in situ.* Genomic and proteomic studies have identified a web of interconnecting signalling pathways and transcription factors that contribute to the regulation of cellular differentiation. Nearly every cell surface and secreted protein is glycosylated. These post-translational modifications have already been shown to effect protein function and a number of cellular processes. Despite evidence for altered glycan profiles of cells at different stages of development, the functional role of glycans in MSC differentiation had not been studied. Here, utilizing immortalised human primary MSCs, the role of glycans in osteogenic differentiation was investigated.

6.1 Osteogenic differentiation of hTERT-MSCs

In chapter 3, hTERT-MSCs were cultured in osteogenic media and their differentiation was confirmed using a variety of cellular methods. Positive osteogenesis was indicated by increased phosphate and ALP staining, increased protein and activity levels of ALP, as well as by increased expression of Runx2, BMP2, and BSP, all of which confirmed the differentiation of hTERT-MSCs into functional osteoblasts. hTERT-MSCs grown in basal media showed a small increase in ALP activity and no visible matrix mineralisation (data not shown). There was also an increase in expression of Runx2, BMP2 and BSP in the hTERT-MSCs cultured for 21 days in basal media compared to day 0 samples, but these levels were lower than cells cultured in osteogenic media. The absence of β-glycerophosphate in the basal media prevented any spontaneous mineralisation as the cells require a phosphate donor in order to produce calcium phosphate. The change in gene expression after 21 days in basal media could be attributed to the confluent culture conditions resulting in pro-osteogenic signalling leading to a change in gene expression. Overall the changes in gene and protein expression, and the mineralised ECM, pointed towards successful osteogenic differentiation of hTERT-MSCs after 3 weeks in osteogenic media.

6.2 Quantitative *N*-glycan analysis of hTERT-MSCs and osteoblasts

A previous study using lectin staining identified differences in the *N*-glycan profiles of mouse MSCs and osteoblasts or adipocytes derived from them. The mouse MSCs and adipocytes were both found to have fewer complex *N*-glycans than the osteoblasts [119]. Heiskanen *et al* (2009) used the more sensitive method of mass spectrometry to profile *N*-glycans on human primary MSCs and osteoblasts derived from them [118]. Their findings agreed with the lectin staining that osteoblasts had more complex type *N*-glycans than MSCs, with an estimate of 34% and 45% abundance in MSCs and osteoblasts respectively. However, importantly, derivitisation of the *N*-glycans prior to mass spectrometry was not included [118]. This step is essential if quantitative results are to be obtained [131]. Permethylation neutralizes the negative charge of sialic acid, which reduces the chemical variation between different *N*-glycan structures leading to more uniform ionization. The inclusion of a permethylation step in my work thus makes the analysis more quantitative, and shows a higher abundance of complex *N*-glycans found in both hTERT-MSCs (46%) and osteoblasts (70%) derived from them (section 3.3.3). Hamouda *et al* (2013) compared the *N*-glycans isolated from the membranes of human primary MSCs and adipocytes derived from them [125]. A permethylation step was included in their method and the *N*-glycans were removed from the membrane proteins by incubation with first EndoH that removed oligomannose type *N*-glycans, followed by incubation with PNGaseF that removed remaining hybrid and complex type *N*-glycans [125]. As analysis was carried out on the *N*-glycans retrieved from each enzyme incubation step separately, conclusions about the relative abundance of different structures in MSCs could not be made. Therefore, the *N*-glycan profiles of hTERT-MSCs and osteoblasts obtained in chapter 3 provides novel data, allowing for the first time the relative abundance of different *N*-glycan structures to be reliably quantified and compared between the cell types. The *N*-glycan profile of hTERT-MSCs and osteoblasts in section 3.1.3, contained the same variety of *N*-glycan structures, only in differing abundance. This was also found to be the case by Heiskanen *et al* (2009) and Hamouda *et al* (2013), but in my work the permethylation step allowed reliable quantification of glycan abundance between spectra enabling the identification of profile characteristics typical to the different cell types. Compared to the vast number of possible glycan structures, the degree of similarity in *N*-glycan profiles between hTERT-MSCs and osteoblasts could be explained by the relative similarity in cell type. Both cell types are of

mesoderm origin, found *in vivo* in the bone marrow. The most abundant *N*-glycans identified by Hamouda *et al* (2013) were also the most abundant in hTERT-MSC profiles. Interestingly, Hamouda *et al* (2013) noted that the structure $Hex_{10}HexNAc_2$ was present in MSCs but absent in adipocytes [125]. The same pattern was observed for hTERT-MSCs and osteoblasts. The structure $Hex_{10}HexNAc_2$ is the oligomannose structure $Hex_9HexNAc_2$ which enters the Golgi, with a branch terminating, glucose still attached. This would normally signal incomplete folding of a protein, resulting in recycling to the ER. It is unclear why MSCs would have more incompletely folded proteins than differentiated cells. In terms of studying the role of glycans in cellular interactions, the analysis of *N*-glycans from just plasma membrane proteins would be beneficial. A potential method to do this is biotinylation of cell-surface proteins and a streptavidin pull-down assay. Hamouda *et al* (2013) centrifuged cell lysates to isolate cell-membrane proteins [125]. Their samples would be enriched for membrane proteins; however this method required up to $13.3x10^6$ cells per sample whilst the FANGS method used in this research required only $1x10^6$ cells per sample. The use of fewer cells per sample allows for the testing of biological repeats or profiling of samples with limited cell numbers.

6.3 Use of *N*-glycans as markers of osteogenic potential

In the study mentioned earlier where adipocytes had fewer complex *N*-glycans, they were also found to be less supportive for haematopoiesis [119]. Investigators then treated MSCs with deoxymannojirimycin (DMJ), a Golgi mannosidase I inhibitor, to block complex *N*-glycan formation. DMJ treatment reduced the myelopoietic supportive capacity of MSCs, showing one role of *N*-glycans in MSC function. The effect of DMJ on MSC differentiation capacity was not tested [119]. Although differences in the *N*-glycan profile of MSCs and osteoblasts had been identified, to date no-one had determined the role (if any) of *N*-glycans in the differentiation of MSCs. To initially investigate this, in chapter 3, the *N*-glycan profiles of different hTERT-MSC lines, with varied differentiation capabilities, were compared. Section 3.1.1, confirmed the varied ability of three hTERT-MSC lines to differentiate into osteoblasts or adipocytes. This finding agrees with the hypothesis that MSCs are a heterogeneous population of cells, with varied differentiation capacity and function in the bone marrow [76]. The ability to identify different MSC subpopulations could improve the effectiveness of cellular therapies in regenerative medicine. The results presented in section 3.1.4, showed that despite the differences in multi-potency, the

three hTERT-MSC lines had similar *N*-glycan profiles. This finding does not rule out a role of glycans during differentiation, but does suggest that *N*-glycan profiles, obtained using these methods, are not a good candidate for identifying multi-potency or immuno-regulatory capacity in subpopulations of MSCs. This is in contrast to the gene and protein expression profiles of the different hTERT-MSC lines that had already been shown to facilitate the isolation of CD317+ subpopulations of the primary human MSCs with specific differentiation and immune-regulatory capacities [122]. Instead of being markers of differentiation potential, glycans could mediate the differentiation process. In order to investigate this, the glycosylation pathway was disrupted genetically and then chemically.

6.4 Genetic disruption of glycosylation

In chapter 4, a genetic approach was taken to disrupt the glycan synthesis pathway and the effect on osteogenesis was monitored. The hTERT-MSCs were utilized again, as their unlimited growth enabled the creation of colonies derived from single cells after genetic manipulation. A subunit of COG was targeted by shRNA, which would hinder the retrograde traffic of vesicles at the Golgi. Following this, Golgi enzyme localization would be disrupted, resulting in aberrant glycan synthesis. Importantly, proteins would still be glycosylated to a degree and correctly trafficked to the cell membrane, allowing the effect of glycosylation to be tested rather than protein localization. Using lenti-virus Y101 hTERT-MSCs were transduced with a plasmid containing a shRNA for Cog4. The transduction efficiency was high, which was fortunate in light of findings that a sequential transduction with retrovirus had an efficacy 3 to 4 fold lower than the initial transduction [162]. There was also no evidence of the Cog4 shRNA plasmid disrupting the expression of hTERT, as cells continued to proliferate during culture.

The effectiveness of the shRNAs was low with many of the colonies expressing similar to WT levels of Cog4 protein. For shRNAs to knock-down target gene expression they need to be processed in the nucleus by Drosha; then transported into the cytosol and processed further by Dicer; and then loaded into the RNA-induced silencing complex (RISC). Of the colonies tested those produced using shRNA B, C or E were more effective than those produced using shRNA A or D. What alters the ability of a shRNA to be processed at each step is currently unknown. Nevertheless, in section 4.3.1 two colonies were identified with <50% WT levels of Cog4, which were produced using shRNAs B and

C. These colonies were further expanded into Cog4KD hTERT-MSC lines and further characterised.

As predicted the disrupted recycling of Golgi resident enzymes, via Cog4 knock-down leads to incomplete glycan chain modulation. This was shown by reduced staining of Cog4KD hTERT-MSCs with the lectin SNA, which binds to sialic acid. Furthermore, staining with PNA, that recognises non-sialylated terminal galactose, was increased in the Cog4KD hTERT-MSCS. These changes are in agreement with the altered glycan profiles of Cog4-CDG patient fibroblasts, which also showed reduced sialylation [65]. In section 4.3.2, the *N*-glycans of Cog4KD hTERT-MSCs were profiled using mass spectrometry. The *N*-glycan profile of Cog4KD hTERT-MSCs was similar to WT, however, the Cog4KD hTERT-MSC profile lacked several complex *N*-glycans. As they were lowly abundant in WT profiles, their loss did not significantly lower the overall abundance of complex *N*-glycans in Cog4KD hTERT-MSCs. The intensity of *N*-glycan peaks did not always decrease linearly with increase in mass, suggesting that the lower abundance of some high mass, complex *N*-glycans was real, rather than a consequence of lower detection by mass spectrometry. In support of this, the lectin staining of WT hTERT-MSCs with SNA (sialic acid binding) was lower than the staining with lectins that bind oligomannose or non-sialylated glycans. The *N*-glycan profiles of serum from CDG patients with mutations in Cog subunits 1, 4, 7, or 8 was on aggregate similar to control serum, but importantly the abundance of sialylated glycans was lower [65]. This supports the lower abundance of sialylated complex *N*-glycans seen in the Cog4KD hTERT-MSCs.

The lectin VVL binds to the Tn antigen structure which is a terminal α-N-acetylgalactosamine linked to serine or threonine. This is the first monosaccharide in an O-glycan structure. The binding of VVL was reduced in Cog4KD hTERT-MSCs. Currently over 24 different polypeptide-N-acetyl-galactosaminyltransferases (ppGalNAcTs) have been identified, which are expressed through-out the Golgi cisternae [32]. Due to the ppGalNAcTs varied substrate specificities, the disruption of enzyme localization in Cog4KD hTERT-MSCs may lead to reduced Tn antigen abundance [32]. As the Tn antigen is the start of an O-glycan chain, fewer extended O-glycan structures would also be a consequence. SNA binds to sialic acid with a α2-6 linkage to galactose or GalNAc, both of which may be present in extended O-glycans [153]. The reduced SNA staining of Cog4KD hTERT-MSCs could therefore be caused by lower abundance of sialylated O-glycans. In

support of this, mass spectrometry or isoelectric focussing of ApoC-III, has shown that CDG-patients with mutations in different COG subunits to have defects in O-glycan sialylation [66, 68, 69, 163]. Overall the change in *N*- and O glycan profile of Cog4KD hTERT-MSCs is consistent with changes seen in samples from COG related CDG patients. In order to determine if sialylated glycans have a functional role in stem cell differentiation, the osteogenic capacity Cog4KD hTERT-MSCs were assessed.

When Cog4KD hTERT-MSCs were cultured in osteogenic media for 21 days, ALP staining was visible but the cells did not form any mineralised extracellular matrix. This change was not caused by reduced proliferation, as data from a MTT assay suggested that the Cog4KD hTERT-MSCs had equal or higher rates of proliferation compared to WT. Results described in section 4.3.4 showed that the Cog4KD hTERT-MSCs had lower levels of ALP activity and ALP protein expression compared to WT. This suggested reduced levels osteogenesis in the Cog4KD hTERT-MSCs. In contrast, real time qPCR data did not support this, showing increases in expression of BMP2 and Runx2 in the Cog4KD hTERT-MSCs during culture in osteogenic media. The expression of BSP, which supports crystal nucleation during bone mineralization, was reduced at day 21 for one Cog4KD line, which supports the notion that Cog4KD hTERT-MSCs were capable of differentiating but had a mineralization defect.

The expression level of Cog4 remained low in the Cog4KD hTERT-MSCs after culture in either basal or osteogenic media for 21 days. This showed that the mild change in phenotype was not due to Cog4 levels returning to normal, due to absence of selective antibiotic in osteogenic media. Complete knock-out of Cog4 may result in a more severe phenotype, however, it's also possible that there is some functional redundancy between the 8 COG subunits, in which case knock-out would not cause a greater change. The reduction in mineralization capacity in Cog4KD hTERT-MSCs is a phenotype shared by Mgat5 -/- MSCs [164]. Mgat5 is an enzyme responsible for the transfer of GlcNAc onto complex *N*-glycans, which initiates the formation of a tetra antennary complex *N*-glycan structure. Mgat5 -/- mice have reduced bone mass density and MSCs isolated from them were unable to mineralise extracellular matrix [164].

In order to confirm the effect of Cog4 knock-down on osteogenesis, ideally rescue experiments with a shRNA resistant form of Cog4 would be carried out. However, the interpretation of the results would be difficult. A lack of rescue could be due to cellular

stress resulting from the third round of genetic manipulation. Also, a previous study found the overexpression of Cog4 in fibroblasts had a dominant negative effect, with defective retrograde vesicle traffic compared to controls [65]. For these reasons, alternative experiments using chemical inhibitors of several Golgi localised, glycan synthesis pathways were carried out to confirm that changes in *N*-or O-glycan synthesis were responsible for the aberrant osteogenic potential of the Cog4KD hTERT-MSCs.

6.5 Chemical disruption of glycosylation

In chapter 5, the *N*-and O-glycan, glycolipid and proteoglycan synthesis pathways were disrupted using chemical inhibitors. Despite significant effects on glycosylation, none of the inhibitors caused changes proliferation at working concentrations. Proliferation was monitored because MSCs need to be viable and able to proliferate, prior to arrest and differentiation into osteoblasts. Also, there have been reports studying cancer cells showing that glycosylation can regulate proliferation. One study suggests that growth receptors that have highly branched glycan structures bind to galectins at the cell surface, forming a lattice. This results in slower turnover of the glycoprotein from the cell membrane and increased signalling. The degree of glycan branching is influenced by metabolic conditions, thus linking growth to glycosylation [165]. Again in cancer cell lines, the removal of all cell surface glycans enzymatically has been shown to induce apoptosis [166]. In contrast, treatment of mice with swainsonine has been shown to cause an increase in HSC proliferation [167]. In agreement with findings in chapter 5, treatment of mammalian cell lines with swainsonine, kifunensine or BadGal has been shown previously to have no effect on cell proliferation [141, 152, 168].

In section 5.2.1, inhibition of mannosidase II with swainsonine, caused a significant change in the *N*-glycan profile of hTERT-MSCs. The profile of treated cells was dominated by hybrid type glycans, with fewer oligomannose and complex *N*-glycans. The addition of swainsonine to osteogenic media did not appear to influence differentiation. The staining of treated cells for ALP and mineralised extracellular matrix was positive, and ALP activity was not significantly different from untreated controls. Since hybrid type glycans can be sialylated, the availability of sialic acid to lectins, would not have altered significantly on swainsonine treated cells. In order to further reduce the abundance of sialylated glycans,

hTERT-MSCs were treated with kifunensine, a mannosidase I inhibitor. This enzyme normally removes mannose oligosaccharides to allow the addition of GlcNAc, which initiates complex or hybrid *N*-glycan assembly. As predicted, the profile of kifunensine treated cells was dominated by oligomannose type *N*-glycans. Also the abundance of fucosylated *N*-glycans was significantly reduced by kifunensine treatment. If the absence of high mass complex *N*-glycans in Cog4KD hTERT-MSCs was responsible for the reduced mineralisation capacity, kifunensine treatment should have reduced the osteogenic potential even further. However, this was not the case. In section 5.2.6, osteogenic assays showed that phosphate staining was increased in kifunensine treated cells. This effect was also seen when a pre-treatment of kifunensine was administered for 48 hours prior to addition of osteogenic media. This indicates that kifunensine was altering the behaviour of a glycoprotein that acts early during osteogenesis, most likely a signalling protein. Western blot analysis of hTERT-MSCs treated with kifunensine for 48 hours showed an increase in active β catenin levels compared to untreated controls. β catenin acts downstream of the Wnt signalling pathway and modulates LEF/TCF transcription factor expression. At odds with this finding is that Wnt pathway stimulation has been shown to suppress MSC differentiation, but enhance osteoblast mineralisation [101]. Due to their poor adipogenic differentiation, the Y101 hTERT-MSCs used in the kifunensine experiments could be described as osteoblast progenitor cells, and the effect of Wnt stimulation of this subpopulation of MSCs could be positive. Further osteogenic analysis of kifunensine continuously and pre-treated hTERT-MSCs was carried out to try and further characterise the mechanism by which kifunensine increased mineralisation activity.

Analysis of ALP protein levels showed that ALP was *N*-glycosylated and levels were reduced in kifunensine treated cells. Both kifunensine treatments caused little change to BMP2 expression levels, but interestingly caused a small decrease in Runx2 expression. If kifunensine was modulating the Wnt signalling pathway the expression of Runx2, the major osteogenic transcription factor, would be expected to increase. Also, despite the increase in mineralised extracellular matrix, BSP expression was lower in kifunensine treated cells compared to untreated. BSP is a major non-collagenous glycoprotein found in bone, and thought to act as a protein nucleator of hydroxyapatite crystal. Transcription of BSP is regulated by Runx2, so the lower levels of BSP may be a consequence of lower Runx2 expression. The real-time qPCR data didn't provide a clearer mechanism of action

of kifunensine treatment on osteogenesis. As with all qPCR data, the levels and activity of a protein may not be reflected by expression levels of mRNA. A speculative explanation for the mechanism of kifunensine, is that a receptor protein sensitive to changes in *N*-glycosylation, triggers a change in response to osteogenic stimuli, resulting in increased levels of β catenin and causing changes to gene and protein expression of osteogenic effectors not looked at in this study, which ultimately enhance ECM mineralisation. Further experiments are required to determine if the mineralisation observed via kifunensine treatment is the result of increased osteogenesis, or aberrant mineralisation by MSCs. Transmission electron microscopy could be used to confirm if the phosphate produced by kifunensine treated hTERT-MSCs is hydroxyapatite, and if the crystals formed have the same structure as those found *in vivo.* Furthermore, the pro-osteogenic effect of kifunensine should be tested in an alternative model to tissue culture.

The loss of nearly all complex *N*-glycans did not phenocopy the Cog4KD hTERT-MSCs. This indicated that the loss of complex *N*-glycans was not the cause of reduced mineralisation. Furthermore kifunensine treatment did not rescue the phenotype of the Cog4KD hTERT-MSCs, showing that the defect was dominant over the positive effector of the kifunensine treatment.

O-glycans are another subset of glycans that are synthesised in the Golgi. In section 5.2.8, flow cytometry with lectins confirmed that BadGal is a competitive inhibitor of O-glycan synthesis. I propose BadGal has two targets, firstly as a competitive inhibitor of the galactose-transferase responsible of forming the T antigen structure. Secondly, the BadGal-Gal disaccharides then act as competitive inhibitors of sialyltransferases. Evidence of both types of inhibition were seen in the BadGal treated hTERT-MSCs, by the increased Jacalin and VVL (Tn antigen binding lectins) staining, and increased PNA (terminal galactose binding lectin) staining. However, the staining with SNA (sialic acid binding) was increased after BadGal treatment. This contradicts the increased PNA staining, which suggested reduced sialylation. The altered availability of substrates for sialyltransferases may have resulted in increased *N*-glycan sialylation, a theory which could be tested by profiling the *N*-glycans of BadGal treated hTERT-MSCs.

O-glycan synthesis inhibition in hTERT-MSCs phenocopied the Cog4 knock-down, with reduced phosphate staining after culture in osteogenic media. Both continuous and pre-treatment with BadGal resulted in reduced phosphate staining, suggesting a change in

differentiation via a signalling pathway. This pathway appears to be different to that affected by kifunensine, as the levels of β catenin were not affected by BadGal treatment. The activity and protein levels of ALP were also not altered by continuous BadGal treatment, although the western blot showed that ALP is O-glycosylated. The expression of Runx2, BMP and BSP were also not changed by continuous BadGal treatment leading to the conclusion that O-glycan inhibition did not affect all of osteogenesis, rather caused a defect specifically in mineralisation, as was the case in the Cog4KDhTERT-MSCs. Just as kifunensine treatment did not rescue the mineralisation of Cog4KD hTERT-MSCs, cells treated with both BadGal and kifunensine also failed to mineralise. This suggests a hierarchy of glycan importance in mineralisation with O-glycans being above *N*-glycans. In this study the O-glycan profile of osteoblasts was not analysed. A previous study found that osteoblasts had more sialylated O-glycans than MSCs [118], and results described here suggest for the first time, that extended O-glycans have a functional role in osteogenic differentiation.

Sharing the Golgi during synthesis with *N*- and O-glycans, are glycolipids and proteoglycans. When hTERT-MSCs were cultured with osteogenic media supplemented with a glycolipid synthesis inhibitor (NB DNJ), ALP and phosphate staining were unaffected showing glycolipid synthesis to be dispensable for the osteogenesis of hTERT-MSCs. It is possible that the concentration of NB DNJ used was ineffective at altering glycolipid synthesis, analysis of NB DNJ treated hTERT-MSCs using thin layer liquid chromatography could be used to disprove this. Proteoglycans are a major component of ECM and osteoblasts deposit ECM during osteogenesis that is then mineralized at later stages. As expected the staining of sulphated GAGs, using alcian blue, increased during hTERT-MSC incubation with osteogenic media for 3 weeks. The addition of sodium chlorate to culture media disrupted GAG sulphation, as seen by the reduced alcian blue staining. This effect was maintained during 3 weeks culture in osteogenic media. Accompanying the decrease in sulphated GAG synthesis, phosphate staining was also reduced in cells cultured with osteogenic media and sodium chlorate. The Cog4knock-down may have affected O-glycan and proteoglycan synthesis leading to reduced mineralisation capacity. The effect of the different chemical inhibitors on glycan profile was assessed here by mass spectrometry, which is a sensitive method, but only semi-quantitative. Lectin staining of cells treated with kifunensine and/or BadGal would validate that the change in phenotype was caused by the intended change in type of

glycan structures produced – rather than change in overall abundance of glycans – which may also have an effect on cellular differentiation. Analysis of the proteoglycans of WT and Cog4KD hTERT-MSCs, by alcian blue staining, or by a more sensitive method such as immuno-histochemistry, would help discern this.

6.6 Future work

Further experiments are required to confirm that glycans have a functional role in mineralisation. The effect of kifunensine and BadGal on primary human MSC differentiation would naturally follow this work, as primary human MSCs are the gold standard cellular model. However, there are reports of variability in responsiveness to treatments between donors, and suggestions that *in vitro* osteogenic assays do not always predict *in vivo* bone forming capacities [137, 169]. An intermediate between the two systems is an *ex vivo* set-up using neonatal rodent calvariae. When the explants are cultured in osteogenic media the calvariae bone continues to develop, and the effect of inhibitors added to the media can be assessed by measuring the thickness of new bone growth. Alongside this, experiments addressing the effect of kifunensine and BadGal on adipogenesis and chondrogenesis are still to be carried out. Considering how important the balance between adipogenic and osteogenic signalling is to stem cell fate, the effect of glycan inhibition on adipogenesis could help identify the mechanism of action of kifunensine and BadGal. Returning to chapter 3, it would be interesting to compare the abundance of sialylated O-glycans between the 3 hTERT-lines. Rather than using flow cytometry, this could be carried out using alkaline β elimination and mass spectrometry. If sialylated O-glycans were identified as a marker of subpopulations of MSCs, this could be used to improve expansion of MSCs for use in regenerative medicine. The experiments with sodium chlorate identified proteoglycans as a possible candidate for causing the reduced mineralization capacity of Cog4KDhTERT-MSCs. The analysis of the proteoglycans present on the Cog4KD hTERT-MSCs is another experiment that would follow this research, as well as analysis of the effect of sodium chlorate on the expression of other osteogenic markers.

6.7 Conclusion

The aim of this research was to determine the role of glycans in the differentiation of MSCs. Mass spectrometry was used to produce quantifiable *N*-glycan profiles of MSCs and osteoblasts derived from them. In agreement with previous research, osteoblasts were found to have more complex type *N*-glycans than MSCs. Disruption of the *N*-glycan synthesis pathway genetically and chemically lead to reduced abundance of sialylated glycans. Kifunensine, which promoted oligomannose type *N*-glycans, appears to be a novel osteogenic stimulator, albeit through an unknown (potentially Wnt-mediated) signalling mechanism. In contrast, inhibition of O-glycan sialylation prevented mineralisation, despite expression of other osteogenic markers, and appears to act via an alternative signalling pathway to kifunensine. Glycolipid synthesis inhibition had no effect on osteogenesis, whilst continued proteoglycan disruption inhibited mineralization. Further experiments in primary human MSCs and *in vivo/ex vivo* are required to confirm these results. Importantly, the data described here shows for the first time a functional role of both *N*- and O-glycans in the osteogenic differentiation of MSCs.

Abbreviations

ALP = Alkaline phosphatase

ApoCII = Apolipoprotein C II

BMP2 = Bone morphogenetic protein 2

BSP = Bone sialoprotein

CDGs = Congenital disorders of glycosylation

CHO = Chinese ovary hamster cell line

COG = Conserved Oligomeric Golgi Complex

ConA = Concanavalin A

COPI = Coatomer protein complex-I

CS = Chondroitin sulphate

CV(hm) = The coefficient of variation (half-max)

DMJ = deoxymannojirimycin

DS = Dermatan sulphate

ECM = Extracellular matrix

EGFR = Epidermal growth factor receptor

EndoH = Endoglycosidase H

ER = Endoplasmic reticulum

FGF = Fibroblast growth factor

FTC = Familial tumoral calcinosis

GAGs = Glycoaminoglycans

GalNAc = N-acetylgalactosamine

GlcNAc = N-acetylglucosamine

GMAP-210 = Golgi microtubule-associated protein 210

GPI = Glycosylphosphatidylinositol

GSL = Glycosphingolipids

HA = Hyaluronan

hESCs = Human embryonic stem cells

Hh = Hedgehog (signalling pathway)

HMRS = Hyperphosphatasia with Mental Retardation Syndrome

HS = Heparan sulphate

HSCs = Hematopoietic stem cells

IHh = Indian Hedgehog

KS = Keratan sulphate

LDL = Low-density lipoprotein

MALDI-TOF/TOF = Matrix-assisted laser desorption/ionization

MALII = Maackia Amurensis Lectin II

Man = Mannose

MOI = Multiplicity of infection

MSCs = Mesenchymal stem cells

MTT = 3-(4,5-dimethylthiazol-2-yl)-2,5-diphenyltetrazolium bromide

NPCs = Neural progenitors cells

OST = oligosaccharyl transferase

PBS = phosphate buffered saline

PBST = phosphate buffered saline with 0.05% v/v Tween

PIGA = phosphatidylinositol glycan class A

PNA = Peanut agglutinin

PNGaseF = Peptide N Glycosidase F

PNH = Paroxysmal nocturnal hemoglobinuria

pNPP = p-Nitrophenyl Phosphate

ppGalNAcTs = polypeptide-N-acetyl-galactosaminyltransferases

qPCR = Quantitative real-time polymerase chain reaction

shRNA = short-hairpin RNA

SNA = Sambucus nigra lectin

TGFβ = Transforming growth factor beta

VSG = Variant surface glycoprotein

VSVG = Vesicular stomatitis virus G protein

VVL = Vicia villosa Lectin

WGA = Wheat germ agglutinin

WT = Wild-type

List of References

1. Golgi, C., *On the structure of nerve cells.* Boll. Soc. Chir. Med. Pavia 1898. **13**: p. 3-16.
2. Dalton, A.J. and M.D. Felix, *Cytologic and cytochemical characteristics of the Golgi substance of epithelial cells of the epididymis in situ, in homogenates and after isolation.* Am J Anat, 1954. **94**(2): p. 171-207.
3. Patterson, G.H., et al., *Transport through the Golgi apparatus by rapid partitioning within a two-phase membrane system.* Cell, 2008. **133**(6): p. 1055-67.
4. Rizzo, R., et al., *The dynamics of engineered resident proteins in the mammalian Golgi complex relies on cisternal maturation.* J Cell Biol, 2013. **201**(7): p. 1027-36.
5. Cottam, N.P. and D. Ungar, *Retrograde vesicle transport in the Golgi.* Protoplasma, 2012. **249**(4): p. 943-55.
6. Jackson, L.P., *Structure and mechanism of COPI vesicle biogenesis.* Curr Opin Cell Biol, 2014. **29**: p. 67-73.
7. Volchuk, A., et al., *Countercurrent distribution of two distinct SNARE complexes mediating transport within the Golgi stack.* Mol Biol Cell, 2004. **15**(4): p. 1506-18.
8. Allan, B.B., B.D. Moyer, and W.E. Balch, *Rab1 recruitment of p115 into a cis-SNARE complex: programming budding COPII vesicles for fusion.* Science, 2000. **289**(5478): p. 444-8.
9. Malsam, J., et al., *Golgin tethers define subpopulations of COPI vesicles.* Science, 2005. **307**(5712): p. 1095-8.
10. Krieger, M., M.S. Brown, and J.L. Goldstein, *Isolation of Chinese hamster cell mutants defective in the receptor-mediated endocytosis of low density lipoprotein.* J Mol Biol, 1981. **150**(2): p. 167-84.
11. Kingsley, D.M., et al., *Three types of low density lipoprotein receptor-deficient mutant have pleiotropic defects in the synthesis of N-linked, O-linked, and lipid-linked carbohydrate chains.* J Cell Biol, 1986. **102**(5): p. 1576-85.
12. Ungar, D., et al., *Characterization of a mammalian Golgi-localized protein complex, COG, that is required for normal Golgi morphology and function.* J Cell Biol, 2002. **157**(3): p. 405-15.
13. Whyte, J.R. and S. Munro, *The Sec34/35 Golgi transport complex is related to the exocyst, defining a family of complexes involved in multiple steps of membrane traffic.* Dev Cell, 2001. **1**(4): p. 527-37.
14. Walter, D.M., K.S. Paul, and M.G. Waters, *Purification and characterization of a novel 13 S hetero-oligomeric protein complex that stimulates in vitro Golgi transport.* J Biol Chem, 1998. **273**(45): p. 29565-76.
15. Cottam, N.P., et al., *Dissecting functions of the conserved oligomeric Golgi tethering complex using a cell-free assay.* Traffic, 2014. **15**(1): p. 12-21.
16. Zolov, S.N. and V.V. Lupashin, *Cog3p depletion blocks vesicle-mediated Golgi retrograde trafficking in HeLa cells.* J Cell Biol, 2005. **168**(5): p. 747-59.
17. Miller, V.J., et al., *Molecular insights into vesicle tethering at the Golgi by the conserved oligomeric Golgi (COG) complex and the golgin TATA element modulatory factor (TMF).* J Biol Chem, 2013. **288**(6): p. 4229-40.
18. Struwe, W.B. and V.N. Reinhold, *The conserved oligomeric Golgi complex is required for fucosylation of N-glycans in Caenorhabditis elegans.* Glycobiology, 2012. **22**(6): p. 863-75.
19. Farkas, R.M., et al., *The Drosophila Cog5 homologue is required for cytokinesis, cell elongation, and assembly of specialized Golgi architecture during spermatogenesis.* Mol Biol Cell, 2003. **14**(1): p. 190-200.
20. Oka, T., et al., *Genetic analysis of the subunit organization and function of the conserved oligomeric golgi (COG) complex: studies of COG5- and COG7-deficient mammalian cells.* J Biol Chem, 2005. **280**(38): p. 32736-45.

21. Shestakova, A., S. Zolov, and V. Lupashin, *COG complex-mediated recycling of Golgi glycosyltransferases is essential for normal protein glycosylation.* Traffic, 2006. **7**(2): p. 191-204.
22. Peanne, R., et al., *Differential effects of lobe A and lobe B of the Conserved Oligomeric Golgi complex on the stability of {beta}1,4-galactosyltransferase 1 and {alpha}2,6-sialyltransferase 1.* Glycobiology, 2011. **21**(7): p. 864-76.
23. Schnaar, R.L., A. Suzuki, and P. Stanley, *Glycosphingolipids*, in *Essentials of Glycobiology*, A. Varki, et al., Editors. 2009: Cold Spring Harbor (NY).
24. Yamashita, T., et al., *A vital role for glycosphingolipid synthesis during development and differentiation.* Proc Natl Acad Sci U S A, 1999. **96**(16): p. 9142-7.
25. D'Angelo, G., et al., *Glycosphingolipids: synthesis and functions.* FEBS J, 2013. **280**(24): p. 6338-53.
26. Varki, A., *Factors controlling the glycosylation potential of the Golgi apparatus.* Trends Cell Biol, 1998. **8**(1): p. 34-40.
27. Nozaki, M., et al., *Developmental abnormalities of glycosylphosphatidylinositol-anchor-deficient embryos revealed by Cre/loxP system.* Lab Invest, 1999. **79**(3): p. 293-9.
28. Nakamura, T., K. Nakamura, and R.A. Stinson, *Release of alkaline phosphatase from human osteosarcoma cells by phosphatidylinositol phospholipase C: effect of tunicamycin.* Arch Biochem Biophys, 1988. **265**(1): p. 190-6.
29. Krawitz, P.M., et al., *PGAP2 mutations, affecting the GPI-anchor-synthesis pathway, cause hyperphosphatasia with mental retardation syndrome.* Am J Hum Genet, 2013. **92**(4): p. 584-9.
30. Brodsky, R.A., *Paroxysmal nocturnal hemoglobinuria.* Blood, 2014. **124**(18): p. 2804-11.
31. Ratajczak, J., et al., *A novel view of paroxysmal nocturnal hemoglobinuria pathogenesis: more motile PNH hematopoietic stem/progenitor cells displace normal HSPCs from their niches in bone marrow due to defective adhesion, enhanced migration and mobilization in response to erythrocyte-released sphingosine-1 phosphate gradient.* Leukemia, 2012. **26**(7): p. 1722-5.
32. Varki, A., et al., *Essentials of glycobiology*. 2nd ed. 2009, Cold Spring Harbor, N.Y.: Cold Spring Harbor Laboratory Press.
33. Prydz, K. and K.T. Dalen, *Synthesis and sorting of proteoglycans.* J Cell Sci, 2000. **113 Pt 2**: p. 193-205.
34. Vertel, B.M., et al., *Xylosylation is an endoplasmic reticulum to Golgi event.* J Biol Chem, 1993. **268**(15): p. 11105-12.
35. Rapraeger, A.C., A. Krufka, and B.B. Olwin, *Requirement of heparan sulfate for bFGF-mediated fibroblast growth and myoblast differentiation.* Science, 1991. **252**(5013): p. 1705-8.
36. Flaumenhaft, R. and D.B. Rifkin, *Extracellular matrix regulation of growth factor and protease activity.* Curr Opin Cell Biol, 1991. **3**(5): p. 817-23.
37. Lamoureux, F., et al., *Proteoglycans: key partners in bone cell biology.* Bioessays, 2007. **29**(8): p. 758-71.
38. Huegel, J., et al., *Heparan sulfate in skeletal development, growth, and pathology: the case of hereditary multiple exostoses.* Dev Dyn, 2013. **242**(9): p. 1021-32.
39. Busse, M., et al., *Contribution of EXT1, EXT2, and EXTL3 to heparan sulfate chain elongation.* J Biol Chem, 2007. **282**(45): p. 32802-10.
40. Koziel, L., et al., *Ext1-dependent heparan sulfate regulates the range of Ihh signaling during endochondral ossification.* Dev Cell, 2004. **6**(6): p. 801-13.
41. Jiao, X., et al., *Heparan sulfate proteoglycans (HSPGs) modulate BMP2 osteogenic bioactivity in C2C12 cells.* J Biol Chem, 2007. **282**(2): p. 1080-6.
42. Lin, X., *Functions of heparan sulfate proteoglycans in cell signaling during development.* Development, 2004. **131**(24): p. 6009-21.
43. Wopereis, S., et al., *Mechanisms in protein O-glycan biosynthesis and clinical and molecular aspects of protein O-glycan biosynthesis defects: a review.* Clin Chem, 2006. **52**(4): p. 574-600.

44. Brockhausen, I., H. Schachter, and P. Stanley, *O-GalNAc Glycans*, in *Essentials of Glycobiology*, A. Varki, et al., Editors. 2009: Cold Spring Harbor (NY).
45. Kufe, D.W., *MUC1-C oncoprotein as a target in breast cancer: activation of signaling pathways and therapeutic approaches.* Oncogene, 2013. **32**(9): p. 1073-81.
46. Sprecher, E., *Familial tumoral calcinosis: from characterization of a rare phenotype to the pathogenesis of ectopic calcification.* J Invest Dermatol, 2010. **130**(3): p. 652-60.
47. Apweiler, R., H. Hermjakob, and N. Sharon, *On the frequency of protein glycosylation, as deduced from analysis of the SWISS-PROT database.* Biochim Biophys Acta, 1999. **1473**(1): p. 4-8.
48. Stanley, P., H. Schachter, and N. Taniguchi, *N-Glycans*, in *Essentials of Glycobiology*, A. Varki, et al., Editors. 2009: Cold Spring Harbor (NY).
49. Ellgaard, L., M. Molinari, and A. Helenius, *Setting the standards: quality control in the secretory pathway.* Science, 1999. **286**(5446): p. 1882-8.
50. Deom, C.M., A.J. Caton, and I.T. Schulze, *Host cell-mediated selection of a mutant influenza A virus that has lost a complex oligosaccharide from the tip of the hemagglutinin.* Proc Natl Acad Sci U S A, 1986. **83**(11): p. 3771-5.
51. Pochec, E., et al., *Glycosylation profile of integrin alpha 3 beta 1 changes with melanoma progression.* Biochim Biophys Acta, 2003. **1643**(1-3): p. 113-23.
52. Wang, X., et al., *Core fucosylation regulates epidermal growth factor receptor-mediated intracellular signaling.* J Biol Chem, 2006. **281**(5): p. 2572-7.
53. Rabinovich, G.A., et al., *Functions of cell surface galectin-glycoprotein lattices.* Curr Opin Struct Biol, 2007. **17**(5): p. 513-20.
54. Metzler, M., et al., *Complex asparagine-linked oligosaccharides are required for morphogenic events during post-implantation development.* EMBO J, 1994. **13**(9): p. 2056-65.
55. Boisson, M., et al., *Arabidopsis glucosidase I mutants reveal a critical role of N-glycan trimming in seed development.* EMBO J, 2001. **20**(5): p. 1010-9.
56. Clark, G.F., *The role of carbohydrate recognition during human sperm-egg binding.* Hum Reprod, 2013. **28**(3): p. 566-77.
57. Freeze, H.H., *Understanding human glycosylation disorders: biochemistry leads the charge.* J Biol Chem, 2013. **288**(10): p. 6936-45.
58. Freeze, H.H., et al., *Solving glycosylation disorders: fundamental approaches reveal complicated pathways.* Am J Hum Genet, 2014. **94**(2): p. 161-75.
59. Marquardt, T. and J. Denecke, *Congenital disorders of glycosylation: review of their molecular bases, clinical presentations and specific therapies.* Eur J Pediatr, 2003. **162**(6): p. 359-79.
60. Wopereis, S., et al., *Apolipoprotein C-III isofocusing in the diagnosis of genetic defects in O-glycan biosynthesis.* Clin Chem, 2003. **49**(11): p. 1839-45.
61. Harms, H.K., et al., *Oral mannose therapy persistently corrects the severe clinical symptoms and biochemical abnormalities of phosphomannose isomerase deficiency.* Acta Paediatr, 2002. **91**(10): p. 1065-72.
62. Wu, X., et al., *Mutation of the COG complex subunit gene COG7 causes a lethal congenital disorder.* Nat Med, 2004. **10**(5): p. 518-23.
63. Foulquier, F., et al., *Conserved oligomeric Golgi complex subunit 1 deficiency reveals a previously uncharacterized congenital disorder of glycosylation type II.* Proc Natl Acad Sci U S A, 2006. **103**(10): p. 3764-9.
64. Kodera, H., et al., *Mutations in COG2 encoding a subunit of the conserved oligomeric golgi complex cause a congenital disorder of glycosylation.* Clin Genet, 2014.
65. Reynders, E., et al., *Golgi function and dysfunction in the first COG4-deficient CDG type II patient.* Hum Mol Genet, 2009. **18**(17): p. 3244-56.
66. Lubbehusen, J., et al., *Fatal outcome due to deficiency of subunit 6 of the conserved oligomeric Golgi complex leading to a new type of congenital disorders of glycosylation.* Hum Mol Genet, 2010. **19**(18): p. 3623-33.

67. Kranz, C., et al., *COG8 deficiency causes new congenital disorder of glycosylation type IIh.* Hum Mol Genet, 2007. **16**(7): p. 731-41.
68. Foulquier, F., et al., *A new inborn error of glycosylation due to a Cog8 deficiency reveals a critical role for the Cog1-Cog8 interaction in COG complex formation.* Hum Mol Genet, 2007. **16**(7): p. 717-30.
69. Paesold-Burda, P., et al., *Deficiency in COG5 causes a moderate form of congenital disorders of glycosylation.* Hum Mol Genet, 2009. **18**(22): p. 4350-6.
70. Morava, E., et al., *A common mutation in the COG7 gene with a consistent phenotype including microcephaly, adducted thumbs, growth retardation, VSD and episodes of hyperthermia.* Eur J Hum Genet, 2007. **15**(6): p. 638-45.
71. Sharon, N. and H. Lis, *History of lectins: from hemagglutinins to biological recognition molecules.* Glycobiology, 2004. **14**(11): p. 53R-62R.
72. Yamamoto, F., *Molecular genetics of ABO.* Vox Sang, 2000. **78 Suppl 2**: p. 91-103.
73. Sumner, J.B. and S.F. Howell, *Identification of Hemagglutinin of Jack Bean with Concanavalin A.* J Bacteriol, 1936. **32**(2): p. 227-37.
74. Boyd, W.C. and E. Shapleigh, *Separation of individuals of any blood group into secretors and non-secretors by use of a plant agglutinin (lectin).* Blood, 1954. **9**(12): p. 1194-8.
75. Zaia, J., *Mass spectrometry and glycomics.* OMICS, 2010. **14**(4): p. 401-18.
76. Pittenger, M.F., et al., *Multilineage potential of adult human mesenchymal stem cells.* Science, 1999. **284**(5411): p. 143-7.
77. da Silva Meirelles, L., P.C. Chagastelles, and N.B. Nardi, *Mesenchymal stem cells reside in virtually all post-natal organs and tissues.* J Cell Sci, 2006. **119**(Pt 11): p. 2204-13.
78. Bartholomew, A., et al., *Mesenchymal stem cells suppress lymphocyte proliferation in vitro and prolong skin graft survival in vivo.* Exp Hematol, 2002. **30**(1): p. 42-8.
79. Kon, E., et al., *Autologous bone marrow stromal cells loaded onto porous hydroxyapatite ceramic accelerate bone repair in critical-size defects of sheep long bones.* J Biomed Mater Res, 2000. **49**(3): p. 328-37.
80. Quarto, R., et al., *Repair of large bone defects with the use of autologous bone marrow stromal cells.* N Engl J Med, 2001. **344**(5): p. 385-6.
81. Ringden, O. and A. Keating, *Mesenchymal stromal cells as treatment for chronic GVHD.* Bone Marrow Transplant, 2011. **46**(2): p. 163-4.
82. Hare, J.M., et al., *A randomized, double-blind, placebo-controlled, dose-escalation study of intravenous adult human mesenchymal stem cells (prochymal) after acute myocardial infarction.* J Am Coll Cardiol, 2009. **54**(24): p. 2277-86.
83. Jang, K.S., et al., *In vivo Tracking of Transplanted Bone Marrow-Derived Mesenchymal Stem Cells in a Murine Model of Stroke by Bioluminescence Imaging.* J Korean Neurosurg Soc, 2010. **48**(5): p. 391-8.
84. Jiang, R., et al., *Transplantation of placenta-derived mesenchymal stem cells in type 2 diabetes: a pilot study.* Front Med, 2011. **5**(1): p. 94-100.
85. Dominici, M., et al., *Minimal criteria for defining multipotent mesenchymal stromal cells. The International Society for Cellular Therapy position statement.* Cytotherapy, 2006. **8**(4): p. 315-7.
86. Cook, D. and P. Genever, *Regulation of mesenchymal stem cell differentiation.* Adv Exp Med Biol, 2013. **786**: p. 213-29.
87. Ducy, P., et al., *Osf2/Cbfa1: a transcriptional activator of osteoblast differentiation.* Cell, 1997. **89**(5): p. 747-54.
88. Komori, T., et al., *Targeted disruption of Cbfa1 results in a complete lack of bone formation owing to maturational arrest of osteoblasts.* Cell, 1997. **89**(5): p. 755-64.
89. Zheng, H., et al., *Cbfa1/osf2 transduced bone marrow stromal cells facilitate bone formation in vitro and in vivo.* Calcif Tissue Int, 2004. **74**(2): p. 194-203.
90. Nakashima, K., et al., *The novel zinc finger-containing transcription factor osterix is required for osteoblast differentiation and bone formation.* Cell, 2002. **108**(1): p. 17-29.

91. Hassan, M.Q., et al., *Dlx3 transcriptional regulation of osteoblast differentiation: temporal recruitment of Msx2, Dlx3, and Dlx5 homeodomain proteins to chromatin of the osteocalcin gene.* Mol Cell Biol, 2004. **24**(20): p. 9248-61.
92. Zhang, J., et al., *Phenotypic analysis of Dlx5 overexpression in post-natal bone.* J Dent Res, 2008. **87**(1): p. 45-50.
93. Dodig, M., et al., *Ectopic Msx2 overexpression inhibits and Msx2 antisense stimulates calvarial osteoblast differentiation.* Dev Biol, 1999. **209**(2): p. 298-307.
94. Hayashi, M., et al., *Comparative roles of Twist-1 and Id1 in transcriptional regulation by BMP signaling.* J Cell Sci, 2007. **120**(Pt 8): p. 1350-7.
95. Yousfi, M., et al., *Increased bone formation and decreased osteocalcin expression induced by reduced Twist dosage in Saethre-Chotzen syndrome.* J Clin Invest, 2001. **107**(9): p. 1153-61.
96. Lee, K.S., et al., *Runx2 is a common target of transforming growth factor beta1 and bone morphogenetic protein 2, and cooperation between Runx2 and Smad5 induces osteoblast-specific gene expression in the pluripotent mesenchymal precursor cell line C2C12.* Mol Cell Biol, 2000. **20**(23): p. 8783-92.
97. Lee, M.H., et al., *BMP-2-induced Osterix expression is mediated by Dlx5 but is independent of Runx2.* Biochem Biophys Res Commun, 2003. **309**(3): p. 689-94.
98. Kulkarni, N.H., et al., *Orally bioavailable GSK-3alpha/beta dual inhibitor increases markers of cellular differentiation in vitro and bone mass in vivo.* J Bone Miner Res, 2006. **21**(6): p. 910-20.
99. Gaur, T., et al., *Canonical WNT signaling promotes osteogenesis by directly stimulating Runx2 gene expression.* J Biol Chem, 2005. **280**(39): p. 33132-40.
100. Boland, G.M., et al., *Wnt 3a promotes proliferation and suppresses osteogenic differentiation of adult human mesenchymal stem cells.* J Cell Biochem, 2004. **93**(6): p. 1210-30.
101. Quarto, N., B. Behr, and M.T. Longaker, *Opposite spectrum of activity of canonical Wnt signaling in the osteogenic context of undifferentiated and differentiated mesenchymal cells: implications for tissue engineering.* Tissue Eng Part A, 2010. **16**(10): p. 3185-97.
102. Hu, H., et al., *Sequential roles of Hedgehog and Wnt signaling in osteoblast development.* Development, 2005. **132**(1): p. 49-60.
103. St-Jacques, B., M. Hammerschmidt, and A.P. McMahon, *Indian hedgehog signaling regulates proliferation and differentiation of chondrocytes and is essential for bone formation.* Genes Dev, 1999. **13**(16): p. 2072-86.
104. Ghaemi, S.R., et al., *Exploring the mesenchymal stem cell niche using high throughput screening.* Biomaterials, 2013. **34**(31): p. 7601-15.
105. Komekado, H., et al., *Glycosylation and palmitoylation of Wnt-3a are coupled to produce an active form of Wnt-3a.* Genes Cells, 2007. **12**(4): p. 521-34.
106. Kurayoshi, M., et al., *Post-translational palmitoylation and glycosylation of Wnt-5a are necessary for its signalling.* Biochem J, 2007. **402**(3): p. 515-23.
107. Mason, J.O., J. Kitajewski, and H.E. Varmus, *Mutational analysis of mouse Wnt-1 identifies two temperature-sensitive alleles and attributes of Wnt-1 protein essential for transformation of a mammary cell line.* Mol Biol Cell, 1992. **3**(5): p. 521-33.
108. Schulte, G. and V. Bryja, *The Frizzled family of unconventional G-protein-coupled receptors.* Trends Pharmacol Sci, 2007. **28**(10): p. 518-25.
109. Jung, H., S.K. Lee, and E.H. Jho, *Mest/Peg1 inhibits Wnt signalling through regulation of LRP6 glycosylation.* Biochem J, 2011. **436**(2): p. 263-9.
110. Marigo, V., et al., *Biochemical evidence that patched is the Hedgehog receptor.* Nature, 1996. **384**(6605): p. 176-9.
111. Filvaroff, E., et al., *Inhibition of TGF-beta receptor signaling in osteoblasts leads to decreased bone remodeling and increased trabecular bone mass.* Development, 1999. **126**(19): p. 4267-79.
112. Kim, Y.W., et al., *TGF-beta sensitivity is determined by N-linked glycosylation of the type II TGF-beta receptor.* Biochem J, 2012. **445**(3): p. 403-11.

113. Saremba, S., et al., *Type I receptor binding of bone morphogenetic protein 6 is dependent on N-glycosylation of the ligand.* FEBS J, 2008. **275**(1): p. 172-83.
114. Hwang, J.B., et al., *Alternative glycosylation of the insulin receptor prevents oligomerization and acquisition of insulin-dependent tyrosine kinase activity.* Biochim Biophys Acta, 2000. **1499**(1-2): p. 74-84.
115. Gooi, H.C., et al., *Stage-specific embryonic antigen involves alpha 1 goes to 3 fucosylated type 2 blood group chains.* Nature, 1981. **292**(5819): p. 156-8.
116. Wearne, K.A., et al., *Use of lectins for probing differentiated human embryonic stem cells for carbohydrates.* Glycobiology, 2006. **16**(10): p. 981-90.
117. Dodla, M.C., et al., *Differing lectin binding profiles among human embryonic stem cells and derivatives aid in the isolation of neural progenitor cells.* PLoS One, 2011. **6**(8): p. e23266.
118. Heiskanen, A., et al., *Glycomics of bone marrow-derived mesenchymal stem cells can be used to evaluate their cellular differentiation stage.* Glycoconj J, 2009. **26**(3): p. 367-84.
119. Morad, V., et al., *The myelopoietic supportive capacity of mesenchymal stromal cells is uncoupled from multipotency and is influenced by lineage determination and interference with glycosylation.* Stem Cells, 2008. **26**(9): p. 2275-86.
120. Sackstein, R., et al., *Ex vivo glycan engineering of CD44 programs human multipotent mesenchymal stromal cell trafficking to bone.* Nat Med, 2008. **14**(2): p. 181-7.
121. Coman, D., et al., *The skeletal manifestations of the congenital disorders of glycosylation.* Clin Genet, 2008. **73**(6): p. 507-15.
122. James, S., et al., *Mutliparameter Analysis of Human Bone Marrow Stromal Cells Identifies Distinct Immunomodulatory and Differentiation-Competent Subtypes.* Stem Cell Reports, 2015. **4**: p. 1-12.
123. Abdul Rahman, S., et al., *Filter-aided N-glycan separation (FANGS): a convenient sample preparation method for mass spectrometric N-glycan profiling.* J Proteome Res, 2014. **13**(3): p. 1167-76.
124. Richardson, B.C., et al., *Structural basis for a human glycosylation disorder caused by mutation of the COG4 gene.* Proc Natl Acad Sci U S A, 2009. **106**(32): p. 13329-34.
125. Hamouda, H., et al., *N-glycosylation profile of undifferentiated and adipogenically differentiated human bone marrow mesenchymal stem cells: towards a next generation of stem cell markers.* Stem Cells Dev, 2013. **22**(23): p. 3100-13.
126. Jaiswal, N., et al., *Osteogenic differentiation of purified, culture-expanded human mesenchymal stem cells in vitro.* J Cell Biochem, 1997. **64**(2): p. 295-312.
127. Bellows, C.G., J.E. Aubin, and J.N. Heersche, *Initiation and progression of mineralization of bone nodules formed in vitro: the role of alkaline phosphatase and organic phosphate.* Bone Miner, 1991. **14**(1): p. 27-40.
128. Valcourt, U. and A. Moustakas, *BMP sigmaling in Osteogenesis, Bone remodeling and repair.* European Journal of Trauma, 2005(31): p. 464-79.
129. Ganss, B., R.H. Kim, and J. Sodek, *Bone sialoprotein.* Crit Rev Oral Biol Med, 1999. **10**(1): p. 79-98.
130. Puchtler, H. and S.N. Meloan, *Demonstration of phosphates in calcium deposits: a modification of von Kossa's reaction.* Histochemistry, 1978. **56**(3-4): p. 177-85.
131. Wada, Y., et al., *Comparison of the methods for profiling glycoprotein glycans--HUPO Human Disease Glycomics/Proteome Initiative multi-institutional study.* Glycobiology, 2007. **17**(4): p. 411-22.
132. Frank, O., et al., *Real-time quantitative RT-PCR analysis of human bone marrow stromal cells during osteogenic differentiation in vitro.* J Cell Biochem, 2002. **85**(4): p. 737-46.
133. Tremblay, L.O. and A. Herscovics, *Characterization of a cDNA encoding a novel human Golgi alpha 1, 2-mannosidase (IC) involved in N-glycan biosynthesis.* J Biol Chem, 2000. **275**(41): p. 31655-60.
134. Hennet, T., *The galactosyltransferase family.* Cell Mol Life Sci, 2002. **59**(7): p. 1081-95.
135. Breckenridge, D.G., et al., *Regulation of apoptosis by endoplasmic reticulum pathways.* Oncogene, 2003. **22**(53): p. 8608-18.

136. Smits, P., et al., *Lethal skeletal dysplasia in mice and humans lacking the golgin GMAP-210.* N Engl J Med, 2010. **362**(3): p. 206-16.
137. Siddappa, R., et al., *Donor variation and loss of multipotency during in vitro expansion of human mesenchymal stem cells for bone tissue engineering.* J Orthop Res, 2007. **25**(8): p. 1029-41.
138. Dorling, P.R., C.R. Huxtable, and S.M. Colegate, *Inhibition of lysosomal alpha-mannosidase by swainsonine, an indolizidine alkaloid isolated from Swainsona canescens.* Biochem J, 1980. **191**(2): p. 649-51.
139. Tulsiani, D.R., H.P. Broquist, and O. Touster, *Marked differences in the swainsonine inhibition of rat liver lysosomal alpha-D-mannosidase, rat liver Golgi mannosidase II, and jack bean alpha-D-mannosidase.* Arch Biochem Biophys, 1985. **236**(1): p. 427-34.
140. Elbein, A.D., et al., *Swainsonine: an inhibitor of glycoprotein processing.* Proc Natl Acad Sci U S A, 1981. **78**(12): p. 7393-7.
141. Elbein, A.D., et al., *Effect of swainsonine, an inhibitor of glycoprotein processing, on cultured mammalian cells.* J Cell Physiol, 1983. **115**(3): p. 265-75.
142. Foddy, L., J. Feeney, and R.C. Hughes, *Properties of baby-hamster kidney (BHK) cells treated with Swainsonine, an inhibitor of glycoprotein processing. Comparison with ricin-resistant BHK-cell mutants.* Biochem J, 1986. **233**(3): p. 697-706.
143. Sun, J.Y., et al., *Suppressive effects of swainsonine on C6 glioma cell in vitro and in vivo.* Phytomedicine, 2009. **16**(11): p. 1070-4.
144. Sun, J.Y., et al., *Inhibition of the growth of human gastric carcinoma in vivo and in vitro by swainsonine.* Phytomedicine, 2007. **14**(5): p. 353-9.
145. Dennis, J.W., *Effects of swainsonine and polyinosinic:polycytidylic acid on murine tumor cell growth and metastasis.* Cancer Res, 1986. **46**(10): p. 5131-6.
146. Galustian, C., et al., *Swainsonine, a glycosylation inhibitor, enhances both lymphocyte efficacy and tumour susceptibility in LAK and NK cytotoxicity.* Immunopharmacology, 1994. **27**(2): p. 165-72.
147. Oredipe, O.A., et al., *Enhanced proliferation of functionally competent bone marrow cells in different strains of mice treated with swainsonine.* Int Immunopharmacol, 2003. **3**(3): p. 445-55.
148. Oredipe, O.A., et al., *Protective effects of swainsonine on murine survival and bone marrow proliferation during cytotoxic chemotherapy.* J Natl Cancer Inst, 1991. **83**(16): p. 1149-56.
149. Shaheen, P.E., et al., *Phase II study of the efficacy and safety of oral GD0039 in patients with locally advanced or metastatic renal cell carcinoma.* Invest New Drugs, 2005. **23**(6): p. 577-81.
150. Varki, A., *Glycan-based interactions involving vertebrate sialic-acid-recognizing proteins.* Nature, 2007. **446**(7139): p. 1023-9.
151. Elbein, A.D., et al., *Kifunensine, a potent inhibitor of the glycoprotein processing mannosidase I.* J Biol Chem, 1990. **265**(26): p. 15599-605.
152. Yamamoto, H., et al., *The apical and basolateral secretion of Wnt11 and Wnt3a in polarized epithelial cells is regulated by different mechanisms.* J Cell Sci, 2013. **126**(Pt 13): p. 2931-43.
153. Shibuya, N., et al., *The elderberry (Sambucus nigra L.) bark lectin recognizes the Neu5Ac(alpha 2-6)Gal/GalNAc sequence.* J Biol Chem, 1987. **262**(4): p. 1596-601.
154. Delannoy, P., et al., *Benzyl-N-acetyl-alpha-D-galactosaminide inhibits the sialylation and the secretion of mucins by a mucin secreting HT-29 cell subpopulation.* Glycoconj J, 1996. **13**(5): p. 717-26.
155. Mistry, P.K., et al., *Glucocerebrosidase gene-deficient mouse recapitulates Gaucher disease displaying cellular and molecular dysregulation beyond the macrophage.* Proc Natl Acad Sci U S A, 2010. **107**(45): p. 19473-8.
156. Platt, F.M., et al., *N-butyldeoxynojirimycin is a novel inhibitor of glycolipid biosynthesis.* J Biol Chem, 1994. **269**(11): p. 8362-5.

157. Kumarasuriyar, A., et al., *De-sulfation of MG-63 cell glycosaminoglycans delays in vitro osteogenesis, up-regulates cholesterol synthesis and disrupts cell cycle and the actin cytoskeleton.* J Cell Physiol, 2009. **219**(3): p. 572-83.
158. Molteni, A., et al., *Alterations of matrix- and cell-associated proteoglycans inhibit osteogenesis and growth response to fibroblast growth factor-2 in cultured rat mandibular condyle and calvaria.* Cell Tissue Res, 1999. **295**(3): p. 523-36.
159. Baeuerle, P.A. and W.B. Huttner, *Chlorate--a potent inhibitor of protein sulfation in intact cells.* Biochem Biophys Res Commun, 1986. **141**(2): p. 870-7.
160. Crocker, P.R., J.C. Paulson, and A. Varki, *Siglecs and their roles in the immune system.* Nat Rev Immunol, 2007. **7**(4): p. 255-66.
161. Hiruma, Y., et al., *Impaired osteoclast differentiation and function and mild osteopetrosis development in Siglec-15-deficient mice.* Bone, 2013. **53**(1): p. 87-93.
162. Walker, P.S., et al., *Viral interference during simultaneous transduction with two independent helper-free retroviral vectors.* Hum Gene Ther, 1996. **7**(9): p. 1131-8.
163. Kodera, H., et al., *Mutations in COG2 encoding a subunit of the conserved oligomeric golgi complex cause a congenital disorder of glycosylation.* Clin Genet, 2015. **87**(5): p. 455-60.
164. Cheung, P., et al., *Metabolic homeostasis and tissue renewal are dependent on beta1,6GlcNAc-branched N-glycans.* Glycobiology, 2007. **17**(8): p. 828-37.
165. Lau, K.S., et al., *Complex N-glycan number and degree of branching cooperate to regulate cell proliferation and differentiation.* Cell, 2007. **129**(1): p. 123-34.
166. Calle, Y., et al., *Removal of N-glycans from cell surface proteins induces apoptosis by reducing intracellular glutathione levels in the rhabdomyosarcoma cell line S4MH.* Biol Cell, 2000. **92**(8-9): p. 639-46.
167. Oredipe, O.A., et al., *Swainsonine stimulates bone marrow cell proliferation and differentiation in different strains of inbred mice.* Pharmacol Res, 2003. **47**(1): p. 69-74.
168. Hennebicq-Reig, S., et al., *Permanent exposure of mucin-secreting HT-29 cells to benzyl-N-acetyl-alpha-D-galactosaminide induces abnormal O-glycosylation of mucins and inhibits constitutive and stimulated MUC5AC secretion.* Biochem J, 1998. **334 (Pt 1)**: p. 283-95.
169. Mendes, S.C., et al., *Relation between in vitro and in vivo osteogenic potential of cultured human bone marrow stromal cells.* J Mater Sci Mater Med, 2004. **15**(10): p. 1123-8.